TRANSPORT AND RETENTION OF FULLERENE-BASED NANOPARTICLES IN WATER-SATURATED POROUS MEDIA

A Thesis
Presented to
The Academic Faculty

By

Yonggang Wang

In Partial Fulfillment
of the Requirement for the Degree
Doctor of Philosophy in Environmental Engineering in the
School of Civil and Environmental Engineering

Georgia Institute of Technology
August 2009

TRANSPORT AND RETENTION OF FULLERENE-BASED NANOPARTICLES IN WATER-SATURATED POROUS MEDIA

Approved by:

Dr. Kurt D. Pennell, Advisor
School of Civil and Environmental Engineering
Georgia Institute of Technology

Dr. Robert L. Snyder, Minor Advisor
School of Materials Science and Engineering
Georgia Institute of Technology

Dr. Joseph B. Hughes
School of Civil and Environmental Engineering
Georgia Institute of Technology

Dr. Jaehong Kim
School of Civil and Environmental Engineering
Georgia Institute of Technology

Dr. Sotira Z. Yiacoumi
School of Civil and Environmental Engineering
Georgia Institute of Technology

Date Approved: June 4, 2009

To my grandfather
Guozhen Wang
for his constant love and support

Acknowledgements

As my Ph.D. journey draws to a close, it is my great pleasure to express heartily appreciations to the individuals below for their support and guidance.

First and foremost, I would like to express my heartily thanks to Xing, my loving wife. Without her love and support, this dissertation would not have been possible. We left our home country to purse my graduate degree in U.S.. It is her constant loves that warm my heart, keep loneliness away, and encourage me to bravely face frustrations.

I am also grateful to my family for their constant belief in me. I thank my grandfather, aunt, and uncle for their generous financial and spiritual support, which provides me with solid foundations for my hopes and dreams. I also thank my parents for raising me in a poor village, where the life instilled in me the value of diligence and persistence.

A special word of thanks must be given to my advisor, Dr. Kurt Pennell. Because he gave a chance and believed in me, I am able to study and do research at Georgia Tech. Over the past three and half years, he has been a constant source of academic advice and encouragement. He always discussed problems that I met during this research like a student and gave me suggestions. He also provided me with valuable opportunities beyond my expectation to help my career development. In addition to be a mentor, he is one of my best friends. He helped me a lot to my personal life. I am deeply thankful for all that he has done for me.

I would like to express my gratitude toward my committee members for their guidance and understanding. I wish to thank Dr. Robert Snyder and Dr. Joseph Hughes for taking time out of their extremely busy schedule to serve on my committee. Great appreciation should also be given to Dr. Jaehong Kim. Especially over the last eight months, he has been helping me a lot on part of this research. Without him, I could not have finished the work presented in Chapter 8. Finally, I thank Dr. Sotira Yiacoumi for her continuous interest in my research and willingness to be a member of my doctoral committee.

Much appreciation is expressed to my collaborators Dr. Yusong Li and Dr. Linda Abriola. Although barely met them, I can sense that they both are nice and fantastic researchers. Through analyzing experimental data and discussing project problems with them, I learned a lot about mathematical modeling. I have enjoyed working with them and wish to have a long last collaboration with them in the future.

I would also like to acknowledge Dr. Shuguang Li, my undergraduate advisor. His experience, achievements in geochemistry and attitude toward science really impressed me. Through working with him, I learned what the scientific research was. In my mind, he has been a model of scientist.

I am indebted to many of my past and present labmates. Dr. Natalie Capiro, Dr. Jed Costanza, Dr. Dave Himmelheber, Emmie Granberry, Namory Keita, Dr. Eric Suchomel, Nivi Ramaswamy, Dr. Lingjun Kong all have been making our research group like a warm family. They are so nice and friendly that I feel I am very lucky to be at Tech. Especially, Dr. Natalie Capiro and Kelly Fletcher have been beyond labmates. Rather, they are my close friends, who share not only late-night working but also happiness and depressions.

I would like to thank all my peers and faculty in the Environmental Engineering program at Georgia Tech. Particular appreciation is expressed to Dr. Guangxuan Zhu for the great help on instrumentations. I also owe my gratitude to the friendship of Dr. John Fortner, Dr. Janet Hatt, Dr. Ulas Tezel, Siv Balachandran, Emily Lantrip, Dr. Yiliang He, Dr. Jinglan Hong, Dr. Bo Zhang, and Xianji Tao.

TABLE OF CONTENTS

LIST OF TABLES

LIST OF FIGURES

LIST OF SYMBOLS AND ABBREVIATIONS

Acronyms

ADR	Advective-dispersive reactive
AP	Appling soil
BTC	Breakthrough curve
CCC	Critical coagulation concentration
CF	Correlation function
CMC	Critical micelle concentration
CNT	Carbon nanotube
DI	Deionized water
DLS	Dynamic light scattering
DLVO	Derjaguin-Landau-Verwey-Overbeek
DMF	N,N-dimethylformamide
EDL	Electronic double layer
GB	Glass beads
GBL	γ-butyrolactone
HPLC	High performance liquid chromatograph
MR	Manufacture-reported
MWNT	Multi-wall nanotube
NMP	N-methylpyrrolidone
NMR	Nuclear magnetic resonance
NOM	Natural organic matter
OS	Ottawa sands
PALS	phase analysis light scattering
PV	Pore volume
SLS	Static light scattering
SRFA	Suwannee River fulvic acids
SRHA	Suwannee River humic acids
SWNT	Single-wall nanotube
TEM	Transmission electron minicroscopy
THF	Tetrahydrofuran
VDW	van der Waals
WB	Webster soil

Symbols

A	Hamaker constant
b	Constant in van de Waals energy calculation
c	Molar concentration
C	Particle effluent concentration
C_0	Particle initial concentration

d	Surface to surface distance
D_0	Diffusion coefficient at infinite dilution
d_c	Mean diameter of collector
D_H	Hydrodynamic dispersion coefficient
D_m	Mutual diffusion coefficient
d_p	Particle diameter
e	Electron charge
E_{edl}	Electronic double layer interaction energy
E_v	van de Waals interaction energy
F	Faraday constant
g	Gravitational constant
k_{att}	Attachment rate
k_b	Boltzman constant
K_D	Solute distribution coefficient
L	Bed length
n	Number of cations
P_e	Peclet number
r	Particle radius
R	Ideal gas constant
R_e	Reynold number
R_F	Retardation factor
S	Particle concentration in solid phase
T	Absolute temperature
U	Darcy velocity
v_p	Pore water velocity
z	Ion valence

Greek Symbols

α	Attachment rate coefficient
γ	Characteristic wavelength
ε	Dielectric constant
ξ	Zeta potential
η_0	Theoretical collector efficiency
θ_w	Volumetric water content
κ	Debye parameter
λ	Filtration coefficient
μ	Dynamic viscosity
μ_e	Electrophoretic mobility
ρ_b	Bulk density
ρ_l	Liquid density
ρ_p	Particle density

SUMMARY

Due to their unique physical and chemical properties fullerene-based nanomaterials are considered to be promising materials for novel nanotechnology applications. Their production, use, and disposal are expected to increase dramatically over the next several decades. While the toxicity of C_{60} nanoparitcles (nC_{60}) and carbon nanotubes (CNTs) in aqueous suspensions has been studied in detail, our current understanding of their fate and transport in subsurface environments is quite limited.

To date, a limited number of column experiments have been conducted to investigate the transport and deposition of nC_{60} in water-saturated porous media. In several of these studies, experimental conditions were not representative of natural conditions, employing clean glass beads at very high flow rates (e.g., pore water velocity of 273 m/d), yielding a condition approaching the laminar flow limit in a porous medium. The resulting steady-state effluent concentration data were interpreted using clean-bed filtration theory. However, the absence of nC_{60} retention data does not allow for validation of this theory and limits a more detailed interpretation of nC_{60} deposition preocess. When compared to nC_{60}, even fewer experiments have been performed to evaluate CNT transport behavior in porous media. In the only study published to date, it was concluded that the physicochemical filtration dominated single-wall carbon nanotube (SWNT) retention in quartz sands. However, potential effects of nanotube length on SWNT transport were not considered. Thus, there is a clear need to develop a

more complete understanding of carbon-based nanoparticle transport and retention behavior in the environment.

The primary objective of this research was to systematically study the transport and retention of aqueous fullerene nanoparticle suspensions in porous media. One-dimensional (1-D) column experiments were conducted. Initial transport experiments were performed using glass beads to allow for direct comparisons with previous studies, quartz sands and natural soils were selected as the porous media for subsequent studies to assess nC_{60} transport and deposition in more realistic subsurface materials. Several extraction protocols were developed to quantify nC_{60} retained by the solid phase. Thus, in addition to effluent concentration data, retention profile data were collected for each column experiment, which allowed for more complete verification of the applicability of clean-bed filtration theory to nanoparticle transport and deposition.

The transport behavior of nC_{60} in quartz sands was evaluated for several sand grain size (20-30, 40-50, 80-100, and 100-140 mesh), flow rates (pore water velocity of 1 and 8 m/d), and electrolyte species (Ca^{2+} and Na^{+}) and concentration (ionic strength of 3 and 30 mM). Experimental results demonstrated that the retention of nC_{60} increased more than 6-fold as mean grain size increased from 20-30 to 100-140 mesh at 8 m/d. Complete retention was observed in 80-100 mesh sands as the pore water velocity of 1 m/d was used. When 1 mM CaCl2 was used as background electrolyte, approximately 33% of total input nC_{60} transported through 40-50 mesh sands, while complete retention was observed as the ionic strength increased to 30 mM. At the ionic strength of 3 mM, the retention of nC_{60} in the presence of Ca2+ was more than 2 orders of magnitude higher than that in the presence of Na+. The attachment of nC_{60} was found to be largely irreversible and an introduction of pH 12 water was required to detach more than 50% of retained nC_{60}. The breakthrough curves and retention profiles in quartz sands suggest that the retention of nC_{60} was primarily associated with Ca^{2+} bridging in the first energy minimum and that clean-bed filtration theory alone was not sufficient for data interpretation. In the presence of stabilizing agents, including surfactant and 20 mg C/L Suwannee River humic and fulvic acids, nC_{60} extraction and quantification protocols were developed. Compared to that in the absence of stabilizing agents, symmetrical effluent breakthrough curves were obtained and the retention of nC_{60} decreased more than 10-fold. In two natural soils, Appling and Webster soil, complete retention of nC_{60} was observed even after introducing up to 65 pore volumes of nC_{60} suspension. However, nC_{60} readily transported through Appling soil in the presence of 1,000 mg/L Tween 80 (an anionic surfactant).

To explore CNT transport, suspensions of multi-wall carbon nanotubes (MWNTs) with three differenet manufacture-reporte (MR) lengths (0.5-2, 10-20, and 50 μm) were prepared using a novel chemical modification method involving a mild acid treatment (no application of ultrasonication or superacids). Column experiments were conducted to evaluate MWNT transport and retention in 40-50 mesh quartz sands with a focus toward effects of tube length. MWNTs even with a MR length of 50 μm were readily transported through quartz sands, where 80% of the injected mass passed through the column.

MWNTs even exhibited either comparable or higher mobility than nC_{60} at similar experimental conditions. Mathematical modeling revealed that clean-bed filtration theory was not able to catch MWNT retention data and physical straining as well as physicochemical interactions played important roles on CNT retention in porous media.

This research contributes to a better understanding of fundamental processes governing nanoparticle transport and retention in porous media and provides experimental data for the development of nanoparticle transport models. The results of this research will help to assess the fate and distribution of nanoparticles in the environement and to prevent or minimize their unintended exposures to the ecosystem. This work, coupling with other components of the proactive nanoparticle risk analysis, will ensure the nanotechnology to be beneficial and environmentally sustainable.

CHAPTER 1

INTRODUCTION AND OBJECTIVES

As allotropes of carbon, fullerene (C_{60}) and carbon nanotubes have attracted particular attention from the scientific community since their discoveries (Iijima, 1991; Kroto et al., 1985). Due to their unique physical and chemical properties of fullerene-based nanomaterials, many applications have been proposed and implemented in various fields, such as superconduction, nonlinear optical material, sensor, personal care, and pharmaceuticals. The commercial production and use of fullerene nanomaterials will inevitably lead to their release into the environment, either from industrial sources or through disposal in municipal waste, landfills, and streams.

Although pure C_{60} is hydrophobic and has extremely low solubility in water (1×10^{-9} mg/L) (Fortner et al., 2005), several methods have recently been developed to disperse C_{60} into water in the form of aggregates without the aid of stabilizing agents (Cheng et al., 2005; Fortner et al., 2005). These fullerene aggregates, referred to as nC_{60}, are comprised of underivatized C_{60}, are negatively charged, and have diameters ranging from 5 to 200 nm. Such stable aqueous suspensions were proposed to be the most relevant form of C_{60} in terrestrial environment. Subsequent cytotoxicity studies have suggested that nC_{60} is toxic to some fish, mice and human cell lines (Oberdorster, 2004a; Sayes et al., 2004), although debates over nC_{60} toxicity continue. Similar to solid C_{60}, carbon nanotubes (CNTs) exhibit very high hydrophobicity and extremely low water solubility. However, with potential applications in biomedical and material science, the research on the preparation of CNT dispersion in water has expanded. Encouragingly, the dispersion of multi-wall nanotubes (MWNTs) into water in the presence of natural organic matter (NOM) has been reported recently (Hyung et al., 2007). Thus, the potential exist for CNTs to naturally enter water to form aqueous suspensions. Additionally, CNTs in suspensions exhibit cytotoxicity to human cell lines (Hussain et al., 2009), raising concerns on their potential impacts on aquatic systems.

Concerns over the potential adverse effects of nC_{60} and CNT exposures have initiated research on their fate and transport in the environment. Results of several recent studies have demonstrated that the stability of fullerene nanoparticles is dependent upon the electrolyte species and concentration, which is attributed to electrostatic interactions (Chen and Elimelech, 2006; Saleh et al., 2008). Based on traditional colloid approaches, the Derjaguin-Landau-Verwey-Overbeek (DLVO) theory has been used to qualitatively interpret nC_{60} stability in aqueous suspensions. Generally, nC_{60} and CNTs can be destabilized by increasing the ionic strength or by addition of multivalent ions (e.g., Ca^{2+}) (Chen and Elimelech, 2006; Saleh et al., 2008). However, the presence of NOM serves to enhance the stability of nC_{60} in suspension, even at very high monovalent electrolyte concentrations (Chen and Elimelech, 2007; Saleh et al., 2008).

In addition to the study of nC_{60} aggregation in batch systems, the transport and deposition behavior of nC_{60} in water-saturated porous media, including glass beads and quartz sands, have been evaluated in few studies (Brant et al., 2005a; Cheng et al., 2005;

Espinasse et al., 2007; Lecoanet and Wiesner, 2004; Lecoanet et al., 2004). The majority of these experiments were conducted in 40-50 mesh glass beads and under flow condition that approaches the limit of turbulent flow, and without particle retention data. In an effort to identify mechanisms governing nanoparticle deposition, clean-bed filtration theory has been directly adopted. However, it is difficult to assess the applicability of clean-bed filtration theory to the deposition of nC_{60} and CNTs in porous media in the absence of retention profile data. Although results of batch experiments have shown that Suwannee River humic (SRHA) and fulvic acids (SRFA) are able to enhance nC_{60} stability, the direct experimental studies in columns have not been reported. In addition, the majority of transport data reported to date have been limited to well-defined porous media, including clean quartz sands and glass beads. Far less attention has been directed toward nanoparicle transport in natural soils, where clay minerals and organic matter often play a dominant role in contaminant fate and transport. Furthermore, CNT transport experiments have been conducted under limited conditions, using SWNT at one length. Thus, there is a clear need to develop a more complete understanding of carbon-based nanoparticle transport and retention behavior in the environment.

The primary objective of this research was to systematically study the transport and retention of fullerene nanoparticles in porous media. MWNTs and nC_{60} were selected as model nanoparticles due to broad applications of MWNTs and C_{60}. The transport and retention of nC_{60} in porous media were evaluated by varying flow rate (pore water velocity of 1 and 8 m/d), mean grain size (20-30, 40-50, 80-100, and 100-140 mesh), and electrolyte species (Ca^{2+} and Na^{+}) and concentrations (ionic strength of 3 and 30 mM). In an effort to understand interactions between nanoparticles with the solid phase, column experiments were conducted in presence of stabilizing agents, including SRHA, SRFA, and Tween 80. During the course of these studies, the complexity of the solid phase was increased from glass beads, an ideal porous media, to quartz sands, and eventually to natural soil.

This document begins with a literature review (Chapter 2), which covers fullerene C_{60} and carbon nanotube properties and applications, methods used to prepare fullerene nanoparticle suspensions, fullerene nanoparitcle toxicity, and potential exposure pathways. Chapter 2 also includes detailed descriptions of DLVO theory and clean-bed filtration theory, which have been used to interpret nanoparticle aggregation and transport kinetics. Details of the materials, experimental protocols, and analytical methods employed in this research are described in Chapter 3. In the following five chapters (Chapters 4-8), experimental results are presented for each of the specific research objectives. In chapter 9, the overall conclusions of this research, as well as recommendations for related and future extended research, are presented. The specific objectives (Chapters 4-8) of this research were:

(1) Investigate the effects of flow velocity and grain size on the transport and retention of nC_{60} in water-saturated quartz sands. One-dimensional (1-D) column experiments were conducted in four size fractions of Ottawa sands (20-30, 40-50,

80-100, and 100-140 mesh). Pore water velocity of 1 and 8 m/d were employed to ensure the laminar flow condition. The transport and retention behavior of nC_{60} were evaluated based upon both effluent and retained nC_{60} concentration data. In order to form a comparison with previous nC_{60} transport studies, additional column experiments were performed in 40-50 mesh glass beads. Experimental results in glass beads and Ottawa sands were then used to evaluate the applicability of clean-bed filtration theory to.nC_{60} transport and retention. (Chapter 4)

(2) Evaluate the influence of electrolyte species and concentration on nC_{60} aggregation and transport in quartz sands. Batch experiments were conducted at various $CaCl_2$ or NaCl concentrations and different suspension preparation mixing sequences to assess aggregation size and electrophoretic mobility. Column experiments were performed with 40-50 and 100-140 mesh Ottawa sands at a pore velocity of 8 m/d. The nC_{60} input suspension were conditioned with either $CaCl_2$ or NaCl at ionic strength of 3 and 30 mM . To further investigate the detachment of nC_{60} from sand grains, pH of the influent solution was altered during a prolonged column elution phase. (Chapter 5)

(3) Assess influences of SRHA, SRFA, and Tween 80 on transport of nC_{60} in water-saturated 40-50 mesh Ottawa sands. An analytical protocol that couples high performance liquid chromatography (HPLC) with liquid-liquid extraction, was developed to quantify nC_{60} and SRHA or SRFA in mixtures. Column experiments were subsequently conducted in the presence of 20 mg C/L SRHA or 20 mg C/L

SRFA in aqueous phase. Effects of Tween 80 on nC_{60} transport were evaluated through either injecting a pulse (5 pore volumes) of nC_{60} suspension that premixed with 1,000 mg/L Tween 80 or introducing nC60 alone (no Tween 80) to sands that were preflooded with 5 pore volumes of 1,000 mg/L Tween 80. (Chapter 6)

(4) Investigate the transport and retention of nC_{60} in water-saturated natural soils. Appling and Webster soil, which contain 0.75 and 3.3% of organic carbon and 9 and 33% of clay, respectively, were used as porous media for the column experiments. Due to strong retention of nC_{60} in both soils, additional column experiments with injection pulse widths of upt to 65 pore volumes were conducted. Interactions between nC_{60} and soil grains were further studied by addition of SRHA or Tween 80. (Chapter 7)

(5) Evaluate the effects of MR tube length on the transport and deposition of MWNTs in quartz sands. Suspensions of MWNTs with three different MR lengths (0.5-2, 10-20, and 50 μm) were prepared using a chemical modification method that involved the treatment with a mild acid and characterized using UV-absorbance photometer, UV-fluorophotometer, dynamic light scattering (DLS), and transmission electron microscopy (TEM). Column experiments were then conducted with two MWNT input concentrations (5 and 90 mg/L) under conditions that allowed for direct comparison to nC_{60} results. (Chapter 8)

CHAPTER 2

LITERATURE REVIEW

2.1 Introduction

Soil, in the outmost layer of the Earth terrestrial surface, consists of primarily unconsolidated (e.g., weathered) minerals and organic matter and supports land plants with nutrients and water. The important feature of soil is that it contains interconnected pores, which occupy 25% to 50% of the total soil volume and allow liquid (typically water) and gas to move (or transport) in subsurface. Based on water content in soil, the subsurface can be divided into mainly three zones: vadose zone, capillary fringe, and saturated zone. The water in saturated zone is referred to as groundwater, which is a vital natural resource for drinking water supply. Due to the permeable soil in upper layers, groundwater in an unconfined aquifer is vulnerable to terrestrial contaminant release. Once reach groundwater, contaminants can transport laterally in the subsurface, which may largely extends exposure to contaminants.

Commercial production and use of engineered nanomaterials are expected to dramatically increase over the next several decades (Maynard et al., 2006) and will inevitably lead to their release into the environment during manufacture, transportation, application, and disposal (Wiesner et al., 2006). It is no doubt that the manufactured nanomaterials, in different forms (e.g., nanoparticles), enter groundwater in many direct and indirect routes, such as infiltration of surface water and leaking from underground storage tanks, and transport with groundwater in subsurface, eventually ending at waste water treatment facilities or water supply.

2.2 Fullerenes

2.2.1 Discoveries

Fullerenes, the third carbon allotrope, are defined as a family of carbon molecules with cage structures. The shapes of fullerene molecules are hollow spheres (e.g., Buckminsterfullerene C_{60}), tubes (e.g., carbon nanotubes), or ellipsoids. The fullerene C_{60} and nanotubes were discovered by Robert F. Curl, Harold W. Kroto and Richard E. Smalley in 1985 (Kroto et al., 1985) and by Sumio Iijima in 1991(Iijima, 1991), respectively.

In September, 1985 Harold W. Kroto and his colleagues accidentally observed C_{60} in a graphite vaporization apparatus (Smalley, 1997), which was developed by Richard E. Smalley's group at Rice University. In this apparatus, graphite was vaporized by a pulsed laser with a wavelength of 532 nm in Helium (He) atmosphere. The vaporized carbon clusters were cooled and partially equilibrated during expansion in the post vaporization region. Next, the carbon clusters entered an ionization region containing an ArF excimer laser. Finally, the carbon clusters were detected using a time-of-flight (TOF) mass spectrometry. Surprisingly, only clusters with even number of carbon were observed and various carbon cluster distributions at the end of expansion were obtained through altering the He pressure, delay time of laser firing, and thermalization time (Curl and Smalley, 1988; Kroto et al., 1991; Kroto et al., 1985). In optimal operational conditions the peak in mass spectra for C_{60} was ca. 40 times stronger than those for other carbon clusters and the stable C_{60} molecule drew particular attentions from the Kroto research group. Based on structure stability, valence satisfaction, and mathematical calculations (Koruga et al., 1993), a sphere structure with pentagons and hexagons was proposed for the structure of C_{60} molecule (Figure 2.1), which was validated with IR and UV spectra (Kratschmer et al., 1990a) and the scanning tunneling microscopy (Koruga et al., 1993). Since the structure is analogous to the simple geodesic dome, C_{60} is named after Buckminster Fuller.

The discovery of CNTs was a direct consequence of intensive research on fullerene synthesis. In 1991, Sumio Iijima, a physicist in the NEC laboratories with strong interest on carbon clusters, observed a novel “needle-like tube” carbon structure (Iijima, 1991) with large length to width aspect ratio, when he studied the carbon soot on the graphite cathode in a fullerene synthesis apparatus. The fullerenes with this type of structure are called CNTs. Although the discovery of CNTs can be tracked back to 1950s (Monthioux and Kuznetsov, 2006), Professor Iijima is traditionally considered as the discoverer of CNTs due to unprecedented stimulation of his 1991 paper on worldwide carbon nanostructure research.

2.2.2 Properties and Applications of C_{60}

Molecular C_{60} has a hollow truncated-icosahedral structure consisting of 12 pentagons and 20 hexagons with one carbon atom on each vertex and a carbon bond (single or double) along each edge (Figure 2.1). This stable soccer-ball like structure exhibits I_h symmetry. The carbon valence (4^{-}) is satisfied by connecting to other carbons with one double bond (at the junction of two hexagons) and two single bonds (at the junction of a hexagon and a pentagon). The lengths of single and double bonds have been characterized by nuclear magnetic resonance (NMR), neutron diffraction, electron diffraction and X-ray as 1.45, 1.45, 1.46, and 1.47 and 1.40, 1.39, 1.40, and 1.36 Å, respectively (David et al., 1991; Hedberg et al., 1991; Hirsch and Brettreich, 2005; Liu et al., 1991; Yannoni et al., 1991). The diameter of C_{60} molecule is directly measured by single crystal X-ray and gas-phase electron diffraction and found to be 7.065 (Liu et al., 1991) and 7.113 Å (Hedberg et al., 1991), respectively. Taking the thickness of π-electron cloud, 3.35 Å (Hirsch and Brettreich, 2005), into account the effective diameter of a C_{60} molecule is ca. 10.44 Å, which agrees with the values measured by X-ray diffraction (Huffman, 1991; Kratschmer et al., 1990b) and STM (Wilson et al., 1990). Since C_{60} consists of 60 carbon molecules, its molecular weight is 720, which results in a signal peak at m/z of 720 (mono-ionized) in mass spectra (Kratschmer et al., 1990b; Kroto et al., 1985). Due to the symmetry of the truncated icosahedral structure, C_{60} has a single line at 143.2 in ^{13}C NMR spectra (Ajie et al., 1990; Hirsch and Brettreich, 2005; Johnson et al., 1990; Taylor et al., 1990) and four IR active bands at 1,429, 1,183, 577 and 528 cm^{-1} (Hirsch and Brettreich, 2005; Kratschmer et al., 1990b; Stanton and Newton, 1988; Weeks and Harter, 1988). The UV-vis spectrum of C_{60} thin film exhibits peaks at 216, 264, 339 and 625 nm, and plateau at 460 and 500 nm (Huffman, 1991; Kratschmer et al., 1990b; Larsson et al., 1987), which may vary with the film thickness (Kratschmer et al., 1990b). The analysis of transition energy between electron orbitals shows molecular C_{60} has very high electron affinity (Larsson et al., 1987; Pierson, 1993), which results in high reactivity of C_{60} with free radicals (Krusic et al., 1991a; Krusic et al., 1991b; McEwen et al., 1992).

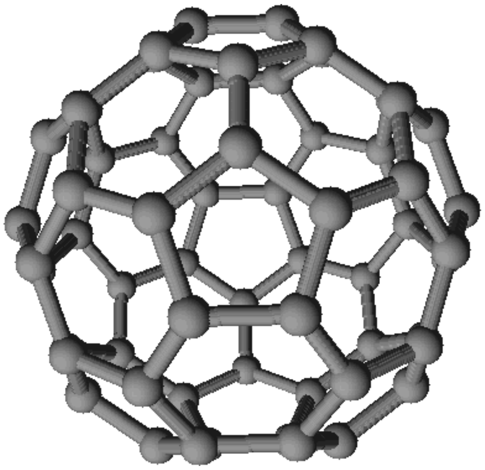

Figure 2.1: The structure of C_{60} in ball-and-sticks view. The structure is drawn through ACD/ChemSketch (www.acdlabs.com/).

Compared to diamond and graphite, solid C_{60} possesses a density of 1.65 g/cm^3, which is even smaller than that of graphite (2.3 g/cm^3). In terms of crystalline lattice, solid C_{60} has the face centered cubic lattice structure with a lattice constant of 14.17 Å (Fischer et al., 1992; Heiney et al., 1991; Pierson, 1993) at 300 K and atmospheric pressure, which is revealed by synchrotron X-ray measurement. At temperature below 260 K, the structure of solid C_{60} transited to simple cubic (Heiney et al., 1991; Prassides et al., 1992). Theoretically, liquid C_{60} can be obtained at high temperature and pressure, which have not been verified yet (Fortner, 2006). At elevated temperatures, sublimation of solid C_{60} occurs at 550 ^{o}C in inert atmosphere (e.g., Ar and He) and at normal pressure (Rausch and Braun, 2001), and at 700 ^{o}C in vacuum (Fortner, 2006; Ismail and Rodgers, 1992).

C_{60} solubility in solvents, which is playing an important role in C_{60} extraction and purification, reaction in solvents and fate in environment, has been widely studied since the beginning of mass production of solid C_{60} in 1990. To date, over 150 solubility values have been reported (Hirsch and Brettreich, 2005; Kulkarni and Jafvert, 2008). Unlike other solids with temperature-dependent solubilities, C_{60} exhibits the maximum solubility in hexane, toluene and CS_2 at ca. 280 K (Ruoff et al., 1993b). Another interesting feature of C_{60} in some solvents, such as bromobenzene (Korobov et al., 1998) and CCl_4 (Nagano and Nakamura, 1997), is the formation of a crystal solvate. The crystal solvate formation in tetrahydrofuran (THF) has been proposed (Kulkarni and Jafvert, 2008), but verification through X-ray has not been reported. Although many scientists have attempted to model and predict C_{60} solubility (Hansen and Smith, 2004; Heymann, 1996a; Kulkarni and Jafvert, 2008; Marcus et al., 2001; Ruoff et al., 1993a; Sivaraman et al., 1992), no direct dependence on certain solvent parameters has been found (Fortner, 2006; Hirsch and Brettreich, 2005). Studies show that C_{60} solubility has good correlation with solvent polarizability (Ruoff et al., 1993a), molecular size (Ruoff et al., 1993a), surface area (Murray et al., 1995), molar volume (Ruoff et al., 1993b) and electron-donor capacity (Talukdar et al., 1997). The solubility of C_{60} in typical solvents is summarized in

Table 2.1.

Table 2.1: C_{60} solubility in several commonly used organic solvents at 25 °C.

Solvent	Solubility (mg/L)
Acetone	1^{b}
Acetonitrile	0.04^{a}
Benzene	$1{,}700^{b}$
Carbon disulfide	$7{,}900^{b}$
Cyclohexane	36^{b}
Ethanol	1.4^{a}
Methanol	0.027^{a}
n-decane	71^{b}
Octanol	42.9^{a}
THF[*]	11^{a}
Toluene	$3{,}000^{a}$
Water	$1.3 \times 10^{-14\,c}$

[a] from Kulkarni and Jafvert (2008)
[b] from Ruoff et al. (1993a)
[c] from Heymann (1996b)
[*] Argument of solvated crystal exists

In solid C_{60}, the analysis of intermolecular distance and the isothermal compressibility reveals that the interaction of C_{60} molecules is dominated by van der Waals (VDW) force (Fischer et al., 1992; Fischer et al., 1991; Huffman, 1991; Kratschmer et al., 1990b). The weak interaction determines that the solid C_{60} is softer than graphite (Fischer et al., 1992), allowing solid C_{60} to be a potential lubricant (Koruga et al., 1993; Pierson, 1993). However, solid C_{60} is able to transform to diamond by applying over 150 atm pressure in less than a second (Regueiro et al., 1992), which makes the solid C_{60} a candidate of abrasive material (Koruga et al., 1996; Koruga et al., 1993). Although solid C_{60} is not electrically conductive at room temperature and one atmosphere, it can be used potentially as a semiconductor due to the band gap energy of 1.5 ev (Pierson, 1993). By doping with other metals, solid C_{60} becomes superconducting at low termperature (Chen and Lieber, 1993; Haddon et al., 1991; Iqbal et al., 1991; Kelty et al., 1991; Koruga et al., 1993).

The presence of double bonds allows the addition of hydrogen, halogen, or cyclo-adducts onto C_{60} molecules (Birkett et al., 1992; Hirsch and Brettreich, 2005). The redox potentials of the hydrogen fullernes (e.g., $C_{60}H_x$) have been studied (Hirsch and Brettreich, 2005; Langa and Nierengarten, 2007), and a $C_{60}H_x$ electrode has been proposed for the fuel cell application (Pierson, 1993). On the other hand, the cycloaddition greatly extends C_{60} applications with various functional groups. Among these derivatives, C_{60}-amino acids (Langa and Nierengarten, 2007; Yang et al., 2007) attracts more attention than others due to its antioxidant feature. Other than antioxidation, certain C_{60} derivatives have the capability to absorb or react with free radicals (Krusic et al., 1991a; Pierson, 1993). Thus C_{60} has been commercially utilized by cosmetic manufactures, such as Vitamin C_{60} BioReserch Corp.(Halford, 2006; Pierson, 1993). In addition, a research team from University of California has synthesized a diamido diacid diphenyl fulleroid derivative, which is able to be functioning as an HIV enzyme inhibitor (Friedman et al., 1993; Sijbesma et al., 1993). Other biological applications of C_{60}, such as drug delivery (Langa and Nierengarten, 2007), DNA cleavage and radio-labeled tracer, have been reported (Jensen et al., 1996; Langa and Nierengarten, 2007). Furthermore, fullerene C_{60} is photo reactive (Arbogast et al., 1991; Sayes et al., 2005; Sayes et al., 2004; Yamakoshi et al., 1998; Yamakoshi et al., 2003), which makes it holds high potential for being used in photodynamic therapy (Jensen et al., 1996) and solar cell (Kamat et al., 2004).

2.2.3 Properties and Applications of CNTs

Similar to the C_{60} molecule, a CNT is a macro-molecule of carbon. But, unlike the spherical C_{60} molecule, the shape of CNTs is tubular with a diameter of few nanometers and a tube length of up to two millimeters (Pan et al., 1998). CNTs consist of ordered hexagon arrays with entirely sp^2 hybridized C-C bonds, which is similar to those in graphite (Iijima, 1991). Based on the architecture, there are two types of CNTs: single-wall nanotubes (SWNT), an analog of seamlessly rolling up one grapheme (a one-atom-thick graphite sheet), and multi-wall nanotubes (MWNT), consisting of multiple concentric SWNTs or a scroll of one sheet of graphite (Iijima, 1991).

In contrast to solid C_{60}, pristine CNTs are not soluble in most common organic solvents, such as toluene, carbon disulfide, and chloroform, owing to high molecular weights and hydrophobicity (Bahr et al., 2001; Bergin et al., 2008). The solubility of derivatized CNTs is not in the scope of this section. Ausman et al. (2000) studied five SWNT suspensions in "best solvents", such as N,N-dimethylformamide (DMF), N-methylpyrrolidone (NMP), and hexamethylphosphoramide, using spectroscopic methods and found that those good solvents for SWNT were Lewis bases with negligible hydrogen bond donation capability. While, Bahr et al. (2001) argued that the SWNT preparation method impacted its dissolution in solvents and found 1,2-dichlorobenzene exhibited higher solubility than DMF or NMP. The authors also pointed out the conceptual ambiguity between solution and suspension in terms of nanotube dissolution. Torrens (2006) theoretically discussed relations between solubility, salvation free energy, and partitioning coefficient for a system consisting SWNT and a solvent. Through calculations, the author confirmed the conclusions from Ausman et al. (2000) and concluded the good correlation between chiral vector and solubility. Furthermore, Bergin et al. (2008) demonstrated that SWNT was truly dissolved in NMP with equilibrium between significant population of pristine individual nanotubes and nanotube bundles, which was further supported by a calculated negative mixing enthalpy, and the maximum dispersibility was reached when the solvent surface energy was equal to that of graphitic surfaces. But the calculation implied that only nanobutes with diameters less than 1 nm or possessing a density higher than 1,700 kg/m^3 were truly soluble in DMP.

Due to the unique tubule structure, electrons in a CNT are confined in by the graphene layer, which leads to the extraordinary electronic properties. Depending on the nanotube structure, a carbon nanobute may exhibit metallic, semimetallic, or semiconductive features (Saito et al., 1992). When SWNT is conductive, the electrical current density can be as high as ca. 4 x 10^9 A/cm^2, which is much higher than that of a typical metal (e.g., copper) (Hong and Myung, 2007). When a SWNT or MWNT is exposed to a high electric field in vacuum, it is able to emit electrons, indicating that CNTs can be potentially used in flat panel displays and electron guns in microscopes (Rinzler et al., 1995). Other than electrical applications, carbon nanobutes can also be used in high tensile strength materials due to their excellent elastic behavior ((Yu et al., 2000), hydrogen storage devices (Cheng et al., 2001; Dillon et al., 1997) due to large surface area and pore volume, and high performance thermal management (Biercuk et al., 2002) due to their high thermal conductivity (e.g., >3,000 W/m·K for MWNT) at room temperature (Kim et al., 2001).

Particularly in environmental applications, CNTs can be used as sorbents to remove gas comtaminants (Kowalczyk and Holyst, 2008), arsenate, and chromium (Di et al., 2006; Peng et al., 2005) due to abundant pore volume. CNTs can also be used in nanofiltration processes with both high flux and high selectivity, when they are aligned (Hinds et al., 2004) or mounted on a porous ceramic support (Brady-Estevez et al., 2008). Since the electrical resistivity of CNTs sensitively changes when exposed to gases, such as NO_2, NH_3, and O_2 (Collins et al., 2000; Kong et al., 2000), at parts per million level, CNTs can additionally be used as novel sensors to monitor gases or chemicals in the environment.

2.3 Fullerenes in Water

2.3.1 Dispersion of C_{60} into Water

Due to the spherical shape, small size and capability of generating singlet oxygen under light irradiation, C_{60} holds high potential to benefit biological and medical applications. However, the extremely low solubility (e.g., 1.3 x 10^{-14} mg/L) of solid C_{60} in water (Heymann, 1996a; Ruoff et al., 1993a) largely hinders its application in these two fields. Hence, the dissolution or solubilization of C_{60} in water has attracted great attention in scientific community. Generally, there are three ways to significantly disperse C_{60} in water: (1) modify C_{60} chemically with hydrophilic groups (Arrais and Diana, 2003; Chiang et al., 1994; Dugan et al., 1997; Lamparth and Hirsch, 1994; Sawada et al., 2003; Yamago et al., 1995), (2) disperse C_{60} with the help of water-soluble surfactants (Bensasson et al., 1994; Guldi et al., 1994), polymers (Ungurenasu and Airinei, 2000; Yamakoshi et al., 1994), natural macromolecules (Andersson et al., 1992; Guldi et al., 1994; Litvinova et al., 2001) and humic substances (Terashima and Nagao, 2007), (3) form stable colloidal aggregates (Andrievsky et al., 1999; Andrievsky et al., 1995; Cheng et al., 2004; Deguchi et al., 2001; Fortner et al., 2005; McHedlov-Petrossyan et al., 1997; Scrivens et al., 1994; Terashima and Nagao, 2007). Unlike the first two methods, the third method delivers C_{60} into water without any stabilizer. Since the size of such aggregate is scaled up to nanometer or even micron, some properties of pristine C_{60}, such as hydrophobicity, are substantially changed (Andrievsky et al., 2002; Fortner et al., 2005). Recently, nanoscale C_{60} aggregates (termed as nC_{60}) have been proposed as the most environmental relevant form of C_{60} (Fortner et al., 2005; Lyon et al., 2006).

To date, five procedures have been proposed and tested to successfully produce stable colloidal nC_{60} in water. The first method was disclosed by Deguchi et al. (Deguchi et al., 2006). Solid C_{60} was placed into an agate mortar and repeat grinding was taken. Hand-ground C_{60} powder was immediately mixed with water and the combined solution was ultrasonicated to disperse C_{60} and filtered to remove large particles. Compared to the first method, the second method is simpler but more time consuming. In this method, solid C_{60} was rigorously mixed with water and gently heated to 40 ^{o}C over 2 to 4 weeks (Brant et al., 2006; Cheng et al., 2004; Lyon et al., 2006). The third method was discovered by Andrievsky et al. (Andrievsky et al., 1995), in which C_{60} was transferred from toluene into water during the proceses of toluene evaporation with ultrasonication. The fourth method was introduced by Scrivens and Tour (Scrivens et al., 1994), in which benzene was saturated with C_{60} by adding excess amount of C_{60} powder. The C_{60}-benzene mixture was sequentially diluted with THF, acetone and water with rapid stirring. The aqueous nC_{60} suspension was finally obtained by evaporating the organic solvents. Brant et al. (Brant et al., 2006) found that benzene can be replaced by toluene at the initial step. Similar to the fourth method, the fifth method was quite simple and less organic solvent was required (Deguchi et al., 2001a; Fortner et al., 2005). Briefly, nitrogen-sparged THF was saturated with excess amount of C_{60} powder (~ 25 mg C_{60} per L THF). An equal volume of water was added into stirred C_{60}-THF solution at 1 L/min. The combined solution was repeatedly evaporated and diluted with water after filtration. The resulting nC_{60} suspension was then concentrated or diluted to desired concentration for experimental use. An alternative procedure for the last method was using C_{60}^{-} as intermediate (Wei et al., 1997). C_{60}^{-} was produced by adding C_{60} powder and Al-Ni alloy or tin in a two phase system containing degassed NaOH and THF. The aqueous nC_{60} suspension was obtained by mixing THF-C_{60}^{-} with water. Unlike the nC_{60} produced with the fifth method, Wei et al. (1997) found that the aggregate in this “aqueous sol” was non-crystaline and its size was ca. 10 nm. The nC_{60} aggregate, prepared using the fifth method, is crystalline, which has been observed using TEM, and is composed of underivatized C_{60}, which has been confirmed by HPLC and ^{13}C NMR analysis. Such stable suspension is monodispersed and has a mean diameter of ca. 100 nm. Although the dependence of nC_{60} physicochemical properties on preparation methods has been reported, the fifth method has higher reproducibility than others. Thus, this method will be chosen to prepare nC_{60} suspensions for all experiments.

Despite of various preparation methods, the nC_{60} produced by all methods is stable for up to 18 months, and confirmed by electrophoresis experiments to possess negative charges. The origin of the negative charge is not completely understood. Two hypotheses have been proposed, nC_{60} produced using the third or fifth method (1) molecular C_{60} is partially oxidized by water to produce amphiphilic C_{60}, by which the pristine core is surrounded (Li et al., 1993); (2) C_{60} accepts electrons from water molecules (Andrievsky et al., 1995; Deguchi et al., 2001; Fortner et al., 2005). The latter is more convincing and supported by ^{13}C NMR result (Fortner et al., 2005).

2.3.2 Dispersion of CNTs into Water

Driven by requirements of in aqueous phase by various biomedical and biophysical applications, the dispersion of CNTs into water has been well studied. To develop a dispersion of CNTs, two interaction forces are required to be counterbalanced: the attractive van de Waal's force between nanotubes and the wetting force between hydrophobic nanotube surface and water. Generally, three strategies have been tested to be effectively disperse CNTs to water: ultrasonication, surface alteration through stabilizing agents (e.g., surfactant), and surface functionalization through chemical reactions.

Although ultrasonication is commonly used in most dispersing methods to initially debundle solid nanotubes, it can be independently used to prepare the CNT suspension. For example, Saleh et al. (2008) prepared MWNT suspensions by solely applying sonication. As the authors observed, ultrasonication significantly broke nanotube lengths from 6.6 μm down to 1.5 μm. However, the stability of this MWNT suspension was not clearly mentioned in this paper.

In the second strategy, various surfactants or polymers, such as polyvinyl pyrrolidone, polystyrene sulfonate, sodium dodecylbenzene sulfonate (NaDDBS), sodium dodecyl sulfate, and Triton X-100 (Chen et al., 2004; Islam et al., 2003; Matarredona et al., 2003; O'Connell et al., 2001; O'Connell et al., 2002), can be used to coat the nanotube surface to induce electrostatic or steric interactions (Hilding et al., 2003) between single tubes or bundles produced through either the pre-sonication or high shear flow. However, CNTs are not favorably dispersed in all surfactants. For example, poly(methyl methacrylate-co-ethyl acrylate), polyvinyl alcohol, polyethylene glycol, and polyallyl amine are observed to not successfully disperse SWNTs (Hilding et al., 2003; O'Connell et al., 2001). The dispersion of nanotubes in surfactant solutions is stable. Islam et al. (2003) observed that the suspension with a SWNT to NaDDBS wight ratio of 1:10 and SWNT concentration of 20 mg/mL remained in dispersed state at least 3 months. Other than surfactant or polymers, NOM (e.g., humic and fulvic acids) is capable of effectively disperse CNTs in water (Hyung et al., 2007; Wang et al., 2008).

The third strategy to disperse CNTs to water is covalently bonding function groups to tube surface and, in turn, impacting the interactions between the tube and water. The traditional surface functionlization is through acidic treatment with HNO3, H2SO4, or the mixture, through which –COOH and –OH are bonded onto nanotubes (Hilding et al., 2003; Kuznetsova et al., 2001; Zhao et al., 2002). Zhao et al. (2002) modified the traditional acidic treatment protocol by using concentrated H2SO4/30% H2O2 and adding a sonication process after reaction and found that the functionalized SWNT suspension was stable for at least a month. Other functional groups leading to dispersion of CNTs to water include some polymers (Sano et al., 2001b; Zhao et al., 2005), crown ethers (Kahn et al., 2002), glucosamines (Pompeo and Resasco, 2002), DNA (Hazani et al., 2003), and some proteins (Huang et al., 2002). However, the formation of covalent bonds with functional groups and acids used in preparation processes may damage pristine CNTs (Garg and Sinnott, 1998; Hilding et al., 2003; Monthioux et al., 2001;

Salzmann et al., 2007; Zhang et al., 2000), such as decreasing strength and increasing side-wall defects.

2.3.3 Toxicity of nC_{60}

The rapid growth of the fullerene market brings concern over potential environmental and heath effects of C_{60} on biological system (Colvin, 2003; Oberdorster et al., 2005). In parallel to the applications of nanosacle fullerenes in biological and medical engineering, toxicity testing of nC_{60} has been conducted intensively in the past few years. Based on exposure targets, these studies can be divided into two categories, eukaryotes and prokaryotes.

Studies on eukaryotes primarily focused on tissue obtained from fish, mouse, pig and human tissue. Oberdorster (Oberdorster, 2004a) found that nC_{60} showed adverse effects on a juvenile largemouth bass. As the fish was exposed to nC_{60} at a concentration 0.5 mg/L over a course of two days, lipid peroxidation in brain tissue and glutathione depletion in gills were observed. Another cytotoxicity study was also conducted on Daphnia magna (Oberdorster, 2004b; Oberdorster et al., 2005), and found the 48 hr LD_{50} of nC_{60} was 0.8 mg/L. Sayes et al. (2004) conducted cytotoxicity study on nC_{60} and observed its damage to membranes of human dermal fibroblasts and lever carcinoma cells. The 30 hour of exposure of nC_{60} at as low as 0.02 mg/L resulted in membrane leakage of these two cultured human cell lines. The superoxide anions generated in fullerene solutions (cell – free) was postulated to be responsible for the observed membrane damage. Further studies by Sayes et al. (2005) showed that nC_{60} with a concentration higher than 0.05 mg/L would be harmful for human dermal fibroblasts, liver carcinoma cells and neuronal human astrocytes. The presence of nC_{60} disrupted the cellular functions through lipid peroxidation. A notable result from this study was the prevention of lipid peroxidation by adding L-ascorbic acid, an antioxidant, which supported the hypothesis of membrane damage by lipid peroxidation. Haasch et al. (2005) conducted a nC_{60} cytotoxicity study within fathead minnow. The results indicated that nC_{60} was able to change gene expression and affect the metabolism of fathead minnows. A study conducted by Isakovic et al. (2006) showed that nC_{60} was toxic to cultured mouse fibrosarcoma, rat glioma and human glioma cells. Cellular membrane damage was caused by reactive oxygen species (ROS) generated by nC_{60}. However, in contrast to the discovery of nC_{60} cytotoxicity to various cells, Scrivens and Tour (1994) found that nC_{60} was not toxic to human keratinocytes using a ^{14}C tracing technology. Similarly, Gharbi et al. (2005) found that nC_{60} showed no acute toxicity to Swiss mice, and even exhibited protection to rat liver. Henry et al. (2007) conducted a study on larval zebrafish to evaluate the toxicity of nC_{60}. They found that nC_{60} itself showed no toxicity, while the THF residual and γ-butyrolactone (GBL) were responsible for the toxicity to the fish. Furthermore, in a study to compare cytotoxicity of various nanomaterials, Jia and co-workers (2005) found nC_{60} was not toxic to alveolar macrophage, which functioned as a defense toward particle invasion to pig lung.

The cytotoxicity study of nC_{60} on prokaryotes has mainly focused on bacteria. Lyon et al. (2005) conducted a cytotoxicity study on *Escherichia coli* and *Bacillus subtilis* and found that nC_{60} at concentrations 0.5 and 1.5 mg/L, was able to inhibit their activity, respectively. Fortner et al. (2005) reported that the growth of *Bacillus subtilis* was inhibited by nC_{60} at a concentration of 0.4 mg/L. A subsequent study by Lyon et al. (2006) indicated that growth of *Bacillus subtilis* was inhibited by nC_{60} regardless of preparation method described previously. In contrast, Tong et al. (2007) observed that the presence of nC_{60} in Drummer soil did not affect any activity of microbial community based on CO_2 production and the activity of four key enzymes (dehydrogenase, phosphatase, β-glucosidase and urease).

2.3.4 Toxicity of suspended CNTs

As the commercial production and application implementations of CNTs are progressing, the risk assessment on them, especially health related subjects, has become more and more important. Similar to nC_{60}, the toxicity of CNTs is controversial in general. But only the toxicity of CNTs in suspension is reviewed here.

The cytotoxicity of CNTs has been recently reviewed by Hussain et al. (2009). Interestingly, all studies are toward to one conclusion: CNTs, either SWNT or MWNT, suspended in water or culture media are toxic to human cells, which include embryo kidney cells (Cui et al., 2005), lung cell line (Davoren et al., 2007), skin and lung fibroblast (Ding et al., 2005), and muscle cells (Raja et al., 2007). Majority of thses nanotube suspensions are prepared through sonication. The inhibition of cell activities has been related to the generation of reactive oxygen species (Garza et al., 2008; Hussain et al., 2009).

Contrast to the cytotoxical studies, the studies on nanotube antimicrobial activities can only be tracked back to two years ago. Liu et al. (2007) conducted the first experiment to investigate the effects of a type of Cu-coated CNTs on E. coli and S. aureus and found the high bactericidal rate (Arias and Yang, 2009). Kang et al. (2007) studied interactions between E.coli and purified SWNTs (not functionalized or coated) and the scanning electron microscopy (SEM) images clearly showed morphological changes, which provided the direct evidence at the first time for cell membrane damages caused by direct contact with nanotubes. Another study (Kang et al., 2008) by the same research group revealed that both purified SWNTs and MWNTs were toxic to E. coli and SWNT exhibited more impact than MWNT. The authors also discovered that the size (diameter) of nanotubes played a key role in their antimicrobial activity and their successive studies on gene expressions implied that oxidative stress was a possible count to the nanotube toxicity mechanisms. Kang et al. (2008) further studied the toxicity of functionalized nanotubes to E. coli and concluded that uncapped, debundled, short and dispersed nanotubes enhanced opportunities of direct contact, which, in turn, increased toxicity. However, the latest study (Arias and Yang, 2009) on the toxicity of functionalized (by –OH or -COOH) CNTs argued that MWNTs were not toxic to Grem-negative/-positive bacteria when nanotube concentration was lower than 500 mg/L. The authors further pointed out that solution buffer and nanotube concentration contributed to SWNT toxicity.

2.3.5 Potential Exposure Pathways

With the rapid expansion of fullerene production, the potential for exposure to carbon nanoparticles exists at any stage in the lifecycle chain from manufacture through consumption and disposal. The likely exposure to nC_{60} and CNTs may take place through the following pathways:

(1) Ingestion. Suspension of nC_{60} are stable in water under various solution conditions (Fortner et al., 2005). The possibility exists that the water containing nC_{60} will be consumed humans. Another possibility is the persistent bioaccumulation of nC_{60} in the food chain (Oberdorster et al., 2005; Wiesner et al., 2006). In addition, the application of water-soluble fullerenes in pharmaceuticals enhances the possibility of exposure to nC_{60} from taking medications (Bush, 2003) and photodynamic therapy (Jensen et al., 1996; Yamakoshi et al., 2003). Although the CNT suspensions are not as stable as nC_{60}, new dispersion method has been developing. Thus, it is still possible for dispersed CNTs to be ingested.

(2) Dermal or skin uptakes. Based on a search of the Nanotechnology Consumer Products Inventory, four fullerene manufactures are listed including Radical Sponge, Yonex, Zelens and Dr. Brandt. Among the six products, five are cosmetics and one is a tennis racquet. Use of these products unavoidably leads

to direct skin contact. It should also be recognized that workers in manufacture plants may also be exposed to fullerenes through dermal contact. For CNTs, the exposure through dermal uptake is in doubt, while through skin ingestion seems to be not possible since the length of majority CNTs exceeds 100 nm (Warheit et al., 2007).

(3) Inhalation. Recent studies have shown that fullerene C_{60} can form in combustion processes (Howard et al., 1992; Oberdorster et al., 2005; Utsunomiya et al., 2002). Thus, the fullerenes produced from power plants or fires, may reach humans and animals during respiration. The inhalation of CNTs may take place when nanotubes are released from products to air like asbestos (Muller et al., 2005; Poland et al., 2008; Service, 2004). Alternatively, exposure to fullerenes may occur through inhalation of ultra fine particles with associated fullerenes (Colvin, 2003).

Industrial scale production of nanoscale fullerenes will inevitably lead to their release into aqueous systems during manufacture, transportation, application, and disposal. Fullerene C_{60} produced through combustion in power plants and wildfires and short CNTs released from natural gas combustion (Murr et al., 2004), coating, and products will eventually fall down to surface water bodies and form stable suspensions with the help of NOM. The terrestrial C_{60}, formed naturally during geological events, will produce nC_{60} through long term contact with water (Buseck, 2002; Chijiwa et al., 1999; Heymann et al., 1996). The fullerenes used in pharmaceuticals and personal care products (e.g., cometics) will enter waste water treatment plants, and eventually aqueous systems. Ultimately, the entire ecosystem may be exposed to fullerene nanoparticles through cycling among the atmosphere, water and subsurface systems (Colvin, 2003).

2.4 Fate and Transport of Fullerene Nanoparticles

2.4.1 Nanoparticle Aggregation

Very recently, several papers have been published to address the stability of nC_{60} under various solution conditions. The methods used to assess nC_{60} stability include the long-time settling in dark (Brant et al., 2005a; Chen and Elimelech, 2006; Deguchi et al., 2001; Fortner et al., 2005) and aggregation kinetic analysis (Chen and Elimelech, 2006; Chen and Elimelech, 2007). In absence of background electrolyte, the hydrodynamic diameter of nC_{60} will not change significantly for periods up to 6 months (Chen and Elimelech, 2006). Interestingly, if salts, such as NaCl and $CaCl_2$, are added, precipitation can occur under certain electrolyte concentration, and is dependent upon the ionic composition. Such agglomeration in the presence of salt suggests nC_{60} stability originates from the electrostatic repulsion (Brant et al., 2005a; Chen and Elimelech, 2006; Deguchi et al., 2001a; Fortner et al., 2005). Due to the negatively charge on C_{60} aggregate surface, the interaction energy based on DLVO theory has been used to explain the stability and aggregation behavior of nC_{60} as a function of ionic strength and composition. The trend of increasing C_{60} diameter with ionic strength is consistent with well with DLVO theory, where the secondary energy minimum is suggested to be responsible for observed agglomeration behavior (Brant et al., 2005a). As ionic strength increases the thickness of the electrical double layer (EDL) of an nC_{60} aggregate is compressed, allowing more aggregates to approach each other (Brant et al., 2005a; Brant et al., 2005b). In terms of ionic species, the presence of multivalent ions, such as Ca^{2+} and Mg^{2+}, stronger surface charge screening, coupled with the formation of surface complexation, largely reduces zeta potential of nC_{60}, which results in a larger aggregate size. On the other hand, Chen and Elimelech (Chen and Elimelech, 2006; Chen and Elimelech, 2007) conducted the aggregation kinetic studies based on real-time observation of nC_{60} diameter change with time. Plots of attachment efficiency (inverse stability ratio) vs. electrolyte concentration exhibited reaction-limited (repulsion dominated) and diffusion-limit (attraction dominated) regions. The nC_{60} critical coagulation concentration (CCC) was 120 mM for NaCl and 4.8 mM for $CaCl_2$. The attachment coefficients at various NaCl concentrations ranging from 0.06 to 0.35 M match the prediction from DLVO theory, if the Harmark constant is chose to be 6.7×10^{-21} J (Chen and Elimelech, 2006). Using a similar approach, nC_{60} aggregation kinetics in presence of humic acids is assessed, although the structure characteristics of nC_{60} (with humic acids) are unknown. The data for electrophoretic mobility and kinetics showed that the adsorption of humic acid to nC_{60} was very rapid and the presence of humic acid even at the concentration level of 1 mg C/L largely reduced nC_{60} aggregate growth rate. Such a reduction in aggregate growth rate was attributed to nC_{60} stabilization due to steric repulsion (Chen and Elimelech, 2006).

The aggregation behavior of suspended CNTs has been studied since 2001 through UV absorbance (Sano et al., 2001a), static light scattering (SLS) (Chen et al., 2004), photoemission (Niyogi et al., 2007), and pseudo-dynamic light scattering (Saleh et al., 2008). Sano et al. (2001a) studied suspensions of acid-treated SWNT using a UV and found that the CCC was described by Schulze-Hardy rule, a simple solid sphere model with only VDW and EDL interactions, in which CCC was proportional to z^{-6}, where z was the electrolyte valency. Chen et al. (2004) employed multi-angle SLS to investigate the aggregation status of pristine SWNTs in Triton X-100 and acid-treated SWNTs in water or Triton X-100 and found those aggregates were fractal-like. When pristine SWNTs were well dispersed in 1% sodium dodecylsulfate, Niyogi et al. (2007) observed light emission of individual nanotubes and found that salts were able to control the aggregation status, reflected by emission intensity pattern. The aggregation behavior of pristine CNTs in suspension was further studied by Saleh et al. (2008) using a SLS instrument at only one angle. Saleh and co-authors found that the plot of attachment efficiency vs. electrolyte concentration exhibited slow and fast aggregation kinetic regions, similar to those of nC_{60} system. The authors pointed out that this feature of MWNT aggregation behaviors with electrolyte concentration indicated that the MWNT suspension was stabilized by DLVO type (electrostatic) interactions. With addition of SRHA to the suspension, lower attachment efficiencies were obtained and such a stability enhancement was attributed to steric repulsions.

DLVO theory is commonly used to predict the stability of colloids by estimating the interactions between colloidal particles. The surface interaction forces between colloids mainly include VDW, EDL, Lewis acid-base and steric forces. Basically, the total interaction energy calculated in DLVO theory is the addition of the contributions from VDW and EDL forces, while in the extended DLVO theory acid-base and steric interactions are also considered.

The VDW interactions are apolar, electrodynamic interactions resulting from randomly oriented dipole-dipole interactions, randomly oriented dipole-induced dipole interactions, and fluctuating dipole-induced dipole interactions. In most cases VDW interactions between two colloid particles immersed in water are attractive. The magnitude of VDW forces depends on the separation distance between particles, the size of the particles, and the Hamaker constant. Hamaker constant is a material parameter and originated from van der Waal's potential integeral over two spheres. In addition, VDW forces are long-range forces and can be effective at large separation distances (e.g., greater than 10 nm). However, at separations greater than ca. 10 nm in free space, retardation effects, largely due to the finite time of propagation (Gregory, 1981), come into play and need to be considered. For nC_{60} aggregates, the VDW interaction energy can be calculated as follows (Gregory, 1981):

$$E_V = -\frac{Ar}{12d}[1 - \frac{bd}{\gamma}\ln(1+\frac{\gamma}{bd})] \tag{2.1}$$

where A is the Hamaker constant and 6.7×10^{-21} J (Chen and Elimelech, 2006) is used for nC_{60}, b is a constant with the value of 5.32, r is the nanoparticle radius, d is the surface to surface distance and γ is the characteristic wavelength of the interaction, assumed to be 100 nm (Schenkel and Kitchener, 1960).

The EDL interactions are Coulombic interactions between charged entities, and can be repulsive or attractive, depending upon the sign and value of particle surface potential. The magnitude of EDL forces is a function of the separation distance, the diameter of particles, the surface potential of particles, electrolyte concentration, and counterion valance. The surface potential is situated at the precise particle-liquid interface and is not directly measurable, but can be derived from the zeta potential, which is measured at the slipping plane by electrokinetic methods such as electrophoresis. For rigid particles, the surface potential is often approximated as the zeta potential by converting electrophoretic mobility (μ_e) using the Henry's equation (Deshiikan and Papadopoulos, 1998):

$$\mu_e = \frac{2\varepsilon\xi f(\kappa r)}{3\mu} \tag{2.2}$$

where ε is the dielectric constant, ξ is the zeta potential, $f(\kappa r)$ is the Henry's function, μ is the dynamic viscosity, and κ is Debye parameter. The Debeye parameter is defined as:

$$\kappa^2 = \frac{F^2 \sum_i c_i z_i^2}{\varepsilon RT} \tag{2.3}$$

where F is the Faraday constant, c in the molar concentration, z is the valence of the ion, and R is the ideal gas constant. The Henry's function can be expressed as (Deshiikan and

Papadopoulos, 1998):

$$f(\kappa r) = 1.000 \qquad (\kappa r \leq 0.1) \qquad (2.4)$$

$$\begin{aligned} f(\kappa r) = 1.0275157930 + 0.0857619670\log(\kappa r) + \\ 0.1058385007(\log(\kappa r))^2 + 0.0464011331(\log(\kappa r))^3 \end{aligned} \qquad (0.1 < \kappa r \leq 3.55) \qquad (2.5)$$

$$\begin{aligned} f(\kappa r) = 1.0622739775 - 0.0740929226\log(\kappa r) + \\ 0.3832612499(\log(\kappa r))^2 - 0.1256407214(\log(\kappa r))^3 \end{aligned} \qquad (3.55 < \kappa r \leq 35.5) \qquad (2.6)$$

$$\begin{aligned} f(\kappa r) = 0.7682190386 + 0.6988704751\log(\kappa r) \\ 0.2263212573(\log(\kappa r))^2 + 0.0248691121(\log(\kappa r))^3 \end{aligned} \qquad (35.5 < \kappa r \leq 1000) \qquad (2.7)$$

$$f(\kappa r) = 1.500 \qquad (\kappa a > 1000) \qquad (2.8)$$

Once the value of the zeta potential is computed, the EDL interaction energy can be calculated from the equation of Gregory (Gregory, 1975):

$$E_{edl} = \frac{64\pi nkTr}{\kappa^2}\tanh^2\left(\frac{ze\zeta}{4k_bT}\right)\exp(-\kappa d) \qquad (2.9)$$

where n is the number of cations, k_b is Boltzmann constant, T is the absolute temperature, z is the charge number, and e is the electron charge. In contrast to the VDW interactions, which are generally not affected by solution ionic strength, the EDLs are strongly dependent upon ionic strength and composition. For example, an increase in ionic strength strongly reduces the zeta potential, and thereby the double layer interaction energy.

2.4.2 Transport and Filtration of Fullerene Nanoparticles

The transport and filtration of colloidal particles, such as latex microspheres, have been extensively studied. However, it is questionable to directly apply the theories developed for colloid to nanoparticles since the retention behavior of particles may dramatically change when the sizes are in nanometer level. To date, only a few column studies have been conducted to study the transport of fullerene nanoparticles in water-saturated porous media (Brant et al., 2005a; Cheng et al., 2005; Espinasse et al., 2007; Jaisi et al., 2008; Lecoanet and Wiesner, 2004; Lecoanet et al., 2004). The transport experiments for nC_{60} aggregates were conducted in either 40-50 mesh glass beads (GB) or a natural soil. The resulting steady-state effluent concentration data were interpreted using clean-bed filtration theory (Yao et al., 1971), where the attachment rate coefficient (α) was calculated from the plateau value of C/C_0 using Eq. 2.10. For an nC_{60} suspension (168-nm dia., C_0 = 10 mg/L) delivered at pore-water velocities (v_p) of ca. 82 and 273 m/d, Lecoanet et al. (2004) obtained steady-state relative effluent concentrations (C/C_0) of 0.56 at an ionic strength of 10 mM NaCl. A value of 0.3 for α was obtained using Eq. 2.10, while a bed length (L) of 10 cm was estimated to achieve a 3-log reduction (99.9% removal) in the influent concentration. At the higher flow rate (v_p = 273 m/d) an unusual drop in effluent concentration was observed after introducing ca. 1.75 pore volumes (PV) of nC_{60} solution, which was attributed to an "affinity transition" that yielded enhanced particle retention (Lecoanet and Wiesner, 2004). However, the flow rate employed in these experiments yields a Reynolds number (Re) of 0.53 ($\mathrm{Re} = \rho_l U d_c / \mu$, where ρ_l is the liquid density, U is the Darcy velocity, and d_c is the mean diameter of sand grain diameter or collector particle), which approaches the limit of laminar flow in porous media (Re < 1-10) (Freeze and Cherry, 1979). Following a similar analytical approach (Eq. 2.10), Espinasse et al. (2007) evaluated the effects of organic macromolecules (tannic acid at 1 mg/L and alginate at 2 mg/L), electrolyte composition ($CaCl_2$ and $MgCl_2$ at 0.01 M; $NaNO_3$ and Na_2SO_4 at 0.01 and 0.1 M; and NaCl at various concentration ranging from 0.01 to 0.6 M), and nC_{60} preparation methods (the benzene-serial dilution and THF methods). The comparison of various α values revealed that transport of nC_{60} was enhanced at low ionic strengths and in the presence of tannic acid, and reduced in the presence of Ca^{2+}, Mg^{2+} and alginate. In addition, the transport of nC_{60} prepared by these two methods differed significantly. Cheng et al. (2005) conducted the nC_{60} transport experiments in Lula soil, rather than GB. Using the similar analytical approach (Eq. 2.10), the authors obtained the values of α ranging from 0.005 to 0.01 for an nC_{60} suspension (100 nm dia., C_0 = 48 mg/L) conditioned with 10 mM NaCl and 10 mM NaN_3 applied at pore-water velocities ranging from 0.86 to 28.3 m/d. Based on Eq. 2.10, bed lengths of 31 to 132 cm would be required to achieve 99.9% of nC_{60} removal. At the lowest flow rate (v_p = 0.86 m/d), Cheng et al. (2005) noted that α approached unity (i.e., all collision result in attachment) after 57 PVs of continuous injection, which was attributed to “filter ripening”. At the same time of nC_{60} transport study, Lecoanet and Wiesner (2004) conducted transport experiments for surfactant modified SWNT (4.5 or 10 mg/L, average length 130 nm and mean diameter 21 nm by DLS) in glass beads at two pore water velocities, ca. 82 and 273 m/d. At the slow flow rate, a bed length (*L*) of 10 m (Lecoanet et al., 2004) was estimated to achieve a 3-log reduction (99.9% removal) in the influent concentration using Eq. 2.10. At the higher flow rate, a dip was observed in SWNT breakthrough curves (BTCs) between 1 and 2 PVs, which was explained using filter ripening. In a pretty recent study, Jaisi et al. (2008) conducted column experiments to investigate effects of electrolyte composition (K^+ and Ca^{2+}) and concentration (0.1 to 55 mM for K^+ and 1 mM for Ca^{2+}) on transport of SWNT in water-saturated quartz sands. The SWNTs (87 mg/L) were functionalized with carboxyl groups and dispersed into water by ultrasonication. Based on the steady-state relative effluent concentrations (C/C_0), α was then calculated by normalizing the obtained attachment rate (k_{att}) to that under favorable condition, where α was equal to 1. Jaisi and co-authors found that α increased with ionic strength, indicating the retention of SWNT followed clean-bed filtration model (physicochemical filtration). Additionally, the authors observed SWNT retention at very low ionic strength (e.g., DI water) and concluded straining was another contributor to the SWNT retention. However, retention profile data were not reported for any of the nanoparticle transport experiments conducted to date.

An important feature of subsurface aquatic system is the ubiquitous presence of natural organic matters (NOM). Thus, effects of NOM must be considered in order to mimic the real nC_{60} transport conditions. As stated above, the presence of NOM is capable to increase the stability of nC_{60} and its potential to enhance the mobility of nC_{60} in porous media has been proposed. However, the direct observation of enhanced mobility has not been reported. Regarding to transport scenario, effects of NOM on transports of colloidal hematite (Amirbahman and Olson, 1993; Kretzschmar and Sticher, 1997), latex microspheres (Amirbahman and Olson, 1995; Davis et al., 2002; Franchi and

O'Melia, 2003), and bacteria (Johnson and Logan, 1996) have been extensively studied. Generally, adsorption of NOM onto particles negatively increases colloid surface charges. For positively charged microspheres, 1 mg C/L of NOM is enough to inverse surface charge. DLS measurements reveal that the thickness of adsorbed NOM layer is statistically less than 10% of particle radius (Amirbahman and Olson, 1995; Franchi and O'Melia, 2003). Promotion of colloidal particle transport qualitatively agrees with the increase of electrostatic repulsion. Franchi and O’Melia (Franchi and O'Melia, 2003) conducted batch sorption and column experiments to investigate the deposition of sulfate latex microspheres (98 nm) to spherical soda-lime GB under various ionic strengths (NaCl) in presence of 1 mg C/L of humic acids. Based on DLVO calculations, authors concluded that, at lower ionic strength (<10 mM), secondary minimum controlled attachment process, while at higher ionic strength, both first and secondary minima contributed to microsphere retention. Davis et al. (Davis et al., 2002) took the effect of Ca^{2+} into account in studying effects of humic acid on colloid transport in porous media. In the presence of Ca^{2+} at 10 mM electrophoretic mobilities of microspheres were not dependent on humic acid concentration. Thus, the enhancement of microsphere transport in presence of both Ca^{2+} and humic acid was attributed to steric repulsion induced by Ca^{2+}. Since nC_{60} is totally different with microspheres, conclusions obtained from colloid transport studies may not be directly applied to nC_{60} aggregates.

2.4.3 Clean-bed Filtration Theory

Two basic conceptual approaches have been employed to describe particle filtration, based on a mass balance approach and trajectory theory. In the former, mass balance calculations are used to describe particle removal by an isolated sphere or collector, with the inherent assumption that a packed bed or porous medium consists of a collection of spherical particles. Yao et al. (1971) presented the following steady-state mass balance filtration equation:

$$\frac{C}{C_0} = \exp\left[-\frac{3}{2}\frac{(1-\theta_w)}{d_c}\alpha\eta_0 L\right] \tag{2.10}$$

where C_0 is the influent particle concentration, η_0 is the theoretical (maximum) collector efficiency, θ_w is the volumetric water content of porous media and L is the length of the bed or column. The above equation may also be expressed as a clean-bed filtration coefficient:

$$\frac{C}{C_0} = \exp(-\lambda L) \tag{2.11}$$

where $\lambda = \frac{3}{2}\frac{(1-\theta_w)}{d_c}\alpha\eta_0$. As colloidal particles migrate through a porous medium several mechanisms may contribute to particle retention and deposition, including straining (sieving), sedimentation, diffusion, inertial impaction, and hydrodynamic forces. In most water treatment applications, it is generally accepted that diffusion (Brownian motion) and sedimentation (gravitational settling) are the predominant mechanisms responsible for particle retention (Amirtharajah, 1988). Trajectory theory was initially developed to describe the single-collector efficiency, η_0, as a function of particle diffusion, interception and sedimentation, where $\eta_0 = \eta_D + \eta_I + \eta_G$ (Yao et al., 1971). Here, η_D, η_I and η_G are the collector efficiencies for diffusion, interception and gravity (sedimentation):

$$\eta_D = 4(\frac{Ud_c}{D_p})^{-2/3} = 4N_{P_e}^{-2/3} \qquad \eta_I = \frac{3}{2}(\frac{d_p}{d_c})^2 = 1.5N_R^2 \qquad \eta_G = \frac{(\rho_p - \rho_l)gd_p^2}{18\mu U} = N_G \quad (2.12)$$

Here, D_p is the bulk particle diffusion coefficient, d_p is the colloid particle diameter, ρ_p is the particle density, and g is the gravitational constant. To simplify the expressions, three dimensionless terms are incorporated: N_{Pe} (Peclet Number), N_R (Interception Number), and N_G (Gravitation Number). The diffusion term given above, η_D, was refined by Yao et al. (1971) to account for collisions generated by diffusion, using the Happel (1958) flow field factor, $A_s = 2(1-p^5)/(2-3p+3p^5-2p^6)$, where $p = (1-\theta_w)^{1/3}$. This model was subsequently refined by Rajagopalan and Tien (1976) so that all terms represent fluid flows in concentric spherical space surrounding the collector particles.

$$\eta_0 = 4A_s^{1/3}N_{P_e}^{-2/3} + A_s N_{L_o}^{1/8} N_R^{15/8} + 0.00338 A_s N_G^{6/5} N_R^{-2/5} \qquad (2.13)$$

where N_{Lo} represents the contribution of van der Waals attractive forces to particle removal and is defined as $N_{Lo} = 4A/9\pi d_p U$. As noted by Logan et al. (1995) this form of the trajectory theory equation is consistent with the mass balance filtration equation presented above. Using the typical values, 1.05 g/cm^3, 0.71 mm, and 0.78 cm/min for particle density, medium size, and pore-water velocity, respectively, the Rajagopalan and Tien trajectory model (corrected) predicted that the minimum theoretical collector efficiency occurs between particle diameters of 1 and 2 μm. For particles with diameters greater than

2 μm, removal efficiency increase rapidly with particle size, indicative of sedimentation and interception mechanisms. For nanoparticles (diameter < 1 μm), the theoretical collector efficiency increases with decreasing particle diameter, which results primarily from the contribution of diffusion to particle deposition.

In a 1-D porous media system, such as column packed with soil, the transport of colloidal particle is dominated by advection, dispersion, attachment and possible reaction. The mass balance for such a system may be expressed as:

$$\frac{\partial(\theta_w C)}{\partial t} = -(J_H + J_{adv}) - \rho_b \frac{\partial S}{\partial t} + \sum Rx \tag{2.14}$$

where, *S* refers to the colloid concentration in solid phase, *t* is the traveling time, ρ_b is the bulk density of the packed porous media, *Rx* is the general term representing flux caused by reaction, and J_H and J_{adv} are the fluxes due to hydrodynamic dispersion and advection, respectively. Assuming conditions of homogeneity, laminar flow, and negligible particle release or decay during the course of transport, Eq. 2.14 can be written as (Tufenkji et al., 2003):

$$\frac{\partial C}{\partial t} + \frac{\rho_b}{\theta_w}\frac{\partial S}{\partial t} = D_H \frac{\partial^2 C}{\partial x^2} - v_p \frac{\partial C}{\partial x} \tag{2.15}$$

where D_H is the hydrodynamic dispersion coefficient, v_p is the pore velocity and *x* is the traveling distance at time *t*. In the conditions where blocking and ripening are not significant and the detachment process is negligible, the term $\frac{\rho_b}{\theta_w}\frac{\partial S}{\partial t}$ can be expressed as (Tufenkji et al., 2003)

$$\frac{\rho_b}{\theta_w}\frac{\partial S}{\partial t} = k_{att} C \tag{2.16}$$

where k_{att} is attachment rate and equal to λv_p. For laboratory column tests, the pulse injection is commonly used. Under such circumstance, the initial and boundary conditions are defined as:

$$C(x,0) = 0$$

$$C(0,t) = \begin{cases} C_0 & 0 < t \le t_0 \\ 0 & t > t_0 \end{cases}$$

$$\frac{\partial C(\infty,t)}{\partial x} = 0$$

Where t_0 is the injection duration. The colloid concentrations in aqueous and solid phases can be analytically solved as (Tufenkji et al., 2003)

$$C(x,t) = \begin{cases} C_A(x,t) = \frac{C_0}{2}[\exp(\frac{v_p - \sqrt{v_p^2 + 4k_{att}D_H}}{2D_H})erfc(\frac{v_p - \sqrt{v_p^2 + 4k_{att}D_H}}{2\sqrt{D_H t}}) + \\ \qquad \exp(\frac{v_p + \sqrt{v_p^2 + 4k_{att}D_H}}{2D_H})erfc(\frac{v_p + \sqrt{v_p^2 + 4k_{att}D_H}}{2\sqrt{D_H t}})] & 0 < t \le t_0 \\ C_A(x,t) - C_A(x,t-t_0) & t > t_0 \end{cases} \tag{2.17}$$

$$S(x,t) = \frac{\theta_w}{\rho_b} k_{att} \int_0^t C(x,t)dt \tag{2.18}$$

For the even simpler case, where the filtration process reaches steady-state and the hydrodynamic dispersion is not significant, the solutions for colloid concentrations in aqueous and solid phases are:

$$S(x) = \frac{t_0 \theta_w k_{att} C_0}{\rho_b} \exp(-\frac{k_{att}}{v} x) \tag{2.19}$$

which predicts a symmetrical effluent BTC and exponentially-decaying retention profile for retained particles with distance.

The mathematical equations and underlying theories described above prodiede a framework from which to interpret and predict the transport of manufactured nanoparticles in water-saturated porous media. In effect, the basic principles developed for the removal of naturally occurring colloidal particles from drinking water have been extended to nanoparticles without any modification (Cheng et al., 2005; Espinasse et al., 2007; Jaisi et al., 2008; Lecoanet and Wiesner, 2004; Lecoanet et al., 2004). While this is a reasonable first approach, almost no research has been undertaken to critically evaluate the applicability of clean-bed filtration theory to nanoparticle transport and retention.

2.4.4 Nanoparticle Retention

The retention mechanisms of colloidal particles in porous media have been extensively studied due to the needs for controlling or predicting colloid movements in subsurface. Initially, the clean-bed filtration theory has been successfully used to interpret data from laboratory and field experiments (Harvey and Garabedian, 1991; Yao et al., 1971). However, recent column studies have shown that the clean-bed filtration theory is not adequate for conditions where the repulsive DLVO energy barrier is present (Bradford et al., 2002; Bradford et al., 2003; Bradford et al., 2009; Li et al., 2004;

Tufenkji et al., 2003). In those conditions, the retention profiles of negatively charged latex microspheres or certain bacteria deviate from the predictions by clean-bed filtration theory, with the distinct hypoexponential or nonmonotonic feature (Figure 2.2), although BTCs are able to be fitted very well. Subsequent studies on such deviations have revealed that the retention of particles in unfavorable conditions (presence of repulsive DLVO energy barrier) is mainly controlled by not only physicochemical interactions (e.g., DLVO), but also hydrodynamics (e.g., drag) (Bergendahl and Grasso, 2000; Li et al., 2005), and physical straining (Bradford et al., 2006). Compared to colloidal particles (e.g., latex microspheres), almost all fullerene nanoparticles (e.g., nC_{60} and MWNTs) suspended in water possess negative surface charges (Fortner et al., 2005; Saleh et al., 2008), indicating the retention of fullerene nanoparticles only occur in unfavorable conditions. It has been reported that physicochemical interactions and straining

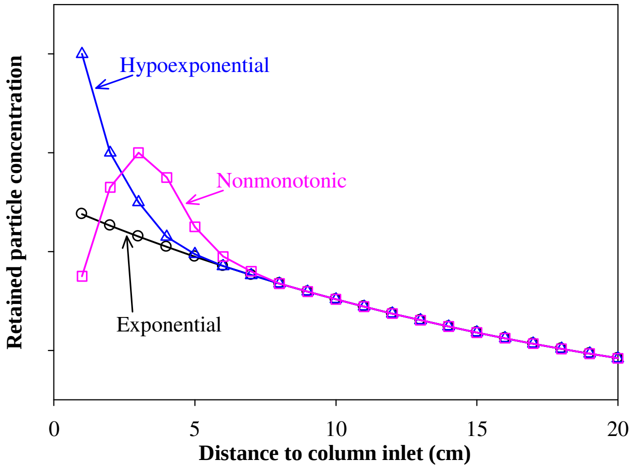

Figure 2.2: Schematic retention profiles of colloidal particles in porous media under unfavorable conditions.

possibly contribute to nanoparticle retention in water-saturated porous media (Brant et al., 2005a; Jaisi et al., 2008). But to my knowledge, no work has been done to address the effects of hydrodynamic forces on nanoparticle transport and retention.

Physicochemical interactions, such as VDW and EDL interactions, are assumed as the primary mechanism for colloidal particle retention in the clean-bed filtration model (Bradford et al., 2009). The DLVO theory is commonly used to calculate the interactions between colloidal particles and soil grains, where the particle-solid system is treated as the sphere-plate model (Tufenkji and Elimelech, 2004). Similar to that in particle-particle system, the total interaction energy in particle-solid system include attractive VDW and repulsive EDL interactions. For VDW interaction energy, Lecoanet and Wiesner (2004) calculated the first Hamaker constant for the fullerene-silica-water system and found it to be 2.76×10^{-20} J. Chen and Elimelech (2006) adopted equations from Gregory (1981) for VDW and Gregory (1975) for EDL calculations in studying the deposition of nC_{60} onto silica surface. However, Guzman et al. (2006) realized that the classical DLVO calculations were based on Derjaguin approximation, which was not valid for nanoparticles. Then the authors proposed to use a surface element integration technique to avoid the assumptions in Derjaguin approximation.

A typical DLVO interaction energy profile of a nanoparticle-water-solid system under unfavorable conditions consists of an energy barrier, the first energy minimum, and the second energy minimum, as illustrated in Figure 2.3. The colloid transport studies have revealed that colloidal particles may be retained on solid surface by the second energy minimum or the first energy minimum by bypassing the energy (Tufenkji and Elimelech, 2004). The retention of particles by the second energy minimum is reversible while the particles held by the first energy minimum can not be released when the ionic strength decreases. Although failures of DLVO theory are observed, a lot of studies have demonstrated that the second energy minimum plays an important role on the retention of colloids at nanometer scale (e.g., 50-200 nm latex microspheres) in water-saturated porous media. Litton and Olson (1996) conducted microsphere (248 nm) detachment experiments and observed 80% of retained particles were released when the column was flushed with an anionic surfactant (e.g., sodium dodecyl sulfate) solution, which provided the direct evidence for the significant particle retention within the second energy minimum. Hahn et al. (2004) conducted experiments to investigate retention and release of submicron colloids (e.g., 72 nm latex and 80 nm hematite) and observed strong detachment when the ionic strength was decrease. A further study by Pelley and Tufenkji (2008) observed the increase of particle attachment kinetics with particle size (50 -1,500 nm) and concluded that larger particles (e.g., 1,500 nm) were held by the second energy minimum while both the first and second energy minimum contributed to the retention of the smallest particles (e.g., 50 nm). Although the second energy minimum has not been correlated to the retention of nC_{60} in porous media, the detachment experiments conducted by Jaisi et al. (2008) indicated that the second energy minimum contributed to the retention of SWNT in quartz sands.

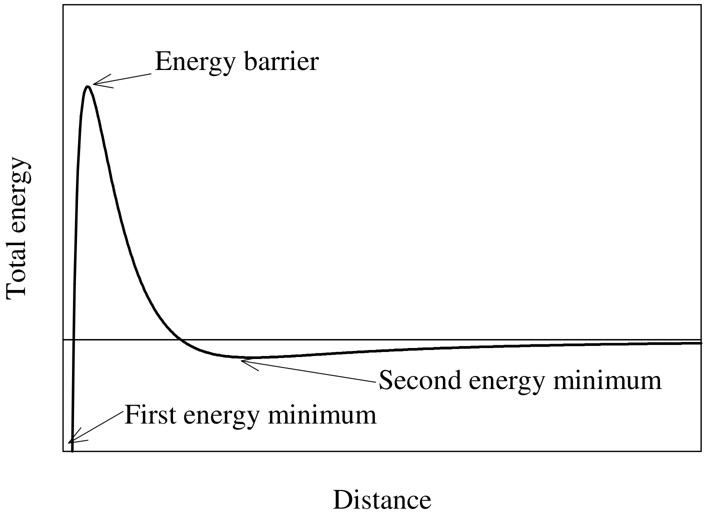

Figure 2.3: A typical Derjaguin-Landau-Verwey-Overbeek (DLVO) interaction energy profile of colloids in porous media.

Physical straining is an important mechanism for colloid retention in porous media and is not considered in clean-bed filtration theory (Bradford et al., 2007). Straining is a result of pore geometry and defined as the retention of colloidal particles in pore throats and the smallest regions that are too small to permit particle passage (Bradford et al., 2006). Herzig et al. (1970) did geometrical (triangular constriction) calculations and found physical straining would contribute significantly to particle retention when the particle/grain diameter ratio was less than 0.05. Xu et al. (2006) reported a critical particle/grain diameter ratio of 0.008. Bradford et al. (2002) even observed microsphere retention due to physical straining at a particle/grain diameter ratio of 0.002. A recent study by Shen et al. (2008) observed that the retention due to straining occurred at a particle/grain diameter ratio of 0.0016, when a 1,156 nm colloid suspension was introduced into a column packed with 0.72 mm glass beads. Although the study on CNT transport (Jaisi et al., 2008) has revealed that physical straining contributes to nanotube retention due to the large aspect ratio, the contribution of straining to nC_{60} retention has not reported yet. If 0.0016 is the smallest critical particle/grain diameter ratio, a mean diameter of 410 nm is required for nC_{60} to allow physical straining to significantly contribute to nC_{60} retention in 40-50 mesh (mean diameter 256 μm) quartz sands. However, studies have revealed that the occurrence of straining during colloid transport is solution chemistry (Bradford et al., 2007; Shen et al., 2008) and particle concentration dependent (Bradford and Bettahar, 2006). Thus, the possibility of straining occurrence in nC_{60} transport exists.

CHAPTER 3

MATERIALS, EXPERIMENTAL PROTOCOLS, AND ANALYTICAL METHODS

3.1 Materials

3.1.1 Chemicals

Solid C_{60} (99.9%; purified by sublimation) was purchased from the Materials Electronics Research Corp. (Tuscon, AZ) to prepare nC_{60} suspensions. The MWNT at three different manufacture-reported (MR) lengths, 0.5-2, 10-20, and 50 µm, were purchased from the Cheap Tubes Inc. (Brattleboro, VT), the Iljin Nanotech co. (Seoul, Korea), and the BuckyUSA (Houston, TX), respectively. The selected properties of MWNT are listed in Table 3.1. THF (99.99%+) was purchased from Fisher Scientific (Fair Lawn, NJ) and used as vehicle solvent during nC_{60} preparation. Optima grade methanol and toluene were obtained from Fisher Scientific for nC_{60} quantification using high performance liquid chromatograph. Various chemicals, such as calcium chloride, sodium chloride, sodium hydroxide, sodium phosphate monobasic, and calcium bromide, with certified ACS or higher grade, were purchased from Sigma-Aldrich (St. Louis, MO) and were used to obtain specific solution characteristics, in addition to being used as non-reactive tracers. Magnesium perchlorate (ACS reagent grade) was purchased from MP Biomedicals, Inc. (Solon, OH) as a destabilizing agent in nC_{60} extraction by toluene. Food grade polyoxyethylene (20) sorbitan monooleate (Tween 80) was purchased from Uniqema (New Castle, DE) and used as a representative surfactant. Tween 80 was selected due to its relative nontoxicity (Pennell et al., 1993) and wide applications in surfactant enhanced aquifer remediation (Pennell et al., 1997; Ramsburg and Pennell, 2001). It has an average molecular weight of 1,310 g/mol and the critical micelle concentration (CMC) is estimated to be 13 mg/L (Pennell et al., 1993; Pennell et al., 1997). Its chemical structure is provided in Figure 3.1. For model NOMs, Suwannee river humic acid (SRHA; standard II) and Suwannee river fulvic acid (SRFA; standard II) were obtained from the International Humic Substances Society (St. Paul, MN). The relevant physical and chemical properties of SRFA and SRHA are summarized in Table 3.2.

Table 3.1: Selected properties of multi-wall nanotubes (MWNTs).

Manufacture	Length (µm)	Purity (wt%)	Inside Diameter (nm)	Outside Diameter (nm)	Other elements
Cheaptubes	0.5-2	>95	5--10	10--20	Cl
Cheaptubes	10-20	>97		10--20	
BuckyUSA	50	95	3--5	8--15	Al, Cl, S

Data provided by manufactures.

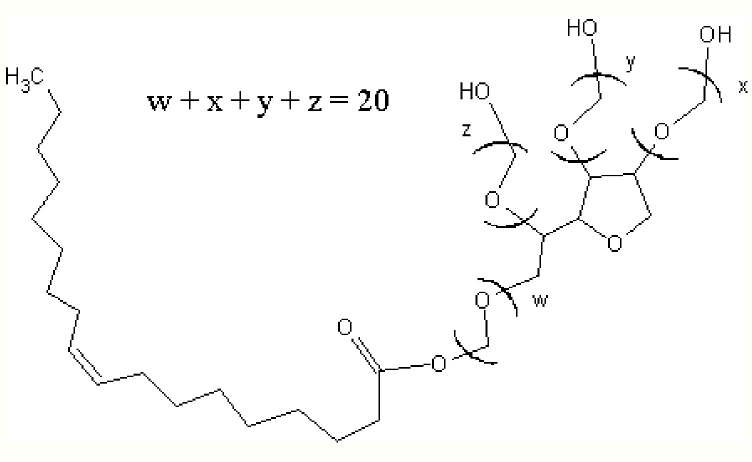

Figure 3.1: Structure of Tween 80. This structure is drawn using ACD/ChemSketch.

Table 3.2: Selected properties of Suwannee River humic acids (SRHA) and fulvic acids (SRFA).

Items	SRHA	SRFA
Mw (Da)	1,000-5,000[a]	2,310[b]
Mn (Da)		1,360[b]
C	52.63	52.34
H	4.28	4.36
O	42.04	42.98
N	1.17	0.67
S	0.54	0.46
P	0.013	0.004
carboxylic acidity (meq/g)	4.8	6.6
Carboxyl	15	17
Aromatic	31	22
Acetal	7	6
Heteroaliphatic	13	16
Aliphatic	29	35

[a] from Hong and Elimelech (1997)

[b] from Chin et al. (1994)

The rest values from International Humic Substances Society (IHSS) (St. Paul, MN)

3.1.2 Porous Media

In this research glass beads (GB), Ottawa sands (OS), Appling soil and Webster soil were selected as porous media. The soda lime GB were purchased from International Surface Preparation (Bellaire, TX) and only the size fraction retained between 40 and 50 mesh sieves was used. This material was selected to allow for direct comparison with previous nC_{60} transport studies (Brant et al., 2005a; Espinasse et al., 2007; Lecoanet and Wiesner, 2004; Lecoanet et al., 2004). Two OS (F-42 and F-70) were obtained from U.S. Silica (Berkeley Springs, WV), and were sieved to obtain four size fractions, 20-30, 40-50, 80-100, and 100-140 mesh. Appling soil was collected from the Ap1 and Ap2 horizons (upper 30 cm of the soil profile) at the University of Georgia Agricultural Experiment Station located near Eastville, GA. The soil is classified as a loamy, coarse sand of the Appling series (clayey, kaolinitic, thermic Typic Hapludult). Appling soil consists of approximately 77% sand, 14% silt and 9% clay. Webster soil, a silty clay loam (mixed, mesic Typic Haplaquoll), was collected from upper 30 cm of the soil horizon at the Agricultural Experiment Station located in Ames, IA. The particle size distribution of Webster soil is estimated to be 23% sand, 44% silt and 33% clay. Selected properties of soils are given in Table 3.3. Prior to use, the GB were washed with pure acetone and hexane solution sequentially, and then soaked in concentrated (12.1 M) hydrochloric acid (HCl) for 12 h. The beads were rinsed several times with deionized (DI) water (>18.0 MΩ·cm, Nanopure Model D4741, Barnstead International, Dubuque, IA) to remove residual HCl and placed in a series of ultrasonic baths containing 0.01 M sodium hydroxide (NaOH), DI water, and 1.0 M nitric acid (HNO_3), each for 20 minutes at room temperature (ca. 23 ^oC). The GB were then rinsed with DI water until pH 7 was achieved, and oven-dried at 70 ^oC for 12 h. Each OS fraction were soaked in a 1.0 M HNO_3 solution, rinsed with DI water, and placed in an ultrasonic bath containing 0.007 M Na_2HPO_4 for at least 10 h, rinsed with DI water until pH 7 was reached, and finally oven-dried at 200 ^oC for 12 h. The air-dried Appling and Webster soils were grounded to pass 10-mesh sieve and packed into the column without any pretreatment.

Table 3.3: Selective properties of natural soils

Soil name	Specific surface area (m^2/g)	Organic carbon content (%wt)	Cation exchange capacity (cmol/kg)	Intrinsic permeability (m^2)
Appling soil	3.50	0.75	7.1	1.2×10^{-11}
Webster soil	8.2	3.32	49.4	NA

Data obtained from (Karagunduz et al., 2001; Pennell et al., 1995)
NA means not available

3.2 Experimental Protocols

3.2.1 Preparation of nC_{60} Suspensions

Stable aqueous suspensions of nC_{60} were prepared following previously described procedures (Deguchi et al., 2001a; Fortner et al., 2005). At room temperature, THF was saturate with excess C_{60} powder after sparging with N_2 to remove dissolved oxygen. Upon saturation, the supernatant was filtered by vacuum through a 0.22 μm nylon membrane (Osmotics Corp., Minnetonka, MN), sparged with N_2 gas, and stored in a 4L amber glass container. An equal volume (250 mL) of DI water was added to a stirred C_{60}-THF solution at a rate of 1 L/min. The resulting solution (500 mL) was loaded into a rotary evaporator (Rotovapor Model R210, Buchi, New Castle, DE) and heated at 75 ^oC until ca. 200 mL of solution remains. The residual solution was diluted with 100 mL of DI water, and the evaporation process was repeated three times to remove THF. The resulting aqueous C_{60} suspension (ca. 250 mL) will be vacuum-filtered through a 0.22 μm cellulose acetate membrane (Corning Inc., Corning, NY) and stored at 4 ^oC in the dark for subsequent use as the nC_{60} stock suspension.

Influent nC_{60} suspensions for the column transport studies were prepared in degassed DI water to which appropriate amounts of background electrolyte, Tween 80, SRHA, or SRFA stock solutions and nC_{60} stock suspension (described above) were added to achieve the desired final concentrations. The background electrolyte stock solution consisted of 0.5 M $CaCl_2$ or 0.1 M NaCl and 0.01 M $NaHCO_3$. The stock solutions of SRHA and SRFA were prepared by dissolving 41.5 mg of SRHA powder and 44.3 mg of SRFA powder, respectively, into 100 mL DI water. After mixing for 24 hrs, both solutions were adjusted to pH 7.0 with 0.1 M NaOH and filtered through a 0.22 μm cellulose acetate membrane.

In the absence of Tween 80, SRHA or SRFA, influent nC_{60} suspensions were prepared by adding 100 mL nC_{60} stock suspension to an equal volume of background electrolyte solution (degassed; with various electrolyte species and concentrations) at a mixing rate of 120 mL/min. To examine potential effects of the suspension preparation method on nC_{60} particle size and stability, additional aqueous nC_{60} suspensions were prepared following the general procedures described above. Several preparation variables were considered, including three electrolyte concentrations (1, 10, 100 mM NaCl or $CaCl_2$), two addition rates (24 and 120 ml/min), two mixing sequences (addition of nC_{60} stock suspension to the electrolyte solution, referred to as E1S2, and addition of the electrolyte solution to the nC_{60} stock suspension, referred to as S1E2), and two final concentrations (~1 and 3 mg/L). For influent nC_{60} suspensions prepared with either Tween 80, SRHA or SRFA, the nC_{60} stock suspension was first mixed with either Tween 80, SRHA or SRFA stock solution in a 200 mL volumetric flask. A predetermined volume of the background electrolyte stock solution (0.5 M $CaCl_2$ and 0.01 M $NaHCO_3$) was introduced to the mixture, and degassed DI water was then added to achieve the desired final concentration of Tween 80, SRHA or SRFA (1,000 mg/L, 20 mg C/L, and 20 mg C/L, respectively) in 1×10^{-3} M $CaCl_2$ and 5×10^{-5} M $NaHCO_3$. At the bicarbonate concentration of 5×10^{-5} M, the pH of nC_{60} influent suspensions before and after the injection period, as well as selected effluent samples, was measured and found to be approximately 7.0. All aqueous nC_{60} suspensions were used within 1 h of preparation.

3.2.2 Preparation of MWNT Suspensions

The protocol used herein to functionalize MWNT by 4-ethoxybenzoic acid (4-EBAc) has been described in detail in (Lee et al., 2008). In brief, 4-ABAc (3.65 mM), MWNT, polyphosphoric acid and Phosphorus Pentoxide (P_2O_5) were mixed in a flask at a weight ratio of 1:1:40:10 under the nitrogen atmosphere. The flask was heated sequentially to 80, 100, and 130 ^{o}C for 1, 1, and 72 h, respectively. Then DI water was added to the mixture to obtain the MWNT stock suspension. The resulting suspension exhibited a shiny green-brown color, which was distinct from other dispersed MWNT via sonication. Since no MWNT loss was observed, the concentration of MWNT in stock suspension was calculated based on the mass of MWNT added and the final volume. To obtain MWNT input suspensions for column experiments at the proper concentrations, such as 5 and 90 mg/L, predetermined amount of MWNT stock suspension was diluted with DI water and the pH was adjusted to 5 using 0.1 or 1 M NaOH solution. In this research, the transport experiments with an input MWNT concentration of 90 mg/L were conducted to form a comparison base to the previous study (Jaisi et al., 2008).

3.2.3 Column Experiments

The 1D column apparatus consisted of a Rainin HPLC pump (model Dynamix SD-200, Varian, Inc. Palo Alto, CA) equipped with a 25 mL pump head and pulse dampener, a syringe pump (model 22, Harvard Apparatus, Inc., Holliston, MA), a borosilicate glass column, and an ISCO fraction collector (Teledyne Isco Inc., Lincoln, NE), which was shown in Figure 3.2. The column had a dimension of 2.5 cm in inside diameter and 15 cm in length for GB and OS, while the column length was shortened to 11 cm for Appling and Webster soil to save costs in nanomaterial purchase. Columns were packed with either GB, one size fraction of OS, Appling soil, or Webster soil in

1-cm increments. For nC_{60} transport experiments, each column endplate was fitted with two 40-mesh nylon screens and a 70 μm nylon filter to support the solid phase and promote uniform flow of the aqueous phase, while a 60-mesh stainless steel screen was used for the endplate in MWNT transport experiments to reduce nanotube retention by supporting filter. Prior to water imbibition, the dry packed column was flushed with CO_2 gas for at least 20 min to facilitate dissolution of entrapped gas phase. At least 10 PVs of degassed background electrolyte solution were introduced into the column in an upflow mode at a pore velocity of 1 or 8 m/d. After complete saturation of the column with background electrolyte, a pulse (e.g., 5 PV) of nC_{60} or MWNT input suspension was introduced into the column with the syringe pump, followed by the injection (e.g., 3 PV) of particle-free solution at the same flow rate. To further investigate the potential effect of sorbed-phase Tween 80 on nC_{60} transport and solid phase interactions, the experimental sequence was modified to include a Tween 80 preflood, which was conducted by injecting 5 PVs of nC_{60}-free Tween 80 solution (1,000 mg/L conditioned with 1×10^{-3} M $CaCl_2$ and 5×10^{-5} M $NaHCO_3$), followed by 3 PVs of background electrolyte solution. Upon completion of the Tween 80 injection sequence, a 5-PV pulse of either a suspension containing nC_{60} alone or a suspension containing Tween 80 mixed with nC_{60} was introduced into the OS or Appling soil column at the same flow rate, followed by 3 PVs of background electrolyte solution. Under such flow conditions, the Reynolds number (*Re*) was equal or less than 0.011, which was several orders-of-magnitude below the limit of laminar flow in a packed bed (*Re* < 1-10).

Column effluents were collected continuously in 15-mL sterile plastic centrifuge tubes (Fisher Scientific, Fair Lawn, NJ). At the conclusion of each transport experiment, the column was dissected into 1.5-cm increments, which were transferred to 30-mL glass vials. The retained nC_{60} aggregates were extracted from GB, OS dissection samples by addition of 10 mL of DI water, agitated for 3 hr (Labquake, Barnstead International, Dubuque, IA), followed by ultrasonication (Model FS20H, Fisher Scientific) for 1 min. For transport experiments conducted in Appling and Webster soils, the sectioned soil samples were oven-dried at 85 ^{o}C over night prior to C_{60} extraction by toluene.

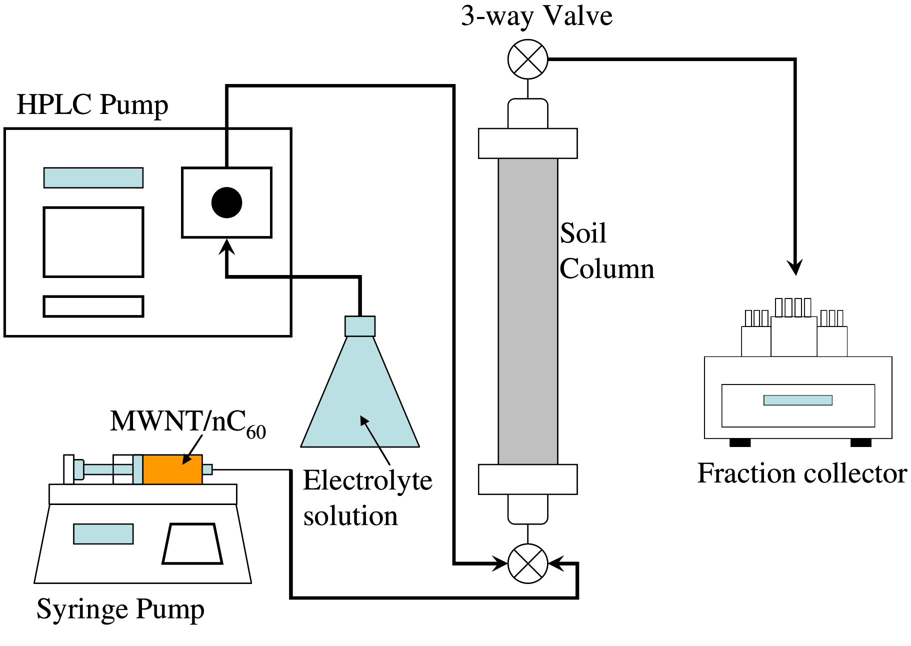

Figure 3.2: Schematic diagram of the experimental apparatus used for the nC_{60} transport and retention studies.

Following complete water saturation of the porous medium, the non-reactive tracer test was conducted in selected columns to assess water flow and hydrodynamic dispersion. Three PV of a 1 x 10^{-3} M $CaBr_2$ and 5 x 10^{-5} M $NaHCO_3$ solution were introduced at a pore velocity of 1 or 8 m/d, followed by three PV of 1 x 10^{-3} M $CaCl_2$ and 5 x 10^{-5} M $NaHCO_3$ at the same flow rate. Effluent samples were collected continuously in centrifuge tubes using a fraction collector and bromide concentrations were measured using an ion selective bromide electrode (Cole-Parmer Instrument Co., Vernon Hills, IL) connected to an Accumet Model 50 pH meter (Fisher Scientific, Fair Lawn, NJ). The probe was calibrated using bromide standards with concentration spanning from 10 to 200 mg/L. The resulting non-reactive tracer BTCs were fit to a 1-D form of the advective-dispersive reactive (ADR) transport equation using CXTFIT ver 2.0 (Toride et al., 1999):

$$R_F \frac{\partial C^*}{\partial t^*} = \frac{1}{P_e} \frac{\partial^2 C^*}{\partial X^2} - \frac{\partial C^*}{\partial X^*} \tag{3.1}$$

$$R_F = 1 + \frac{\rho_b K_D}{\theta_w}; \quad C^* = \frac{C}{C_0}; \quad t^* = \frac{v_p t}{L}; \quad P_e = \frac{v_p L}{D_H}; \quad X^* = \frac{x}{L} \tag{3.2}$$

where R_F was the retardation factor, K_D was the solute distribution coefficient; t^* was dimensionless pore volumes, P_e was the Peclet number, and X was dimensionless distance. In the absence of physical nonequilibrium (e.g., immobile water), the value of $R_F = 1$ for a non-reactive tracer, and hence, the only parameter that was fit was the Peclet number (Pe), from which the hydrodynamic dispersion coefficient (D_H) was obtained.

3.2.4 Batch Retention Experiments

Batch reactor experiments were performed in 30 mL borosilicate glass vials to independently assess the attachment characteristics of nC_{60} particles to GB or OS. Approximately 13 g of dry OS or GB were combined with 13 mL of nC_{60} suspension at initial concentrations of ranging from 0.08 to 12.78 mg/L, prepared in DI water or 1.0 mM $CaCl_2$ buffered to pH 7 with 0.05 mM $NaHCO_3$. The contents of the batch reactors were mixed on an oscillating shaker for 4 h, which corresponds to approximate duration of an nC_{60} transport experiment.

3.3 Analytical Methods

The mean diameter and size distribution of nC_{60} aggregates in aqueous suspension were determined using a Zetasizer Nano ZS analyzer (Malvern Instruments Ltd. Southborough, MA) operated in non-invasive back scattering (NIBS$^{®}$) mode at an angle of 173°. Measurement of particle size distribution by photon correlation spectroscopy, commonly referred to as dynamic light scattering (DLS), is based on the change in scattered light intensity collected over different time intervals. These data are described using an electric field correlation function (*CF*), for which the decay rate (Γ) may be expressed as:

$$\Gamma = q^2 D_m \tag{3.3}$$

where D_m is the mutual diffusion coefficient and q is the scattering vector magnitude, defined as:

$$q = \frac{4n\pi \sin(\theta/2)}{\lambda_0} \tag{3.4}$$

where n is the refractive index of the solution, θ is the scattering angle (173^{o}), and λ_0 is the laser wavelength (532 nm). Assuming that the particles are: (i) in Brownian motion (dilute solution), (ii) spherical in shape with a diameter that is small relative to the molecular dimensions, and that (iii) D_m is approximately equal to the diffusion coefficient extrapolated to infinite dilution (D_0), Stokes' Law can be used to calculate the effective hydrodynamic radius (r) of a particle:

$$r = \frac{k_b T}{6\pi\mu D_0} \tag{3.5}$$

where k_b is the Boltzman constant, T is the temperature in degrees Kelvin, μ is the dynamic viscosity of the solution. Approximately 1 mL of nC_{60} suspension was loaded into a disposable cuvette (DTS0012, Malvern Instruments Ltd., Southborough, MA) and analyzed using a green laser (DPSS source, 50.0mW) at 532 nm and a C_{60} refractive index of 2.20 (Huffman, 1991). A refractive index of 1.33 (water) was used for all aqueous samples. The instrument obtains scattering intensity fluctuation data to obtain a correlation function, which is converted into natural log form and fit to a polynomial function:

$$ln(CF) = a + bt + ct^2 + dt^3 + et^4 + ... \tag{3.6}$$

where the terms a, b, c, d and e are fitting parameters, with the value of b corresponding to the mutual diffusion coefficient (D_m) in eq 3.3, while eq 3.5 was used to obtain the aggregate radius. Based on a measured set of correlation functions, an intensity distribution is generated from which the mean aggregate size is obtained. All DLS measurements were performed in triplicate, and the accuracy of the system was checked using monodisperse polystyrene spheres (3100A, Nanosphere Size Standards, Duke Scientific Corp., Palo Alto, CA), with a mean diameter of 97 ± 3 nm. A typical size distribution (by intensity) of nC_{60} suspension is shown in Figure 3.3.

The size and shape of the nC_{60} aggregates were further characterized by transmission electron microscopy (TEM) following the procedures of Fortner et al. (Fortner et al., 2005). Briefly, two drops of concentrated (*ca.* 25 mg/L) nC_{60} suspension were placed on a 300-mesh carbon-coated copper grid (Electron Microscopy Sciences, Hatfield, PA), air-dried at room temperature, and imaged using a JEOL 100CX II transmission electron microscope (Peabody, MA) operated at 100 kV. A representative TEM image of the nC_{60} aggregates is shown in Figure 3.4. The sample preparation method for MWNTs was slight modified and was described in Chapter 8.

The electrophoretic mobility of nC_{60} aggregates or MWNT in aqueous samples was determined using a Zetasizer Nano ZS analyzer. The instrument monitored the direction and velocity of particles (i.e., electrophoretic mobility) in response to an applied electric field. Particle movement was tracked using a combination of laser doppler velocimetry (LDV) and phase analysis light scattering (PALS), which enabled detection of particles with diameters ranging from 5 nm to 10 μm. For nC_{60}, the electrophoretic mobility was converted to a zeta potential using Eq. 2.2.

The aqueous phase concentration of nC_{60} in the absence of SRHA or SRFA was determined using a Cary 3E UV-Vis spectrophotometer (Varian Inc., Palo Alto, CA)

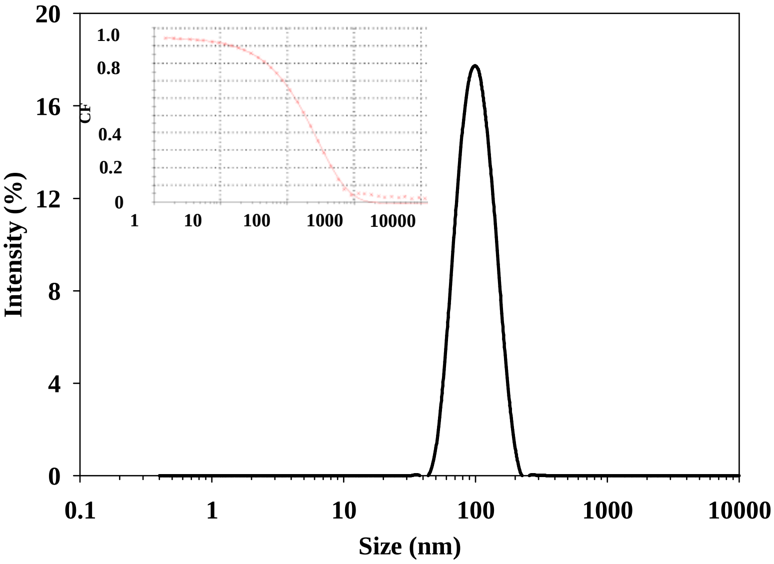

Figure 3.3. Size distribution of an nC_{60} suspension (pH 7, C_{60} concentration = 6.7 mg/L, DI water) determined by dynamic light scattering. The inset shows the corresponding correlation function (*CF*).

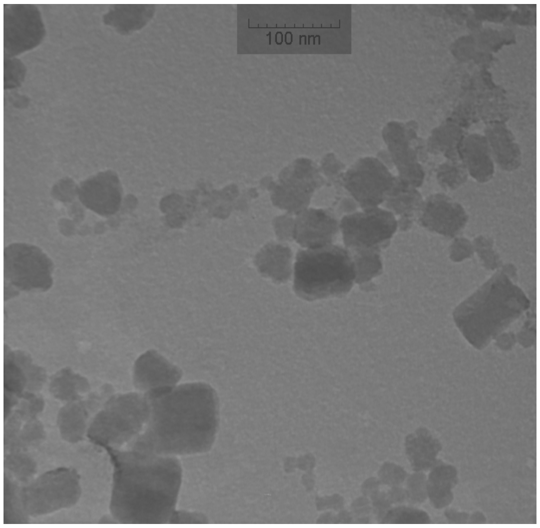

Figure 3.4. Transmission electron microscope (TEM) image of nC_{60} aggregates dried on a 300-mesh carbon-coated copper grid.

scanned over wavelength range of 190 to 500 nm. The absorbance response at a wavelength of 344 ± 1 nm was used for nC_{60} quantification based on a 5-point calibration curve prepared by serial dilution of a known C_{60} stock solution (9.5 mg/L). Concentrations of nC_{60} in stock solution and samples in presence of SRHA or SRFA were determined using a liquid-liquid extraction process (Fortner et al., 2005; Xia et al., 2006). An aliquot (2 mL) of aqueous sample was destabilized with 0.8 mL of 0.1 M $Mg(ClO_4)_2$, to which 2.0 mL of neat toluene were added to extract C_{60} from the aqueous phase. The extraction vials were placed on a table shaker and mixed at 400 rpm for 10 min, followed by mixing at 250 rpm for 12 h (Innova 2100, New Brunswick Scientific Co., Inc., Edison, NJ). After mixing, the toluene phase was transferred to a 1.5 mL centrifuge tube (VWR International, West Chester, PA) and spun at 5000 rpm for 10 min (Eppendorf centrifuge 5415D, Brinkmann Instruments Inc., Westbury, NY). An aliquot (0.3 mL) of toluene was transferred into 1.2 mL methanol and the combined solution was loaded onto an high performance liquid chromatograph (HPLC) after mixing for 1 min on a vortexer (Touch mixer model 232, Fisher Scientific). Quantitative analysis of C_{60} in the toluene-methanol solution was performed using an Agilent model 1100 HPLC equipped with an Alltima C18 column (150 mm length x 4.6 mm i.d., 5 um particle size) and a diode array detector (DAD) monitored at a wavelength of 334 nm. The HPLC was operated at a constant flow rate of 1 mL/min with an isocratic mobile phase consisting of 55% toluene and 45% methanol (Isaacson et al., 2007). Reference C_{60} standards were prepared by placing 2 mg of fullerene powder into an amber vial containing 10 mL of toluene, which was placed in a sonication bath for 3 hrs, and then diluted to prepare a calibration curve.

To quantify the concentration of SRHA or SRFA, the aqueous phase from the extraction vial was analyzed using the Cary 3E UV-Vis spectrophotometer at a wavelength of 290 nm, where the minimum interference of magnesium perchlorate was observed. To determine the concentration of Tween 80 in the presence of nC_{60}, effluent samples was filtered through 0.02 μm membrane filter (Whatman International Ltd., Maidstone, Kent, UK) to remove nC_{60}. The filtrate was then analyzed using the Cary 3E UV-Vis spectrophotometer operated at a wavelength of 234 nm. Quantification of Tween 80 was obtained using a 5-point calibration curve prepared over a concentration range of 10 to 1,500 mg/L.

Analysis of THF and its toxic daughter product, GBL, in aqueous samples was performed using an Agilent 6890 gas chromatograph (GC) equipped with a DB-1ms column (30 m length × 0.25 mm outside diameter × 0.25 um film thickness, J&W Scientific Inc., Folsom, CA) connected to an Agilent Model 5975 mass selective detector (MSD). Approximately 2 mL of effluent sample were treated with 2 g of NaCl before loading onto an HT3 headspace autosampler (Teledyne-Tekmar, Mason, OH) that was connected to the GC-MS system. To measure the concentration of GBL, another aliquot (1 mL) of aqueous samples was mixed with equal volume of methylene chloride for 30 min on an oscillating shaker. After extraction, GBL in methylene chloride was analyzed using GC-MS system. GBL standards were pretreated and analyzed using the same protocol.

In order to determine amount of nC_{60} retained by the Appling or Webster soil, nC_{60} was extracted from oven-dried (85 ^{o}C) dissection samples by adding 20 mL of neat toluene. The extraction vials were then placed in an ultrasonication bath for 4 hr and mixed at 250 rpm for 12 hours at 30 ^{o}C. The C_{60} concentration in toluene phase was determined using the same HPLC method described in liquid-liquid extraction above. A five-point calibration curve over a concentration range of 1 to 100 μg nC_{60} per 13 g Appling or 11 g Webster soil was prepared following similar sample drying and toluene extraction processes. The detection limit of the solid-phase extraction method was 0.35 and 0.11 μg/g for Appling and Webster soil, respectively.

The concentration of MWNT in input suspensions and effluents from experiments with 90 mg/L as input concentration were determined using a Cary 3E UV-Vis spectrophotometer at 450 nm, where an absorbance shoulder was constantly observed, a Shimadzu spectrofluorophotometer (Shimadzu Scientific Instruments, Columbia, MD) operated with an excitation wavelength of 450 nm was used to quantify MWNT concentrations of those from experiments with 5 mg/L as input concentration. The fluorescence was scanned from 400 to 700 nm and the intensity at 515 ± 5 nm was employed herein.

CHAPTER 4*

TRANSPORT AND RETENTION OF FULLERENE (C_{60}) NANOPARTICLES: EFFECTS OF FLOW VELOCITY AND GRAIN SIZE

4.1 Introduction

The production of fullerene (C_{60}) nanomaterials has reached industrial level and the market demands for these products are still expanding (Trembley, 2002; Xie et al., 2008). Despite improved controls, it is inevitable that these materials will enter the environment during their manufacture, transportation, application, and disposal. Although the inherent aqueous solubility of C_{60} in water is extremely low ($< 10^{-9}$ mg/L), stable suspensions of C_{60} aggregates with diameters ranging from 25 to 500 nm have been prepared at concentrations of up to 100 mg/L using relative simple preparation methods (Andrievsky et al., 1995; Cheng et al., 2004; Deguchi et al., 2001b; Fortner et al., 2005; Yamakoshi et al., 1994). In addition, recent studies have shown that NOM can stabilize nC_{60} and MWNTs in aqueous suspensions (Hyung et al., 2007; Terashima and Nagao, 2007). Thus, the potential exists for nC_{60} to enter the water supply through a number of pathways, including groundwater recharge and runoff into surface water bodies. A detailed understanding of the processes governing nC_{60} transport and retention in porous media is

---

*The data in this chapter is partially published in Enviornmental Science and Technology, vol. 42, page 3588-3594 and vol. 42, page 7174-7180 in 2008.

required to accurately assess the fate and distribution of nC_{60} in the environment, and to design effective removal strategies for drinking water treatment.

To date, a limited number of column studies have been conducted to study the transport of nC_{60} water-saturated porous media (Brant et al., 2005a; Cheng et al., 2005; Espinasse et al., 2007; Lecoanet and Wiesner, 2004; Lecoanet et al., 2004). In the majority of these experiments, nC_{60} were observed to readily transport through columns leading to the development of a pseudo steady-state in effluent concentrations. Based on clean-bed filtration theory (Eq. 2.10), this concentration plateau was then used to obtain α and to estimate bed length required for 99.9% (3-log) removal. However, retention profile data were not reported in any of these transport experiments, and all observations of nC_{60} transport and deposition behavior were limited to 40-50 mesh glass beads, an idealized porous medium. In addition, these experiments were conducted at flow rates approaching a turbulent flow condition.

The primary objectives of this research were to investigate the effects of flow velocity and grain size on the transport and retention of nC_{60} in water-saturated quartz sands. To allow for direct comparisons with previous work, nC_{60} transport experiments were also conducted in 40-50 mesh glass beads. Then, the transport behavior of nC_{60} were further studied in four size fractions of Ottawa sand (20-30, 40-50, 80-100, or 100-140 mesh) at pore-water velocities of either 1 or 8 m/d. In addition, batch retention experiments were conducted to independently assess the distribution of nC_{60} between water and Ottawa sand or glass beads.

4.2 Results and Discussion

Eight column experiments were conducted to quantify the nC_{60} transport in 40-50 mesh GB and OS. These column experiments were conducted at the beginning of this research for three reasons, (1) to start experiments with the least complex porous medium, (2) to allow for direct comparisons to previous nC_{60} transport work (Brant et al., 2005a; Espinasse et al., 2007; Lecoanet and Wiesner, 2004; Lecoanet et al., 2004), (3) to evaluate differences of nC_{60} transport and retention behavior in glass beads and quartz sands at similar experimental conditions. The experimental conditions are summarized in Table 4.1.

4.2.1 Transport and Retention of nC_{60} in GB and OS

Effluent BTCs for nC_{60} aggregate transport through water-saturated columns packed with either 40-50 mesh glass beads or Ottawa sand are shown in Figures 4.1A and 4.1B, respectively. Pulse injections (3 or 5 PV) of the nC_{60} suspensions containing 1.0 mM $CaCl_2$ as a background electrolyte yielded asymmetrical BTCs that gradually increased to a maximum value before declining sharply to relative concentrations (C/C_0) approaching zero. For the glass bead columns, nC_{60} appeared in the column effluent after injecting ca. 1.1 PV of suspension, while in columns packed with Ottawa sand nC_{60} breakthrough occurred at ca. 1.8 PV. These data indicate that Ottawa sand had a greater capacity to retain nC_{60} aggregates relative to glass beads possessing the same mean grain

Table 4.1: Experimental conditions of nC_{60} transport studies conducted in water-saturated conditions.

Column	Size[a] (mesh)	θ_w[b]	C_0[c] (mg/L)	PW[d] (pv)	IS[e] (mM)	MB[f] (%)	Retained (%)
GB-1	40-50	0.38	2.44	3.0	3.065	95.8	8.6
GB-2	40-50	0.38	1.34	3.0	3.065	100.5	33.8
GB-3	40-50	0.38	1.34	3.0	3.065	94.6	48.9
GB-4	40-50	0.38	3.06	3.0	0.0	100.6	0.0
OS-1	40-50	0.36	2.33	3.0	3.065	98.4	77.0
OS-2	40-50	0.37	2.25	4.56	3.065	97.6	48.1
OS-3	40-50	0.37	1.34	3.0	3.065	102.2	59.7
OS-4	40-50	0.35	2.31	3.45	0.0	100.2	4.8
2030F-1	20-30	0.34	3.00	5.0	3.065	100.3	14.3
2030F-2	20-30	0.35	2.93	5.0	3.065	103.7	17.8
2030S-1	20-30	0.34	3.34	5.0	3.065	98.3	26.2
2030S-2	20-30	0.35	3.08	5.0	3.065	94.2	22.6
4050F-1	40-50	0.36	3.03	5.0	3.065	103.8	36.2
4050F-2	40-50	0.37	3.16	5.0	3.065	101.6	29.7
4050S-1	40-50	0.37	3.05	10	3.065	91.7	27.0
4050S-2	40-50	0.36	3.12	9.9	3.065	97.4	37.2
80100F-1	80-100	0.39	3.10	5.0	3.065	93.7	66.5
80100F-2	80-100	0.39	3.21	5.0	3.065	104.1	73.2
80100S-1	80-100	0.39	3.38	5.0	3.065	100.5	99.9
80100S-2	80-100	0.39	2.95	5.0	3.065	93.8	100.0
100140F-1	100-140	0.39	3.27	4.7	3.065	101.6	99.9
100140F-2	100-140	0.39	3.08	5.0	3.065	103.2	100.0
100140F-3	100-140	0.39	3.04	3.8	0.0	102.6	6.6
100140S-1	100-140	0.40	3.07	10	3.065	99.7	99.8
100140S-2	100-140	0.40	3.26	5	3.065	92.6	99.9

[a] grain size of porous media. [b] volumetric water content. [c] influent nC_{60} concentration. [d] pulse width expressed in dimensionless pore volumes. [e] ionic strength. [f] mass balance of nC_{60}. In column names, F representing fast flow and S representing slow flow.

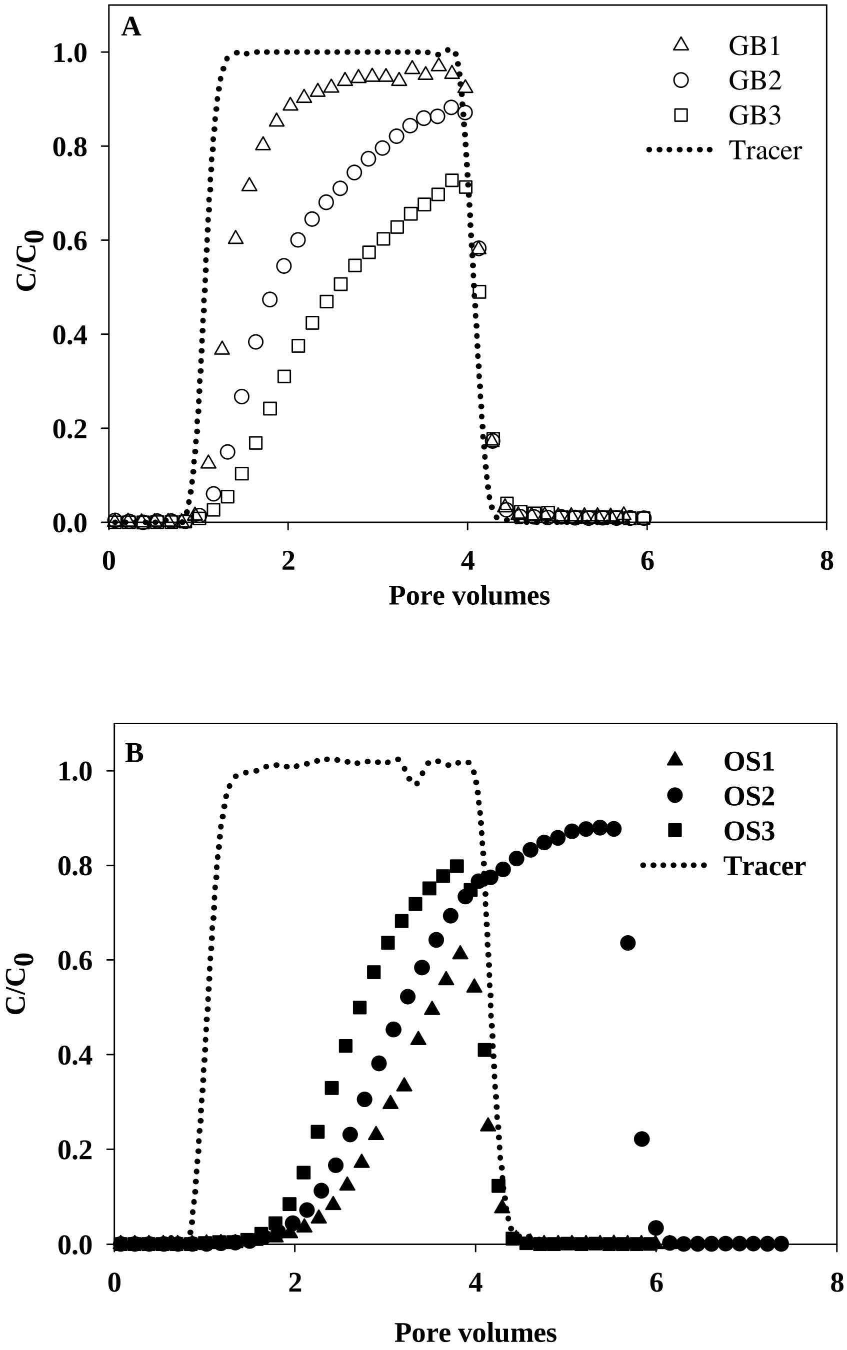

Figure 4.1: Measured nC_{60} breakthrough curves (A and B) in water-saturated columns packed with either 40-50 mesh glass beads (open symbols) or Ottawa sand (solid symbols), respectively. Aqueous nC_{60} suspensions contained 1.0 mM $CaCl_2$, buffered to pH 7 with 0.065 mM $NaHCO_3$, applied at a Darcy velocity of 2.8 m/d.

size. During the initial breakthrough period, the area above the nC_{60} BTC (i.e., the region between the measured data points and a relative concentration (C/C_0) of 1.0) corresponds to the mass of nC_{60} particles retained by the solid phase. Under ideal conditions (i.e., reversible, equilibrium) this retained mass would be eluted from the column upon the re-introduction of nC_{60}-free water, and would appear in the BTC as gradual decline in effluent concentration. However, the sharp reduction in relative concentration observed in the distal portion of the BTCs indicates that retained nC_{60} aggregates were not released from the solid phase and that the detachment coefficient approaches zero under these experimental conditions. Such irreversible attachment is consistent with the findings of Chen and Elimelech (Chen and Elimelech, 2006), who reported that nC_{60} aggregates deposited on a silica-coated quartz surface in a 0.6 mM $CaCl_2$ solution at pH 5.2. These deposited nC_{60} were not released until the rinse solution contained DI water adjusted to pH 12.3.

For comparison purposes, representative BTCs obtained for 3 PV pulse injections of non-reactive tracer (Br^-) are shown in Figure 4.2 (also in Figures 4.1A and 4.1B). The CXTFIT program (ver. 2), which employs a least squares procedure to obtain the desired parameters (i.e., R_F and Pe), was used to simulate the non-reactive tracer effluent BTCs (Toride et al., 1999) through solving Eq. 3.1 and 3.2. As anticipated, the fitted R_F for all of the tracer studies were equal to 1.0 ± 0.02, while the Peclet numbers for the glass bead and Ottawa sand columns were approximately 230 and 180, respectively. The Peclet numbers correspond to hydrodynamic dispersivity values ($\alpha_D = D_H / v_p$) of 0.065 and 0.084 cm, respectively, which are consistent with the relatively small values of α_D reported for laboratory-scale columns packed with uniform sand (Pennell et al., 1993). Additionally, the symmetrical shape and absence of tailing in the non-reactive tracer BTCs indicate that physical nonequilibrium processes, such as rate-limited mass transfer into regions of immobile water and preferential flow paths, did not contribute to retention of nC_{60} aggregates or the observed asymmetry in the nC_{60} BTCs (Figure 4.2).

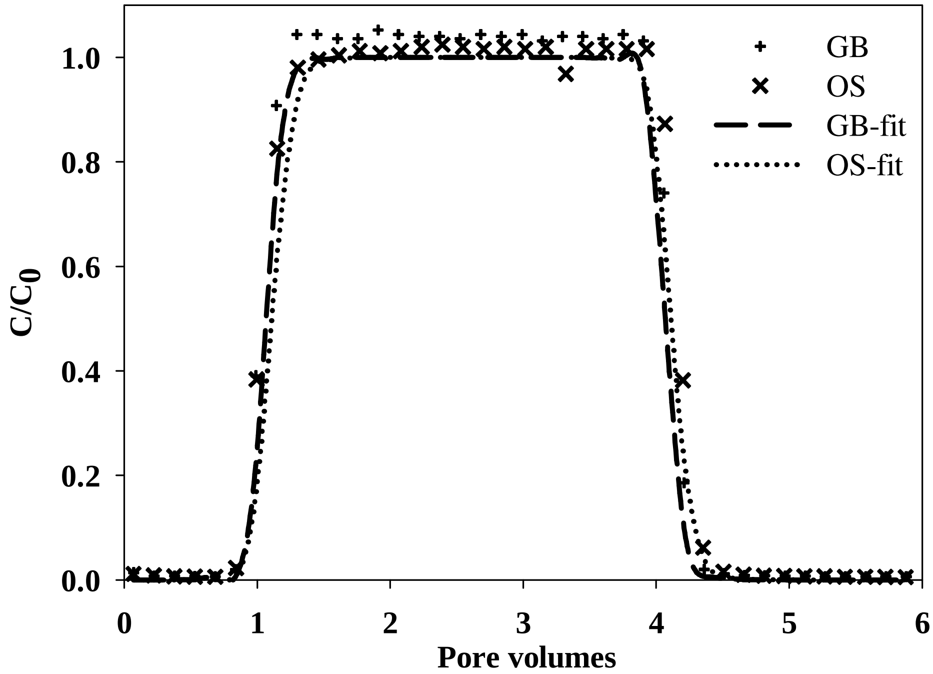

Figure 4.2: Measured and simulated non-reactive tracer breakthrough curves in columns packed with either 40-50 mesh glass beads (GB) or Ottawa sand (OS).

A nearly 2-fold increase (1.34 to 2.44 mg/L) in the concentration of nC_{60} injected into the glass bead columns (exp. GB-1) resulted in a steeper rise to a maximum relative concentration. At the lower concentration of 1.34 mg/L, the maximum or plateau concentration was not achieved after injecting 3 PV of nC_{60} suspension (exps. GB-2 and GB-3). However, the distal portion of the BTCs exhibited an identical shape irrespective of input concentration, suggesting that the capacity of the solid phase to retain nC_{60} had not been exceeded. For the Ottawa sand columns, increasing the input concentration did not yield a discernable change in the shape of the nC_{60} BTCs. At the higher input concentration of 2.44 mg/L, a 5 PV pulse of nC_{60} was required to reach a maximum relative effluent concentration of ca. 0.85 (exp. OS-2). The larger applied volume of nC_{60} (5 PV vs. 3 PV) required to reach a maximum effluent concentration indicates that Ottawa sand possesses a greater capacity to retain nC_{60} aggregates relative to glass beads, which is consistent with the delayed nC_{60} breakthrough observed in the Ottawa sand columns.

The nC_{60} retention profiles for the glass bead and Ottawa sand columns are plotted in Figures 4.3A and 4.3B, respectively, where a distance of 0 cm corresponds to the column inlet. Overall mass balance recoveries were computed from the ratio of the nC_{60} mass injected and the sum of the mass recovered from the column effluent and solid phase extraction, and ranged from 95 to 102%. For the glass bead columns, nC_{60} aggregate retention decreased with distance from the column inlet. In contrast, the retention of nC_{60} in the Ottawa sand columns was relatively uniform over the entire length of the column, and was similar in magnitude regardless of the input concentration (Table 4.1). The relatively constant deposition profile in the Ottawa sand columns

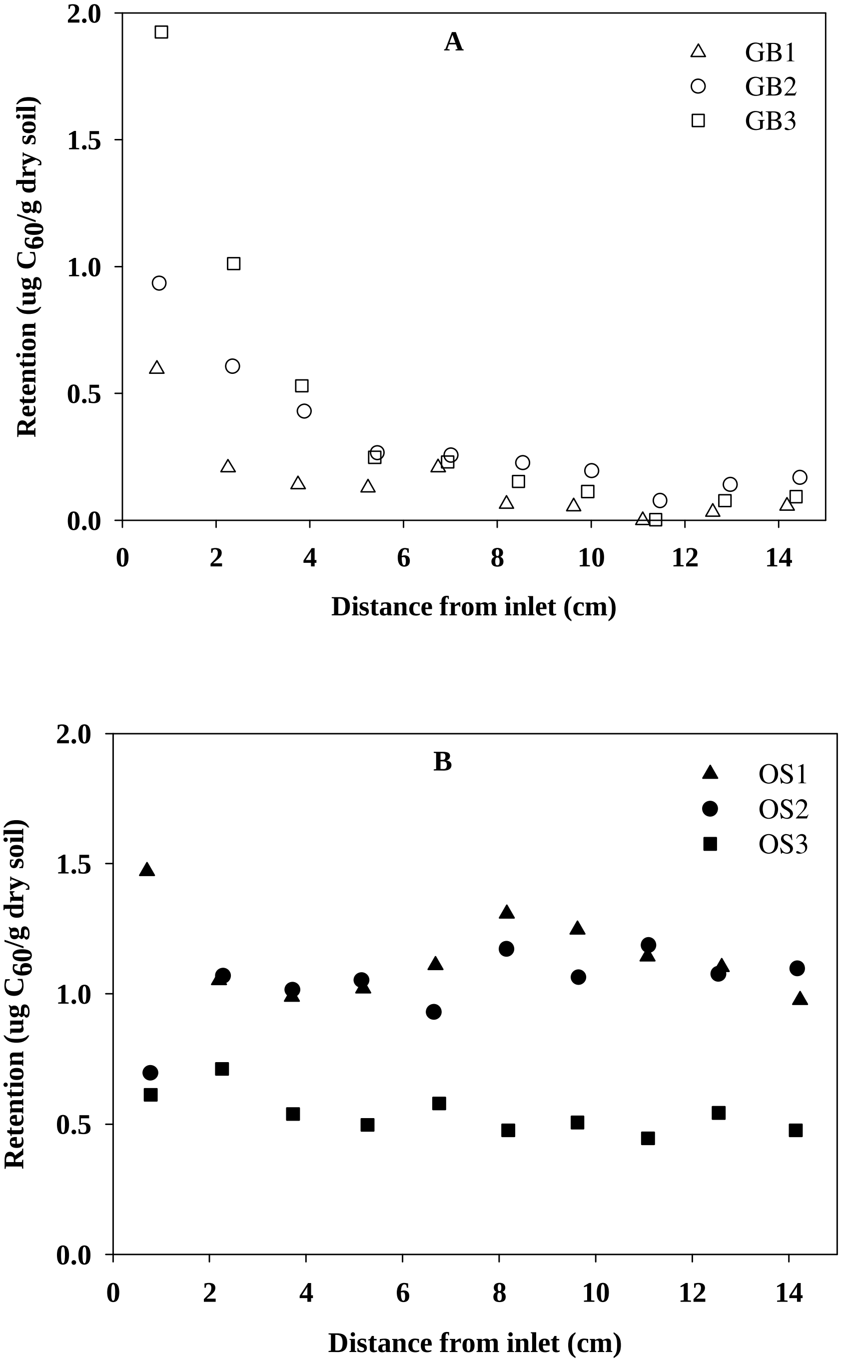

Figure 4.3. Measured nC_{60} retention profiles (A and B) in water-saturated columns packed with either 40-50 mesh glass beads (open symbols) or Ottawa sand (solid symbols), respectively. Aqueous nC_{60} suspensions contained 1.0 mM $CaCl_2$, buffered to pH 7 with 0.065 mM $NaHCO_3$, applied at a Darcy velocity of 2.8 m/d.

indicates that nC_{60} deposition approached a limiting capacity under these experimental conditions.

4.2.2 Effects of Solution Ionic Strength

Two additional column experiments (GB-4 and OS-4) were performed with DI water alone (i.e., no background electrolyte or pH buffer) to investigate the role of electrostatic interactions in nC_{60} aggregate retention. The resulting nC_{60} effluent BTCs obtained at a Darcy velocity of 2.8 m/d are shown in Figure 4.4. In contrast to the column experiments conducted at an ionic strength of 3.065 mM, nC_{60} effluent BTCs for both the glass bead and Ottawa sand columns coincided with the non-reactive tracer (Br^-), indicating that there was minimal retention of nC_{60} aggregates by the solid phase (Figures 4.4A and 4.4B). Subsequent column extraction revealed that no measurable amounts of nC_{60} were retained by the glass beads, while less than 5% of the injected mass was recovered from the Ottawa sand column (Figures 4.4C and 4.4D). The observed enhancement in nC_{60} transport coincided with the larger absolute value of the zeta potential in DI water alone (-64.0 ± 2.0 mV) compared to that in 1.0 mM $CaCl_2$ (-23.9 ± 3.1 mV). These data are consistent with the reported increase in nC_{60} aggregate mobility when the ionic strength was reduced from 100 mM NaCl to 1 mM (Brant et al., 2005a), and further support the important role of electrostatic interactions in nC_{60} retention.

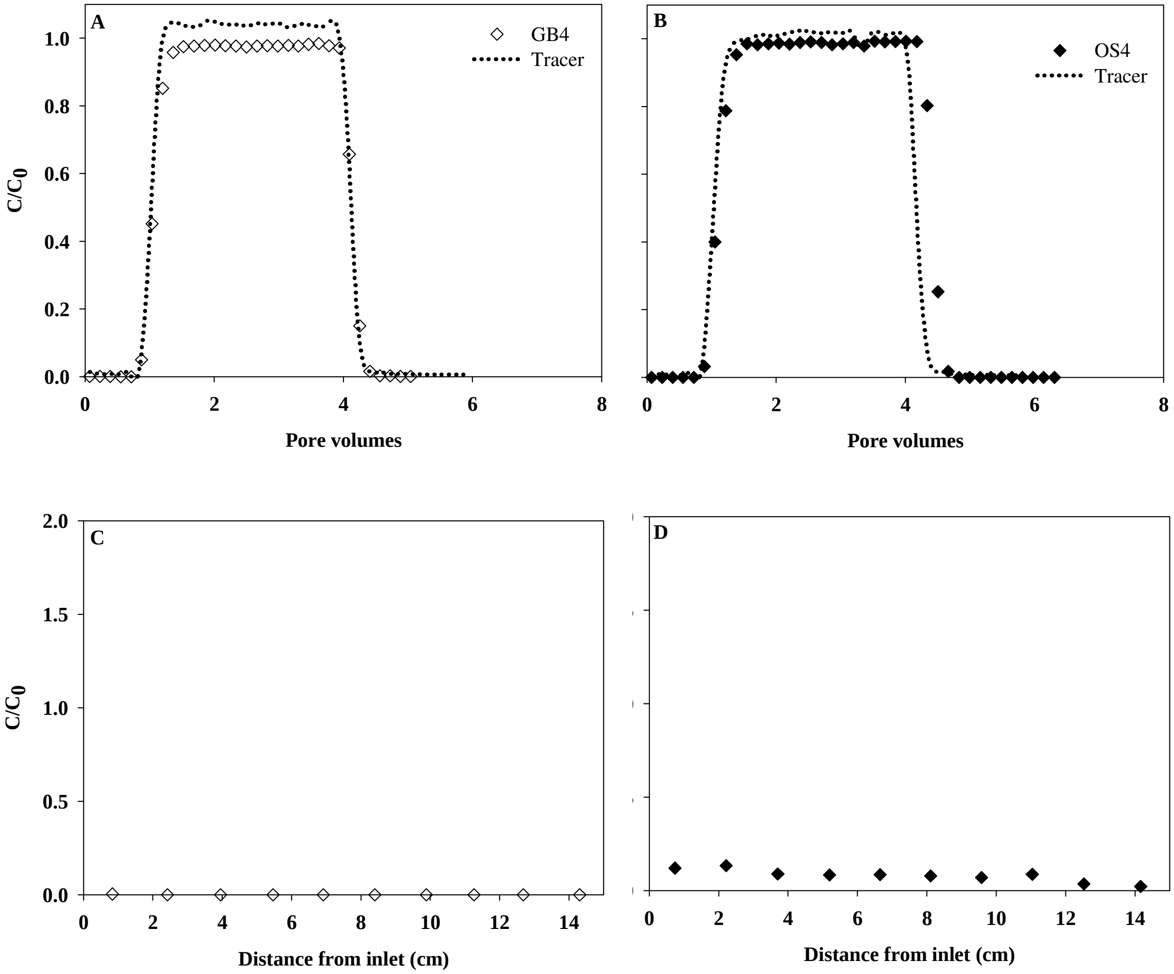

Figure 4.4: Measured nC_{60} breakthrough curves (A and B) and retention profiles (C and D) in water-saturated columns packed with either 40-50 mesh glass beads (open symbols) or Ottawa sand (solid symbols), respectively. Aqueous nC_{60} suspensions were prepared in DI water, and were applied at a Darcy velocity of 2.8 m/d.

4.2.3 Batch Retention Experiments

To independently assess nC_{60} retention behavior, batch reactor experiments were conducted in which aqueous suspensions of nC_{60} were gently mixed with Ottawa sand and glass beads for a period of 3h. The resulting nC_{60} retention data are plotted in Figure 4.5 as concentration of nC_{60} associated with the solid phase (*S*) versus the final aqueous phase concentration (*C*). In the presence of 1.0 mM $CaCl_2$, Ottawa sand exhibited the greatest retention capacity, which was most closely fit (r^2 = 0.97) by the Freundlich sorption model ($S = K_F C^N$), where K_F (1.37) provides a measure of the sorption or

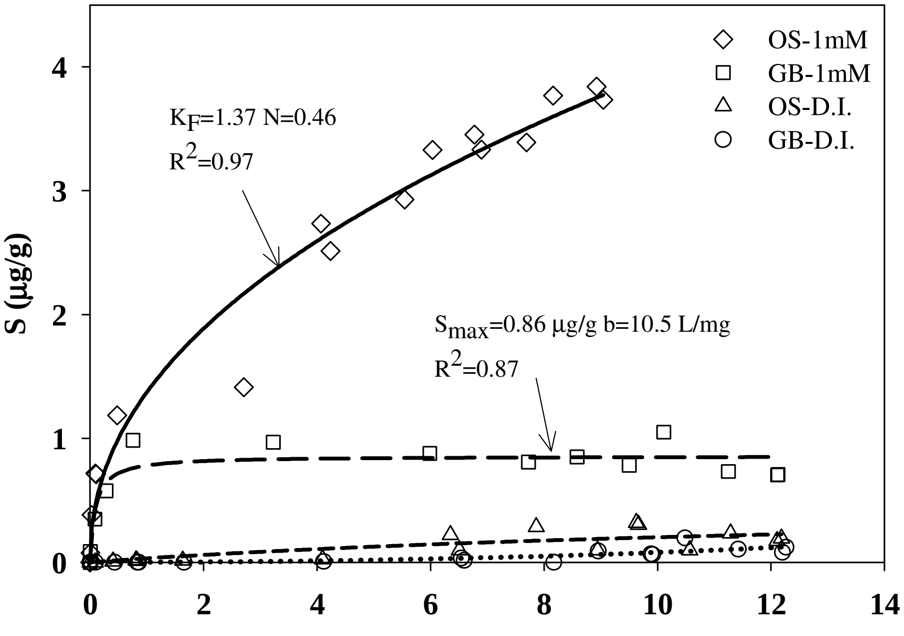

Figure 4.5: Retention of nC_{60} aggregates in batch reactors containing either glass beads (GB) or Ottawa sand (OS) in 1.0 mM $CaCl_2$ aqueous solution or DI water.

retention capacity of the solid phase and N (0.46) characterizes the intensity of interaction between nC_{60} particles and the solid surface. In the absence of background electrolyte, retention of nC_{60} by Ottawa sand decreased substantially, yielding a solid phase concentration of 0.07 ug/g at the applied concentration of 2.3 mg/L, consistent with magnitude of nC_{60} retention observed in column experiment OS-4 (Figure 4.4D). As expected from the column results, batch retention of nC_{60} by the glass beads was considerably less than that measured for Ottawa sand. In the presence of 1.0 mM $CaCl_2$, nC_{60} retention by the glass beads conformed to the Langmuir sorption model ($S = S_m bC/[1+bC]$), where S_m (0.86 ug/g) is the monolayer or limiting sorption capacity and b (10.5) is the ratio of the adsorption and desorption rate coefficients. In the absence of background electrolyte, retention nC_{60} by glass beads was negligible, consistent with the retention profile observed in column experiment GB-4 (Figure 4.4C).

4.2.4 Effects of Flow Rate and Grain Size

Seventeen more column experiments were performed to quantify the transport and retention of nC_{60} aggregates in OS as a function of pore-water velocity and sand grain size. The experimental conditions are summarized in Table 4.1.

Prior to the nC_{60} pulse injection, the tracer tests were conducted for each size fractions at two pore water velocities (1 and 8 m/d) to assess the water flow and hydrodynamic dispersion. The resulting BTCs were simulated using the similar approach described previously. The experimental and fitting results were summarized in Table 4.2.

The fitted retardation factors (R_F) for all of the tracer studies were equal to 1.03 ± 0.02 and the shape of all tracer BTCs were symmetrical, indicating that the physical nonequilibrium processes (e.g., immobile water) did not contribute to nC_{60} retention even in finer sands (e.g., 100-140 mesh OS). The calculated Reynolds number (*Re*) for all experiments were at least 2 orders magnitude less than the laminar flow limit. As anticipated, the hydrodynamic dispersivity was as small as 0.064 and 0.058 cm for 8 and 1 m/d, respectively, and relative constant as a function of grain size.

Table 4.2: The experimental and fitting results for tracer tests in various size fractions and at the pore velocity of 8 and 1 m/d. Trace breakthrough curves s were fitted using CXTFIT.

Size (mesh)	8 m/d				1 m/d			
	α_D[a] (cm)	P_e[b]	R_e[c]	R_F[d]	α_D (cm)	P_e	R_e	R_F
20-30	0.064	236.9	0.027	1.03	0.055	274.3	0.004	1.01
40-50	0.064	238.4	0.013	1.03	0.057	265.1	0.002	1.06
80-100	0.063	243.3	0.007	1.04	0.067	224.9	0.001	1.02
100-140	0.065	236.1	0.005	1.03	0.052	291.1	0.001	1.04

[a] hydrodynamic dispersivity. [b] Peclet number. [c] Reynold number. [d] retardation factor.

Effluent BTCs of nC_{60} in transport experiments conducted at pore-water velocities of 8 m/d and 1 m/d are shown in Figure 4.6A and 4.6B, respectively. At the higher flow rate (e.g., 8 m/d), nC_{60} were observed to breakthrough columns in all size fractions of OS except 100-140 mesh (e.g., exps 100140F-1,2) with an introduction pulse width of 5 PV. The breakthrough time increased from 1.1 to 2.5 PV when the sand grain size decreased from 20-30 to 80-100 mesh. In columns packed with 20-30 and 40-50 mesh OS, the concentration plateau was developed near the end of pulse injection, indicating that steady state was reached, while the nC_{60} relative concentrations in 80-100 mesh OS monotonically increased during the pulse introduction. Under the slower flow condition (e.g., 1 m/d), the breakthrough of nC_{60} was only observed in column experiments conducted with 20-30 or 40-50 mesh OS size fractions. While a 5-PV pulse injection led to the development of concentration plateau in 20-30 mesh OS, a pulse width of at least 9 PV was required to reach the steady state in 40-50 mesh OS. Consistent with previous results, once breakthrough, BTCs of nC_{60} were asymmetric with a gradually ascending portion and a sharply declining distal, implying the retention of nC_{60} in OS was irreversible. The delay of nC_{60} breakthrough time in the same size fractions of OS was increase at lower flow rate. For instance, nC_{60} broke through columns packed with 40-50 mesh OS at 1.5 PV when the pore water velocity was 8 m/d, while a breakthrough time at 3.2 PV was observed in the same size fraction when experiments were performed at the pore velocity of 1 m/d. Once nC_{60} breaking through columns, the sharp reduction feature was shared with all size fraction OS, indicating the detachment of nC_{60} was negligible in OS.

The retention profiles of nC_{60} aggregates, expressed as the retained mass normalized to the total injected nC_{60} mass per gram of dry soil, as a function of distance from the column inlet at the pore velocity of 8 and 1 m/d are shown in Figures 4.7A and 4.7B, respectively. Similar to the previous results (e.g., OS-1), relatively flat retention

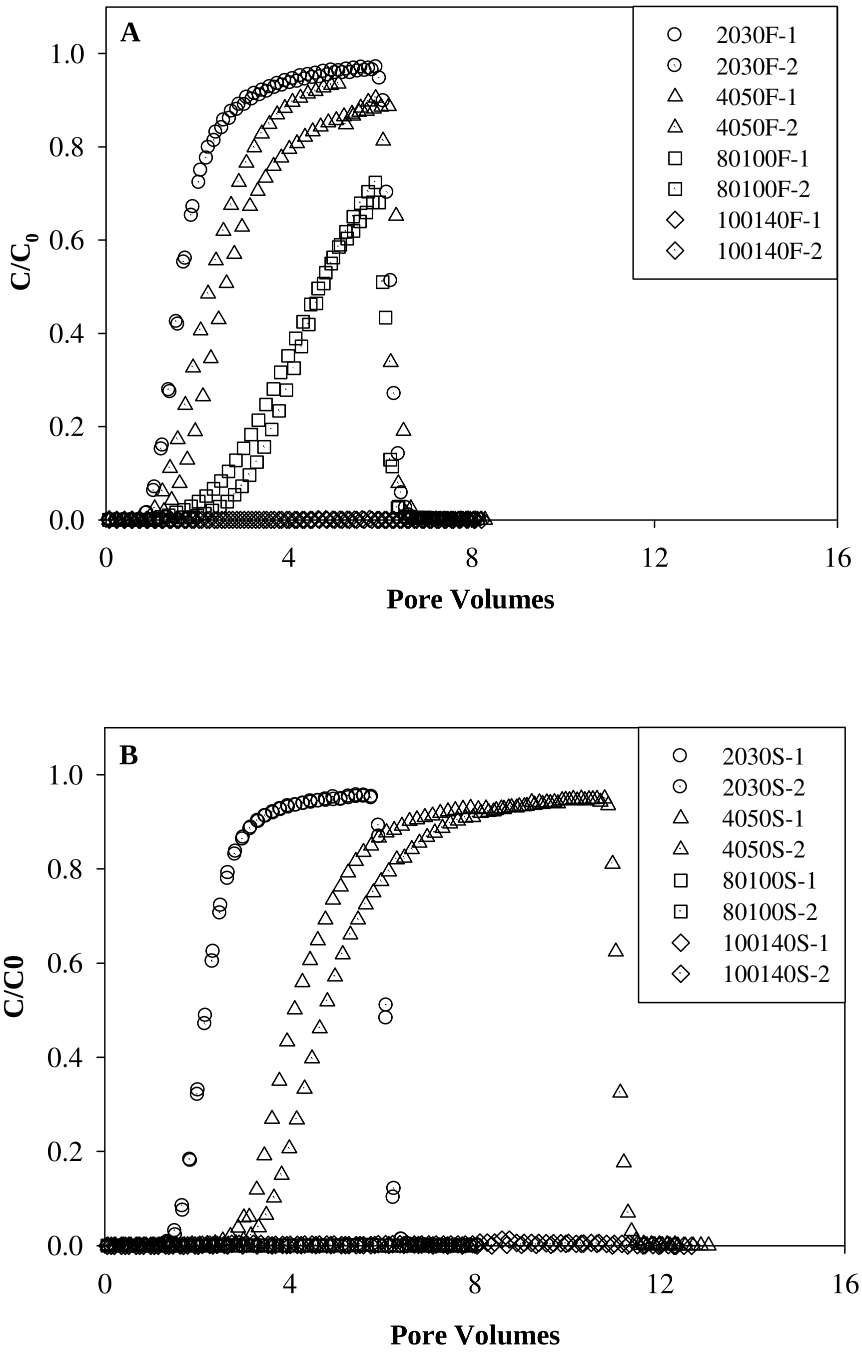

Figure 4.6: Measured nC_{60} breakthrough curves in water-saturated columns packed with various size fractions of Ottawa sands at a pore velocity of 8 m/d (A) and 1 m/d (B), respectively. Aqueous nC_{60} solutions contained 1.0 mM $CaCl_2$, buffered to pH 7 with 0.065 mM $NaHCO_3$.

profiles were observed for experiments conducted at 8 and 1 m/d when the breakthrough of nC_{60} in columns was observed, indicating the transport of nC_{60} in OS was affected by retention capacity filling processes. For those experiments without measurable breakthrough of nC_{60} (i.e., 80100S-1,2, 100140S-1,2, and 100140F-1,2), nC_{60} concentrations in solid phase were generally concentrated near the column inlet and nonmonotonically decreased with distance. In those columns, the presence of concentration plateau and successive descending portions in retention profiles indicated that the retention capacity of Ottawa sands had not fully reached. A simple comparison of the flat nC_{60} retention profiles in the same OS size fraction revealed that the retention capacity of OS was flow rate dependent: the slower the flow rate, the higher the retention capacity, which was not consistent with the findings in Espinasse et al. (2007).

Complete retention of nC_{60} in 100-140 mesh OS was observed in experiments both conducted at 8 and 1 m/d (Figure 4.6). To further investigate the role of electrostatic interactions in nC_{60} retention, a transport experiment of nC_{60} with DI water (i.e., no background electrolyte) was conducted in the 100-140 mesh fraction of OS. The resulting nC_{60} effluent BTCs and retention profiles are shown in Figure 4.8A and 4.8B, respectively. Similar to the experimental results obtained in 40-50 mesh Ottawa sands with DI water (Figure 4.4), nC_{60} effluent BTCs matched with that of non-reactive tracer and less than 7% of the injected nC_{60} mass was recovered from the solid phase. These data suggested that the physical straining did not significantly contribute to the retention of nC_{60} in finer sands, but further strengthened the importance of physicochemical

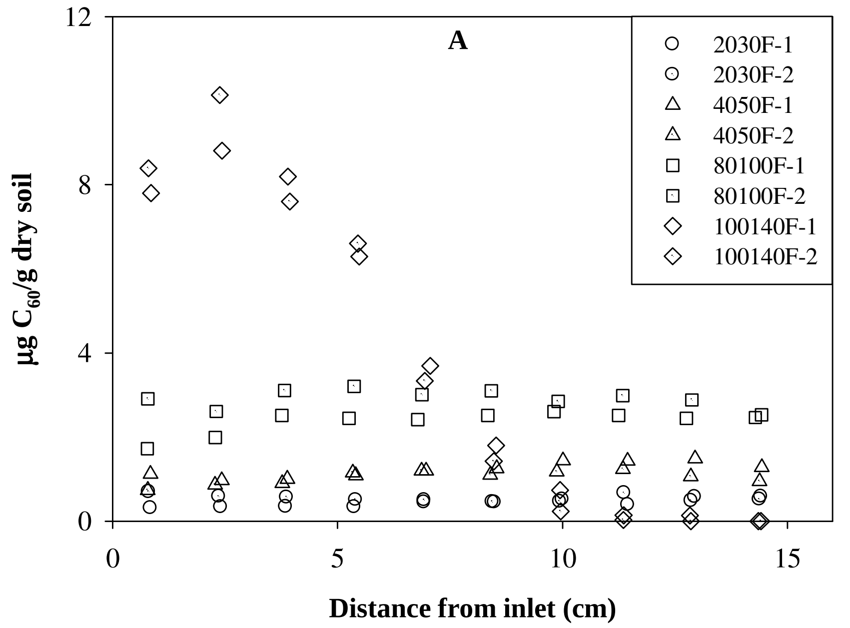

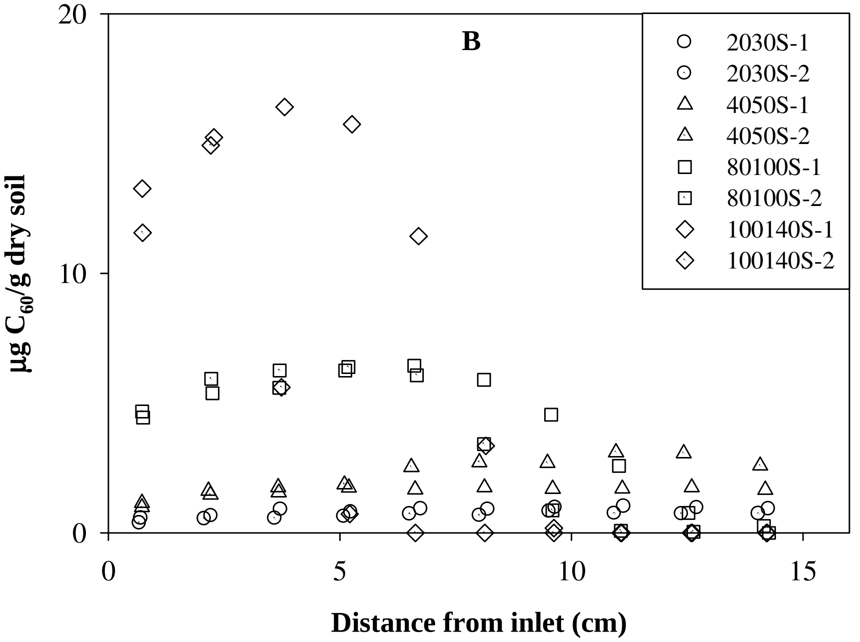

Figure 4.7: Measured nC_{60} retention profiles in water-saturated columns packed with various size fraction of Ottawa sands at a pore velocity of 8m/d (A) and 1m/d (B), respectively. Aqueous nC_{60} solutions contained 1.0 mM $CaCl_2$, buffered to pH 7 with 0.065 mM $NaHCO_3$.

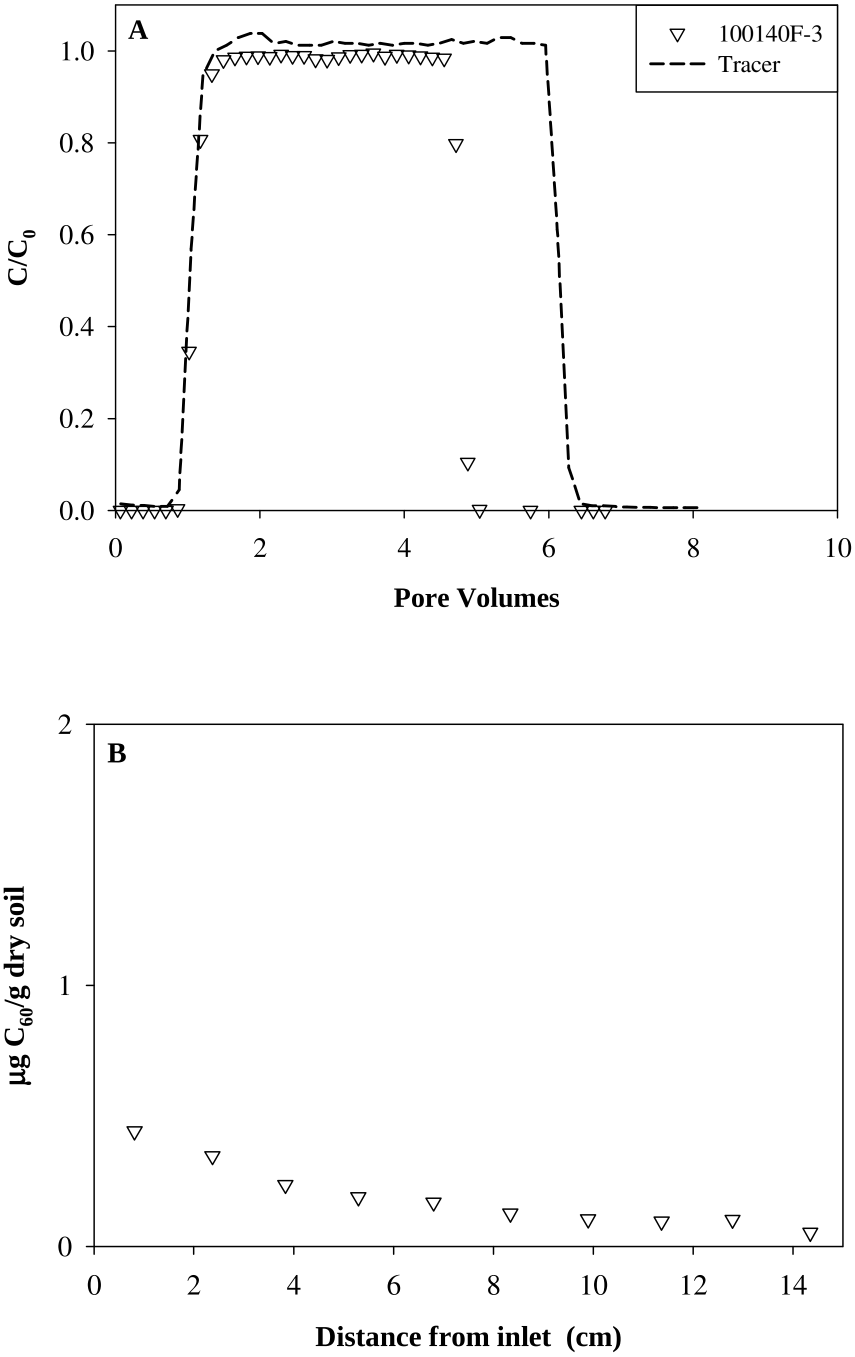

Figure 4.8: Measured nC_{60} breakthrough curves (A) and retention profiles (B) in water-saturated columns packed with 100-140 mesh. Aqueous nC_{60} suspensions were prepared in DI water, and were applied at a pore velocity of 8 m/d.

interactions on nC_{60} transport in water-saturated sands.

Clean-bed filtration theory has been successfully used to interpret colloid transport data (Bradford et al., 2009) and tentatively used in all previous nC_{60} transport studies conducted to date (Brant et al., 2005a; Cheng et al., 2005; Espinasse et al., 2007; Lecoanet and Wiesner, 2004; Lecoanet et al., 2004). The findings in this study clearly support the dominant contribution of physicochemical interactions to nC_{60} retention in OS. However, as asymmetrical BTCs were observed in all cases, and retention profiles did not exhibit exponential decay, both of which contradict clean-bed filtration theory. Thus, simulations using the clean-bed filtration theory did not accurately describe the effluent concentration profiles or retention profiles, which was verified by my collaborators at Tufts University.

4.3 Summary and Conclusions

A series of column experiments was initially conducted to investigate the transport and retention of nC_{60} in columns packed with either 40-50 mesh glass beads or Ottawa sands at a pore water velocity of 8 m/d. In addition to the nC_{60} BTCs, expressed as relative effluent concentrations versus pore volumes injected, columns were dissected at the conclusion of each experiment and retained nC_{60} aggregates were extracted from solid phase to obtain retention profiles. At a pore water velocity of 8 m/d and in the presence of 1.0 mM $CaCl_2$, effluent BTCs obtained for nC_{60} in 40-50 mesh glass beads and 40-50 mesh Ottawa sands exhibited an asymmetrical shape with a gradual increase portion during the pulse injection period and a sharp decreasing distal upon reintroduction of nC_{60}-free solution. These findings are distinct from nC_{60} effluent concentration data presented in previous studies, where a continuous pulse of nC_{60} was applied. The concentration of retained nC_{60} in glass beads monotonically decreased with distance, while retention profiles in Ottawa sands were relative constant, which suggests that the retention of nC_{60} in Ottawa sand was strongly influenced by retention processes. Retention of nC_{60} in the glass bead columns ranged from 8 to 49% of the introduced mass, while up to 77% of the mass was retained in the Ottawa sand columns. These findings indicate that the nC_{60} surface interactions were considerably lower for glass beads compared to Ottawa sands. Independent batch retention experiments revealed that nC_{60} attachment processes were conformed to nonlinear isotherm models (e.g., Langmuir).

The effects of flow rate and grain size on nC_{60} transport and retention under water-saturated conditions were further studied in column experiments conducted at two pore-water velocities (1 and 8 m/d) and with four size fractions of Ottawa sand (20-30, 40-50, 80-100, and 100-140 mesh). Generally, the nC_{60} breakthrough concentrations decreased with increasing grain size or flow rate. At the higher flow rate complete retention of nC_{60} occurred for a 5-PV injection of nC_{60} in 100-140 mesh OS. At the lower flow rate complete retention of nC_{60} was observed even after a 10-PV injection of nC_{60} in either 80-100 or 100-140 mesh OS. All BTCs observed were asymmetrical, suggesting that the attachment of nC_{60} onto OS grains was not a reversible process, a feature that did not vary with flow rate or grain size. The retention profiles of nC_{60} in Ottawa sands were either relatively flat or nonmonotically decayed with distance. The fairly flat retention profiles, obtained as the breakthrough of nC_{60} from columns was observed, imply that the retention capacity of Ottawa sand was reached. The retention capacity of Ottawa sand to nC_{60} particles increased with decreasing flow rate or mean grain size. The nC_{60} BTCs and retention profiles at low ionic strength (e.g., DI water alone) support the hypothesis that the retention of nC_{60} was dominated by physicoelectrical interactions between nC_{60} and quartz sands as opposed to physical straining.

CHAPTER 5*

INFLUENCE OF ELECTROLYTE SPECIES AND CONCENTRATION ON THE AGGREGATION AND TRANSPORT OF FULLERENE NANOPARTICLES IN QUARTZ SANDS

5.1 Introduction

Commercial production and use of engineered nanomaterials is anticipated to increase dramatically over the next several decades (Maynard et al., 2006), which inevitably will lead to their release of them into the environment. Recent studies have shown that pure C_{60} can be readily dispersed into water using organic solvents or long-term mixing in water (Brant et al., 2006; Deguchi et al., 2001b; Fortner et al., 2005). Stable nanoparticles (nC_{60}) in such suspensions possess negative surface charges, and have been found to be toxic to microbes, fish, and human cell lines (Fortner et al., 2005; Oberdorster, 2004a; Sayes et al., 2005). In addition, naturally occurring organic matter is capable of further stabilizing suspensions and facilitating nC_{60} transport through water saturated porous media (Chen and Elimelech, 2007; Espinasse et al., 2007; Xie et al., 2008), which raises concerns about the extent of nC_{60} impacts on humans and ecosystem through subsurface pathways, including groundwater transport and recharge to surface water bodies. Thus, studies on the fate and transport of nC_{60} in groundwater systems are

---

*The data in this chapter is partially published in Environmental Toxicology and Chemistry, vol. 27, page 1860-1867 in 2008.

needed to develop a more complete understanding of the mechanisms governing these processes.

Similar to colloidal particles, an important feature of nanoparticles is their agglomeration in presence of salts, which substantially impacts their fate and transport in subsurface. Brant et al. (2005a) evaluated the effects of NaCl concentration on nC_{60} aggregation behavior and observed that the size of nC_{60} (initial mean diameter of 168 nm) increased with ionic strength, confirming that the electrostatic interactions arising from negative surface charge were the principle mechanism for suspension stability (Deguchi et al., 2001b). Another study by the same research group (Brant et al., 2005b) involved batch experiments to study effects of electrolyte species (e.g., Na^+ and Ca^{2+}) on the zeta potential of nC_{60} and found a general decreasing trend (more negative) with increasing $CaCl_2$ concentration, except at 0.0001 M, for which the nC_{60} surface charge was positive. Zeta potentials of nC_{60} were calculated based on the Smoluchowski equation, which ignores the contribution of particle sizes by setting Henry's function to 1.5 (Deshiikan and Papadopoulos, 1998). However, the effects of electrolyte species and concentration on nC_{60} aggregation have not been systematically studied.

Several studies have been conducted to address nC_{60} transport in groundwater, which was commonly simulated in laboratories using a column packed with water-saturated glass beads (Brant et al., 2005a; Espinasse et al., 2007; Lecoanet and Wiesner, 2004; Lecoanet et al., 2004) or quartz sands (Cheng et al., 2005). A pseudo steady-state effluent concentration was achieved in all of these transport experiments, which was interpreted using clean-bed filtration theory (Yao et al., 1971). However, all of the experiments conducted to date, except those of Espinasse et al. (2007), were conducted with 10 mM NaCl as background electrolyte, which is not representative of the chemical composition of groundwater. Espinasse et al. (2007) studied nC_{60} transport in glass beads as a function of electrolyte species (Na^+, NH_4^+, Ca^{2+}, and Mg^{2+}) and concentration (10-600 mM for NaCl, 10 mM for Ca^{2+} and Mg^{2+}). The authors observed that the nC_{60} retention increased with ionic strength, and that Ca^{2+} had a greater impact on nC_{60} retention than Na^+ at the same ionic strength, supporting the hypothesis that physicochemical interactions played an important role in nC_{60} deposition. However, nC_{60} retention mechanisms in porous media were not addressed in any of these studies.

In the present study, the influence of electrolyte species and concentration on the aggregation and transport of nC_{60} in water-saturated quartz sands was investigated using a combination of batch and column studies. The mean diameter, size distribution and surface charge of nC_{60} particles were quantified in aqueous suspensions containing either NaCl or $CaCl_2$ as background electrolyte. A series of 1-D column studies was performed to assess the transport, deposition and recovery of nC_{60} particles in either 40-50 mesh (d_{50} = 0.335 mm) or 100-140 mesh (d_{50} = 0.125 mm) quartz sand. Effluent concentration data and solid-phase retention profiles were obtained after pulse injections (5 PVs) of nC_{60} suspensions prepared with either NaCl or $CaCl_2$ at ionic strengths of 3.05 and 30.05 mM. For conditions that yielded near complete retention of the introduced nC_{60} particles, a prolonged elution phase was conducted to evaluate the ability of increased flow rate, reduced ionic strength, increasing pH, and the addition of a cosolvent or surfactant to recover deposited nC_{60} particles. Experimental data are interpreted within the context of particle-particle and particle-surface electrostatic interactions, providing a mechanistic framework to explain the transport, deposition and release of nC_{60} in water-saturated quartz sands.

5.2 Results and Discussion

5.2.1 Characterization of nC_{60} Aggregate Suspensions

The mean diameter and size distribution of nC_{60} aggregates in aqueous suspension were systematically studied in batch experiments as a function of electrolyte species and concentration, solution addition rate, mixing sequence and target nC_{60} concentration. In general, the diameter of nC_{60} aggregates increased with electrolyte concentration (Figure 5.1A), in agreement with previous reports of nC_{60} aggregate formation and stability behavior (Brant et al., 2005a; Chen and Elimelech, 2006; Fortner et al., 2005). At low electrolyte concentrations ($\leq$ 1.0 mM), the diameter of nC_{60} aggregates was consistent with the initial stock suspension value of 92 nm regardless the electrolyte species, solution addition rate, or mixing sequence. At electrolyte concentrations greater than 1.0 mM, however, nC_{60} aggregate size was dependent upon electrolyte species and solution addition sequence, especially in the presence of $CaCl_2$. For example, when the concentration of $CaCl_2$ was increased from 1 to 100 mM the mean nC_{60} aggregate diameter increased from 92 nm to more than 500 nm regardless of mixing rate and

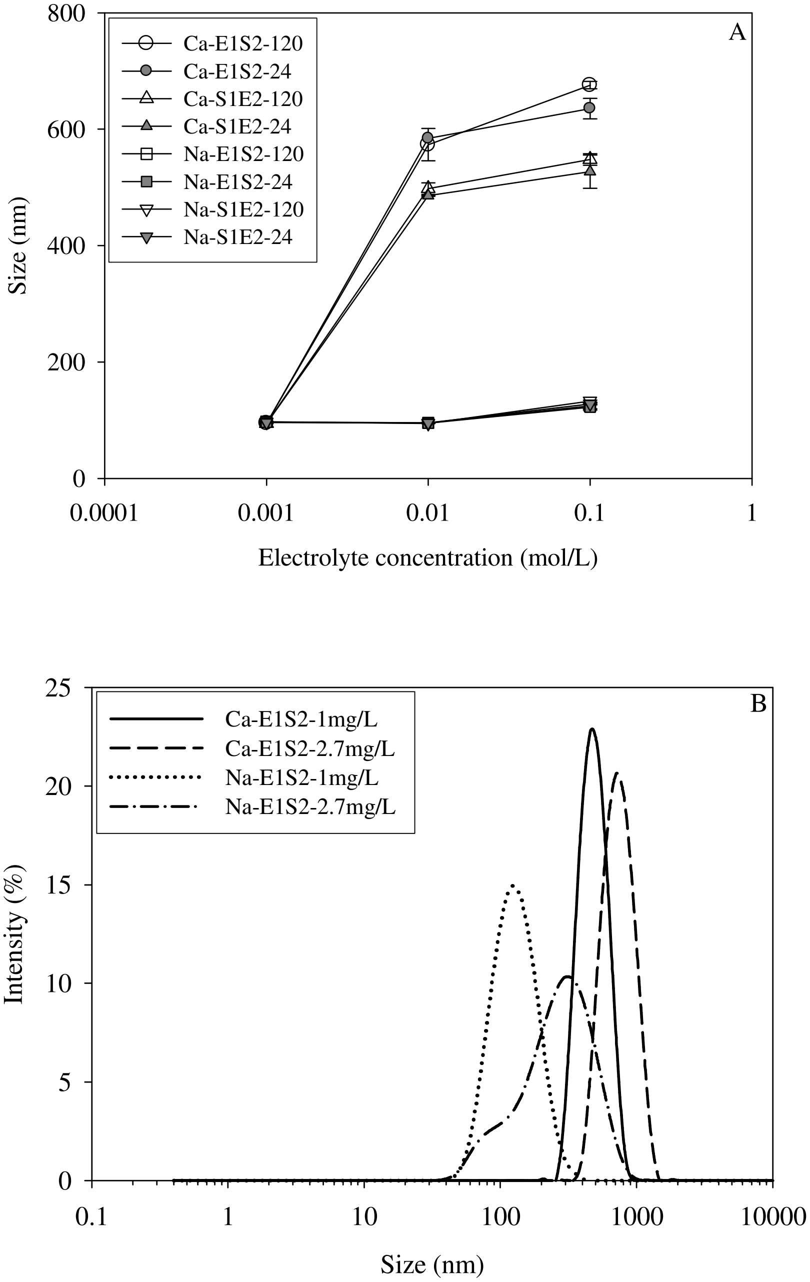

Figure 5.1: Effect of electrolyte concentration, suspension addition rate (24 or 120 mL/min), and dilution sequence (E1S2 or S1E2) on (A) the mean nC_{60} aggregate diameter and (B) the intensity-weighted size distribution of nC_{60} aggregates as a function of target concentration (1.0 and 2.7 mg/L). E1S2 refers to the sequence of adding the electrolyte solution to the nC_{60} stock suspension, while S1E2 refers to the sequence of adding the nC_{60} stock suspension to the electrolyte solution. Error bars represent the standard deviation of duplicate or triplicate measurements.

sequence (Figure 5.1A). The corresponding nC_{60} aggregate growth factors, defined as the ratio of the aggregate diameter measured in the prepared aqueous suspension to that of the initial stock suspension, ranged from 5.3 to 7.3 in the presence of 10 and 100 mM $CaCl_2$ (Figure 5.1A). The nC_{60} aggregate diameter in aqueous suspension was dependent upon the mixing sequence; with addition nC_{60} stock suspension to aqueous $CaCl_2$ solutions (referred to E1S2) resulting in an nC_{60} aggregate diameter that was approximately 25% greater than when the addition sequence was reversed (referred to S1E2). In the presence of NaCl, changes in nC_{60} aggregate diameter as a function of electrolyte concentration and mixing condition were relatively minor (Figure 5.1A). Over the range of NaCl concentrations considered (1 to 100 mM), the mean nC_{60} aggregate diameter increased from 92 to 135 nm, corresponding to aggregate growth factors of less than 1.4.

Representative intensity-weighted nC_{60} aggregate size distributions are shown in Figure 5.1B for suspensions prepared by addition of nC_{60} stock suspensions to aqueous solutions (E1S2 sequence) containing either NaCl or $CaCl_2$ at an ionic strength of 30.05 mM and an addition rate of 120 mL/min. Interestingly, the mean aggregate diameter was dependent upon the target nC_{60} concentration (either 1.0 or 2.7 mg/L), with a shift toward larger aggregate clusters at the higher target concentration. These trends were less pronounced at lower ionic strength, but nevertheless, demonstrate the sensitivity of the aggregation process to different suspension preparation methods. The shape of the size distribution of nC_{60} aggregates in NaCl at a target concentration of 2.7 mg/L is indicative of a bimodal distribution, with two distinct aggregates diameters of approximately 100 nm and 300 nm (Figure 5.1B). These findings suggest that the initial 100-nm diameter aggregates formed larger nC_{60} clusters or agglomerates in the presence of higher electrolyte and nC_{60} concentrations. We hypothesize that the nC_{60} aggregation or agglomeration process was enhanced at higher nC_{60} concentrations due to greater collision efficiency, consistent with the findings of Chen and Elimelich (Chen and Elimelech, 2006) who concluded that nC_{60} aggregation is a diffusion-controlled process.

The role of electrolyte species and concentration on nC_{60} aggregation behavior was evaluated using DLVO theory (Eq. 2.1 and 2.9). The resulting interaction energies between two nC_{60} aggregates as a function of distance are presented in Figure 5.2 for suspensions containing either NaCl or $CaCl_2$. Here, negative values represent a net attractive force, while positive values correspond to a net repulsive force. In the presence of $CaCl_2$ (Figure 5.2A), the energy minimum became more negative and approached the surface as the electrolyte concentration was increased, consistent with strong suppression of the EDL by divalent cations. Under these conditions, VDW attractive forces dominate, which lead to the formation of agglomerates consisting of multiple n-scale aggregates as shown in Figure 5.1. In the presence of NaCl, a large negative interaction energy minimum was maintained for all but the highest concentration considered (100 mM), while a small secondary minimum was observed at a separation distance of approximately 10 nm (Figure 5.2B). These findings indicate that a strong repulsive force existed between nC_{60} aggregates, consistent with the suspension stability and

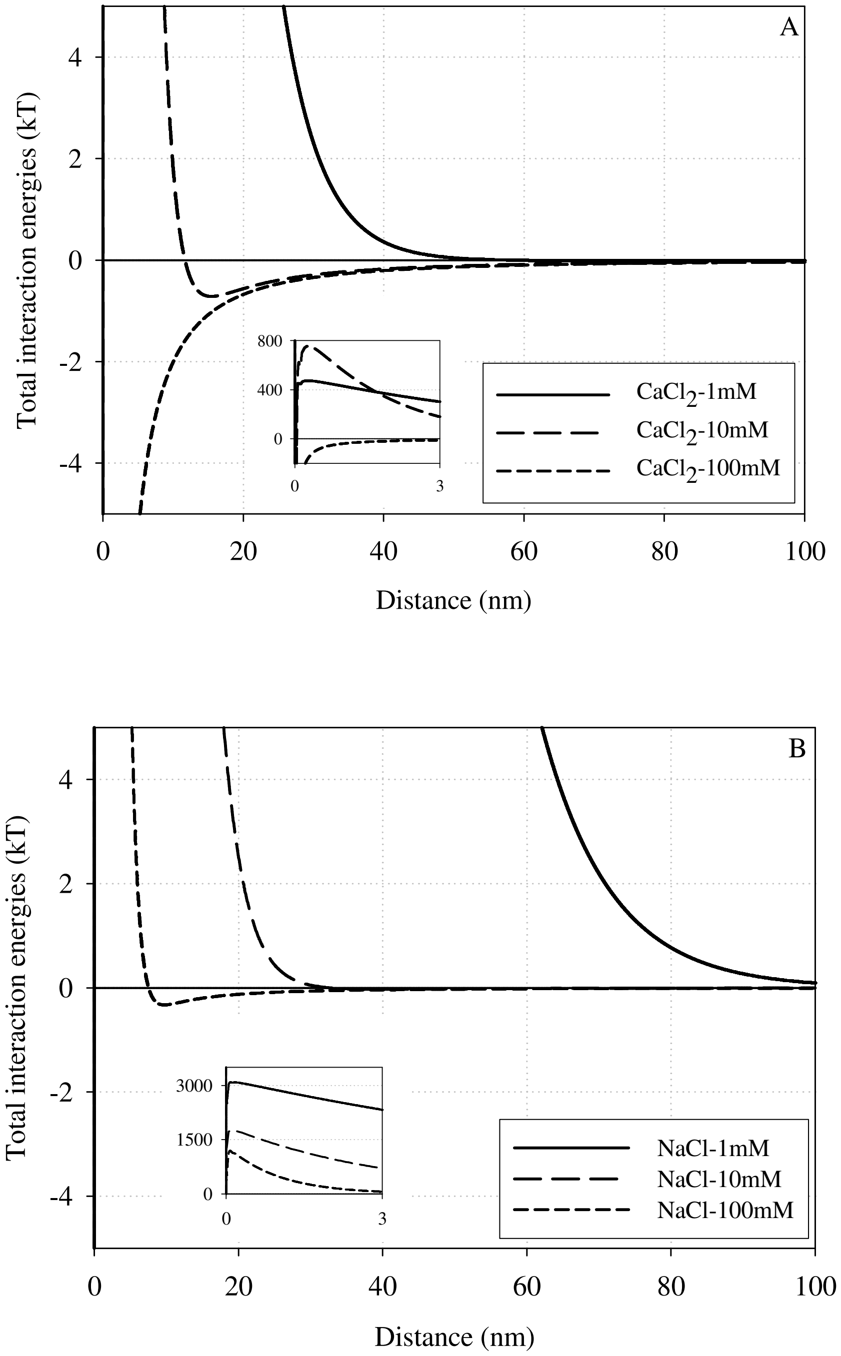

Figure 5.2: Interaction energies (E_i) between two nC_{60} aggregates as a function of (A) $CaCl_2$ and (B) NaCl concentrations at pH 7.

relatively constant diameter of nC_{60} aggregates observed over the range of NaCl concentrations considered (Figure 5.1).

To further explore the role of surface charge on the aggregation process, the zeta potential of nC_{60} aggregates was measured as a function of electrolyte species and concentration (Figure 5.3). As the concentration of both NaCl and $CaCl_2$ was reduced, the surface charge (electrophoretic mobility) of the nC_{60} aggregates became more negative, trends that are consistent with previous findings (Brant et al., 2005a; Chen and Elimelech, 2006). In the presence of 1 and 10 mM $CaCl_2$, the zeta potential of nC_{60}

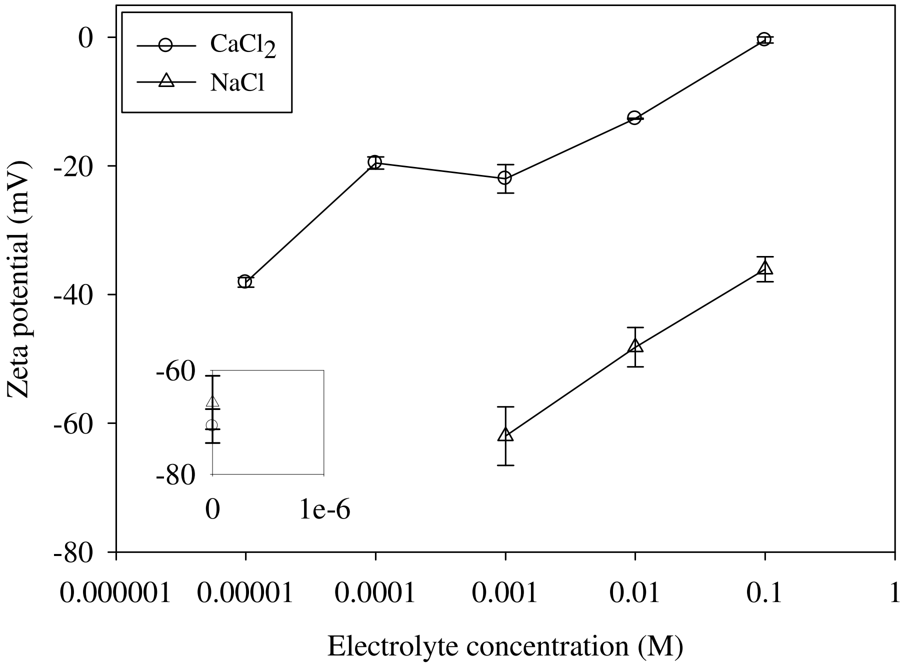

Figure 5.3: Zeta potential of nC_{60} aggregates as a function of electrolyte concentration in 1 mg/L suspensions containing either $CaCl_2$ or NaCl. The inset shows the zeta potential of nC_{60} in DI water, while the error bars represents the standard deviation of triplicate measurements.

aggregates was similar to the values reported by Brant et al. (Brant et al., 2005b). Although the zeta potential of nC_{60} generally became more negative as the concentration of $CaCl_2$ decreased, a shoulder was observed at a concentration of 0.1 mM. Although much more pronounced, Brant et al. (Brant et al., 2005b) observed a charge reversal +18 mV at the same $CaCl_2$ concentration (0.1 mM), which was attributed to an excess of counter-ions surrounding the charged aggregate surface. In the presence of NaCl, the zeta potential of nC_{60} aggregates was considerably more negative (by approximately -40 mV) compared to $CaCl_2$ over the same ionic strength range (Figure 5.3). This difference has been attributed to the stronger screening effect of Ca^{2+} on nC_{60} surface charge than that of Na^+ and may also indicate specific adsorption of Ca^{2+} ions on the surface of nC_{60} aggregates (Brant et al., 2005b).

5.2.2 Effects of Electrolyte Species and Concentration

A total of twelve column experiments (Table 5.1) were conducted to evaluate the effects of electrolyte species and concentrations on the transport and deposition of nC_{60} in Ottawa sands. Concentrations of nC_{60} aggregates transported through 40-50 mesh (MS) and 100-140 (FS) Ottawa sand (OS) in the presence of $CaCl_2$ at two ionic strengths (3.05 and 30.05 mM) are shown in Figure 5.4A. These data are expressed as effluent BTCs, where the relative concentration (C/C_0) is plotted against the number of pore volumes (PV) introduced. For comparison purposes, a representative BTC obtained for a non-reactive tracer (bromide) is also shown in Figure 5.4A. In the experiments conducted

Table 5.1: Experimental conditions for nC_{60} column studies conducted with two Ottawa sand size fractions (40-50 mesh or 100-140 mesh), two electrolyte species (NaCl or $CaCl_2$), and two ionic strengths (3.05 mM or 30.05 mM).

Column Identifier[a]	d_{50}[b] (mm)	θ_w[c]	IS[d] (mM)	Electrolyte	C_0[e] (mg/L)	d_a[f] (nm)	Retention (%)	MB[g] (%)
Ca-MS-3a	0.335	0.363	3.05	$CaCl_2$	3.03	121	36.2	103.8
Ca-MS-3b	0.335	0.367	3.05	$CaCl_2$	3.16	121	29.7	101.6
Ca-MS-30a	0.335	0.366	30.08	$CaCl_2$	2.60	989	99.7	93.9
Ca-MS-30b	0.335	0.369	30.08	$CaCl_2$	2.60	817	99.8	95.9
Ca-FS-3a	0.125	0.395	3.05	$CaCl_2$	3.27	117	99.9	101.6
Ca-FS-3b	0.125	0.391	3.05	$CaCl_2$	3.08	117	100	103.2
Ca-FSR-3a	0.125	0.391	3.05	$CaCl_2$	2.50	99.2	94.8	87.9
Ca-FSR-3b	0.125	0.389	3.05	$CaCl_2$	2.71	99.2	97.5	93.1
Ca-FSR-3c	0.125	0.392	3.05	$CaCl_2$	2.69	98.8	43.2	105.2
Na-MS-3	0.335	0.368	3.05	NaCl	3.12	92.7	0.04	98.4
Na-MS-30	0.335	0.368	30.05	NaCl	3.00	225	95.4	99.9
Na-FS-3	0.125	0.386	3.05	NaCl	2.96	92.6	7.7	102.7

[a] Ca = calcium chloride, Na = sodium chloride, MS = medium sand, FS = fine sand, FSR = fine sand recovery, 3 = ionic strength of 3.05 mM, 30 = ionic strength of 30.05 mM; [b] mean grain diameter; [c] volumetric water content; [d] ionic strength; [e] influent nC_{60} concentration; [f] mean nC_{60} aggregate diameter; [g] mass balance.

with 40-50 mesh OS at the lower ionic strength (Ca-MS-3a,b), nC_{60} aggregates appeared in the column effluent after approximately 1.4 PV and gradually increased to a maximum relative concentration of approximately 0.9 after introduction of 2.5 to 3.0 PV of the nC_{60} suspension. The small decline in effluent concentration observed in experiment Ca-MS-3b at approximately 5 PV occurred following a 12-hour period of flow interruption. Such behavior is characteristic of a rate-limited deposition or retention process, indicating that a local equilibrium assumption (LEA) is not valid for these experimental conditions. Following reintroduction of nC_{60}-free solution, the effluent

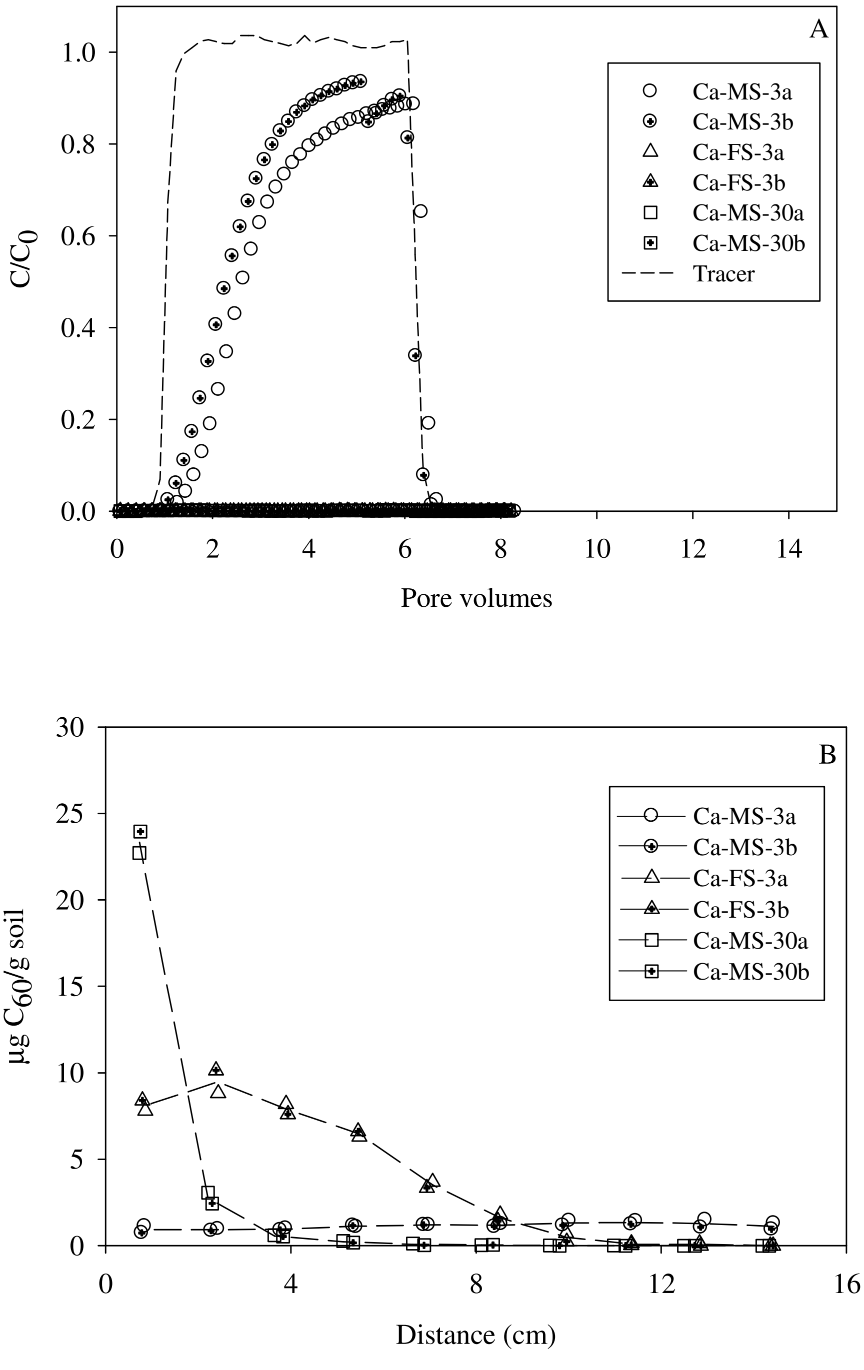

Figure 5.4: Effluent concentrations (A) and retention profiles (B) after pulse injections of nC_{60} aggregate suspensions in columns packed with either 40-50 mesh or 100-140 mesh Ottawa sand with $CaCl_2$ as the background electrolyte. The dotted line in (B) represents the predicted retention profile based on clean-bed filtration theory at an ionic strength of 30.08 mM.

concentration of nC_{60} declined sharply, approaching a value of zero at approximately 6.5 PV. The asymmetric shape of the BTC indicates that deposited nC_{60} aggregates were not released from the Ottawa sand. This irreversible attachment of nC_{60} aggregates is consistent with the findings of Chen and Elimelech (Chen and Elimelech, 2006) and in Chapter 4. In contrast to the experiments discussed above, when either the ionic strength was increased from 3.05 to 30.05 mM or the sand grain size was decreased from 0.335 to 0.125 mm, virtually no nC_{60} aggregates were detected in the column effluent (Figure 5.4A). At the conclusion of each column experiment, sand was removed in 1.5-cm increments and extracted with DI water to obtain nC_{60} aggregate deposition profiles (Figure 5.4B). As anticipated, nC_{60} aggregate retention was greatest near the column inlet and declined rapidly with distance for the column experiments conducted in 40-50 mesh Ottawa sand at an ionic strength of 30.05 mM. When the ionic strength was increased from 3.05 to 30.05 nM ($CaCl_2$), the mean diameter of the nC_{60} aggregates in the influent suspension increased from approximately 120 nm to 817 and 989 nm (Table 5.1). For 100-140 mesh Ottawa sand at an ionic strength of 3.05 mM, a more gradual decrease in aggregate retention with distance from the column inlet was observed. In contrast, the deposition profile obtained in 40-50 mesh Ottawa sand at an ionic strength of 3.05 mM was essentially flat, suggesting that a limiting retention capacity was achieved throughout the column, similar to the findings of in Chapter 4.

When NaCl was employed as the background electrolyte, much greater transport of nC_{60} aggregates was observed through Ottawa sand compared similar experimental

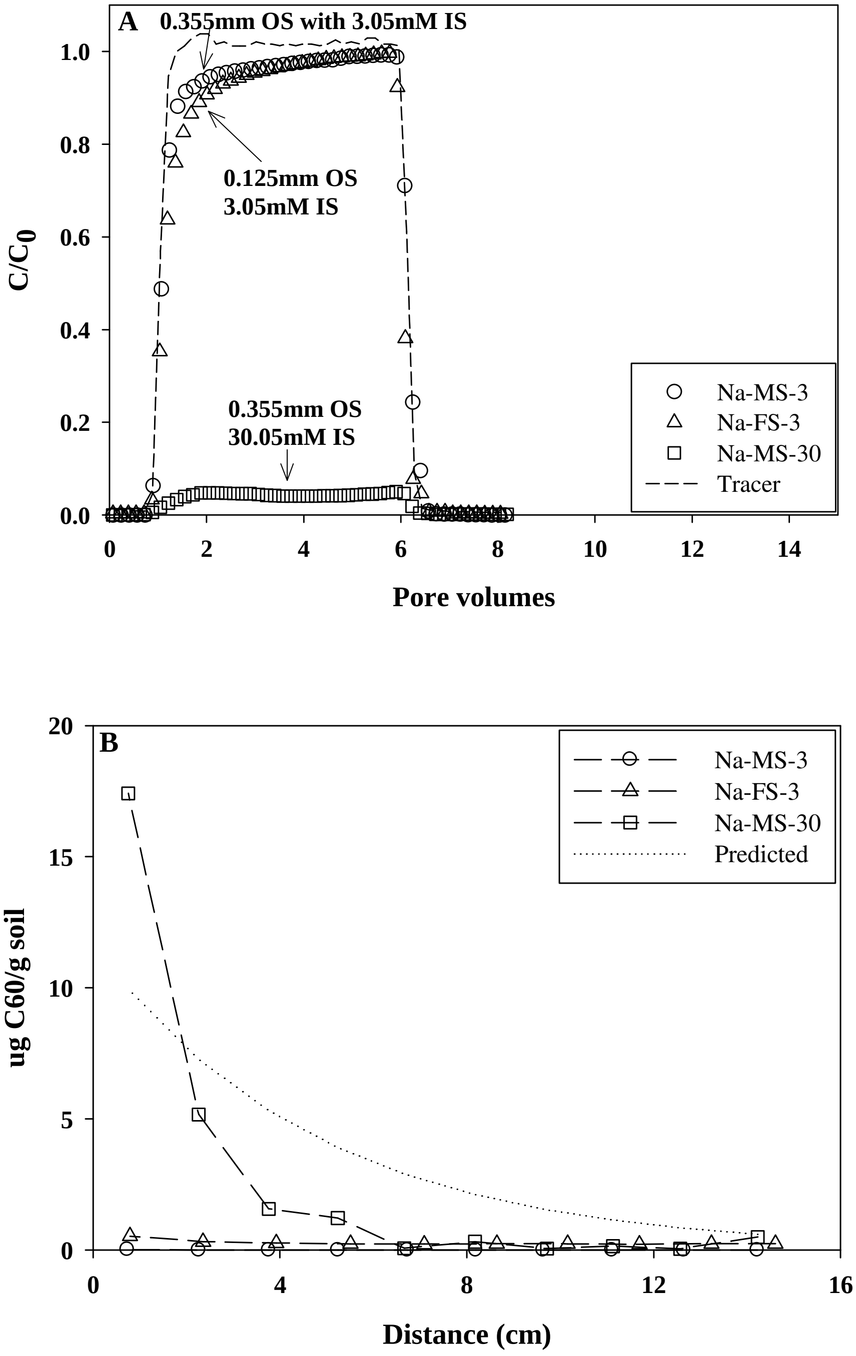

Figure 5.5: Effluent concentrations (A) and retention profiles (B) after pulse injections of nC_{60} aggregate suspensions in columns packed with either 40-50 or 100-140 mesh Ottawa sand with NaCl as the background electrolyte. The dotted line in (B) represents the predicted retention profile based on clean-bed filtration theory at an ionic strength of 30.05 mM

conditions with $CaCl_2$ (Figure 5.5A). For example, in both 40-50 and 100-140 mesh Ottawa sand at an ionic strength 3.05 mM (experiments Na-MS-3 and Na-FS-3), nC_{60} aggregates appeared in the column effluent at approximately 1 PV, rapidly increased to relative concentration of 0.8, and then gradually approached a relative concentration of 1.0 after 6 PV. Thus, the nC_{60} effluent BTCs under these conditions nearly coincided with the non-reactive tracer BTC (dashed line, Figure 5.5A). When the ionic strength was increased to 30.05 mM (NaCl), a small amount ($C/C_0 < 0.1$) of nC_{60} still appeared in the column effluent over the duration of the pulse injection. As anticipated from the BTCs, the retention on nC_{60} aggregates in experiments conducted at ionic strength of 3.05 mM (NaCl) were minimal, while the experiment conducted at the higher ionic strength (30.05 mM) exhibited considerable retention near the column inlet, and decreased rapidly with distance from the column inlet (Figure 5.5B). For all of the nC_{60} column experiments, the total mass balance recovery (i.e., the sum of mass retained and in column influent versus the introduced mass) ranged from 88 to 105%, with the majority of experiment yielding recoveries of greater than 95%.

Based on the column results, it is clear that both the ionic strength and species have dramatic impacts on the transport and retention of nC_{60} aggregates in quartz sand. To explore these effects in more detail, DLVO theory was used to calculate electrostatic interaction energy profiles for quartz sand and nC_{60} aggregates as a function of electrolyte species and concentration. The double layer energy (E_{edl}) and VDW attraction energy (E_V) were calculated using the approach of Guzman et al. (Guzman et al., 2006), which accounts for the small size of nC_{60} aggregates,

$$\begin{aligned}&E_{edl} = \pi\varepsilon_0\varepsilon_r\kappa(\psi_p^2+\psi_s^2)\times \\ &\int_0^a \left(-\coth\left[\kappa(d+a-a\sqrt{1-(r/a)^2}\right]+\coth\left[\kappa(d+a+a\sqrt{1-(r/a)^2}\right]\right)rdr + \\ &\int_0^a \frac{2\psi_s\psi_p}{\psi_s+\psi_p}\left(\csc h\left[\kappa(d+a-a\sqrt{1-(r/a)^2}\right]-\csc h\left[\kappa(d+a+a\sqrt{1-(r/a)^2}\right]\right)rdr\end{aligned} \tag{5.1}$$

$$E_V = -\frac{A}{6}\left[\frac{a}{d}+\frac{a}{d+2a}+\ln(\frac{d}{d+2a})\right] \tag{5.2}$$

where ε_0 is the permittivity of a vacuum, ε_r is the relative dielectric constant, and ψ_s and ψ_p are the surface potentials of the sand surface and nC_{60} aggregate, respectively. Under low ionic strengths, thickness of stern layer is very small. Thus, surface potential is approximately equal to zeta potential. The zeta potential of Ottawa sand was estimated to be -30 and -22 mV in CaCl2 solutions (Kaya and Yukselen, 2005) and -53 and -34.7 mV in NaCl solutions (Saiers and Lenhart, 2003) at ionic strengths of 3.05 and 30.05 mM, repectively, the nC_{60} zeta potential was measured (Figure 5.3), and the C_{60}-water-slilica Hamaker constant of 4.71×10^{-21} J was estimated from a C_{60}-C_{60} Hamaker number of 7.5×10^{-21} J (Chen and Elimelech, 2006). The resulting interaction energy profile for $CaCl_2$ at the lower ionic strength (3.05 mM) indicates a net repulsive force near the sand surface (~35 kT), which should prevent deposition of nC_{60} aggregates (Figure 5.6A). However, divalent cations are known to form complexes with negatively charged surface sites, thereby reducing the repulsive surface charge (Chen and Elimelech, 2006; Israelachvili, 1992), an effect not accounted for by DLVO theory. In addition, a small secondary attractive region (-0.5 kT) existed approximately 35 nm from the surface, which could

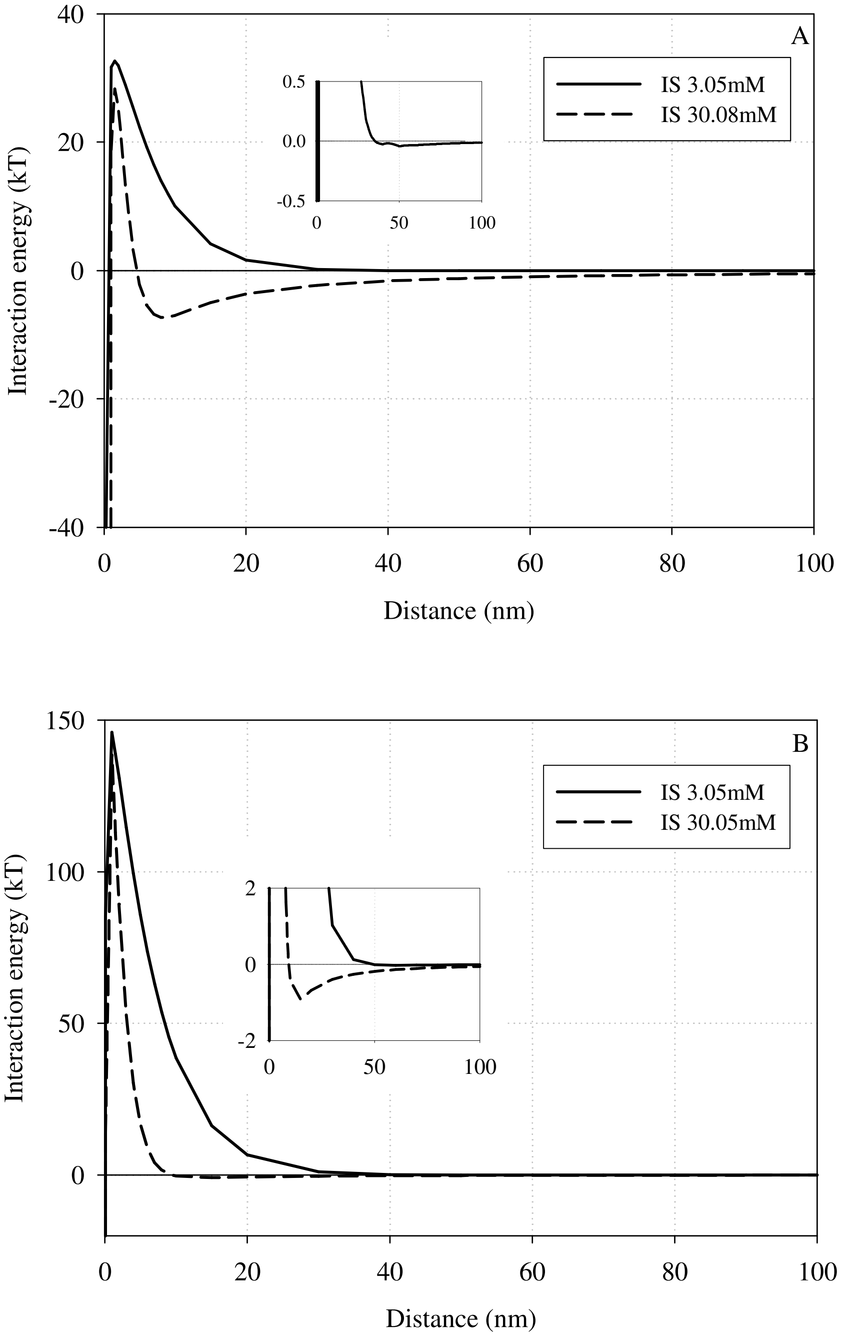

Figure 5.6: Interaction energies between an nC_{60} aggregate and quartz sand as a function of ionic strength in (A) $CaCl_2$ and (B) NaCl at ionic strengths of 3.05 and 30.05 or 30.08 mM. The inset shows the secondary minimum attractive region at an ionic strength of 3.05 mM.

also contribute to nC_{60} aggregate retention. At the higher ionic strength (30.05 mM), a primary attractive force existed near the surface, consistent with strong tendency for nC_{60} aggregates to be retained by Ottawa sand in the column studies (Figure 5.4). In the presence of NaCl at 3.05 mM, a large primary repulsive force (~ 145 kT) existed near the surface. This large repulsive force is consistent with the minimal retention of nC_{60} aggregate observed in column experiments Na-MS-3 and Na-FS-3 (Figure 5.5). At the higher ionic strength (30.05 mM), the primary repulsive force was reduced to approximately 125 kT, while the secondary attractive region became stronger, consistent the much greater retention of nC_{60} aggregates in experiment Na-MS-30 (Figure 5.5).

While the relatively flat or constant retention profiles obtained at low ionic strength (Ca-MS-3, Na-FS-3 and Na-MS-3) are consistent with a limiting retention capacity (Henry et al., 2007; Lecoanet et al., 2004), the sizable aggregate deposition observed near the inlet of column experiments Na-MS-30 and Ca-MS-30 is suggestive of clean-bed filtration theory, which typically yields an exponential decrease in particle retention with distance from the inlet (Elimelech and Omelia, 1990; Harvey and Garabedian, 1991). The predicted nC_{60} aggregate retention profiles from classical filtration theory, shown in Figures 5.4B and 5.5B as dotted lines, failed to capture the high solid-phase concentrations observed at the column inlet. While the observed discrepancies could be attributed to simplifications inherent to Eq 2.19, these data are also suggestive of particle straining (Bradford et al., 2002) or interactions with previously deposited aggregates. This line of reasoning is further supported by the considerably larger mean aggregates diameters (>500 nm) observed in batch suspensions prepared at higher ionic strength (30.05 mM, Figure 5.1).

To further evaluate nC_{60} aggregate retention, the fractional surface coverage was calculated from the effluent BTCs following the approach of Tufenkji et al. (Tufenkji et al., 2003),

$$\theta = \frac{\pi a^2 r_c q N_0 \int_0^t (1 - N/N_0) dt}{3L(1 - \theta_w)} \tag{5.3}$$

where, r_c is the radius of the collector or sand grains, q is the superficial or Darcy velocity, N_0 is the influent concentration expressed as the number of aggregates per mL, N is the effluent aggregate concentration, and L is the column length. At the lower ionic strength (3.05 mM), nC_{60} aggregate deposition approached limiting surface coverages of approximately 0.25% and 0.15% in the presence of $CaCl_2$ and NaCl, respectively (Figure 5.7). These relatively small surface coverages are consistent with both the stability of the nC_{60} aggregate suspension and the strong primary repulsive force at an ionic strength of 3.05 mM (Figures 5.2 and 5.6). At the higher ionic strength (30.05 mM), the fractional surfaces coverages were smaller than those at 3.05 mM, which was attributed to the larger aggregate size and the corresponding decrease in the applied aggregate concentration (N_0). This effect was less pronounced in the presence of NaCl because the change in nC_{60} aggregate diameter was relatively small, from 93 to 225 nm, with increasing ionic strength, while in the presence of $CaCl_2$ the aggregate diameter increased by more than 7-fold (Table 5.1). However, the coverages shown in Figure 5.7

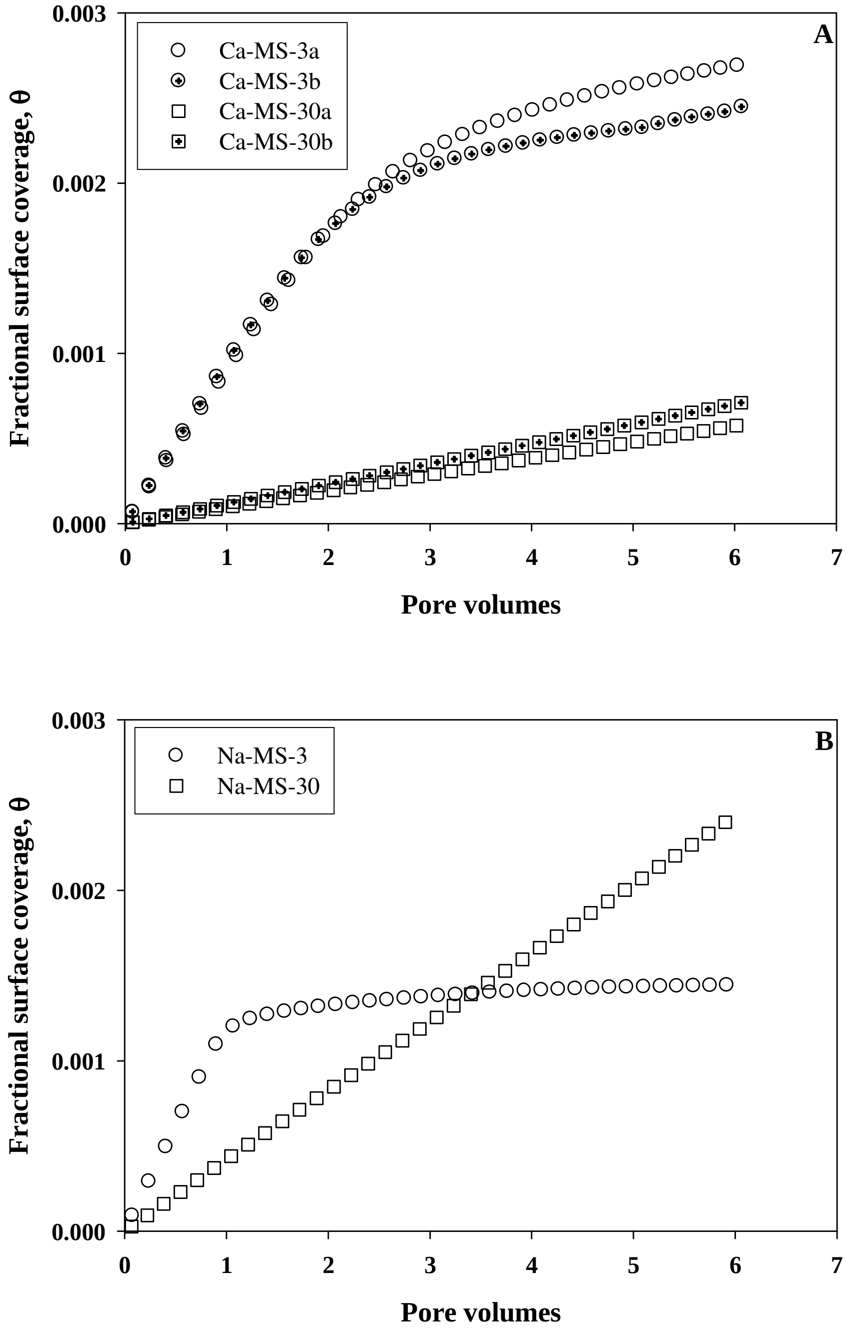

Figure 5.7. Change in the fractional surface coverage of 40-50 mesh Ottawa sand with time following the introduction of nC_{60} aggregates suspensions containing either (A) $CaCl_2$ or (B) NaCl at two ionic strengths.

at the higher ionic strength are representative of early time, and are likely to increase as more mass is applied to the column.

As noted previously, the sharp decrease in the distal portion of the nC_{60} BTCs is indicative of irreversible aggregate attachment (Figures 5.4 and 5.5). To further investigate the aggregate detachment process, a series of recovery experiments were conducted in which nC_{60} aggregates were deposited in columns packed with 100-140 mesh Ottawa sand with 1.0 mM $CaCl_2$, followed by changes in flow rate, ionic strength or solution pH, addition of cosolvent or surfactant. Approximately 1% of the deposited nC_{60} aggregates were removed when the column was flushed with DI water (IS ≈ 0) or 50% ethanol, while doubling the flow rate or flushing with 0.1% Tween 80 resulted in negligible recovery of deposited nC_{60} aggregates (Experiments Ca-FS-3a,b; effluent data not shown). In contrast, injection of DI water (3 PV) adjusted to pH 10.0 and 12.0 and containing no background electrolyte, resulted in substantial increases in nC_{60} effluent concentration, corresponding to 17.2 and 27.6% of deposited mass, respectively (Figure 5.8A). The final nC_{60} retention profile indicates a maximum solid phase concentration of approximately 3.5 μg/g (Figure 5.8B) compared to a maximum value of approximately 10 μg/g for the analogous deposition experiments (Figure 5.4B, Experiments Ca-FS-3a,b). Overall, the sequential injection of DI water at increasing pH resulted in the recovery of more than 50% of deposited nC_{60} aggregates. These data are consistent with the behavior of C_{60} nanoparticles deposited on a silica-coated quartz surface, which were

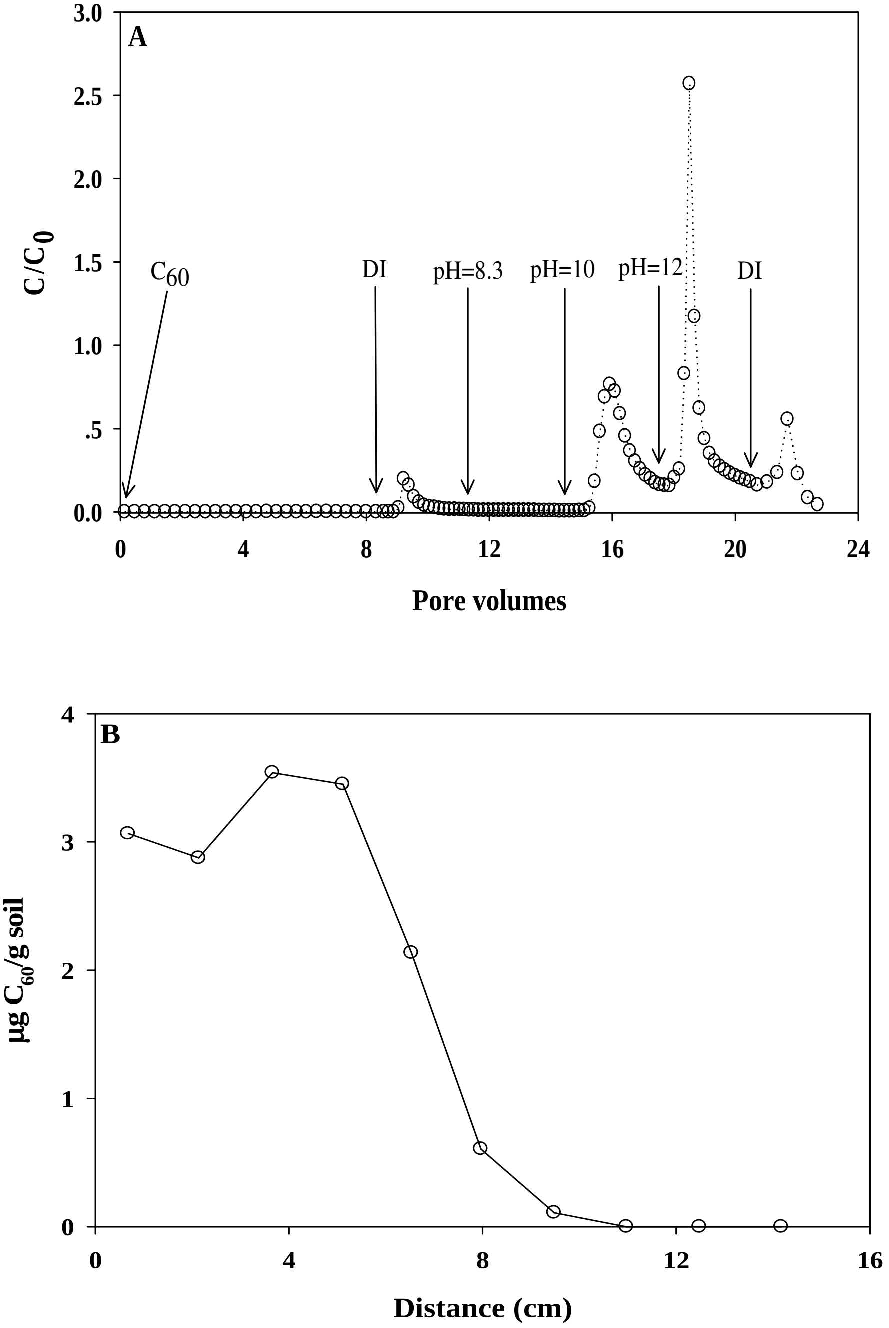

Figure 5.8: Effluent concentrations (A) of nC_{60} with time after introducing an nC_{60} aggregate suspension containing 3.05 mM $CaCl_2$, followed by sequential injections of DI water at pH 7.0, 8.3, 10.0, 12.0 and 7.0, and (B) the final nC_{60} retention profile in 100-140 mesh Ottawa sand.

not released until the pH of DI rinse water was raised from 5.2 to 12.3 (Chen and Elimelech, 2006). These findings suggest that nC_{60} aggregates are retained in the primary energy minimum, and therefore a substantial change in the surface potential of the sand surface and nC_{60} aggregates is required to achieve detachment.

5.3 Summary and Conclusions

Batch and column experiments were conducted to systematically assess effects of electrolyte species (Na^+ and Ca^{2+}) and concentration (ionic strength of 3 and 30 mM) on nC_{60} aggregation and transport in water-saturated quartz sands. Results from electrophoresis experiments clearly demonstrated that nC_{60} aggregates possess a negative surface charge and that the charge density decreased with increasing electrolyte concentration. The change in nC_{60} particle diameter was minimal in the presence of NaCl, but increased by more than 7-fold in the presence of $CaCl_2$, when the electrolyte concentration increased from 1 to 100 mM. Theoretical analysis using DLVO theory in a sphere-sphere model revealed that the agglomeration of individual nC_{60} particles in the presence of $CaCl_2$ (e.g., 100 mM) was consistent with a net attractive force between particles and suppression of the EDL. Similar to colloid (e.g., latex microsphere) deposition in porous media, column experiment data showed that the retention of nC_{60} in quartz sands increased with decreasing grain size or increasing ionic strength, consistent with interaction energy calculations based on DLVO theory in a sphere-plate model. Data obtained from subsequent recovery experiments conducted in 100-140 mesh OS demonstrated that the retained nC_{60} was partially released only when the solution pH was increased to 10.0 or 12.0, and that the second energy minimum that typically plays an important role in colloid retention, did not contribute significantly to nC_{60} retention as reflected by removal of less than 1% of retained nC_{60} by DI water flush. The irreversible attachment process and difficulty of retained nC_{60} removal observed in this study indicates that the primary energy minimum was responsibile for nC_{60} retention in quartz sands, which may be facilitated by bridging to surface-adsorbed Ca^{2+} ions.

CHAPTER 6

EFFECTS OF STABILIZING AGENTS ON FULLERENE (C_{60}) NANOPARTICLE TRANSPORT AND DEPOSITION IN QUARTZ SANDS

6.1 Introduction

Fullerene (C_{60}) has attracted particular attention from scientific community since its discovery in 1985 (Kroto et al., 1985) and its production has been rapidly expanding due to commercial demands in many areas (Li et al., 2008; Lyon et al., 2006; Xie et al., 2008). Development of several facile methods to disperse C_{60} into water without the aid of stabilizing agents makes it possible for C_{60} to exist in aquatic environments in the form of aggregates. These stable aggregates (nC_{60}) are within nanoscale (e.g., 5 – 200 nm), possess negative surface charge and have been proposed to be the most likely form of C_{60} in environment (Fortner et al., 2005; Lyon et al., 2006). Although the toxicity of nC_{60} is a controversial topic, several studies have identified nC_{60} toxicity to certain microorganisms, fish, and human cell lines (Fortner et al., 2005; Oberdorster, 2004a; Sayes et al., 2005). While the potential health impacts of nC_{60} have been considered in detail, far less attention has been focused on understanding the processes that govern the transport of fullerene nanoparticles in subsurface environments, which is a critical component of risk assessment and life-cycle analysis.

Natural organic matter (NOM), often considered to be a “natural surfactant” (Terashima and Nagao, 2007), is ubiquitous in aquatic systems and has been shown to enhances transport of natural colloidal particles (e.g., iron oxides) in the subsurface, which has been attributed to the formation of adsorption of surfactant monomers (Amirbahman and Olson, 1993; Deshiikan et al., 1998; Franchi and O'Melia, 2003; Mylon et al., 2004) on particle surfaces. An aggregation kinetics' study revealed that the presence of NOM (e.g., SRHA) stabilizes nC_{60} in aqueous phase (Chen and Elimelech, 2007). For example, the critical aggregation of NaCl required for aggregation of an nC_{60} suspension increased by more than 4 fold when 1 mg C/L SRHA was added, compared to that required in the absence of SRHA. Recently, Espinasse et al. (2007) conducted column experiments to study the transport of nC_{60} through water-saturated glass beads in the presence of tannic acids, which are considered to be similar to humic and fulvic acids (Espinasse et al., 2007). The authors collected only effluent nC_{60} concentration data, which were presented as BTCs. A clean-bed filtration model was employed to interpret the BTCs, and to calculate the the attachment efficiency factor (α) based on the plateau value on BTC (Yao et al., 1971). Enhancements of nC_{60} transport enhancement in presence of 1 ppm tannic acids was evident based on decreased α values compared to those in absence of tannic acids and was attributed to increased electrostatic and steric repulsions. To date, experimental observations of enhanced nC_{60} transport in porous media in the presence of SRHA or SRFA, as model NOM, has not been reported because of challenges associated with the quantification of nC_{60} and NOM separately from mixtures.

Surface active agents (surfactants) have been utilized in subsurface remediation technologies, including surfactant-enhanced aquifer remediation (SEAR), enhanced bioremediation, and soil washing. Surfactants recover subsurface contaminants by either micellar solubilization and the reduction in liquid-liquid interfacial tension (Pennell et al., 1993). Polyoxyethylene (20) sorbitan monooleate (Tween 80), a nonionic surfactant with a CMC of 13 mg/L (Pennell et al., 1993; Pennell et al., 1997), has been well studied and applied successfully in remediation of dense nonaqeous phase liquids (DNAPLs) (Abriola et al., 2005; Ramsburg et al., 2005). Solubilization studies with C_{60} indicate that surfactants are capable of dispersing solid C_{60} in water, and resulting stable nC_{60} suspension (Bensasson et al., 1994). However, our previous work in Chapter 5 suggest that the presence of 1,000 mg/L Tween 80 in background solution was not sufficient to recover previously attached nC_{60} in quartz sands. However, the potential exists that Tween 80, when mixed with the influent suspension, could facilitate the transport and reduce the attachment of nC_{60}.

The purpose of this study was to investigate the effects of SRHA, SRFA and Tween 80 on nC_{60} transport and deposition in water-saturated quartz sands. The experimental protocol for quantification of SRHA or SRFA and nC_{60} in mixtures was developed using high performance liquid chromatography (HPLC) and liquid-liquid extraction. A series of nC_{60} transport experiments were conducted in the presence of tetrohydroforun (THF), Tween 80, SRHA or SRFA using 1-D columns packed with water-saturated 40-50 mesh Ottawa sands. Effluent and solid-phase concentration data were collected to construct effluent BTCs and retention profiles, to evaluate the effects of stabilizing agents on nC_{60}

transport behavior.

6.2 Results and Discussion

6.2.1 Quantification of nC_{60} and SRHA or SRFA

Quantification of nC_{60} and SRHA or SRFA from their mixtures is challenging. A typical UV spectrum of SRHA or SRFA exhibits featureless increase in absorbance with the decrease of wavelength (Chin et al., 1994). The UV absorbance at 220, 267, or 344 nm, which are nC_{60} characteristic wavelengths, becomes useless for nC_{60} quantification due to the nonlinear overlap of spectra when SRHA or SRFA is added to nC_{60} suspensions. Hyung et al. (2007) developed a method using Thermal Optical Transmittance (TOT) to quantify SRHA and MWNTs. However, when a nC_{60} and SRHA mixture sample is burnt in TOT, uncertainties are introduced due to the sublimization of solid C_{60} at ca. 700 ^{o}C (Fortner, 2006). Since the average diameter of nC_{60} is around 100 nm and SRHA or SRFA is soluble in water, one may think that they could be separated using size exclusion chromatography. However, a preliminary test was conducted using a HiTrap desalting column and nC_{60} exhibited very high affinity to the column packing media, leading to the removal of nC_{60} from aqueous phase. In addition, the size exclusion chromatography may give a very broad peak for humic or fulvic acids due to the separation of compounds in them (Her et al., 2002). The quantification protocol for nC_{60} and SRHA/SRFA in the present study was based on the principle that toluene was capable of selectively dissolving C_{60} and apolar components of humic/fulvic acids and the results were presented as follow.

At a mobile phase flow rate of 1 mL/min, C_{60} molecule in standard toluene solution was eluted at 8.0 min as a single peak (Figure 6.1), while the HPLC column dead time was determined to be ~ 3.8 min using a tracer (KI) test. Retention time of toluene-extracted C_{60} in the presence of SRHA or SRFA (Figure 6.1) was same with that of the pristine C_{60} in toluene, indicating dissolved NOM in toluene phase had minimum impact on elution of extracted C_{60} and C_{60} was not derivatized in nC_{60} aggregates (Fortner et al., 2005) regardless the presence of SRHA or SRFA. The dissolved C_{60} in toluene exhibited a maximum absorbance at 334 nm on the UV spectrum captured by DAD, which is consistent with the finding in Fortner et al. (2005) and Xia et al. (2006). Various methanol percentages in sample preparations and injection volumes were tested with a fixed C_{60} concentration (e.g., 1 mg/L in toluene) and 20% (vol.) methanol and 900 μL were found to give the sharpest peak on C_{60} chromatograms (data not shown). With the injection volume of 900 μL no sample cross contamination was observed. The toluene to methanol ratio, 55/45, in mobile phase was adopted from Issacson et al. (2007) and Heymann et al. (1996). Starting from the column dead time (ca. 3.8 min), a noticeable broad peak followed by a relative sharp dip was observed on C_{60} chromatogram, which was believed to be due to the flow front between sample and mobile phase.

To quantify both nC_{60} and NOM in aqueous mixtures, calibration curves were prepared and presented in Figure 6.2. An expected, areas of chromatographic peaks (at 8

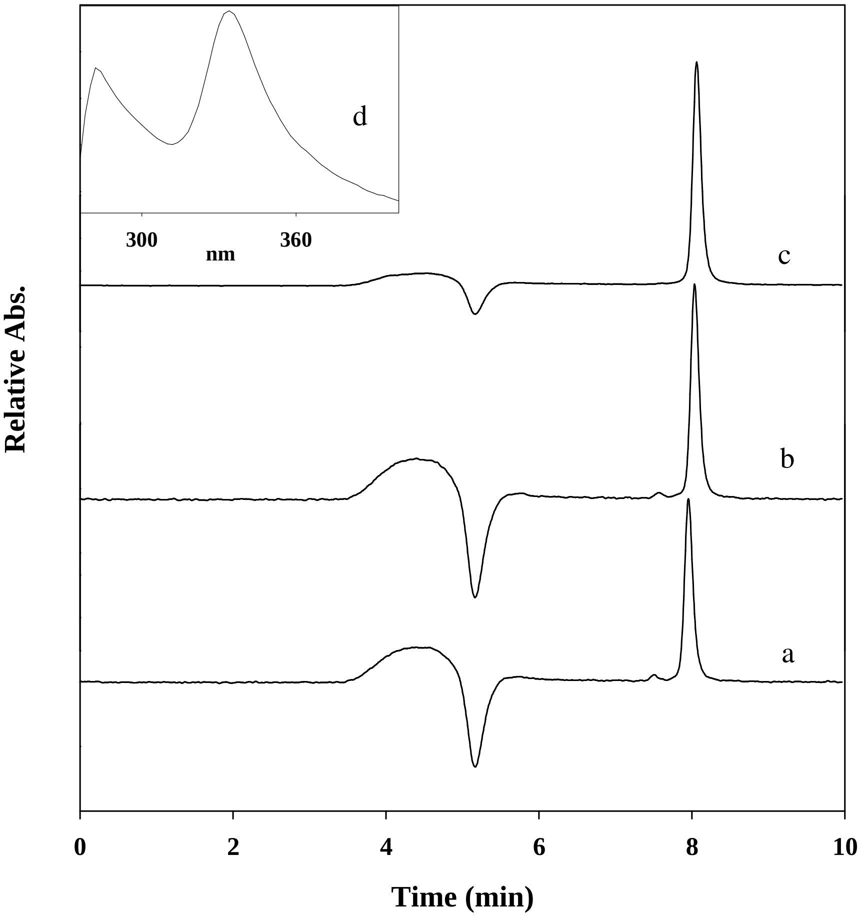

Figure 6.1: Selected HPLC chromatograms of C_{60} with a toluene/methanol (55:45) mobile phase; (a) C_{60} extracted from 0.24 mg/L nC_{60} spiked with 10 mg C/L of Suwannee River humic acids (SRHA); (b) C_{60} extracted from 0.24 mg/L nC_{60} spiked with 10 mg C/L of Suwannee River fulvic acids (SRFA); (c) standard 1 mg/L C_{60} in toluene; (d) a UV-vis spectrum of C_{60} in the mobile phase scanned by diode array detector (DAD).

min) and concentrations of pristine C_{60} in toluene showed excellent positive linear relationship (R^2 = 1.00; Figure 6.2A), which was held for C_{60} up to 10 mg/L. The detection limit of the pristine C_{60} in toluene was determined to be 0.002 mg/L using Hubaux-Vos approach (Hubaux and Vos, 1970). When nC_{60} was extracted from aqueous phase using the liquid-liquid extraction, the calibration curve of nC_{60} in presence of SRHA or SRFA coincided with nC_{60} alone (Figure 6.2B), suggesting the apolar portion of SRHA or SRFA was either completely eluted out of HPLC column before 8.0 min or not contributing to C_{60} absorbance at the wavelength of 334 nm. Since the extraction efficiency of C_{60} to toluene was high when $Mg(ClO_4)_2$ was used as destabilizing agent (Fortner et al., 2005; Xia et al., 2006), interference of residual C_{60} to NOM UV spectra after extraction was negligible, which allowed quantification of NOM in aqueous phase using a UV-vis spectrometer without further treatments. The UV absorbance at a wavelength range of 250 to 260 nm (Her et al., 2002; Hyung et al., 2007; Wu et al., 2007) was commonly measured to determine concentration of SRHA and SRFA in aqueous phase. However, the presence of $Mg(ClO_4)_2$ largely altered UV spectrum (200 to 300 nm) of SRHA or SRFA after the liquid-liquid extraction (Figure 6.3). Although a linear relationship can be developed between SRHA/SRFA initial concentration and UV absorbance at 254 nm, a reference correction (pure $Mg(ClO_4)_2$ solution at a concentration of 28.6 mM) is required. Apparently, no UV absorption was observed for pure $Mg(ClO_4)_2$ solution at 290 nm. Thus, the UV response at 290 nm was selected to construct calibration curves for SRHA/SRFA quantification in aqueous phase after liquid-liquid

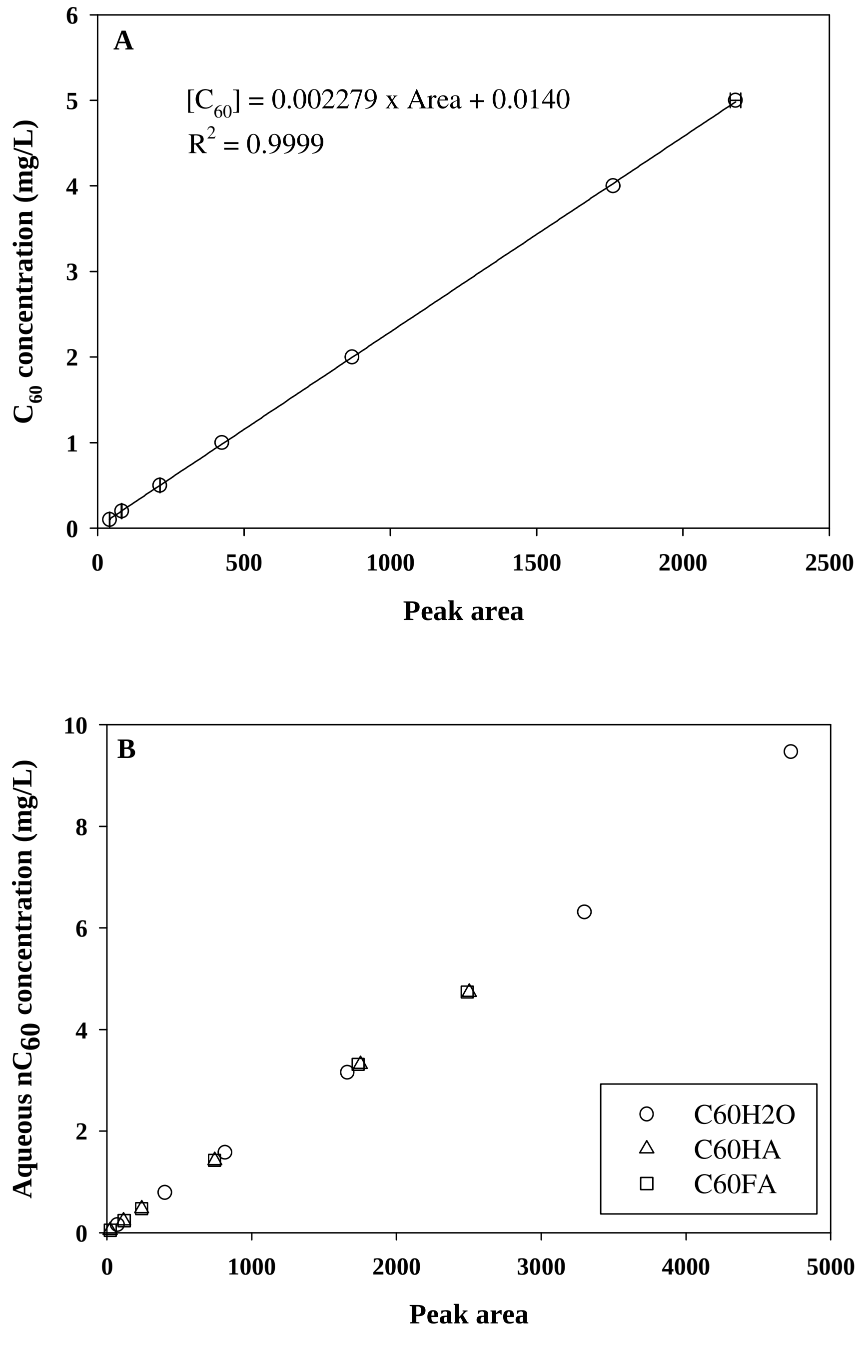

Figure 6.2: Calibration curves for the pristine C_{60} in toluene (A) and nC_{60} in aqueous suspensions based on the liquid-liquid extraction method (B). Error bars represent the standard deviation of duplicate or triplicate measurements.

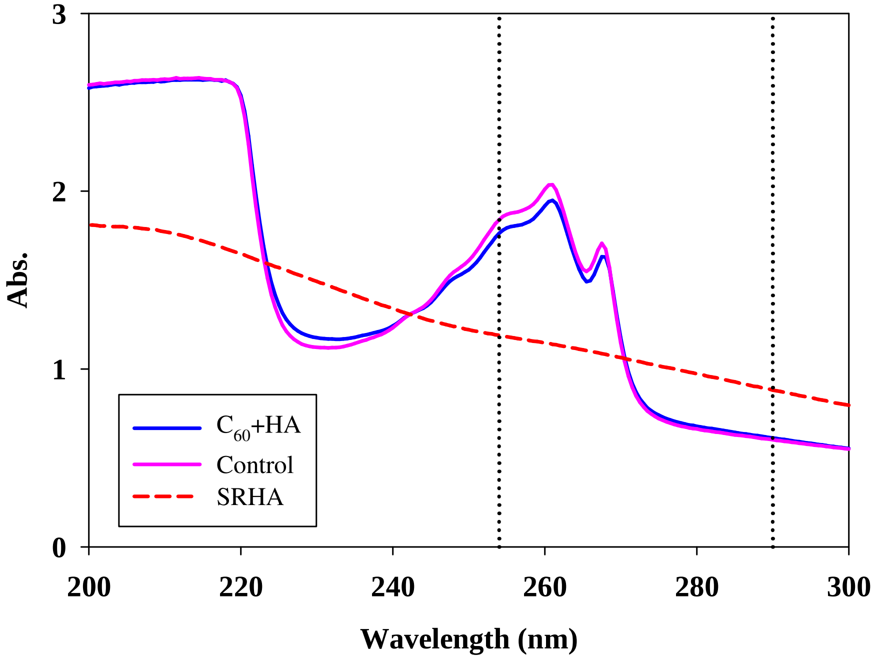

Figure 6.3: UV-vis spectra of Suwannee River humic acids (SRHA) at 20 mg C/L before (dash line) and after liquid-liquid extraction (solid blue). The control sample consisted of 20 mg C/L SRHA, 28.6 mM $Mg(ClO_4)_2$, and toluene.

extraction. In the current experimental conditions, the oxidation of SRHA or SRFA by $Mg(ClO_4)_2$ was not considered, since $Mg(ClO_4)_2$ was only a mild oxidant (Fortner et al., 2005).

6.2.2 Transport Experiments in Presence of Stabilizing Agents

A total of 11 transport experiments were conducted to investigate the effects of THF, SRHA, SRFA, and Tween 80 on nC_{60} transport and retention in columns packed with 40-50 mesh Ottawa sands. All experiments were performed at a Darcy velocity of 2.8 m/d with 1.0 mM $CaCl_2$, conditioned with 0.05 mM $NaHCO_3$ to pH 7, as a background electrolyte. The experimental conditions, such as input concentration and particle zeta potential, are summarized in Table 6.1.

Table 6.1: Experimental conditions for nC_{60} column studies conducted in 40-50 mesh Ottawa sand with 1.0 mM $CaCl_2$, conditioned with 0.05 mM $NaHCO_3$ to pH 7, as a background electrolyte.

Column Identifier	C_0 [a] (mg/L)	PW [b] (pv)	ξ [c] (mv)	d_a [d] (nm)	Retention [e] (%)	MB [f] (%)
C_{60}	4.7	5.0	-23.5	94.2	29.0	92.9
THF+C_{60}	4.7	5.0	-25.8	95.4	27.4	89.5
TW80+C_{60}-1	4.9	5.0	-15.1	92.5	0.0	103.1
TW80+C_{60}-2	5.0	5.0	-17.0	92.6	0.0	103.1
TW80,C_{60}-1	4.2	5.0	-24.2	90.6	6.3	96.1
TW80,C_{60}-2	4.3	5.0	-22.9	93.6	7.1	96.4
SRHA+C_{60}	3.9	5.0	-19.1	96.9	1.2	96.7
SRHA+C_{60}-eq	3.9	5.2	-15.6	104.0	2.9	99.4
SRFA+C_{60}	4.4	5.4	-23.6	95.6	0.8	100.1
SRHA	20.8	2.0	ND	ND	ND	90.7 *
SRFA	19.9	2.0	ND	ND	ND	93.2 *

[a] input concentration of nC_{60}, SRHA or SRFA. [b] pulse width. [c] average zeta potential of nC_{60}. [d] nC_{60} mean diameter. [e] mass percentage of retained nC_{60}. [f] mass balance. * mass retained in column was not measured. ND not determined.

6.2.2.1 Effects of THF.

The THF-as-vehicle method was used here to prepare nC_{60} suspension because it was reproducible and easily manipulated to produce consistent particle diameter (Fortner et al., 2005). However, presences of THF residual and THF decay products raise concerns that the toxicity of nC_{60}, in part, results from byproducts produced during preparations (Andrievsky et al., 2005; Brant et al., 2005b; Lyon et al., 2006; Zhu et al., 2006). Henry et al. (Henry et al., 2007) even detected ca. 158 ppm of GBL in a nC_{60}

suspension, prepared using the similar method, and found that GBL was responsible for nC_{60} toxicity. In the present study, the concentration of THF residual in nC_{60} stock solution was determined to be 1.57 mg/L two days after preparation, with no detectable level of GBL, suggesting that repeating evaporation process three times greatly reduced THF level and oxidation of THF. Due to the presence of THF in nC_{60} suspension as a type of organic matter, effects of THF on nC_{60} transport need to be studied in the first step of this study.

Effluent BTCs and retention profiles of nC_{60} in presence of 44.5 mg/L THF transporting through 40-50 mesh water saturated Ottawa sands are shown in Figure 6.4A and 6.4B, respectively. To form a basis for comparison, transport column experiment of normal nC_{60}, in which the concentration of THF residual was expected to be less than 0.8 mg/L, was also conducted (denoted by circles in Figure 6.4). Consistent with the previous results in Chapter 5, the shape of normal nC_{60} BTC was asymmetric, with a gradual ascent before ca. 5 PV followed by a sharp drop at the end of pulse injection. When THF was spiked to nC_{60} suspension with a final concentration of 44.5 mg/L, both BTC and retention profile were identical to those of normal nC_{60}. These findings suggested that presence of THF with a concentration up to 44.5 mg/L contributed negligibly to nC_{60} transport and deposition in 40-50 mesh Ottawa sands.

Besides nC_{60} concentrations, THF and GBL concentrations in effluent samples were measured and GBL levels were found to be below detection limit. In contrast to transport behavior of nC_{60}, the THF BTC (Figure 6.5) was symmetric, with sharp ascent

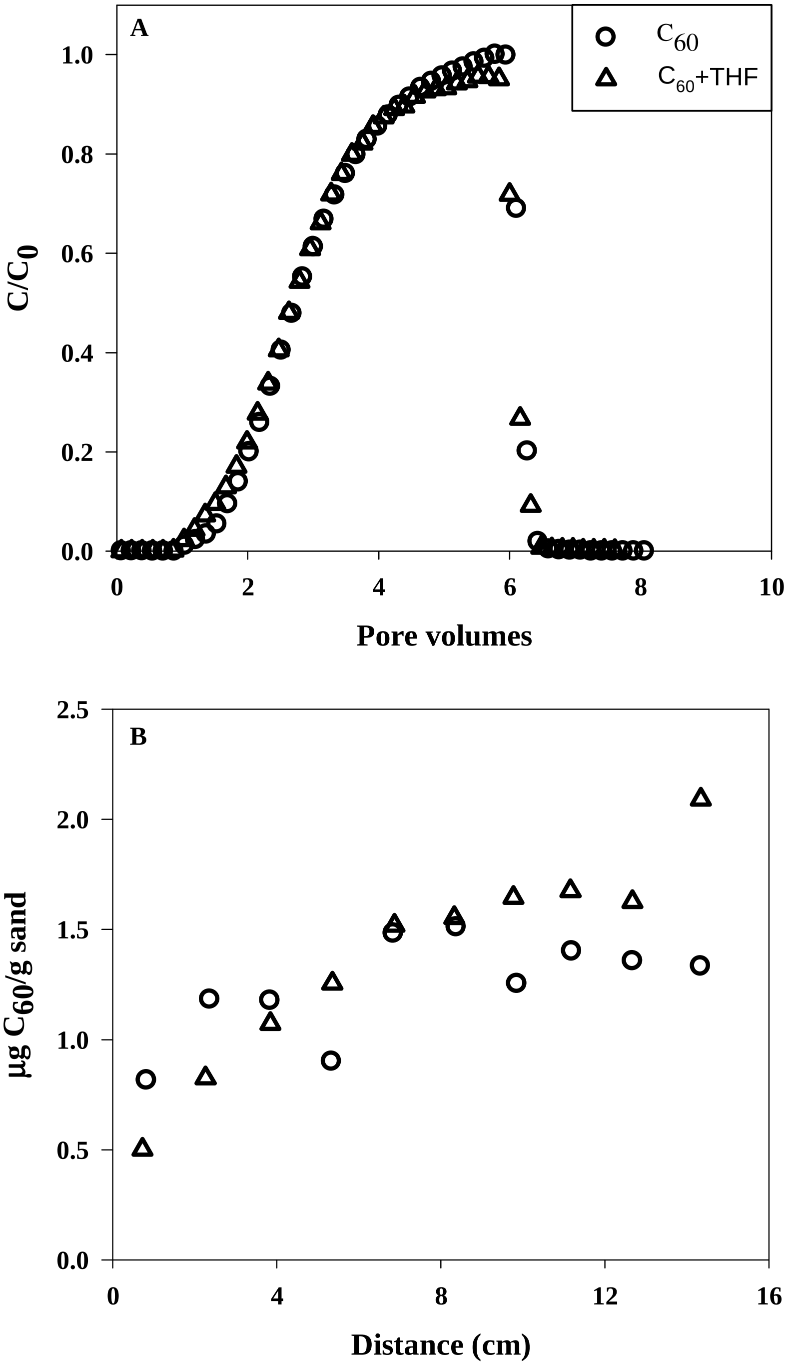

Figure 6.4: Effluent breakthrough curves (A) and retention profiles (B) of nC_{60} for pulse injections of normal nC_{60} and nC_{60} + THF (44.5 mg/L) in columns packed with 40-50 Ottawa sand. Aqueous nC_{60} contained 1.0 mM $CaCl_2$ and 0.05 mM $NaHCO_3$, applied at a Darcy velocity of 2.8 m/d.

and descent at ca. 1 and 6 PV, respectively. Once THF broke through sand column, a plateau was developed with an average THF relative concentration (*C/C_0*) of 0.89, indicting less than 11% of input THF was retained in sands. The retention of THF was mainly attributed to adsorption of THF to Ottawa sand and enclosure of THF molecules in structure of retained nC_{60} (Brant et al., 2005a; Fortner et al., 2005). Since the presence of THF at a concentration of 44.5 mg/L did not impact nC_{60} transport and deposition in water saturated sands, the contribution of THF (< 0.8 mg/L) in nC_{60} input suspensions to nC_{60} retention was negligible and THF concentrations were not monitored in the rest of experiments conducted in this study.

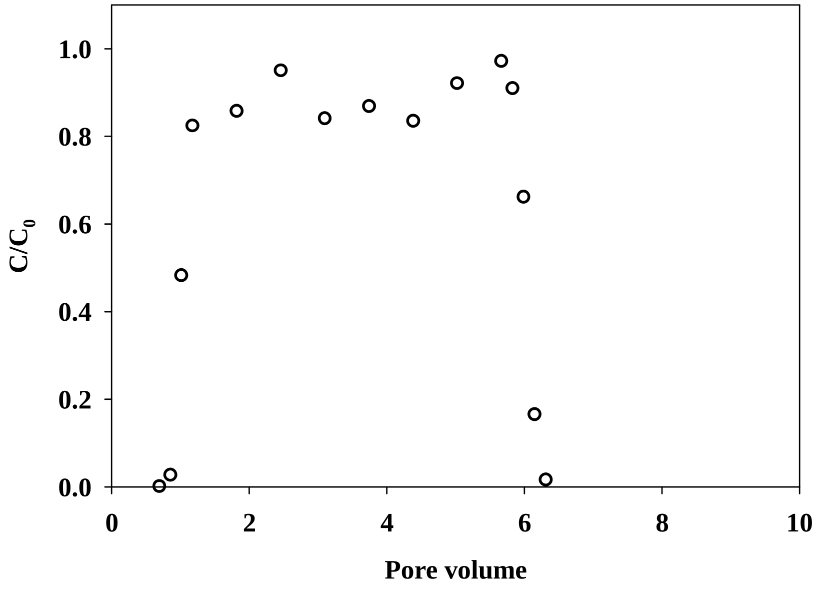

Figure 6.5: Relative concentrations of THF in effluent samples for a 5-PV injection of nC_{60} + THF (44.5 mg/L) in water-saturated Ottawa sand.

6.2.2.2 Effects of Tween 80

To investigate effects of surfactant, a classic type of stabilizing agent, on nC_{60} transport and deposition in water saturated Ottawa sands, Tween 80, was chosen to alter either nC_{60} particle or sand grain surface physiochemical properties. The resulting nC_{60} BTCs in experiments, where Tween 80 is present in aqueous suspension at a concentration of 1,000 mg/L Tween 80 or in solid phase, are shown in Figure 6.6A. When nC_{60} suspension was premixed with Tween 80 (TW80+C_{60}-1,2), nC_{60} BTCs were identical to that of non-reactive tracer with a C/C_0 plateau value of 1.0, indicating that the physical straining (Bradford et al., 2002) due to narrow pore throat was not contributing to nC_{60} retention in 40-50 mesh Ottawa sands. When nC_{60} alone (no Tween 80) was introduced into Ottawa sands pre-flooded with 5 PV 1,000 mg/L Tween 80 followed by 3 PV elution of background electrolyte solution (TW80,C_{60}-1,2), relative concentrations (C/C_0) of nC_{60} rapidly reached a maximum value of 0.9 right after 1 PV and declined slightly till a sharp drop at ca. 6 PV, yielding 6.3 to 7.1% of input nC_{60} were retained in columns, although sharp ascent and descent were identical in both cases.

Corresponding to the plateau value of 1.0 in BTCs, nC_{60} in solid phase were not measurable when 1,000 mg/L Tween 80 was present in nC_{60} input suspensions (Figure 6.6B). While nC_{60} alone transported through Tween 80 coated sands, retained nC_{60} hypoexponentially decreased along transport distance with more than 77% total retained nC_{60} mass concentrated in the first 5 cm of column from inlet (Figure 6.6B).

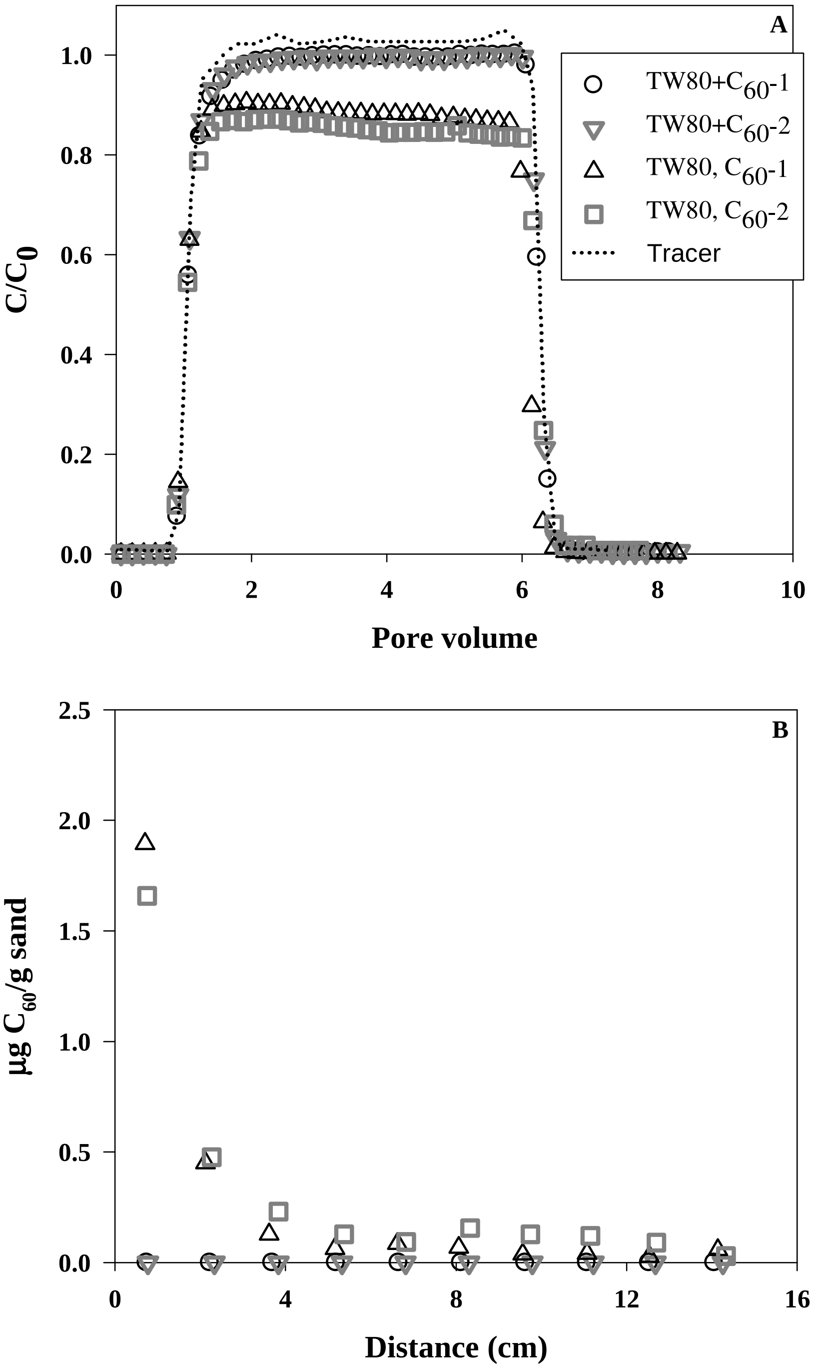

Figure 6.6: Effluent breakthrough curves (A) and retention profiles (B) of nC_{60} for a 5-PV injection of nC_{60} + Tween 80 (1,000 mg/L) mixture in 40-50 Ottawa sands (TW80+C_{60}-1,2) or nC_{60} alone in Ottawa sands preflooded with 5 PVs of Tween 80 (1000 mg/L) (TW80,C_{60}-1,2).

While effluent nC_{60} concentrations were monitored, concentration of Tween 80 in effluent samples (TW80+C_{60}-1,2) were determined to assess possible effects of nC_{60} on Tween 80 transport and their relative concentrations were plotted in Figure 6.7. The Tween 80 BTC in a Tween 80 alone transport experiments are shown in Figure 6.7 as a reference. In these three experiments, Tween 80 appeared in effluent at ca. 1 PV and then their effluent concentration sharply increased to initial levels, followed by a sharp drop. Effluent Tween 80 concentrations in nC_{60} tranpsort experiments (e.g., TW80+C_{60}-1,2) arbitrarily scattered around 1.0 due to little uncertainties introduced by filtration processes. The t-test of data points between 1.57 and 5.89 PV from these three

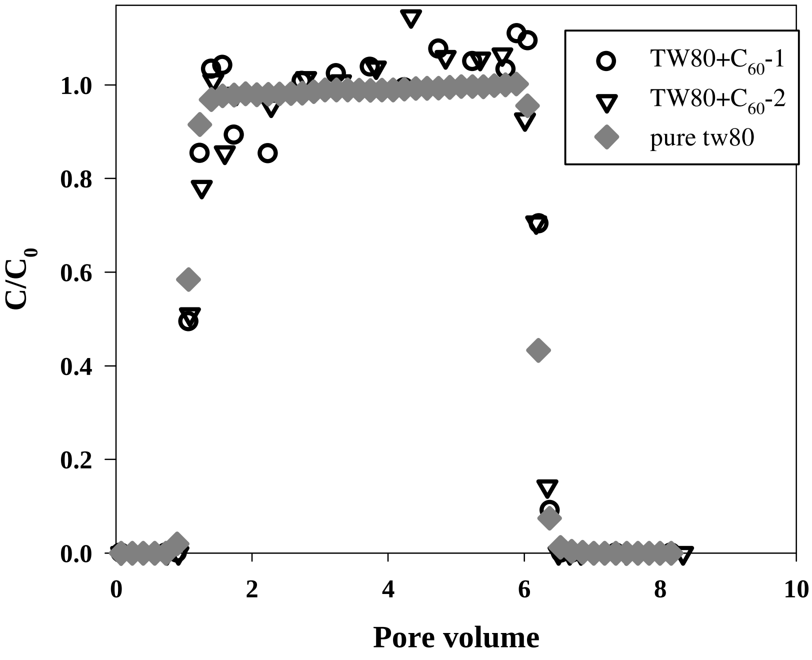

Figure 6.7: Effluent relative concentrations of Tween 80 from experiments with 5-PV pulse injection of nC_{60} and Tween80 (hollow points) and with Tween 80 alone injection (solid points).

experiments revealed that those plateau concentrations were not significantly different. These findings suggested that the filtration process was able to effectively detach Tween 80 associated with nC_{60} and there was significant amount of free Tween 80 in effluents.

When mixed with Tween 80, nC_{60} suspension was stabilized by micellar solubilization processes, since the concentration of Tween 80 used here was 76 times higher than its CMC (ca. 13 mg/L). During solubilization, surface of nC_{60} particles was covered with Tween 80 molecules, which was reflected by the significant reduction (less negative) of nC_{60} zeta potentials (Table 6.1). The DLS results showed that the mean hydrodynamic diameter of nC_{60} in the presence of 1,000 mg/L Tween 80 was slightly smaller than that in the absence of Tween 80 (e.g., 94.2 nm) (Table 6.1). However, the reduction of nC_{60} size in the presence of Tween 80 did not necessarily mean the occurrence of disaggregation (Xie et al., 2008). Rather, this was believed to be due to the change of mixing sequence: stock nC_{60} (no salt) was mixed with Tween 80 prior to $CaCl_2$ addition, where effects of $CaCl_2$ on nC_{60} size were reduced by the preaddition of Tween 80. A careful examination of DLS results revealed that the size of nC_{60} in the presence of Tween 80 (1.0 mM $CaCl_2$) was ca. 0.5 nm greater than that in stock suspension (92.0 ± 0.3 nm), implying that Tween 80 molecules on nC_{60} particles were not radically assembled with lipophilic tails associating with nC_{60} surface and hydrophilic moieties (Figure 3.1) towards water molecules, since the hydrodynamic diameter of a micelle in 1,000 mg/L Tween 80 (no nC_{60}) was determined to be ca. 10 nm, which was consistent with the molecule length (ca. 5 nm) of Tween 80 under maximum stretch conditions.

Possibly hydrophilic heads of Tween 80 were located close to nC_{60} surface similar to their tails (Figure 6.8) due to interactions between cycloether ring and π-system of C_{60} (Hungerbuhler et al., 1993). But the exact structure of Tween 80 coated on nC_{60} is still not clear.

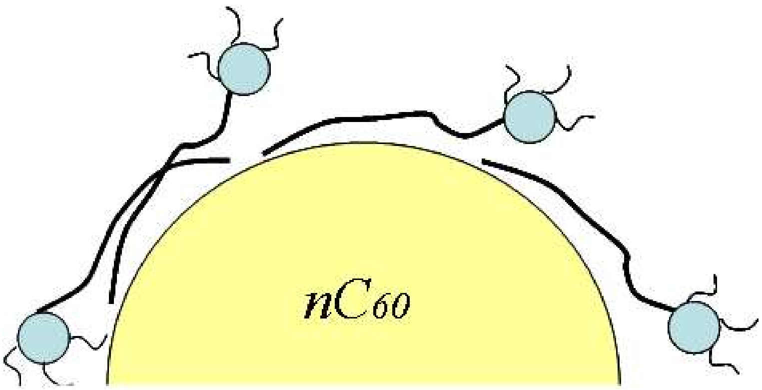

Figure 6.8: Proposed Tween 80 coating conformation on an nC_{60} particle based on current findings.

The comparison between nC_{60} BTCs in the presence of Tween 80 and those in the absence of Tween 80 clearly demonstrated the nC_{60} transport enhancement due to Tween 80 coating. Due to the presence of free Tween 80, sand grains were coated with Tween 80 during the pulse introduction of nC_{60} and Tween 80. The zeta potentials of Ottawa sands coated with Tween 80 following the similar experimental procedures were determined to be -30.3 mV using a streaming potential instrument in the University of California, Riverside, while a slight higher zeta potential (-31.4 mV) was obtained for uncoated Ottawa sands. Intuitively, based on DLVO theory (sphere-plate model), a common approach to study nanoparticle transport, zeta potential reductions (less negative) of both

nC_{60} and Ottawa sands in the presence of Tween 80 should result in higher nC_{60} retention when 1,000 mg/L Tween 80 was added to nC_{60} input suspensions (e.g., TW80+C_{60}-1,2), which was not consistent with observations in this study. Thus, steric repulsions induced by coated Tween 80, rather than physicochemical interactions, were primarily responsible for the enhancement of nC_{60} transport in the presence of Tween 80.

Transport and deposition of nC_{60} in Tween 80 coated Ottawa sands exhibited two striking features: slightly declined effluent concentration “plateau” and hypoexponentially decayed retention profiles (Figure 6.6). Intuitively, the slight decline of plateau in BTCs may imply the occurrence of filter ripening (Ginn et al., 2002), in which attached particles further serve as collectors causing more particle deposition near the injection point. However, findings in Chapter 4 and 5, such as unfavorable interactions between nC_{60} and nC_{60} or Ottawa sand with 1 mM $CaCl_2$ as a background electrolyte, may suggest that ripening processes do not contribute to nC_{60} deposition. On the other hand, the hypoexponential decay of retained particles has been reported in colloid transport studies and attributed to various particle attachment rates (k_{att}) with traveling distance (Li et al., 2004; Tufenkji et al., 2003). A mathematic model coupling a lognormal distribution of k_{att} with clean bed filtration theory has been developed by collaborators in Tufts University and used to simulate data here. Although predictions from the model matched both BTCs and retention profiles, the selection of distribution function was arbitrary. A careful investigation on retention profiles revealed that the maximum nC_{60} concentrations on solid phases were consistent with retention capacity (e.g. 1.98 μg/g) reported in Chapter 4, which suggested retention capacity of nC_{60} was reached the near column inlet. Thus, it is hypothesized that nonexponentially decayed retention profiles in Tween 80 coated Ottawa sands are results of production of available surface by gradually washing off Tween 80 attached on sand surface. This hypothesis has been confirmed by mathematical modeling at Tufts University.

6.2.2.3 Effects of NOM

Effluent BTCs and retention profiles of nC_{60} premixed with 20 mg C/L SRHA or SRFA in water saturated 40-50 mesh Ottawa sands are shown in Figure 6.9A. Interestingly, when 20 mg C/L of SRHA was added to the input suspension with an nC_{60} concentration of 3.9 mg/L, the nC_{60} zeta potential immediately decreased to -20.6 ± 0.8 mV and further decreased to -17.7 ± 1.7 mV at the end of the column experiment (Exp. SRHA+C_{60}). Another independent test showed that nC_{60} zeta potential in the presence of 20 mg C/L SRHA did not remain constant until the suspension was quiescently placed on bench for 4 days. The input suspension equilibrated for 5 days was used for Exp. SRHA+C_{60}-eq to study possible effects from the equilibration process. The variation of nC_{60} zeta potentials with time was not observed in the presence of 20 mg C/L SRFA. Regardless of interaction equilibrium in input suspensions, presence of 20 mg C/L SRHA or SRFA resulted in breakthrough of nC_{60} through sand columns at ca. 1 PV, which was 0.5 PV earlier than that in absence of stabilizing agents (e.g., Exp. C_{60}). Once nC_{60} broke through sand columns, relative nC_{60} concentrations increased rapidly to a plateau value

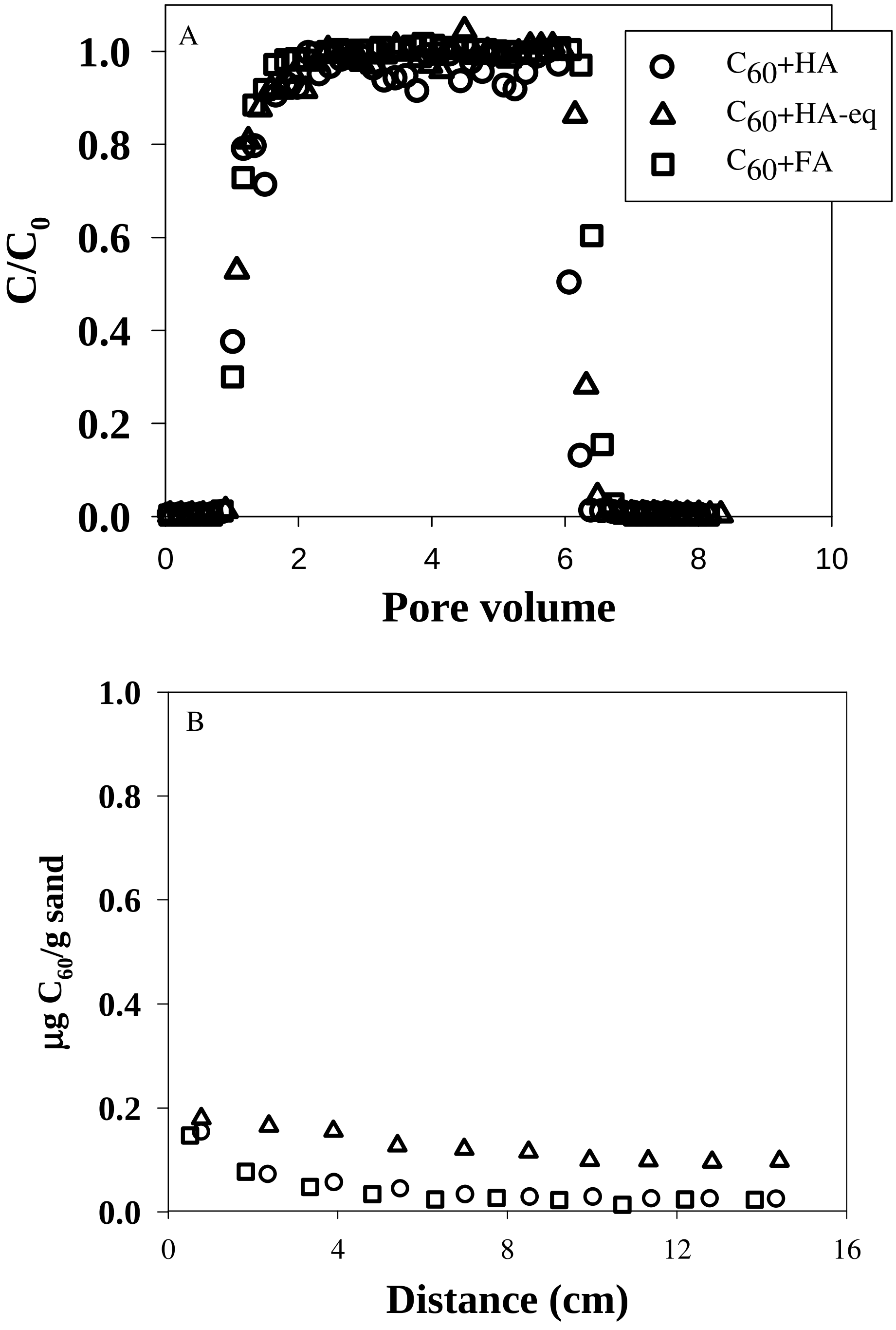

Figure 6.9: Effluent breakthrough curves (A) and retention profiles (B) of nC_{60} for a 5-PV injection of nC_{60} + SRHA/SRFA (20 mg C/L) mixture in 40-50 Ottawa sands.

greater than 0.98, followed by sharp descents to approach zero at the end of pulse injection. When equilibrium of interactions between nC_{60} and SRHA was achieved prior to pulse injections, the nC_{60} BTC exhibited identical characteristics to those at nonequilibrium status (e.g., Exp. SRHA+C_{60}). These findings suggested that the presence of SRHA or SRFA enhanced nC_{60} transport in saturated 40-50 mesh Ottawa sands.

At the conclusion of each transport experiment, the column was sectioned into ten 1.5 cm increments, from which retained nC_{60} and SRHA or SRFA were extracted through sonication and liquid-liquid extraction processes described in Chapter 3. The resulting retention profiles of nC_{60} are shown in Figure 6.9B. Generally, Concentrations of nC_{60} in solid phase decreased gradually with traveling distance. While the retention profile of nC_{60} in the presence of SRFA was not discernable from that in the presence of nonequilibrated SRHA, the reach of nC_{60} and SRHA interaction equilibrium in input suspension resulted in relative higher nC_{60} retention (Figure 6.9B). Regardless of equilibrium in input suspensions, the maximum solid phase concentrations of nC_{60} were identical (0.18 μg/g) and observed near column inlets. The nC_{60} mass underneath BTCs and retention profiles were integrated to calculate the overall mass balance (Table 6.1). A mass recovery of greater than 96% was obtained for all column experiments, reflecting the good accuracy of nC_{60} and SRHA/SRFA quantification protocols described in Chapter 3.

Although NOM has been considered at natural surfactant, the SRHA/SRFA concentration (20 mg C/L) used in this study was well below reported CMCs, such as ca.

500 and 15,000 mg C/L for certain humic and fulvic acids, respectively (Hayase and Tsubota, 1983). In addition, no detectable aggregates with diameter greater than 0.6 nm (DLS detection limit) formed in pure SRHA/SRFA solutions at the concentration of 20 mg C/L. Thus, nC_{60} suspensions were stabilized by SRHA/SRFA not through micellar solubilization. Electrophoresis measurements showed that adsorption of SRHA molecules onto nC_{60} particles reduced (less negative) the zeta potential of nC_{60} from ca. -23 to -16 mV, while change of nC_{60} zeta potential after mixing with SRFA was discernable (Table 6.1). These findings did not agree with previous studies (Amirbahman and Olson, 1993; Deshiikan et al., 1998; Franchi and O'Melia, 2003), where surface charge of negatively charged colloidal particles increased due to adsorption of NOM. In mixture of nC_{60} and SRHA, screening effect of Ca^{2+} on nC_{60} surface charges was enhanced due to complexation of Ca^{2+} with carboxyl groups (Kalinichev and Kirkpatrick, 2007; Nguyen and Chen, 2007), which was considered dominated in SRHA. Compared to SRHA, SRFA possess smaller molecular weight and less affinity to nC_{60} (Terashima and Nagao, 2007). Thus, SRFA did not alter nC_{60} zeta potential, although they had similar carboxyl content with SRHA (IHSS website).

In studies of colloid (e.g., latex microsphere) transport, the reduction of particle deposition in presence of NOM has been attributed to increasing electrostatic repulsion and steric interaction (Franchi and O'Melia, 2003). In this study, the total DLVO interaction energy was calculated based on equations proposed by (Guzman et al., 2006) and shown in Figure 6.10. In presence of 20 mg C/L SRHA at equilibrium, an energy barrier with 18 kT was found at ca. 2.5 nm, while a relative higher barrier (ca. 36 kT) was observed at ca. 1.5 nm in presence of SRFA at the same concentration. In Chapter 5, it has been demonstrated that nC_{60} particles are able to overcome energy barrier as high as 35 kT and held on quartz sands by the primary energy minimum. By assuming the presence of SRHA does not charge particle energy (e.g., kinetic energy), nC_{60} particles in this study should be able to overcome the current energy barrier (18 kT), resulting in more nC_{60} retention, which is not consistent with current observations. While in the presence of SRFA, the sizable energy barrier slightly increased compared to that in absence of stabilizing agents, which was consistent with the reduction of nC_{60} retention.

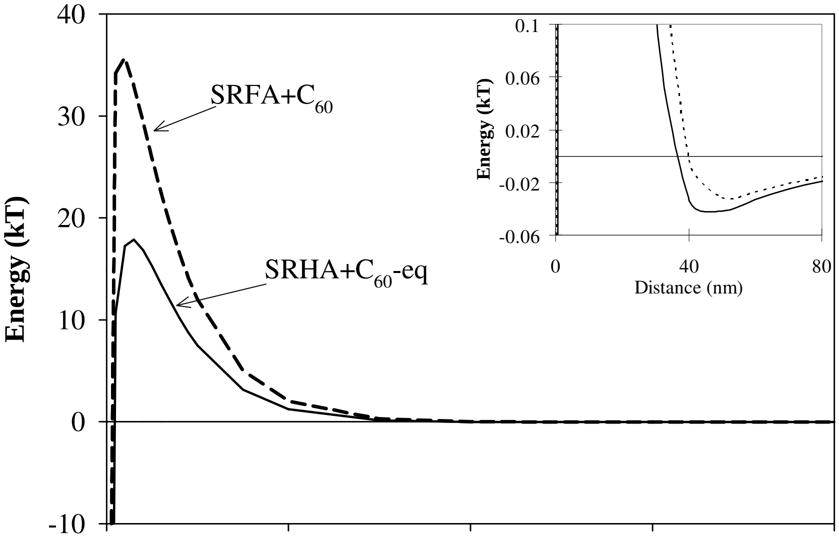

Figure 6.10: Derjaguin-Landau-Verwey-Overbeek (DLVO) interaction energy of nC_{60} and quartz sands in presence of Suwannee River humic acids (SRHA, at equilibrium, solid line) and Suwannee River fulvic acids (SRFA, dash line). The inset shows the secondary minimum attractive region.

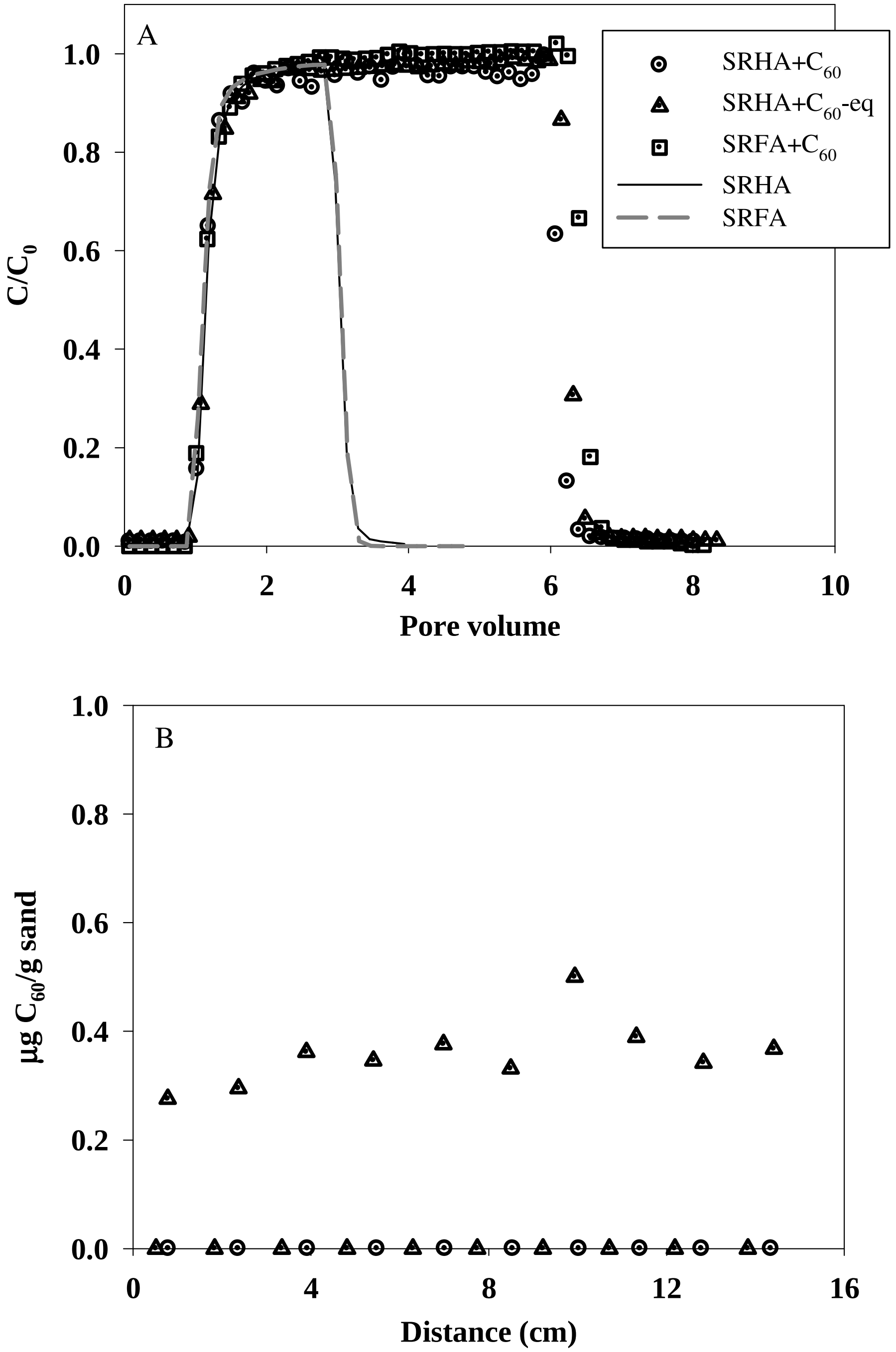

Figure 6.11: Relative concentrations of Suwannee River humic acids (SRHA) and fulvic acids (SRFA) in effluents (A) and solid phase (B).

However, steric repulsions between coated humic or fulvic acids on nC_{60} and quartz sands dominated when surface distance of particle and sand was less than 1.5 or 2 nm. Steric interactions effectively prevented attachment of nC_{60} particles and, in turn, enhanced nC_{60} transport. Although first energy barriers became less than or comparable to that of pure nC_{60}-sand system (Chapter 5), small secondary minima were still observed at distance of ca. 44 and 50 nm in presence of SRHA and SRFA, respectively. These secondary minima mainly contributed to small nC_{60} retentions (Table 6.1).

After nC_{60} removal through liquid-liquid extraction, concentrations of SRHA or SRFA in effluents and solid phase were determined and plotted in Figure 6.11A and 6.11B. Since toluene extracts more than 90% of nC_{60} out of mixtures, the SRHA and SRFA determined here may include not only free SRHA and SRFA in aqueous phase, but also those adsorbed to nC_{60} particles. BTCs of SRHA and SRFA were identical to those in experiments with SRHA or SRFA alone injection (Exp. SRHA and SRFA), regardless of interaction equilibrium in input suspensions. Similar to nC_{60} retention, more SRHA were retained when interaction equilibrium in input suspensions was reached, while very small amount of SRHA or SRFA was observed in solid phase. When SRHA or SRFA alone at 20 mg C/L was introduced to sand columns, it was observed that 9.3% or 6.8% of input SRHA or SRFA were retained in sands, respectively. These findings suggested that transport of SRHA and SRFA in porous media were also facilitated by presence of nC_{60} transport due to their adsorption to nC_{60} particles.

6.3 Summary and Conclusions

An analysis protocol was developed using HPLC coupled with liquid-liquid extraction to quantify nC_{60} and SRHA or SRFA separately in mixtures. This analytical method allowed for direct quantification of enhancements in nC_{60} transport in presence of SRHA or SRFA.

Following development of the extraction methodology, a series of column experiments were conducted in water-saturated 40-50 mesh Ottawa sands to investigate effects of THF, SRHA, SRFA, or Tween 80 on nC_{60} transport behavior. Experimental results showed that the presence of the residual THF (at concentrations up to 44.5 mg/L) exhibited no measurable effects on nC_{60} transport and retention in quartz sands. When SRHA (20 mg C/L), SRFA (20 mg C/L), or Tween 80 (1,000 mg/L) was mixed with the influent nC_{60} suspensions, transport of nC_{60} was dramatically enhanced, as evidenced by the disappearance of gradual ascent in nC_{60} BTCs and a sharp reduction in solid-phase concentrations. Subsequent transport experiment performed in Tween 80-coated quartz sands revealed that solid phase Tween 80 enhanced nC_{60} transport, while gradual release of adsorbed Tween 80 resulted in greater nC_{60} retention. The corresponding nC_{60} retention profiles exhibited hyperexponential decay with distance from the column inlet. Steric repulsions are considered to be the likely mechanism for the enhancement of nC_{60} transport observed in this study.

CHAPTER 7

TRANSPORT AND RETENTION FULLERNE (C_{60}) NANOPARTICLES IN NATURAL SOIL

7.1 Introductions

As the nanotechnology market proceeds to $1 trillion (Nel et al., 2006), the production of fullerene C_{60} nanomaterials has reached industrial levels (Xie et al., 2008). In every stage of their lifecycle, such as manufacturing, application, and disposal, the release of C_{60} into the environment is possible (Wiesner et al., 2006). It has been reported that nanoscale C_{60} readily enters water in an aggregate form (Brant et al., 2005b; Deguchi et al., 2006; Duncan et al., 2008; Terashima and Nagao, 2007) even though the solubility of pure C_{60} in water is less than 10^{-9} mg/L (Fortner et al., 2005). Such C_{60} nanoparticles (nC_{60}) are negatively charged and suspensions of nC_{60} are stable for months due to particle-particle electrostatic repulsive forces. Some toxicology studies can suggest that nC_{60} is toxic to microorganisms (Fortner et al., 2005; Lyon et al., 2005; Sayes et al., 2004), fish (Oberdorster, 2004a), and human cell lines (Sayes et al., 2004), which raises concerns regarding adverse impacts of nC_{60} on aquatic systems and human health. Once C_{60} enters an aqueous system, exposure to nC_{60} may occur through several pathways (Colvin, 2003) including groundwater, and their distribution in the environment can be potentially extended via groundwater transport. Thus, it is important to understand the transport and retention of nC_{60} in natural soils and aquifer materials.

To date, most nC_{60} transport experiments have been conducted in columns packed with well-defined porous media, such as glass beads (Brant et al., 2005a; Espinasse et al., 2007; Lecoanet and Wiesner, 2004; Lecoanet et al., 2004). Although the use of glass beads and quartz sands provide researchers with reproducible matrix conditions and renders a transport experiment protocols and the subsequent data interpretation less complex, these materials do not adequately represent natural soils with respect to texture, clay, and organic matter content. For example, Shani et al. (Shani et al., 2008) conducted colloid transport experiments in both natural and cleaned sands and observed greater retention in the natural sand.

To our knowledge, only one nC_{60} transport study has been conducted in natural porous media (Cheng et al., 2005). The solid phase was Lula aquifer material, collected from Lula, OK, contained of 2% clay and 0.27% organic matter. The mean diameter (d_c) of Lula soil (as collector) was estimated to be 250 μm based on the fraction of coarse grains (e.g., 106-500 μm). At a pore-water velocity of 0.38 m/d, a nC_{60} suspension conditioned with 0.1 M NaCl and 0.1 M NaN_3, was continuously introduced into soil column and nC_{60} breakthrough was observed at 3.2 PVs. Although no effluent nC_{60} concentration plateau was developed, Eq. 2.10, which is based on the clean-bed filtration theory (Yao et al., 1971), was still applied by using an average C/C_0 value 0.33 to calculate an α (attachment efficiency factor) of 0.0046. After injecting 56.5 PV of the nC_{60} suspension, Cheng et al. (Cheng et al., 2005) observed a sharp drop in the nC_{60} relative concentration to zero, which was attributed to filter ripening. However, the distribution of nC_{60} retained was not quantified in this experiment, which rendered such an interpretation.

In this chapter, a series of column experiments (Table 7.1) were conducted to investigate the transport and retention of nC_{60} in natural soils. Two natural soils, Appling soil and Webster soil, were selected as representative porous media due to different clay and organic matter content. The concentration of nC_{60} in effluents and soil phase were determined to construct nC_{60} BTCs and retention profiles, respectively. To investigate the role of stabilizing agent on nC_{60} behavior in soils, transport experiments were performed in presence of SRHA and surfactant (e.g., Tween 80). Experimental data are interpreted within the context of particle-surface electrostatic interactions.

7.2 Results and Discussion

7.2.1 Transport of nC_{60} Alone

Complete retention of nC60 was observed in Appling and Webster soil following 5-PV pulse injections. The breakthrough of nC_{60} was not observed in any column packed with Appling or Webster soil when SRHA or Tween 80 was absent in aqueous or solid phase. Thus, nC_{60} BTCs were not shown. These findings indicate that the transport of nC_{60} in natural soil is distinct from that observed in glass beads and quartz sands (Brant et al., 2005a; Espinasse et al., 2007; Lecoanet and Wiesner, 2004; Lecoanet et al., 2004), in which nC_{60} were consistently observed in column effluent and steady-state concentrations were developed. Even when the injected pulse width was extended to 64.7 PV in Appling soil, no nC_{60} breakthrough was observed, in contrast with data of Cheng et

Table 7.1: Experimental conditions for nC_{60} transport studies conducted in Appling (AP) and Webster (WB) soils with 1.0 mM $CaCl_2$ and 0.05 mM $NaHCO_3$ as background electrolytes.

Column Identifier[a]	θ_w[b]	C_0[c] (mg/L)	PW[d] (pv)	ξ[e] (mV)	d_a[f] (nm)	MB[g] (%)	Ret[h] (%)
APC_{60}-5pv	0.41	4.31	5.0	-23.4	110	94.8	100.0
APC_{60}-32pv	0.40	4.37	32.5	-22.9	121	101.9	100.0
APC_{60}-65pv	0.37	4.26	64.7	-25.3	98.6	102.4	100.0
APC_{60}SRHAmix-I	0.39	4.69	5.0	-19.6	98.5	99.0	100.0
APC_{60}SRHAmix-II	0.34	4.15	5.3	-16	110.6	103.4	99.2
APC_{60}TW80mix-5pv-I	0.34	4.14	5.2	-15.9	102.5	96.8	43.2
APC_{60}TW80mix-5pv-II	0.34	4.27	5.2	-14.1	103.5	92.7	44.1
APC_{60}TW80mix-15pv	0.33	4.26	15.1	nd	nd	93.1	29.2
APC_{60}TW80coat	0.41	4.21	5.0	-25.2	94.1	99.9	100.0
APC_{60}TW80mix,coat	0.33	4.32	5.1	-14.6	104	92.3	36.4
WBC_{60}-I	0.46	4.42	4.8	-23.9	99.9	85.0	100.0
WBC_{60}-II	0.46	4.41	4.8	-23.9	99.9	89.1	100.0
WBC_{60}TW80mix	0.45	4.67	5.0	-15.6	100.1	96.2	100.0

[a] AP = Appling soil, WB = Webster soil, SRHA = Suwannee River humic acids, pv = pore volume, mix = nC_{60} premixed with SRHA or Tween 80, coat = Appling soil preflushed with Tween 80. [b] porosity determined gravimetrically. [c] nC_{60} concentrations in input suspensions. [d] pulse width. [e] zeta potential of nC_{60}. [f] mean hydrodynamic diameter of nC_{60}. [g] mass balance. [h] retention.

al. (2005), where nC_{60} appeared in column effluent at 3.2 PV, and then disappeared from effluent after 56.7 PVs. Inspection of the soil physical properties reveals that the clay and organic carbon contents of Appling soil were ca. 4 and 3 times greater than those in Lula soil (Table 3.3), respectively, which may have been responsible for higher nC_{60} retentions observe herein.

Retention profiles for nC_{60} in Appling and Webster columns are depicted in Figure 7.1. When a 5-PV pulse (ca. 100 mL) of nC_{60} suspension was introduced, the spatial distributions of retained nC_{60} in Appling and Webster soil were similar, with a maximum concentration (ca. 38 µg/g dry soil) near the column inlet and non-exponentially

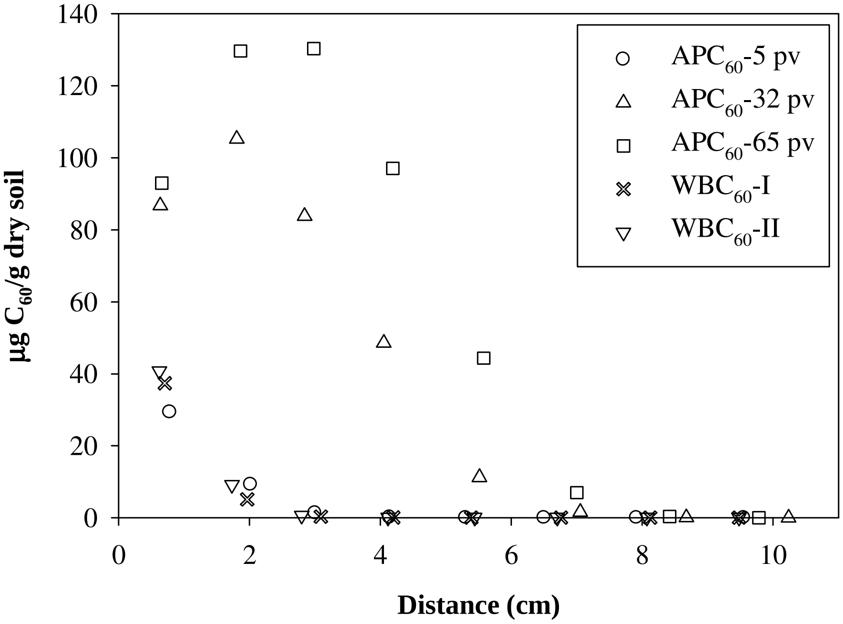

Figure 7.1: Retention profiles of nC_{60} in water-saturated columns packed with Appling (AP) or Webster (WB) soils. Aqueous nC_{60} suspensions were prepared in absence of stabilizing agents and contained 1.0 mM $CaCl_2$, applied at a pore water velocity of 7.9 m/d. No nC_{60} breakthrough was observed in all these experiments.

decreasing to zero at ca. 4 cm from the inlet. When the pulse width of transport experiment in Appling soil increased to 32.5 PV, the nC_{60} retention profile exhibited a concentration of ca. 110 μg/g dry soil at ca. 2 cm from inlet and nC_{60} was not absent in soil until ca. 7 cm from the column inlet. A concentration plateau with a value of 130 μg/g dry soil was developed at the first 2 – 3 cm and nC_{60} was present in the first 8.5 cm of the column, when the pulse width was further doubled to 64.7 PV. The presence of concentration plateau implied that the maximum retention of nC_{60}, 130 μg/g, in Appling soil was reached. The features of nC_{60} retention profiles, such as the concentration peak and plateau, were similar to those observed in fine Ottaws sands (Chapter 4), which strengthened the importance of the presence of clay component on nC_{60} retention. Natural soil is complicated and the broad particle size distribution may result in the presence of narrow pores. Thus, physical straining may occur and contribute to nC_{60} retention, especially when pore throats are even narrower than the particle/grain diameter ratio of 0.0016 (Shen et al., 2008). In addition, Cheng et al. (2005) suggested that filter ripening contributed to nC_{60} retention in natural soil. However, the low concentrations near column inlet and presence of concentration plateau in nC_{60} retention profiles did not support the occurrence of filter ripening, with which a monotonic decay would be expected in retention profile.

For further investigating interactions between nC_{60} nanoparticles and soil grains, streaming potentials of Appling soil were measured in University of California, Riverside and found to be -5.68 ± 0.55 mV, which was ca. 5.5-fold less than the zeta potential of

Ottawa sands. Following the sphere-plate DLVO model (Chapter 5), an energy barrier of ca. 1.7 kT and secondary energy minimum of ca. -0.08 kT were obtained for nC_{60}-Appling soil system Figure 7.2. The sphere-plate model was used here because the soil grain size was estimated to be 0.98 μm by assuming that clay particles were spherical and contributed to the majority of specific surface area (3.50 m^2/g). Compared to nC_{60}-sand system (Chapter 5) at the same chemical condition (e.g., 1 mM $CaCl_2$), the energy barrier (1.7 kT) was 20 times less, although the secondary attractive minimum was comparable, which was consistent with the higher retention in Appling soil. Due to difficulties on measuring Webster soil streaming potential, the direct DLVO energy

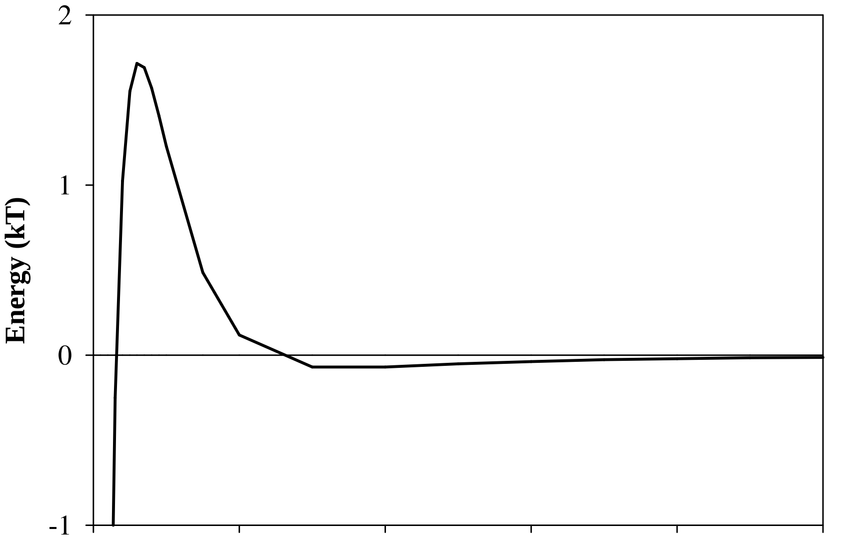

Figure 7.2: Interaction energy between a fullerene nanoparticle and Appling soil grain. The suspension was conditioned with 1.0 mM $CaCl_2$ and 0.05 mM $NaHCO_3$.

calculation for nC_{60}-Webster soil system is not available, yet the contribution of electrostatic interactions to nC_{60} retention in Webster soil is presumable. In addition, interactions of nC_{60} with soil organic matter due to inherent hydrophobicity of nC_{60} is likely to have contributed to nC_{60} retention in Appling soil and Webster soil.

7.2.2 Tracer Tests

The bromide concentrations in effluent samples (C) collected during the nonreactive tracer transport experiment were normalized to the influent concentration (C_0) and the resulting relative concentrations (C/C_0) were plotted against time in a unit of PV to construct a BTC. A representative tracer (Br^-) BTC in columns packed with Appling soil is presented in Figure 7.3. The bromide BTCs were fit to the 1-D advective-dispersive reactive (ADR) transport equation in a dimensionless form (Eq. 3.1 and 3.2) using the CXTFIT model (Toride et al., 1999). For BTCs in Appling soil columns, Pe and R_F were chosen as fitting parameters, and their resulting average fitted values were 100.4±26.3 and 1.00±0.08, respectively. Following a similar modeling procedures, however, the average fitted R_F (0.72±0.01) of Br^- in water-saturated Webster soil columns was less than unity when the gravimetrically-determined porosity (ca. 0.46) was used. The early breakthrough of bromide in Webster soil was attributed to an over-estimation of porosity and/or anion exclusion effects of clay particles, since the contribution from immobile water and preferential flow can be excluded by the symmetrical shape of tracer BTCs. As an alternative, the porosity of Webster soil was determined using the soil particle density

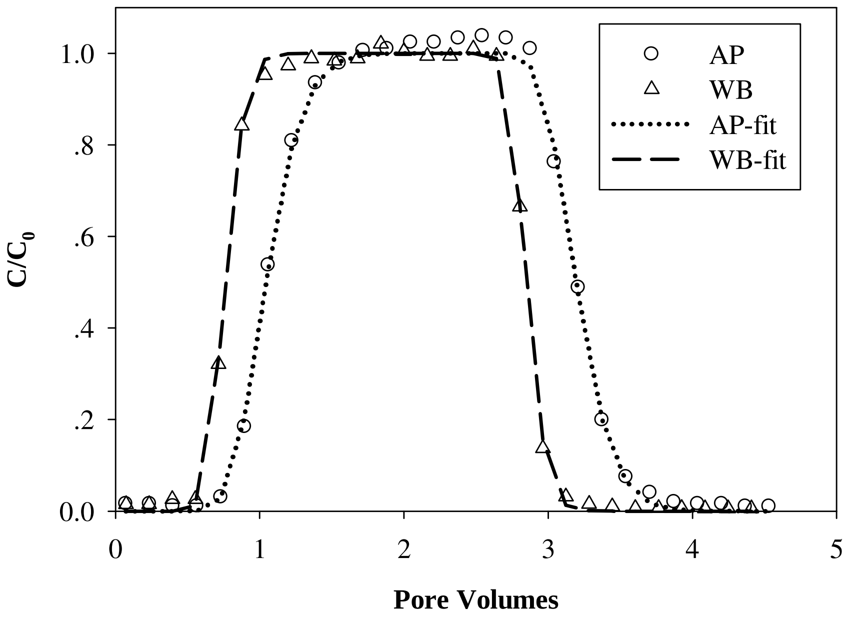

Figure 7.3: Measured and simulated representative non-reactive tracer breakthrough curves in columns packed with Appling (AP) or Webster (WB) soils.

(ρ_p) and bulk density (ρ_b) as follows:

$$\theta_w = 1 - \frac{\rho_b}{\rho_p} \tag{7.1}$$

The particle density of Webster soil was measured to be 2.63 g/cm^3 using the pycnometer method developed by Blake and Hartge (1986). With an average bulk density of 1.45 g/cm^3, the porosity of Webster soil was calculated to be 0.45, which was consistent with gramimetrically-determined porosity of 0.46, suggesting that the initial value was correct. The effect of anion exclusion on bromide tracer tests has been observed in fine-textured soils (Dousset et al., 2007; Gamerdinger et al., 1990). The anion exclusion volume can be estimated based on double layer theory (Dehaan, 1964) as follows:

$$V_{ex} = SSA \times d^{-} \tag{7.2}$$

where *SSA* is the specific surface area of particles (e.g., 8.2 cm^3/g), and d^- is the equivalent distance of exclusion. The value of d^- can be estimated from solution properties as (Bolt and Bruggenwert, 1976):

$$d^{-} \approx \frac{\omega}{z^{+}\sqrt{N_t}} \tag{7.3}$$

where, ω is a constant and equal to 6 for Br^-, z^+ is the valance of the dominant cation and equal to 2 for Ca^{2+}, and N_t is the total electrolyte concentration and equal to 0.003 keq/m^3 in this study. Based on these values, an effective exclusion distance of 5.5 nm was obtained. Then the anion exclusion volume was estimated to be 5% of the total pore volume based on the following equation:

$$Exlusion\% = \frac{clay\% \times V_{ex} \times \rho_b}{\theta_w} \tag{7.4}$$

where, the clay content of Webster soil was 33% and the porosity was 0.45. Thus, a retardation factor of 0.95 would be obtained if anion exclusion was the only contributor to early breakthrough. Since the experimentally determined value was 0.72, other mechanisms are likely to have contributed to early tracer breakthrough in Webster soil, such as soil compression and development of vertical soil fractures.

7.2.3 Effects of SRHA

No nC_{60} nanoparticles were detected in column effluent when a 5-PV pulse of the nC_{60} input suspension premixed with 20 mg C/L of SRHA, was introduced into the

Appling soil column. Thus, only the nC_{60} retention profile is shown in Figure 7.4, which exhibits a peak concentration of ca. 15 µg/g dry soil at ca. 3 cm from the column inlet before declining gradually to solid phase concentration approaching zero at ca. 8 cm. The nC_{60} input suspension was injected to the soil column immediately after mixing with 20 mg C/L of SRHA, when relative higher nC_{60} zeta potentials (e.g., -19 mV) were obtained than those of the equilibrated nC_{60}-SRHA suspensions (e.g., -16 mV in Chapter 6).

Commonly, a bed length required to achieve a 99.9% removal was calculated based on clean-bed filtration theory to evaluate the mobility of nanoparticles in porous media (Chen and Elimelech, 2007; Chen and Elimelech, 2008; Espinasse et al., 2007; Lecoanet and Wiesner, 2004; Lecoanet et al., 2004; Pelley and Tufenkji, 2008). However, such an

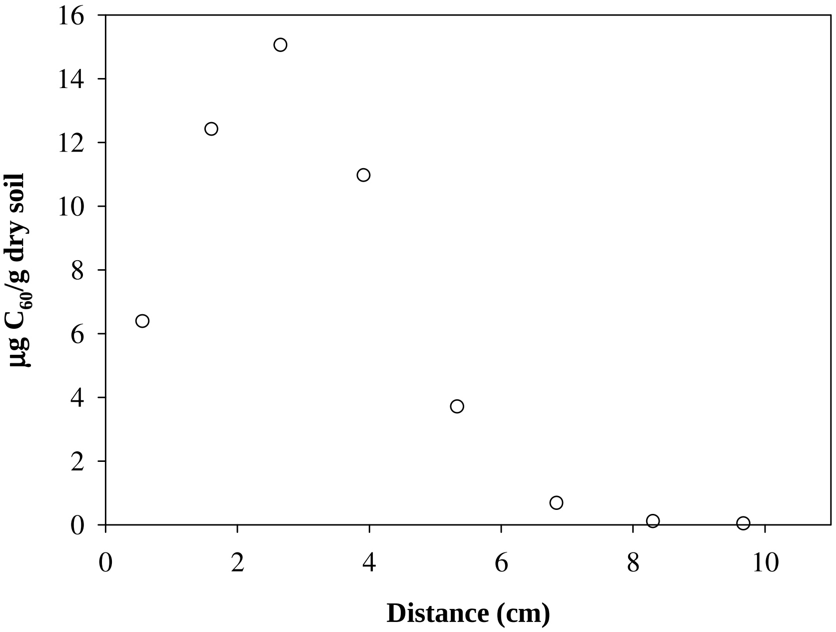

Figure 7.4: Retention profiles of nC_{60} in presence of 20 mg C/L Suwannee River humic acids (SRHA) in columns packed with Appling soils. No breakthrough of nC_{60} or SRHA was observed.

approach was not applicable in this study to evaluate effects of SRHA on nC_{60} transport due to the absence of nC_{60} breakthrough and the invalidation of clean-bed filtration theory in this system, indicated by the non-exponential decay of retention profile. Rather, the particle presence length, defined as the column depth where the nC_{60} soil phase concentration was first observed to approach zero, was used. Compared to the retention profile in the absence of SRHA (e.g., C_{60}-5pv), the nC_{60} presence length increased to 8.5 cm from 3 cm, indicating the presence of SRHA with a concentration of 20 mg C/L facilitated nC_{60} transport in Appling soil.

Consistent with results in Chapter 6, the zeta potentials (Table 7.1) of nC_{60} was observed to be negatively reduced (less negative) yet the mobility of nC_{60} was enhanced in the presence of 20 mg C/L SRHA. Similar to nanoparticle-SRHA-quartz systems (Chen and Elimelech, 2008; Pelley and Tufenkji, 2008), the enhancement of nC_{60} transport in the presence of SRHA was attributed to steric repulsions. However, such repulsions between SRHA-coated nC_{60} and soil grains were expected to occur through certain length in packed soil, since the retention capacity of soil to SRHA was not fully reached within 5 PV of suspension injection, reflected by the absence of SRHA breakthrough. The attachment to fine clay particles and partitioning to soil organic carbons were likely mechanisms for strong SRHA retention in Appling soil. Wherever soil surface is coated with SRHA, steric repulsions occur, resulting in less nC_{60} retention in soil. Thus, relative lower nC_{60} solid phase concentrations before 3 cm were possibly due to the coating of SRHA onto soil. Although nC_{60} were able to transport through retention-unfavorable regions near column inlet due to steric repulsions, they were further retained in later part of soil column, where Appling soil were barely covered with SRHA.

7.2.4 Effects of Tween 80

7.2.4.1 Solid Phase Tween 80 in Appling Soil

When the pure 1,000 mg/L Tween 80 solution (e.g., no nC_{60}) conditioned with 1.0 mM $CaCl_2$ and 0.05 mM $NaHCO_3$ was introduced to the Appling soil column, Tween 80 broke through at ca. 1.6 PV and a steady state was developed at 5.2 PV (Figure 7.5B), yielding a retention of 25% of total input Tween 80. The retardation of breakthrough and the strong retention were attributed to adsorption of Tween 80 onto fine clay particles and soil organic carbons. Assuming uniform distribution of coated Tween 80 along the column, a surface loading of 387.5 µg/g dry soil was obtained. The coating of Tween 80 slightly decreased Appling soil streaming potentials from -5.7 ± 0.5 to -5.2 ± 0.2 mV (University of California, Riverside). Immediately following Tween 80 preflushing process, nC_{60} suspension alone (e.g., no SRHA or Tween 80) was pulse-injected into the Appling column to investigate effects of sorbed Tween 80 on nC_{60} transport. However, coating Appling soil with Tween 80 did not lead to nC_{60} breakthrough (nC_{60} BTCs not shown). The concentration of retained nC_{60} non-exponentially decayed with distance with a maximum value of 17 µg/g dry soil near the column inlet and a particle presence length of 7 cm (Figure 7.5A). The longer particle presence length than that in C_{60}-5pv (e.g., 3 cm) indicated Tween 80 coating on Appling soil enhanced nC_{60} transport in Appling soil.

Similar to observations in Chapter 6, solid phase concentrations of nC_{60} hypoexponentially decayed with distance (Figure 7.5A). This feature of nC_{60} retention profile was attributed to more available sites for nC_{60} deposition produced when preattached Tween 80 were gradually washed off from solid phase during nC_{60} injection. The mathematic model (developed by Linda Abriola's research group at Tufts University), simultaneously coupling the release of attached Tween 80 and the nC_{60} attachment, has successfully captured both BTC and retention profile.

7.2.4.2 Aqueous Phase Tween 80 in Appling Soil

Interestingly, when 1,000 mg/L Tween 80 was present in input suspensions, nC_{60} readily transport through columns packed with Appling soil, regardless applications of the Tween 80 coating process (Figure 7.6A), indicating that Tween 80 (1,000 mg/L) exhibited stronger effects on nC_{60} transport compared to SRHA (20 mg C/L), which was not discovered in quartz sand columns (Chapter 6). When a 5-PV of nC_{60} (ca. 4.3 mg/L) and Tween 80 (1,000 mg/L) mixture was introduced into uncoated Appling soil, nC_{60} broke through columns at 1.2 PV and the resulting asymmetrical BTCs gradually ascended to a maximum value (ca. 0.7) before sharply descending to the relative concentration approaching zero, yielding that ca. 44% of total input nC_{60} were retained in Appling soil. When the pulse width was extended to 15 PV, the gradual increase of nC_{60}

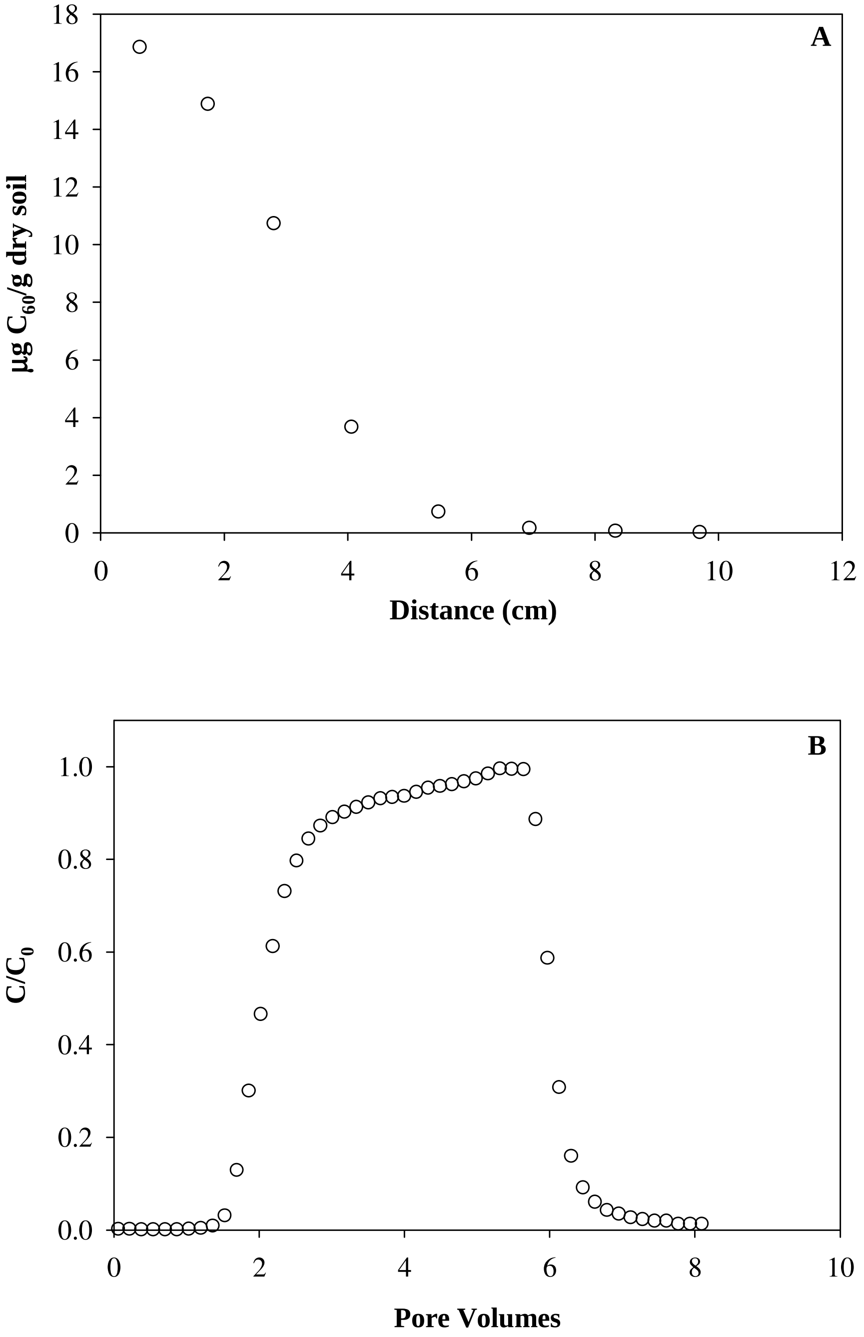

Figure 7.5: Retention profiles (A) of nC_{60} in the absence of Tween 80 in a column packed with Tween 80-preflushed Appling soils. Relative concentrations of Tween 80 in effluent samples in the preflushing process are shown in B. The concentration of input Tween 80 is 1,000 mg/L.

relative concentration continued till 13.5 PV, from which a plateau was developed before sharply descending. The presence of plateau in nC_{60} BTCs suggested that steady-state was reached, where the nC_{60} attachment rate was equal to the detachment rate. While an nC_{60} and Tween 80 mixture was introduced into Appling soil precoated with Tween 80, as anticipated, nC_{60} broke through the column at as early as 0.6 PV and then gradually increased to a maximum relative concentration of 0.64, which was slightly lower than that when Tween 80 was only present in aqueous phase (e.g., Exp. C_{60}TW80mix-5pv-I, II).

Solid phase concentrations of C_{60} in presence of Tween 80 are plotted in Figure 7.6B. When Tween 80 at 1,000 mg/L was present in input suspensions, nC_{60} appeared in all dissected samples and the nC_{60} retention profiles exhibited a concentration peak consistently at ca. 1.8 cm off the column inlet. When 5 PV of nC_{60} and Tween 80 mixture were introduced, the concentration of retained nC_{60} ranged from 0.8 to 2.2 μg/g. When the pulse width was tripled, the concentration range of retained nC_{60} increased to from 2.1 to 4.2 μg/g. Preflushing the soil column with 1,000 mg/L Tween 80 prior to introduction of the nC_{60} and Tween 80 mixture resulted in slight lower nC_{60} solid phase concentrations, but similar profile pattern. The reason causing this profile pattern is still unclear and the mathematical modeling for retention data is needed.

Effluent BTCs and retention profiles of nC_{60} clearly showed that the transport of nC_{60} was greatly enhanced in the presence of aqueous phase Tween 80, while the retention nC_{60} was reduced nearly 3 folds (Table 7.1). Consistent with results in Chapter

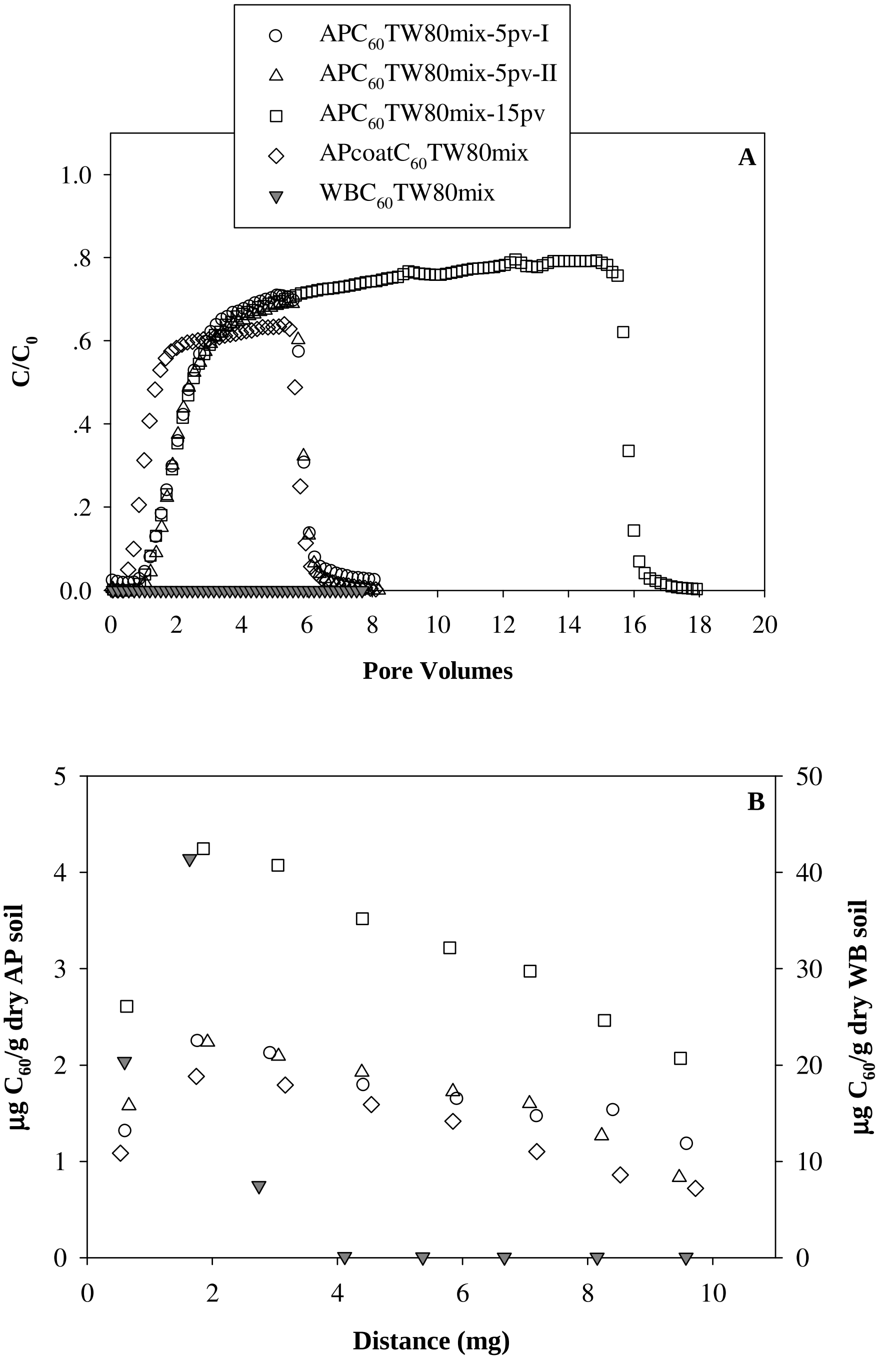

Figure 7.6: Breakthrough curves (A) and retention profiles (B) of nC_{60} premixed with 1,000 mg/L Tween 80 (TW) in columns packed with Appling (AP), Webster (WB; solid symbol), or Tween 80-preflushed Appling (APcoat) soils. No breakthrough of nC_{60} or Tween 80 was observed in Webster soil columns.

6, the presence of Tween 80 negatively reduced (less negative) zeta potentials of both nC_{60} and Appling soil, which would promote nC_{60} retention based on DLVO theory. Thus, the significant decrease of nC_{60} retention than that in Exp. C_{60}-5pv was primarily attributed to the steric repulsion between coated nC_{60} ("laying-on-surface" model in Chapter 6) and soil surface. In contrast with SRHA, a 5-PV pulse injection of 1,000 mg/L Tween 80 was sufficient to coat all packed soil grains (Figure 7.5B), suggesting that the aqueous phase Tween 80 coated soil surface, partially, through competing with nC_{60} for available adsorption sites, when input suspensions premixed with 1,000 mg/L Tween 80 were introduced into uncoated soil columns. Such competition between nC_{60} and aqueous phase Tween 80 was absent when nC_{60} and Tween 80 mixtures were injected into soil precoated with Tween 80 (Exp. APcoatC_{60}TW80mix), resulting in earlier breakthrough and steeper ascending portions in BTCs. The data in Chapter 6 clearly demonstrated that interactions between nC_{60} and quartz in the presence of aqueous phase Tween 80 were minimized. Thus, it is speculated that attachments of nC_{60} to quartz surface (e.g., not coated with organic carbons) negligibly contributed to nC_{60} retention when Tween 80 were present in both aqueous and solid phases (Exp. APcoatC_{60}TW80mix). Rather, the retention of nC_{60} in this case was mainly due to their adsorptions to soil organic carbons, resulting in lower maximum C/C_0 value than that in the presence of only aqueous Tween 80, where nC_{60} attachments occurred on both quartz and organic carbon sites. In addition, distal portions of nC_{60} BTCs were coincident with tracer tests, indicating that nC_{60} did not release once attached. Thus, secondary energy minima did not contribute significantly to nC_{60} retention in the presence of Tween 80.

To further investigate fullerene nanoparticle retention in Appling soil, the fractional surface coverage (*θ*) was calculated from effluent BTCs based on Eq. 5.3. When Tween 80 were absent, the surface coverage of Appling soil by nC_{60} particles linearly increased with time to a maximum surface coverage 0.0036% at the end of 5PV pulse injection (Figure 7.7). In the presence of only aqueous Tween 80, however, the surface coverage nonlinearly increased with time to a maximum value of 0.0011%, while a maximum value of 0.0009% was obtained at the end of 5 PV of introduction of the nC_{60} and Tween 80 mixture into Appling soil preflushed with Tween 80. These findings are consistent

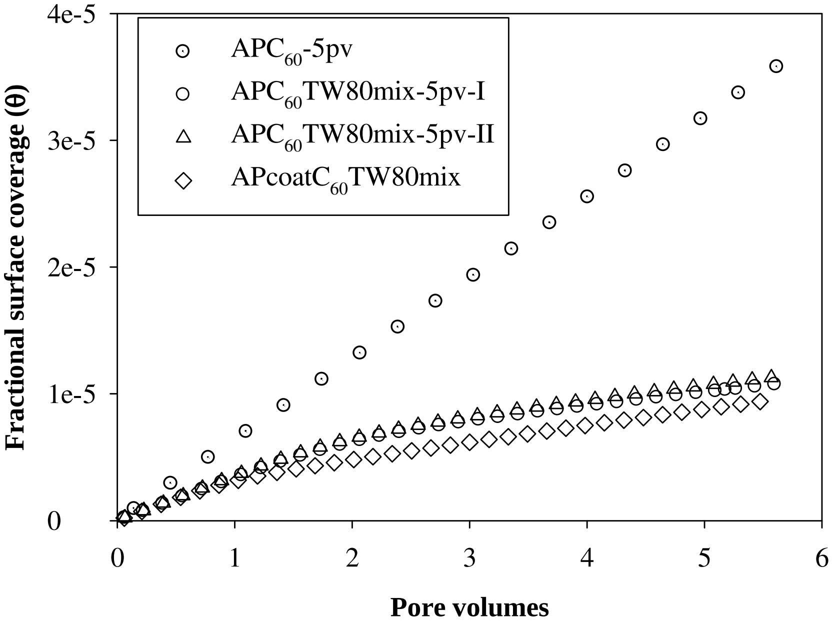

Figure 7.7: Change in the fractional surface coverage of Appling soil with time following the introduction of nC_{60} aggregates suspensions in the absence and presence of Tween 80.

with sequentially decreasing nC_{60} retentions in the absence of Tween 80, in the presence of only aqueous Tween 80, and in the presence of both aqueous and solid phase Tween 80 (Figure 7.1 and 7.6).

7.2.4.3 Aqueous Tween 80 In Webster soil

The BTCs and retention profiles of nC_{60} in the presence of 1,000 mg/L Tween 80 in columns packed with Webster soil are shown in Figure 7.6A and 7.6B, respectively. Contrast to in Appling soil columns, 100% of both input nC_{60} and Tween 80 were retained in Webster soil, indicating Webster soil exhibited even higher retention capacity than Appling soil due to higher organic matter content (3.3%) and higher clay content. The retained nC_{60} exhibited a concentration peak at ca. 1.8 cm off inlet, rather than monotonic decrease in the absence of Tween 80, with a particle presence distance of 4 cm, which was 1 cm further than that in the absence of Tween 80, indicating the presence of Tween 80 in input suspension enhanced nC_{60} transport in Webster soil. The presence of peak in the nC_{60} retention profiles was possible due to the partial filling of Webster soil retention capacity to Tween 80.

7.3 Summary and Conclusions

A series of column experiments was conducted to investigate nC_{60} transport in two natural soils, Appling and Webster soil. The data obtained from these transport experiments demonstrated that nC_{60} transport and retention behaviors were different than in well-defined porous media, such as glass beads and quartz sands. The presence of fine particles (e.g., clay) and soil organic matter dramatically reduced nanoparticle transport, while retention was greatly enhanced. For instance, in absence of stabilizing agents (e.g., SRHA or Tween 80), complete retention of input nC_{60} was observed in experiments even after introducing 65 PVs (ca., 1,300 mL) of nC_{60} suspensions (ca. 4.5 mg/L). The concentration of retained nC_{60} in Appling soil, which contained 0.75%wt. of organic carbon and 9%wt. of clay, was as high as 130 µg/g.

Appling soil exhibited strong retention capacity not only to nC_{60}, but also SRHA, which was attributed to the presence of soil organic matter. The injection of 5 PV of 20 mg C/L SRHA was sufficient to enhance the transport of nC_{60}, reflected by a longer nC_{60} retention profile length than that in absence of stabilizing agents. The mobility of nC_{60} was greatly enhanced in the presence of aqueous Tween 80 at a concentration of 1,000 mg/L. Steric repulsions developed between Tween 80 coated nC_{60} and Tween 80 treated soil surface significantly reduced nC_{60} retention, resulting in more than 55% of total input nC_{60} being transported through the column. Webster soil, which contained higher organic carbon and clay than Appling soil, exhibited even greater retention to nC_{60} and Tween 80, strengthening the agreement that clay minerals and soil organic matter play an important role in nanoparticle retention.

These findings indicate that natural soils will exhibit less transport and greater retention to nC_{60} transport when compare to quartz sands of similar particle size. The presence of NOMs and surfactants, however, may greatly enhance nC_{60} mobility in natural subsurface environments.

CHAPTER 8

TRANSPORT AND RETENTION OF MULTI-WALL NANOTUBES IN QUARTZ SANDS

8.1 Introduction

Carbon nanotubes (CNTs) are tubular carbon macro-molecules with diameters of few nanometers and lengths of up to several centimeters (Zheng et al., 2004). Due to their unique physical properties, CNTs have been considered as promising materials for various applications, such as solar cells, biomedical, sensors, and high tensile strength materials (Gannon et al., 2007; Kong et al., 2000; Li et al., 2007). There is little doubt that CNTs will be released into the environment with commercial production and use, either from industrial sources or through disposal in municipal waste. Although CNTs are insoluble in water due to their hydophobicity and large aspect ratio, a recent study by Hyung et al. (2007) has demonstrated that stable aqueous MWNT suspensions can be prepared with the aid of NOM, which is ubiquitous in aquatic systems. In addition, cytotoxicity studies have shown that suspended CNTs in water or culture media exhibit toxic responses in to human cell lines, such as kidney and lung cells (Hussain et al., 2009). The aqueous solubility and health concerns of CNTs necessitate a more complete understanding on CNT fate and transport in porous media, which is also needed to design effective removal strategies for drinking water treatment.

To date, a single study has been published (Jaisi et al., 2008) that addresses CNT transport and deposition behavior in quartz sands. In these column experiments, influent suspensions of carboxyl-functionalized SWNTs (87 mg/L) were prepared using ultrasonication, conditioned with KCl at various concentrations and buffered to pH 7. The mean hydrodynamic diameter of SWNTs conditioned with 0.1 mM KCl was determined to be ca. 118 nm at the start of the transport experiment using DLS and slightly increased (ca. 130 nm) after passing through the column at a Darcy velocity of 15.7 m/d. TEM images showed single tubes with aspect ratios of up to 1000 (Jaisi et al., 2008). During column experiments, authors observed the presence of plateau on symmetrical BTCs, which was further interpreted using clean-bed filtration theory (Eq. 2.10). An attachment efficiency factor (α) of 0.98 or 1.04 was obtained at an ionic strength of 7 or 55 mM, respectively. Jaisi and coauthors (2008) also studied the release of retained SWNTs, concluding that physicochemical filtration dominated SWNT retention in quartz sand although physical straining did contribute to retention. No solid-phase retention data, however, were reported in the study.

The large aspect ratio of CNTs is a unique feature compared to from other fullerene-based nanomaterials (e.g., C_{60}), and has been found to be a determinant of their electronic, thermal, and mechanical properties (Hong and Myung, 2007; Kim et al., 2001; Saito et al., 1992; Yu et al., 2000). Similarly, the aspect ratio has been observed to impact bacterial and colloid transport in porous media (Salerno et al., 2006; Weiss et al., 1995; Xu et al., 2008), although the ratio is typically less than 4. A recent modeling study by Xu et al. (2008) suggests that particles with an aspect ratio of greater than 1 pass through pores with a preferential orientation, in which the major axis matches the local flow direction. The adoption of this preferential orientation became more pronounced as the aspect ratio increased. Although drawing an analogy between CNTs and rod-like colloidal particles may not be appropriate, the aspect ratio (i.e., tube length) of CNTs is anticipated to strongly influence transport in porous media. However, the effects of nanotube lengths were not considered in the study (Jaisi et al., 2008).

In this study, the primary objective was to investigate transport and retention behavior of MWNTs in water saturated quartz sands as a function of tube length. A new chemical modification method, which effectively dispersed nanotubes in water without or with minimal structural damage, was used to prepare MWNT suspensions with three indicated MR tube lengths: 0.5 to 2 (short), 10 to 20 (medium), and 50 µm (long). The MWNT suspensions were characterized using TEM, DLS, UV-vis photometer, and UV fluorophotometer. Then a series of transport experiments was conducted in 1-D columns packed with 40-50 mesh Ottawa sands at two input concentrations (5 and 90 mg/L). Both MWNT effluent BTCs and retention profiles were constructed, and compared to SWNT and nC_{60} transport data.

8.2 Results and Discussion

8.2.1 MWNT Suspension Characterization

Although CNTs are promising nanomaterials for nanotechnology, their practical applications in various areas, such as biology and material science, have been considerably hindered by their extreme insolubility in water or solvents. Studies have shown that CNTs can be effectively dispersed in water through ultrasonication (Saleh et al., 2008), surface alteration via stabilizing agents (e.g., surfactant) (Chen et al., 2004), and chemical modification (Zhao et al., 2002). However, ultrasonication and current chemical modification methods significantly alter CNTs, especially the length to width ratio, due to localized high temperatures (Hilding et al., 2003) and utilization of strong acids (Lee et al., 2008). Although certain surfactants facilitate CNT dispersion in water with slight impacts on CNT properties, the separation of CNTs and associated surfactants in later processing stages is problematic. A chemical modification method was developed by Lee et al. (2008) to functionalize MWNTs with 4-substituted benzoic acids (e.g., 4-ethoxybenzoic acid) in a mild acid environment. It has been reported that this chemical method uniformly and covalently coats MWNT surface with ethoxybenzoyl moieties, and exhibits no or minimal damage to MWNT structure integrity (Lee et al., 2008) A schematic structure of such functionalized MWNTs is shown in Figure 8.1.

Through the preparation protocol described previously, concentrations of short (0.5-2 μm), medium (10-20 μm), and long (50 μm) MWNTs in stock suspensions were determined gravimetrically to be 2,700, 1,875, and 1,875 mg/L, respectively. In order to make experimental conditions as close to natural water, and to maintain MWNT suspension stablility, the pH of each input suspension was adjusted from ca. 2 to 5 with NaOH (0.1 or 1 M). At the lower MWNT concentrations (5 mg/L), input suspensions were conditioned to an ionic strength of 5.0 mM with NaCl after pH adjustment, while ionic strengths of input suspensions at the higher MWNT concentrations (90 mg/L) were

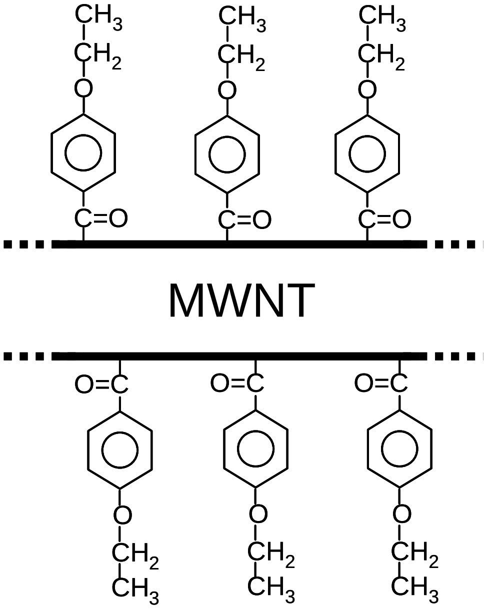

Figure 8.1: Schematic structure of a multi-wall nanotube (MWNT) functionalized with 4-ethoxybenzoic acid. Modified from Lee et al. (2008).

very close to 50 mM after pH adjustment and were not further adjusted with NaCl. Prior to each transport experiments, MWNT suspensions were characterized using UV-vis spectrometer, fluorophotometer, DLS, and TEM as discussed bellow.

8.2.1.1 UV-vis Spectra

The MWNT suspension at each MR length was scanned from 200 to 800 nm before and after pH adjustment and representative spectra at a concentration of 5 or 90 mg/L were shown in Figure 8.2A or 8.2B, respectively. At each concentration, the spectrum slightly varied before and after pH adjustment (to pH 5), indicating very little impact of pH adjustment on MWNT spectra. At the lower concentration (5 mg/L), the spectrum for medium (10-20 μm) MWNTs exhibited a peak and shoulder at ca. 245 and 450 nm, respectively, in contrast to those of nC_{60}, which exhibited strong absorbance peaks at 218, 266, and 344 nm and a shoulder at 460 nm. The UV absorbance peak at 245 nm was consistent with findings in previous studies (Jiang et al., 2003). Generally, the low UV absorbance was observed spanning from 0.07 to 0.36, which suggests that quantification of MWNTs through UV response was not feasible when concentrations were lower than 5 mg/L. At the higher MWNT concentration (90 mg/L), the absorbance peak at 245 nm was observed by spectrum saturation and the absorbance range was dramatically enhanced to from 1.2 to 2.7, allowing MWNT quantification by UV absorption. Thus, the UV response at 450 nm was used to determine MWNT concentration in aqueous suspensions using a 5-point calibration curve prepared over a concentration range of 1 to 100 mg/L. Based on Hubaux-Vos method (1970), the detection limit of this quantification method was 3.9, 2.8, and 6.8 mg/L for short, medium, and long MWNTs, respectively. Although data were not shown, short and long MWNTs exhibited similar UV-vis spectra, except that the absorbance peak at 450 nm was absent in short MWNT spectra.

8.2.1.2 UV-fluorescence Spectra

A striking feature of the MWNT suspension prepared in this study was that it exhibited green color when illuminated with a flashlight, which had not been observed in CNT suspensions prepared using either ultrasonication or superacid modification methods (Saleh et al., 2008; Zhao et al., 2002). The green fluorescence was believed to

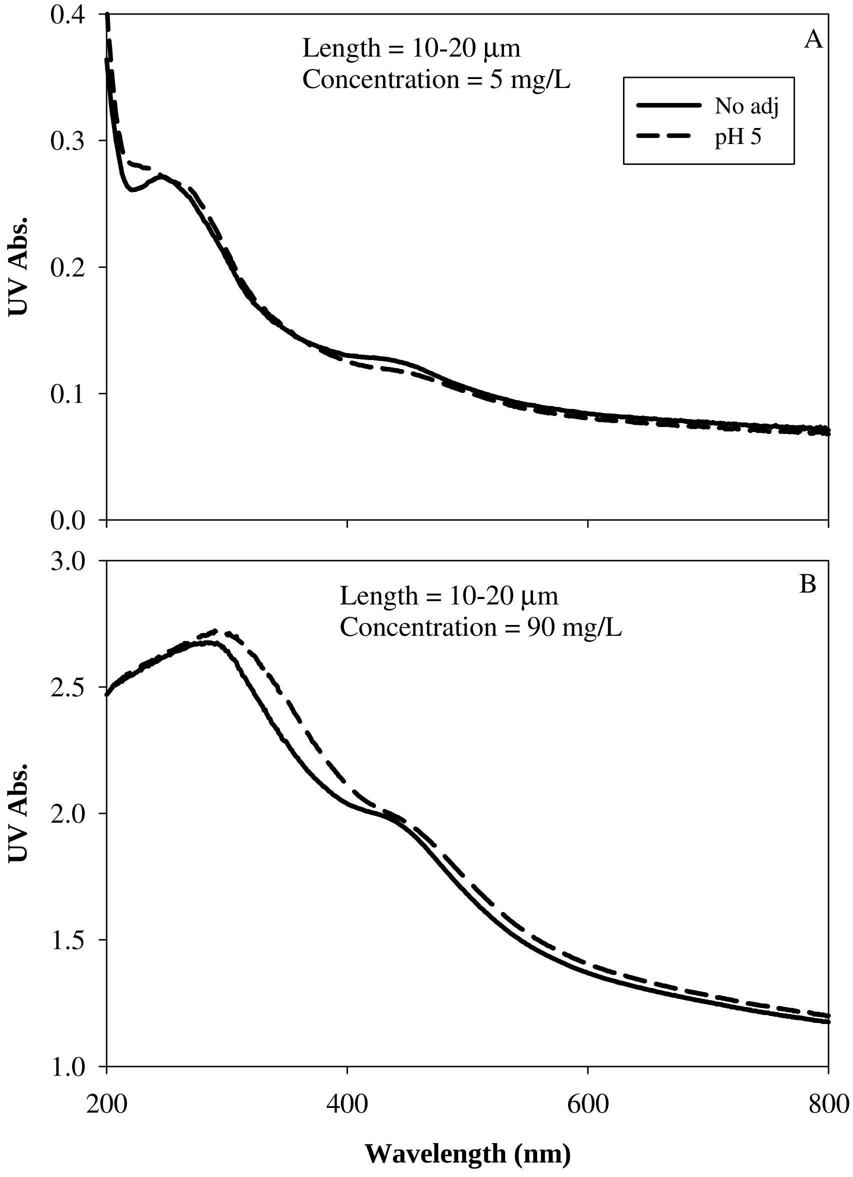

Figure 8.2: Representative UV spectra of functionalized multi-wall nanotubes (MWNTs) at two different concentrations before (dash lines) and after (solid lines) pH adjustment.

be due to a charge complex formed between the ether-link (electron withdrawal) and ethoxide group (electron donation). Regardless of the MR length of MWNTs, the strongest fluorescence emission was observed when suspensions were excited at ca. 450 nm (Figure 8.3A). At an excitation wavelength of 450 nm, the maximum fluorescence emission was observed at an emission wavelength of ca. 515 nm (Figure 8.3B), which was consistent with the green color observed under a flashlight. When the pH of each suspension was adjusted to 5,, a few-nanometers shift was observed for the maximum emission wavelength and the maximum fluorescence intensity decreased slightly. In addition, the fluorescence data suggest that the maximum emission wavelength shifted toward violet with the increasing MR length. For example, a maximum emission wavelength of 517 and 511 nm was observed for short or long MWNTs, respectively. Although the maximum fluorescence wavelength varied with pH and MR length, the fluorescence intensity at the excitation wavelength of 450 nm was sufficient to provide quantification of MWNTs at lower concentrations (e.g., less than 5 mg/L). A 5-point calibration curve over a concentration range of 0.1 to 5 mg/L was prepared for MWNTs at each length. As expected, the fluorescence intensities and MWNT concentrations showed a positive linear relationship ($R^2 = 0.99$; data not shown). With this quantification protocol, concentrations as low as 0.73, 0.68, and 0.39 mg/L were measurable for short, medium, and long MWNTs, respectively, which allowed for measurement of MWNT transport at lower input concentrations.

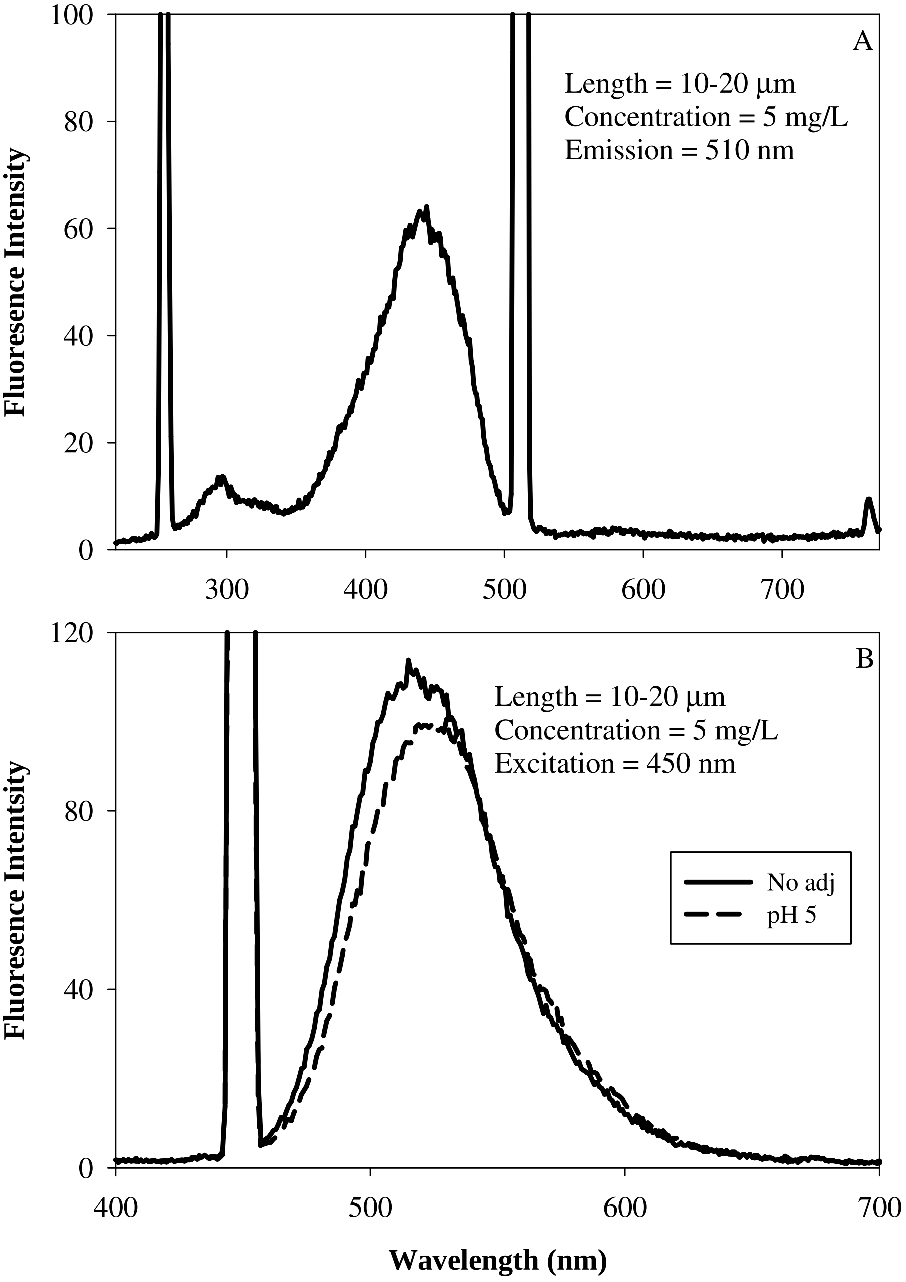

Figure 8.3: UV-fluorescence excitation scan (A) and emission scan (B) spectra of medium multi-wall nanotubes (MWNTs) with a concentration of 5 mg/L.

8.2.1.3 Electrophoretic Mobility

To assess the surface charge of MWNTs, electrophoresis experiments were performed, where measured electrophoretic mobilities (EMs) were plotted against MR length in Figure 8.4. All dispersed MWNTs prepared through chemical modification were negatively charged regardless of the initial concentration, MR length and suspension pH, with EMs ranging from -2.3 to -4.5 x 10^{-8} $m^2V^{-1}s^{-1}$. Saleh et al. (2008) reported that suspended bare MWNTs prepared through ultrasonication were also negatively charged, but their EMs at similar chemical solution conditions were all ca. -2.5 x 10^{-8} $m^2V^{-1}s^{-1}$. The relatively more negative values observed in this study may

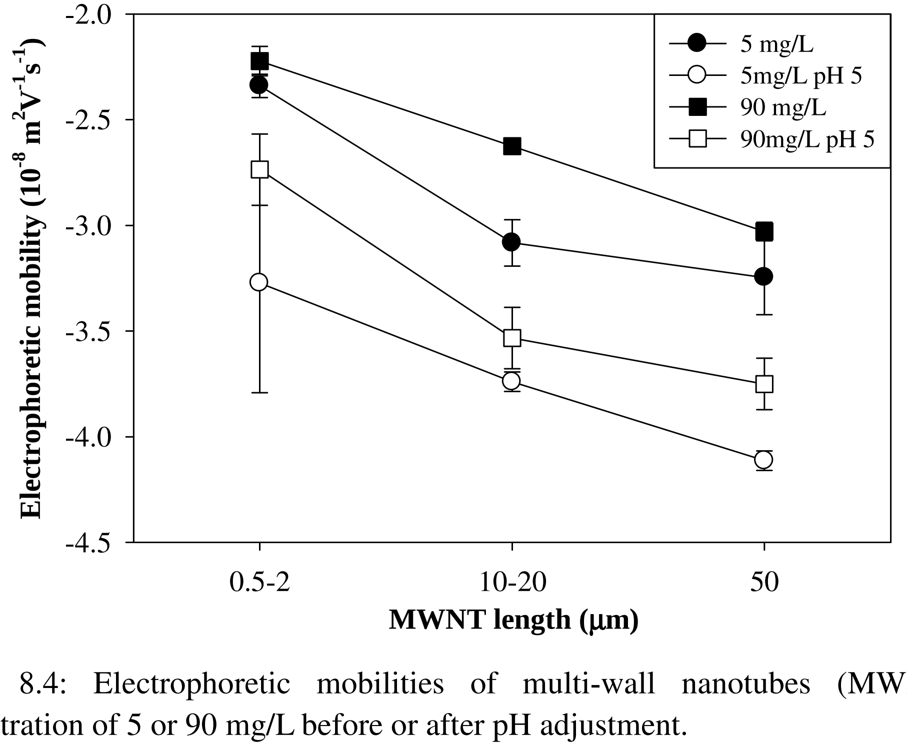

Figure 8.4: Electrophoretic mobilities of multi-wall nanotubes (MWNTs) at a concentration of 5 or 90 mg/L before or after pH adjustment.

indicate that covalently bonded ethoxybenzoyl moieties contribute to MWNT surface charge, possibly through acid-base interactions (e.g, interaction between ether link and phosphate ions). When the suspension pH was increased to pH 5, MWNT EMs increased (more negative) ca. 1.3-fold, which was in contrast to the pH effect observed for nC_{60} zeta potentials. The increase ikn MWNT EMs was not unexpected because concentrations of phosphate ions, such as $H_2PO_4^-$, HPO_4^{2-}, and PO_4^{3-}, increased and phosphoric acid (H_3PO_4) became less dominant when the suspension pH was increased to 5. Thus, EMs of MWNTs negatively decreased with increasing concentration, since lower pH values were observed in suspensions with higher MWNT concentrations. In addition, the experimental results showed that MWNT EMs negatively increased with the increasing MR length, which was attributed to the increase in ethoxybenzoyl moiety density with MR length.

8.2.1.4 TEM and DLS

For TEM samples that were prepared following the method described previously (Fortner et al., 2005), salt crystals (e.g., NaH_2PO_4) surrounding MWNT aggregates were observed, compromising the TEM images for nanotube configurations in suspension. Therefore, the sample preparation protocol was modified by dropping ca. 0.2 mL MWNT suspension onto a copper grid placed on a piece of Parafilm® cover paper, through which the excess suspension was gradually absorbed. The resulting TEM images of samples prepared using this method were throught to be more representative of the true conformation of MWNTs in aqueous suspension. TEM images of MWNTs at each MR length after adjustment to pH 5 are shown in figure 8.5. Generally, individual nanotubes were observed in all samples, indicating that the chemical modification described previously debundled pristine MWNTs without the use of ultrasonication. Clearly, the TEM images revealed that the observed lengths of short and medium MWNTs matched the MR values, with no single tubes longer than 20 μm in the long MWNT samples. The long individual tubes could exist in large aggregates, but a length examination of the pristine MWNTs was still necessary. In addition to single tubes, nanotube aggregates with diameters of ca. 200 nm and 5 μm were observed in short and medium MWNT samples, respectively. In contrast to short or medium MWNT samples, there were large quantities of aggregates with diameters ranging from less than 1 μm to more than 10 μm in the long MWNT samples, and the majority of single tubes were associated with aggregate bundles. These findings suggest that the chemical modification method described previously is able to disperse MWNTs in water, but that agglomeration occurs in the resulting suspension. Further modifications should be explored to prevent aggregation of single MWNTs in order to obtain well-dispersed suspensions.

As described in Chapter 3, the measurement of nanoparticle size via DLS is based on particle diffusion in a fluid (Eq. 3.5), with the size reported as an intensity-weighed hydrodynamic diameter. Thus, for rod-like particles, the hydrodynamic diameter reported by DLS refers only to a diameter of a “spherical” particle with the equal diffusion coefficient. Therefore, unlike nC_{60}, hydrodynamic diameters of MWNTs determined

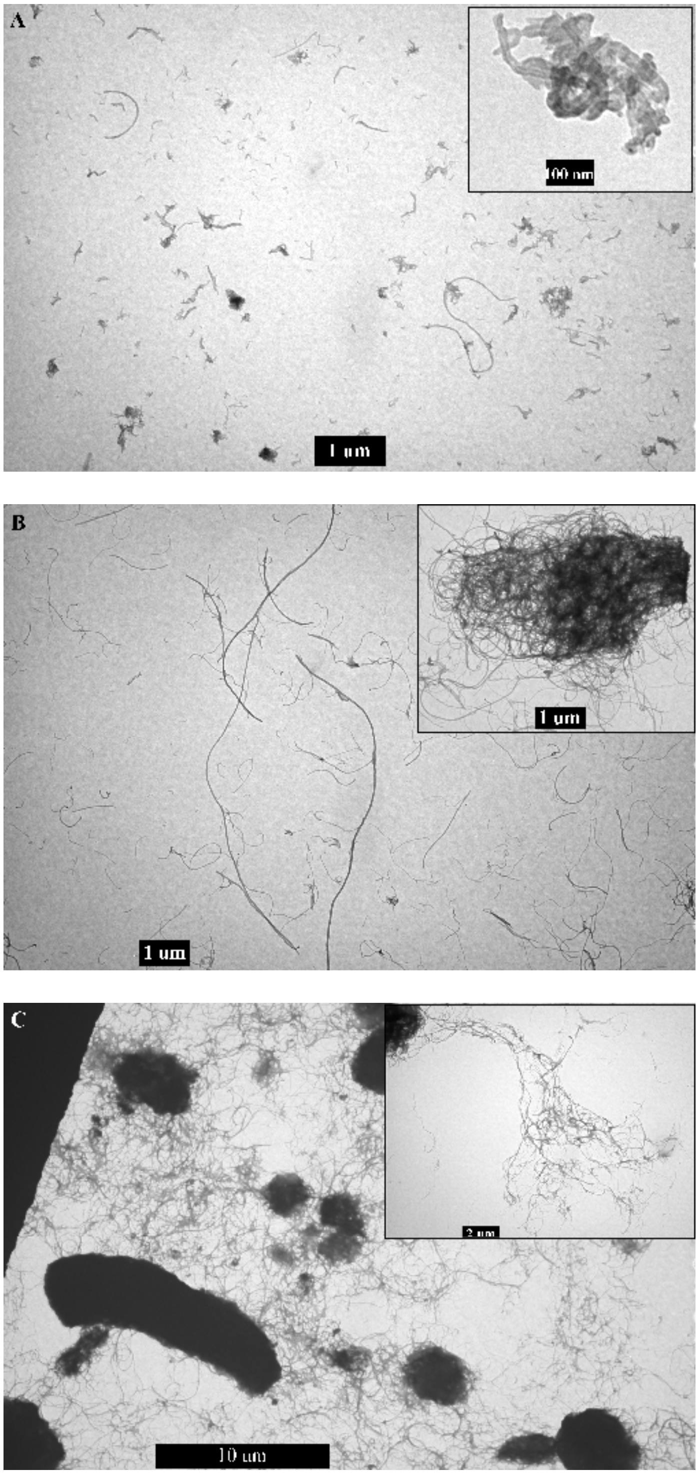

Figure 8.5: Representative transmission electron micrograph (TEM) images of short (A), medium (B), and long (C) multi-wall nanotubes (MWNTs) at pH 5.

using DLS do not represent the true nanotube size, but changes in hydrodynamic diameter are still captured by DLS results. The intensity-weighed hydrodynamic diameters and size distributions of dispersed MWNTs in aqueous phase are shown in Figure 8.6 and 8.7, respectively. The data for long MWNTs were not reported here because noisy correlation curves were observed and instrument quality criteria were not met (e.g., fit errors very high). The hydrodynamic diameters of short and medium MWNTs were determined to be ca. 200 and 500 nm, which are consistent with aggregate dimensions observed in TEM images (insets in Figure 5A and 5B) and larger than SWNT values reported by Jaisi et al. (2008). As anticipated, hydrodynamic diameters of

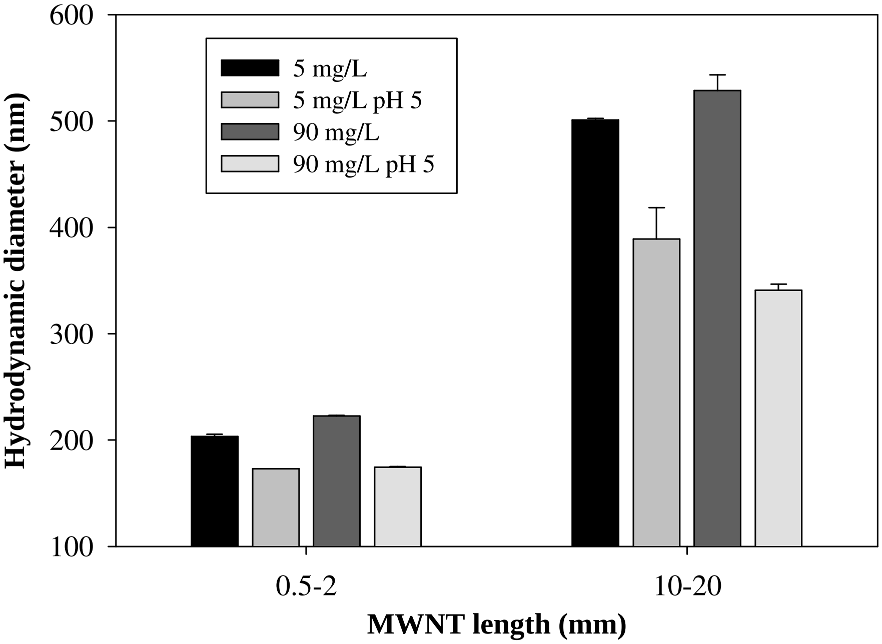

Figure 8.6: Hydrodynamic diameters of mutli-wall nanotubes (MWNTs) as a function of concentration, pH, and manufacture-reported (MR) length.

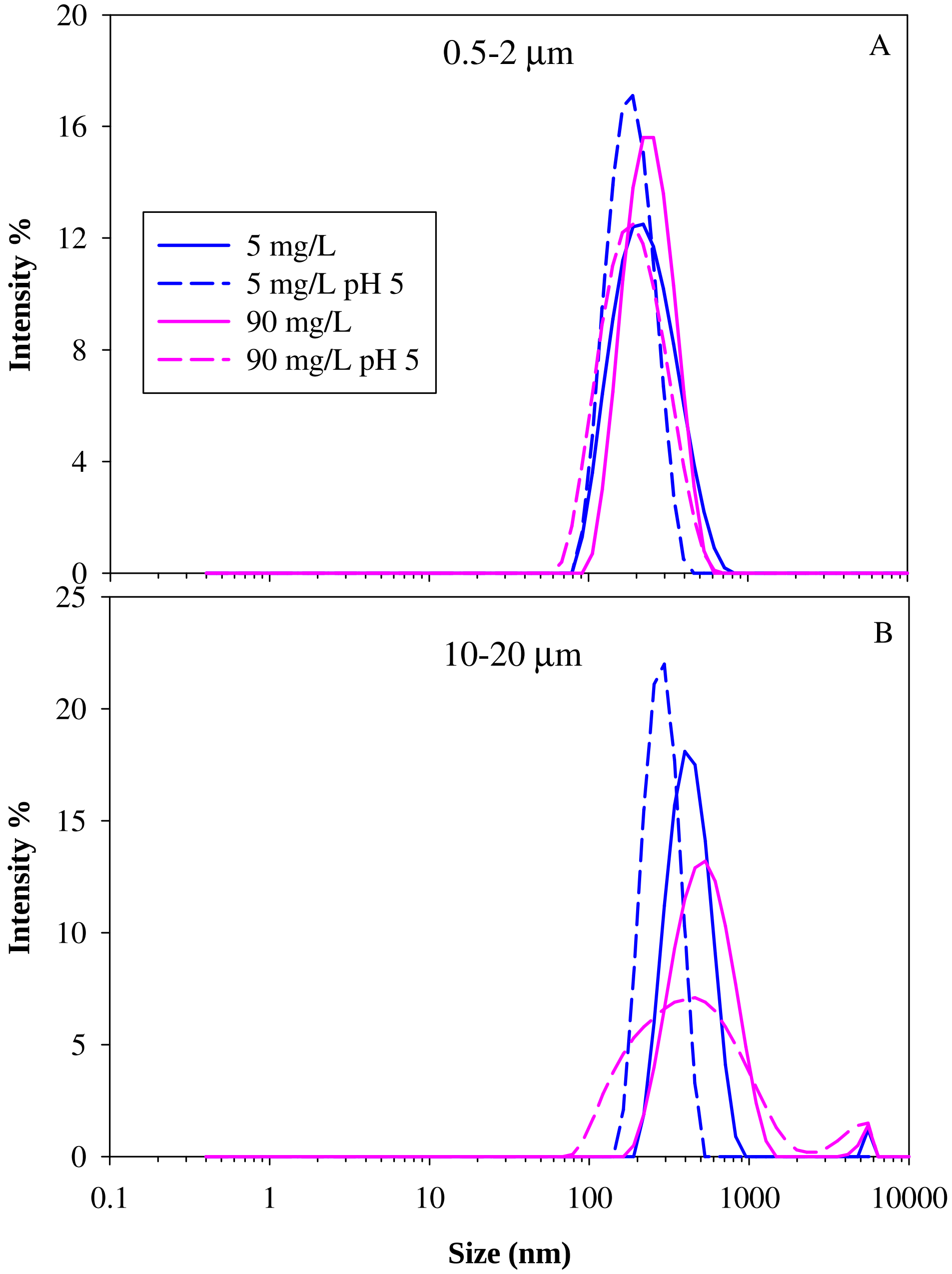

Figure 8.7: Representative size distribution of multi-wall nanotubes (MWNTs) as a function of concentration of concentration, pH, and manufacture-reported (MR) length.

MWNTs increased with the increasing MR length. At the same MR length, hydrodynamic diameters of MWNTs increased slightly with concentration. For example, the diameter of medium MWNTs increased from 501.0 ± 1.4 to 528.5 ± 14.8 nm when the concentration increased from 5 to 90 mg/L (Figure 8.6). This shift was possibly because more MWNTs of longer size were sampled during the preparation of 90 mg/L nanotube suspension. When the suspension pH increased to 5, MWNT sizes decreased considerably. For short MWNTs, single peaks were observed in the size distribution curves for all samples, while bimodal distributions were observed in medium-size MWNTs.

8.2.2 Column Experiments

A total of 7 column experiments were conducted to measure the transport and retention of MWNTs in water saturated 40-50 mesh Ottawa sand. Transport experiments with input concentrations of either 5 or 90 mg/L were performed to develop data that could be compared to nC_{60} and SWNT transport. The experimental conditions are summarized in Table 8.1.

Effluent BTCs for MWNTs with an input concentration of 5 mg/L in 40-50 mesh Ottawa sands are shown in Figure 8.8. Regardless of the MR length, MWNTs effluent concentrations exhibited a sharp increase at ca. 1 PV, followed by a corresponding decrease in effluent concentration at the end of the pulse injection. When 5 PV of short MWNT suspension were introduced into the columns, relative MWNT concentrations

Table 8.1: Experimental conditions for multi-wall nanotubes (MWNT) transport studies in columns packed with either 40-50 or 100-140 mesh Ottawa sands.

Column Identifier[a]	θ_w[b]	C_0[c] (mg/L)	IS[d] (mM)	Sand (mesh)	EM[e] (μm·cm/V·s)	d_H[f] (nm)	Ret[g] %	MB[h] %
2μm-5-M-1	0.38	3.1	5.0	40-50	-2.90	186.4	0.12	81.6
2μm-5-M-2	0.37	3.8	5.0	40-50	-2.96	177.2	1.11	81.2
2μm-90-M	0.37	88.8	40.7	40-50	-2.93	186.5	3.57	101.9
20μm-5-M	0.37	4.6	5.0	40-50	-3.60	362	0.15	96.2
20μm-90-M	0.37	97.3	49.7	40-50	-3.53	289	9.61	104.1
50μm-5-M	0.37	4.5	5.0	40-50	-4.48	389.75	0.1	72.9
50μm-90-M	0.37	89.0	49.8	40-50	-3.87	338.5	20.3	105.5

[a] 2μm, 20μm, and 50μm represent MWNTs with MR length of 0.5-2, 10-20, and 50 μm, 5 and 90 represent expected input concentration, M = 40-50 mesh sand. [b] porosity. [c] measured input concentration of MWNTs. [d] ionic strength calculated based on chemical speciation. [e] electrophoretic mobility. [f] hydrodynamic diameter of MWNTs. [g] retention. [h] mass balance.

gradually increased to a concentration plateau of 0.85 at 5 PV. In contrast, a relative concentration plateau was developed at ca. 2.5 PV with a C/C_0 value of 0.98 for medium MWNTs. The earlier plateau development and higher plateau value observed for medium MWNT compared to the short MWNT BTC are consistent with the more negative EM values for medium MWNTs. For a 5-PV pulse injection, long MWNTs followed similar breakthrough pattern to the short MWNTs, yet with 10% lower effluent concentrations. These findings suggest that presence of large nanotube aggregates (e.g., 10 μm, Figure 8.5C) exhibit more pronounced impacts on MWNT transport than electrostatic repulsions resulting from negative surface charge. A close data examination of the breakthrough

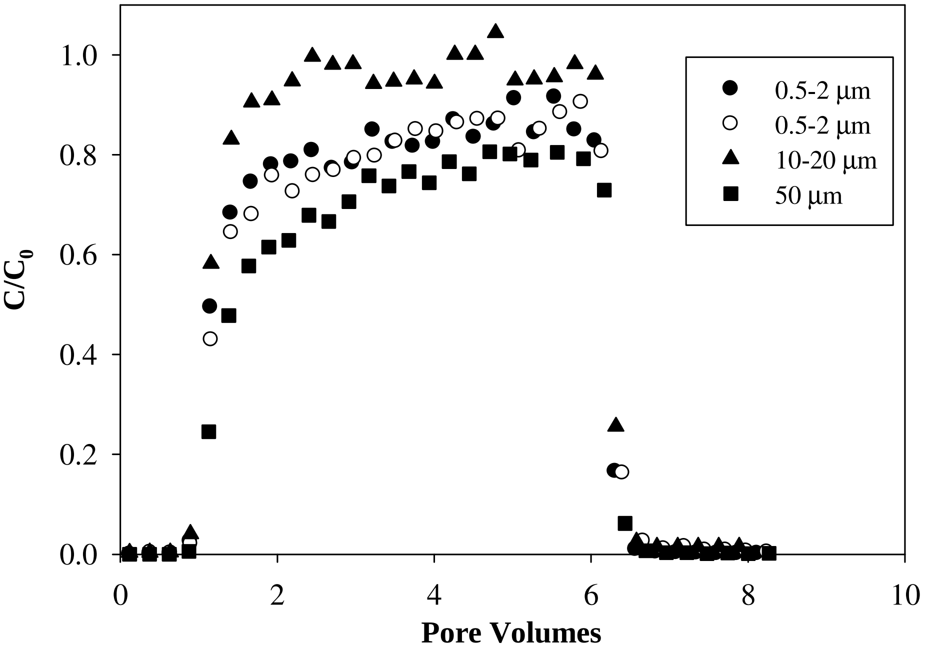

Figure 8.8: Effluent breakthrough curves of multi-wall nanotubes (MWNTs) with an input concentration of ca. 5 mg/L in columns packed with 40-50 mesh Ottawa sands. The pH of input suspensions was adjusted to 5 and a final ionic strength of 5 mM was obtained by adding NaCl.

data revealed that the medium MWNT BTC was comparable to that of nC_{60} (Chapter 5) under similar solution conditions (e.g., similar ionic strength and EM). Since MWNTs at medium MR length exhibited a hydrodynamic diameter greater than 100 nm and single tubes were present in suspensions, it was expected that much greater retention would occur for MWNTs than for nC_{60}. Thus, the comparable effluent BTCs suggest that adoption of preferential orientation occurs as suspended MWNTs approach pore throats (Xu et al., 2008), which could counteract MWNT retention caused by greater particle size and physical straining. Although the extraction method developed for solid phase nC_{60} was utilized, retained MWNTs were barely released even after 1 min of sonication, yielding very low and unreliable mass recoveries (Table 8.1). Thus, MWNT retention profiles in experiments at the lower input concentration (5 mg/L) are not presented herein. The recovery method for solid phase MWNTs should be further explored to obtain better nanotube release efficiency while maintaining the UV-fluorescence feature.

When the input MWNT concentration was increased 16-fold to ca. 90 mg/L, an effluent concentration plateau developed for MWNTs at each MR length within 2.5 PV and the steady-state C/C_0 value decreased with the increasing MR length (Figure 8.9A). Compared to MWNT BTCs at input concentration of 5 mg/L, little change was observed in medium MWNT BTC, while BTCs for short and long MWNTs increased considerably, which was not consistent with their decreasing EM values (Figure 8.6) with MR length. In addition, at a similar ionic strength (e.g., 50 mM), the obtained plateau values were much higher than that of SWNTs observed by Jaisi et al. (2008), which was attributed to higher EMs of MWNTs (Figure 8.4). On the other hand, MWNTs exhibited much higher mobility than nC_{60} under similar solution conditions. For instance, a small C/C_0 value (less than 0.1) was observed when an nC_{60} suspension conditioned with 30 mM NaCl was pulse injected into a column packed with 40-50 mesh Ottawa sands (Chapter 5).

Following a similar extraction protocol for experiments with lower input concentration (5 mg/L), retained MWNTs at 90 mg/L were quantified and resulting mass balances for these column experiments were between 102 and 105% (Table 8.1). Similar to the distribution of nC_{60} retained in quartz sands (Chapter 5), MWNT retention profiles decreased monotonically with distance, and the highest solid phase concentrations

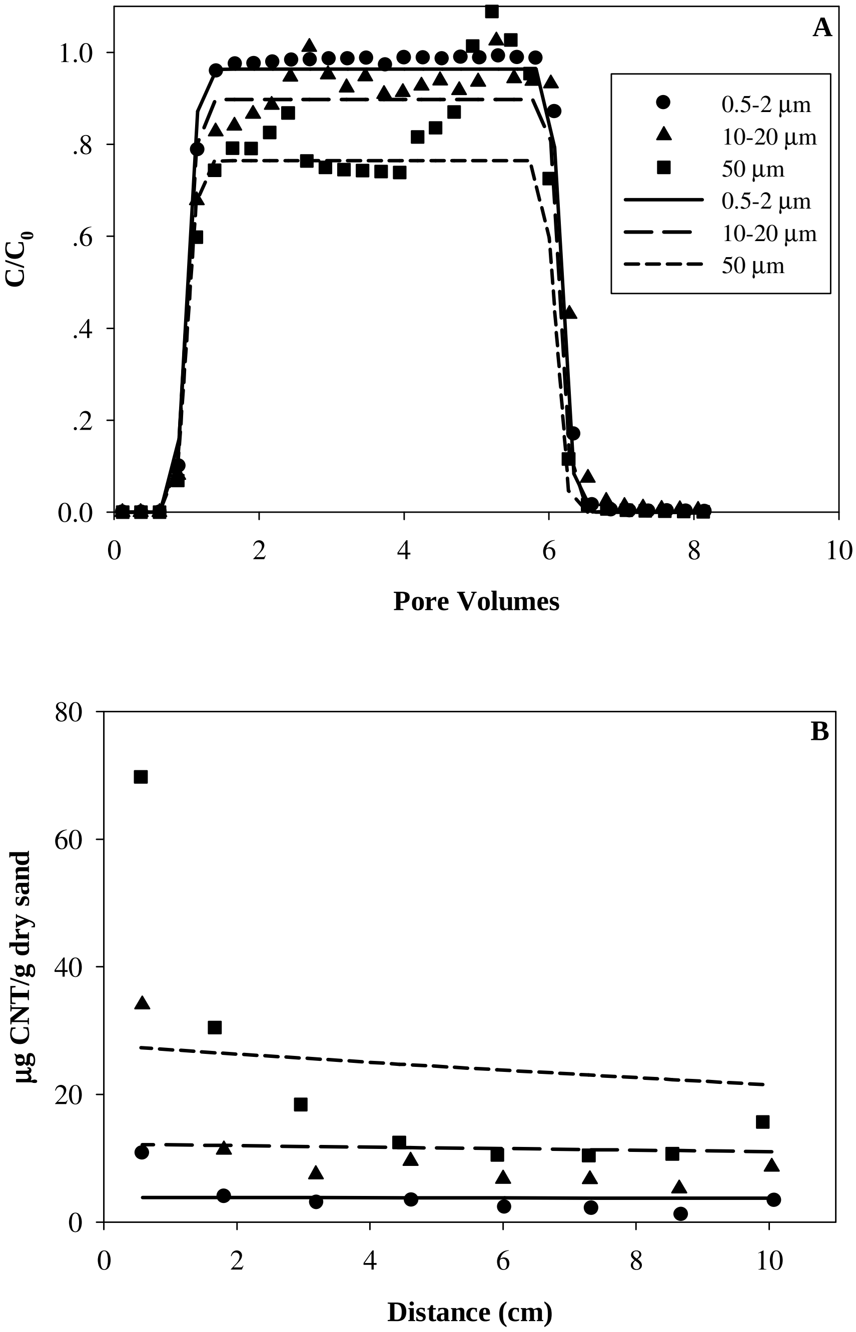

Figure 8.9: Measured and simulated breakthrough curves (A) and retention profiles (B) of multi-wall nanotubes (MWNTs) with the input concentration of ca. 90 mg/L in columns packed with 40-50 mesh Ottawa sands. The input suspension pH was adjusted to 5.

occurred near the column inlet. With an increase of MR length, higher MWNT solid phase concentrations were observed along the entire column.

To further investigate MWNT and sand interactions, both MWNT BTCs and retention profiles were fit using the 1D-ADR equation (Eq. 2.15), with first order attachment kinetics (Eq. 2.16). The attachment rate (k_{att}) for MWNTs at each MR length was estimated by minimizing differences between experimental data and predictions by Eq. 2.15 and 2.16. The simulated BTCs and retention profiles are shown in Figure 8.9. The fitted k_{att} for short, medium, and long MWNTs were 1.5, 9.1, and 14 ($\times 10^{-4}$ s^{-1}), repectively. Although BTCs matched well, a simple attachment model that does not account for physical straining, ripening, or particle detachment was not capable of describing the observed MWNT retention profiles. The discrepancy suggests that physical straining plays an important role in MWNT retention at higher input concentrations, which was under evaluated by Jaisi et al. (2008). Compared to findings from Jaisi et al. (2008) at similar experimental conditions, the simulated k_{att} values for MWNTs were 1 to 2 orders-of-magnitude smaller, suggesting that suspended MWNTs, even with the occurrence tube agglomerations, were more mobile in water-saturated porous media than SWNTs under the experimental conditions employed herein.

8.3 Summary and Conclusions

A novel chemical modification method was employed to disperse solid MWNTs in water. The resulting MWNT suspensions emit green fluorescence at an excitation wavelength of 450, which provides with means to quantify MWNT at concentrations lower than 5 mg/L. Through this treatment, MWNTs are debundled and dispersed in water, although agglomerations occurred in all suspensions and were more pronounced in long (50 μm) MWNT suspensions than in short (0.5-2 μm) or medium (10-20 μm) suspensions. These findings suggest that MWNT suspensions with significant populations of individual tubes are not kinetically stable.

After characterization of the suspended MWNTs, a series of column experiments were conducted to investigate the effects of MR length on MWNT transport and retention in a water-saturated quartz sand. MWNTs were readily transported through 40-50 mesh Ottawa sands regardless of the MR length. At the lower input concentrations (5 mg/L) medium MWNTs exhibited comparable mobility with nC_{60} nanoparitcles that are spherical and possess smaller hydrodynamic diameters (100 vs. 362 nm), suggesting possible adoption of preferential orientation (e.g., parallel with local flow direction) by MWNTs. At the higher input concentrations (90 mg/L), the retention of MWNTs with longer MR length was more than 2- and 5-fold greater than those of MWNTs with medium (10-20 μm) and short (0.5-2 μm) MR length, respectively. A BTC comparison revealed that MWNTs exhibited higher mobility than nC_{60} and SWNTs at the similar ionic strength. Application of a 1-D ADR transport equation with the attachment model suggest that physical straining played an important role in MWNT retention.

CHAPTER 9

CONCLUSIONS AND RECOMMENDATIONS

9.1 Conclusions

The research presented herein focused on the transport and retention of fullerene-based nanoparticles in subsurface environments, with nC_{60} (C_{60} nanoparticle) and MWNTs employed as reprentative nanoparticles. The key findings of this work are highlighted below:

nC_{60} transport and retention in quartz sands

1. The transport of nC_{60} decreased and the retention increased as (a) the mean grain size of quartz sand was decreased from 710 μm (20-30 mesh) to 130 μm (100-140 mesh) and (b) the pore-water velocity was decreased from 8 to 1 m/d.
2. Complete retention of input nC_{60} occurred in 130 μm Ottawa sands at a pore-water velocity of 8 m/d, and in both 160 μm (80-100 mesh) and 130 μm Ottawa sands at 1 m/d.
3. The presence of Ca^{2+} as the background electrolyte increased in the retention of nC_{60} by more than two order-of-magnitude compared to Na^+ at the same ionic strength.
4. Electrostatic interactions play an important role in C_{60} retention.
    - The retention of nC_{60} increases with increasing solution ionic strength for both Na^+ and Ca^{2+}.
    - When DI water alone (e.g., no background electrolyte) was used in column

experiments, nC_{60} was transported through the sand column like a tracer, with only 4.8% and 6.6% of input nC_{60} retained in 40-50 and 100-140 mesh Ottawa sands, respectively.

5. C_{60} retention was attributed to the primary energy minimum.
    - The attachment of nC_{60} in quartz sands was largely irreversible.
        - The minimal detachment (6.9% of retained nC_{60}) was observed even after sequentially flushing columns with low ionic strength solution (deionized water), solutions containing surfactant (1,000 mg/L Tween 80), and cosolvent (50% vol. ethanol).
        - Introduction of pH 12 water was required to detach more than 50% of retained nC_{60}.
    - Only 2.3% of retained nC_{60} were held on sand surface due to the attachment associated with the secondary energy minimum (DI water flushing).
    - Ca^{2+} bridging possibly contributed to nC_{60} retention.
6. Presence of stabilizing agents significantly enhanced nC_{60} transport in quartz sands and natural soil.
    - The presence of SRHA (20 mg C/L), SRFA (20 mg C/L), or Tween 80 (1,000 mg/L) resulted in less than 2% of input nC_{60} retained in 40-50 Ottawa sands.
    - The transport data, together with DLS and electrophoresis data, suggest that adsorbed Tween 80 coat the surface of nC_{60}.

  - More than 55% of total input nC_{60} transport through columns packed with natural soils when Tween 80, at a concentration of 1,000 mg/L, was present in the aqueous phase, while breakthrough of nC_{60} remained absent when the input nC_{60} suspension was premixed with 20 mg C/L SRHA.
  - When nC_{60} aggregate and quartz sand surfaces were coated with stabilizing agents, steric repulsion was the likely cause of the observed enhancement in nC_{60} transport.
7. Complete retention of input nC_{60} was observed in Appling and Webster soils, even after introducing up to 65 PVs of nC_{60} suspension.
   - Appling and Webster soil exhibited much higher retention capacity to nC_{60} (e.g., 130 μg/g dry Appling soil) compared to glass beads and quartz sands, which was attributed to the presence of appreciable amounts of clay minerals and organic matter.
8. Clean-bed filtration theory was not able to adequately describe nC_{60} transport and retention data in quartz sand and natural soils.
   - Effluent breakthrough curves of nC_{60} were not symmetric and retention profiles did not follow exponential decay.
   - Coupling clean-bed filtration theory with a rate-limited attachment coefficient and a limiting retention capacity term was required to capture both nC_{60} breakthrough and retention data.

MWNT transport and retention

1. The MWNT suspension, prepared using a chemical modification method that involved a mild acid environment, exhibited green fluorescence.
    - The presence of fluorescence allowed for quantification of MWNTs at low concentration levels (< 5 mg/L).
2. TEM imaging results demonstrated that agglomerations occur in MWNT suspensions.
3. MWNTs with MR length of 0.5-2, 10-20, or 50 μm were readily transported through 40-50 mesh quartz sands.
    - At a lower input concentration (5 mg/L), 10-20 μm long MWNTs exhibited comparable mobility to nC_{60} possibly due to the adoption of preferential orientation.
    - At the higher input concentrations (90 mg/L), the transport of MWNTs decreased with the increasing MR length, and MWNT exhibited higher mobility than nC_{60} and SWNTs at the similar solution conditions.

In summary, this work systematically studied fullerene-based nanoparticle transport and retention behavior in water-saturated porous media. The findings of this research advanced our understanding of fundamental processes governing fullerene-based nanoparticles in porous media. The results will aid in assessing the distribution of nanoparticles in the environment and in designing effective removal strategies for groundwater and drinking water treatment. The work presented herein, coupling with other components of proactive nanoparticle risk analysis, will aid in refining current disposal guidelines for engineered nanomaterials, ensuring the nanotechnology to be socially beneficial and environmentally sustainable.

9.2 Recommendations

Based upon the experimental results decribed in previous chapters, the following four areas of research regarding carbon-based nanoparticle transport are recommended for future study.

Although the work presented herein greatly expands our knowledge of the transport and retention of fullerene-based nanoparticles in porous media, it would be beneficial to evaluate nC_{60} transport behavior in a two-dimensional (2-D) aquifer cell, where both latitude and horizontal transport can be evaluated. In addition, a 2-D cell allows for consideration of subsurface heterogeneity, such as presence of low permeability lenses. In this manner, the potential retention of nanoparticles at textural interfaces could be measured.

In Chapter 7, experimental results implied that the sizable retention of nC_{60} in natural soils was related to presence of clay minerals and soil organic matter. In order to further explore the role of clay particles and organic matter in nanoparticle retention, additional natural soils with varying clay and organic carbon contents should be evaluated. This could provide critical insight into nC_{60} retention in natural soils.

As illustrated in previous chapters, retention profile data are essential for understanding processes governing particle transport and retention in porous media.

However, retention profiles for MWNTs at the lower input concentration (5 mg/L) were not reported in Chapter 8 due to the low efficiency of the extraction method. Therefore, modifications of the method, or development of new extraction protocol should be developed to improve MWNT extraction efficiencies from the solid phase, while maintaining the fluorescence feature.

Following the release or deposition on the soil surface, nC_{60} will have to transport through the unsaturated zone and capillary fringe to reach groundwater. Understanding the transport of nC_{60} in water-unsaturated zone and capillary fringe is of importantance to groundwater protection. Therefore, it is also recommended to evaluate nC_{60} transport and retention behavior in water-unsatured porous media through column experiments.

REFERENCES

Abriola, L.M., C.D. Drummond, E.J. Hahn, K.F. Hayes, T.C.G. Kibbey, L.D. Lemke, K.D. Pennell, E.A. Petrovskis, C.A. Ramsburg, and K.M. Rathfelder. 2005. Pilot-scale demonstration of surfactant-enhanced PCE solubilization at the Bachman Road site. 1. Site characterization and test design. Environ. Sci. Technol. 39:1778-1790.

Ajie, H., M.M. Alvarez, S.J. Anz, R.D. Beck, F. Diederich, K. Fostiropoulos, D.R. Huffman, W. Kratschmer, Y. Rubin, K.E. Schriver, D. Sensharma, and R.L. Whetten. 1990. Characterization of the soluble all-carbon molecules C_{60} and C_{70}. J. Phys. Chem. 94:8630-8633.

Amirbahman, A., and T.M. Olson. 1993. Transport of humic matter-coated hematite in packed-beds. Environ. Sci. Technol. 27:2807-2813.

Amirbahman, A., and T.M. Olson. 1995. The role of surface conformations in the deposition of humic maater-coated colloids in porous media. Colloids and Surfaces a-Physicochemical and Engineering Aspects 95:249-259.

Amirtharajah, A. 1988. Some theoretical and conceptual views of filtration. Journal American Water Works Association 80:36-46.

Andersson, T., K. Nilsson, M. Sundahl, G. Westman, and O. Wennerstrom. 1992. C-60 embedded in gamma-cyclodextrin - a water-soluble fullerene. Journal Of The Chemical Society-Chemical Communications:604-606.

Andrievsky, G., V. Klcohkov, and L. Drevyanchenko. 2005. Is the C_{60} fullerene molecule toxic?! Fullerenes, Nanotubes, and Carbon Nanostructures 13:363-376.

Andrievsky, G.V., M.V. Kosevich, O.M. Vovk, V.S. Shelkovsky, and L.A. Vashchenko. 1995. On the production of an aqueous colloidal solution of fullerenes. Journal Of The Chemical Society-Chemical Communications:1281-1282.

Arbogast, J.W., A.P. Darmanyan, C.S. Foote, Y. Rubin, F.N. Diederich, M.M. Alvarez, S.J. Anz, and R.L. Whetten. 1991. Photophysical properties of C_{60}. J. Phys. Chem. 95:11-12.

Arias, L.R., and L.J. Yang. 2009. Inactivation of bacterial pathogens bycarbon nanotubes in suspensions. Langmuir 25:3003-3012.

Arrais, A., and E. Diana. 2003. Highly water soluble C-60 derivatives: A new synthesis. Fullerenes Nanotubes and Carbon Nanostructures 11:35-46.

Ausman, K.D., R. Piner, O. Lourie, R.S. Ruoff, and M. Korobov. 2000. Organic solvent dispersions of single-walled carbon nanotubes: Toward solutions of pristine nanotubes. J. Phys. Chem. B 104:8911-8915.

Bahr, J.L., E.T. Mickelson, M.J. Bronikowski, R.E. Smalley, and J.M. Tour. 2001. Dissolution of small diameter single-wall carbon nanotubes in organic solvents? Chem. Commun.:193-194.

Bensasson, R.V., E. Bienvenue, M. Dellinger, S. Leach, and P. Seta. 1994. C_{60} in model biological-systems - a visible-UV absorption study of solvent-dependent parameters and solute aggregation. J. Phys. Chem. 98:3492-3500.

Bergendahl, J., and D. Grasso. 2000. Prediction of colloid detachment in a model porous media: hydrodynamics. Chem. Eng. Sci. 55:1523-1532.

Bergin, S.D., V. Nicolosi, P.V. Streich, S. Giordani, Z.Y. Sun, A.H. Windle, P. Ryan, N.P.P. Niraj, Z.T.T. Wang, L. Carpenter, W.J. Blau, J.J. Boland, J.P. Hamilton, and J.N. Coleman. 2008. Towards solutions of single-walled carbon nanotubes in common solvents. Adv. Mater. 20:1876-1881.

Biercuk, M.J., M.C. Llaguno, M. Radosavljevic, J.K. Hyun, A.T. Johnson, and J.E. Fischer. 2002. Carbon nanotube composites for thermal management. Appl. Phys. Lett. 80:2767-2769.

Birkett, P.R., P.B. Hitchcock, H.W. Kroto, R. Taylor, and D.R.M. Walton. 1992. Preparation and characterization of $C_{60}Br_6$ and $C_{60}Br_8$. Nature 357:479-481.

Blake, G.R., and K.H. Hartge. 1986. Paritcle density, p. 377-382, *In* A. Klute, ed. Methods of Soil Analysis. Part I. Physical and Mineralogical Methods Second Edition, 2 ed. American Society of Agronomy, Inc. Soil Science Society of America, Inc. Madison, Wisconsin USA.

Bolt, G.H., and M.G.M. Bruggenwert. 1976. Soil chemistry: Basic elements Elsevier Science Ltd, St. Louis, MO.

Bradford, S.A., and M. Bettahar. 2006. Concentration dependent transport of colloids in saturated porous media. J. Contam. Hydrol. 82:99-117.

Bradford, S.A., S. Torkzaban, and S.L. Walker. 2007. Coupling of physical and chemical mechanisms of colloid straining in saturated porous media. Water Res. 41:3012-3024.

Bradford, S.A., S.R. Yates, M. Bettahar, and J. Simunek. 2002. Physical factors affecting the transport and fate of colloids in saturated porous media. Water Resour. Res. 38:1327-1338.

Bradford, S.A., J. Simunek, M. Bettahar, M.T. Van Genuchten, and S.R. Yates. 2003. Modeling colloid attachment, straining, and exclusion in saturated porous media. Environ. Sci. Technol. 37:2242-2250.

Bradford, S.A., J. Simunek, M. Bettahar, M.T. van Genuchten, and S.R. Yates. 2006. Significance of straining in colloid deposition: Evidence and implications. Water Resour. Res. 42:W12s15.

Bradford, S.A., S. Torkzaban, F. Leij, J. Simunek, and M.T. van Genuchten. 2009. Modeling the coupled effects of pore space geometry and velocity on colloid transport and retention. Water Resour. Res. 45:W02414.

Brady-Estevez, A.S., S. Kang, and M. Elimelech. 2008. A single-walled-carbon-nanotube filter for removal of viral and bacterial pathogens. Small 4:481-484.

Brant, J., H. Lecoanet, and M.R. Wiesner. 2005a. Aggregation and deposition characteristics of fullerene nanoparticles in aqueous systems. J. Nanopart. Res. 7:545-553.

Brant, J., H. Lecoanet, M. Hotze, and M. Wiesner. 2005b. Comparison of electrokinetic properties of colloidal fullerenes (n-C_{60}) formed using two procedures. Environ. Sci. Technol. 39:6343-6351.

Brant, J.A., J. Labille, J.-Y. Bottero, and M.R. Wiesner. 2006. Characterizing the impact of preparation method on fullerene cluster structure and chemistry. Langmuir 22:3878.

Buseck, P.R. 2002. Geological fullerenes: review and analysis. Earth. Planet. Sci. Lett. 203:781-792.

Bush, L. 2003. Merck and C sixty to pursue fullerene antioxidant technology [Online] http://www.encyclopedia.com/doc/1P3-500897071.html (verified Mar. 21).

Chen, C.C., and C.M. Lieber. 1993. Isotope effect and superconductivity in metal-doped C_{60}. Science 259:655-658.

Chen, K.L., and M. Elimelech. 2006. Aggregation and deposition kinetics of fullerene (C-60) nanoparticles. Langmuir 22:10994-11001.

Chen, K.L., and M. Elimelech. 2007. Influence of humic acid on the aggregation kinetics of fullerene (C-60) nanoparticles in monovalent and divalent electrolyte solutions. J. Colloid Interface Sci. 309:126-134.

Chen, K.L., and M. Elimelech. 2008. Interaction of fullerene (C-60) nanoparticles with humic acid and alginate coated silica surfaces: Measurements, mechanisms, and environmental implications. Environ. Sci. Technol. 42:7607-7614.

Chen, Q., C. Saltiel, S. Manickavasagam, L.S. Schadler, R.W. Siegel, and H.C. Yang. 2004. Aggregation behavior of single-walled carbon nanotubes in dilute aqueous suspension. J. Colloid Interface Sci. 280:91-97.

Cheng, H.M., Q.H. Yang, and C. Liu. 2001. Hydrogen storage in carbon nanotubes. Carbon 39:1447-1454.

Cheng, X., A.T. Kan, and M.B. Tomson. 2004. Naphthalene adsorption and desorption from aqueous C_{60} fullerene. J. Chem. Eng. Data 49:675-683.

Cheng, X., A.T. Kan, and M.B. Thomson. 2005. Study of C_{60} transport in porous media and the effect of sorbed C_{60} on naphthalene transport. J. Mater. Res. 20:3244-3254.

Chiang, L.Y., L.Y. Wang, J.W. Swirczewski, S. Soled, and S. Cameron. 1994. Efficient synthesis of polyhydroxylated fullerene derivatives via hydrolysis of polycyclosulfated precursors. J. Org. Chem. 59:3960-3968.

Chijiwa, T., T. Arai, T. Sugai, H. Shinohara, M. Kumazawa, M. Takano, and S. Kawakami. 1999. Fullerenes found in the Permo-Triassic mass extinction period. Geophysical Research Letters 26:767-770.

Chin, Y.P., G. Aiken, and E. Oloughlin. 1994. Molecular-weight, polydispersity, and spectroscopic properties of aquatic humic substances. Environ. Sci. Technol. 28:1853-1858.

Collins, P.G., K. Bradley, M. Ishigami, and A. Zettl. 2000. Extreme oxygen sensitivity of electronic properties of carbon nanotubes. Science 287:1801-1804.

Colvin, V.L. 2003. The potential environmental impact of engineered nanomaterials. Nat. Biotechnol. 21:1166-1170.

Cui, D.X., F.R. Tian, C.S. Ozkan, M. Wang, and H.J. Gao. 2005. Effect of single wall carbon nanotubes on human HEK293 cells. Toxicol. Lett. 155:73-85.

David, W.I.F., R.M. Ibberson, J.C. Matthewman, K. Prassides, T.J.S. Dennis, J.P. Hare, H.W. Kroto, R. Taylor, and D.R.M. Walton. 1991. Crystal-structure and bonding of ordered C_{60}. Nature 353:147-149.

Davis, C.J., E. Eschenazi, and K.D. Papadopoulos. 2002. Combined effects of Ca^{2+} and humic acid on colloid transport through porous media. Colloid. Polym. Sci. 280:52-58.

Davoren, M., E. Herzog, A. Casey, B. Cottineau, G. Chambers, H.J. Byrne, and F.M. Lyng. 2007. In vitro toxicity evaluation of single walled carbon nanotubes on human A549 lung cells. Toxicology in Vitro 21:438-448.

Deguchi, S., R.G. Alargova, and K. Tsujii. 2001a. Stable dispersions of fullerenes, C-60 and C-70, in water. Preparation and characterization. Langmuir 17:6013-6017.

Deguchi, S., R.G. Alargova, and K. Tsujii. 2001b. Stable dispersions of fullerenes, C_{60} and C_{70}, in water. Preparation and characterization. Langmuir 17:6013.

Deguchi, S., S. Mukai, M. Tsudome, and K. Horikoshi. 2006. Facile generation of fullerene nanoparticles by hand-grinding. Adv. Mater. 18:729-732.

Dehaan, F.A.M. 1964. Negative adsorption of anions (anion exclusion) in systems with interacting double layers. J. Phys. Chem. 68:2970-2977.

Deshiikan, S.R., and K.D. Papadopoulos. 1998. Modified Booth equation for the calculation of zeta potential. Colloid. Polym. Sci. 276:117-124.

Deshiikan, S.R., E. Eschenazi, and K.D. Papadopoulos. 1998. Transport of colloids through porous beds in the presence of natural organic matter. Colloids and Surfaces a-Physicochemical and Engineering Aspects 145:93-100.

Di, Z.C., J. Ding, X.J. Peng, Y.H. Li, Z.K. Luan, and J. Liang. 2006. Chromium adsorption by aligned carbon nanotubes supported ceria nanoparticles. Chemosphere 62:861-865.

Dillon, A.C., K.M. Jones, T.A. Bekkedahl, C.H. Kiang, D.S. Bethune, and M.J. Heben. 1997. Storage of hydrogen in single-walled carbon nanotubes. Nature 386:377-379.

Ding, L.H., J. Stilwell, T.T. Zhang, O. Elboudwarej, H.J. Jiang, J.P. Selegue, P.A. Cooke, J.W. Gray, and F.Q.F. Chen. 2005. Molecular characterization of the cytotoxic mechanism of multiwall carbon nanotubes and nano-onions on human skin fibroblast. Nano Lett. 5:2448-2464.

Dousset, S., M. Thevenot, V. Pot, J. Simunek, and F. Andreux. 2007. Evaluating equilibrium and non-equilibrium transport of bromide and isoproturon in disturbed and undisturbed soil columns. J. Contam. Hydrol. 94:261-276.

Dugan, L.L., D.M. Turetsky, C. Du, D. Lobner, M. Wheeler, C.R. Almli, C.K.F. Shen, T.Y. Luh, D.W. Choi, and T.S. Lin. 1997. Carboxyfullerenes as neuroprotective agents. Proceedings of the National Academy of Sciences of the United States of America 94:9434-9439.

Duncan, L.K., J.R. Jinschek, and P.J. Vikesland. 2008. C-60 colloid formation in aqueous systems: Effects of preparation method on size, structure, and surface, charge. Environ. Sci. Technol. 42:173-178.

Elimelech, M., and C.R. Omelia. 1990. Kinetics of deposition of colloidal particles in porous-media. Environ. Sci. Technol. 24:1528-1536.

Espinasse, B., E.M. Hotze, and M.R. Wiesner. 2007. Transport and retention of colloidal aggregates of C-60 in porous media: Effects of organic macromolecules, ionic composition, and preparation method. Environ. Sci. Technol. 41:7396-7402.

Fischer, J.E., P.A. Heiney, and A.B. Smith. 1992. Solid-state chemistry of fullerene-based materials. Acc. Chem. Res. 25:112-118.

Fischer, J.E., P.A. Heiney, A.R. McGhie, W.J. Romanow, A.M. Denenstein, J.P. McCauley, and A.B. Smith. 1991. Compressibility of solid C_{60}. Science 252:1288-1290.

Fortner, J.D. 2006. C_{60} in water: aggregation characterization, reactivity and behavior. Ph.D. Dissertation, Rice University, Houston, TX.

Fortner, J.D., D.Y. Lyon, C.M. Sayes, A.M. Boyd, J.C. Falkner, E.M. Hotze, L.B. Alemany, Y.J. Tao, W. Guo, K.D. Ausman, V.L. Colvin, and J.B. Hughes. 2005. C_{60} in water: Nanocrystal formation and microbial response. Environ. Sci. Technol. 39:4307-4316.

Franchi, A., and C.R. O'Melia. 2003. Effects of natural organic matter and solution chemistry on the deposition and reentrainment of colloids in porous media. Environ. Sci. Technol. 37:1122-1129.

Freeze, R.A., and J.A. Cherry. 1979. Groundwater Prentice-Hall Inc., Englwood Cliffs, New Jersey.

Friedman, S.H., D.L. Decamp, R.P. Sijbesma, G. Srdanov, F. Wudl, and G.L. Kenyon. 1993. Inhibition of the HIV-1 protease by fullerene derivatives - model-building studies and experimental-verification. JACS 115:6506-6509.

Gamerdinger, A.P., R.J. Wagenet, and M.T. Vangenuchten. 1990. Application of 2-site 2-region models for studying simultaneous nonequilibrium transport and degradation of pesticides. Soil Science Society of America Journal 54:957-963.

Gannon, C.J., P. Cherukuri, B.I. Yakobson, L. Cognet, J.S. Kanzius, C. Kittrell, R.B. Weisman, M. Pasquali, H.K. Schmidt, R.E. Smalley, and S.A. Curley. 2007. Carbon nanotube-enhanced thermal destruction of cancer cells in a noninvasive radiofrequency field. Cancer 110:2654-2665.

Garg, A., and S.B. Sinnott. 1998. Effect of chemical functionalization on the mechanical properties of carbon nanotubes. Chem. Phys. Lett. 295:273-278.

Garza, K.M., K.F. Soto, and L.E. Murr. 2008. Cytotoxicity and reactive oxygen species generation from aggregated carbon and carbonaceous nanoparticulate materials. International Journal of Nanomedicine 3:83-94.

Gharbi, N., M. Pressac, M. Hadchouel, H. Szwarc, S.R. Wilson, and F. Moussa. 2005. [60]Fullerene is a powerful antioxidant in vivo with no acute or subacute toxicity. Nano Lett. 5:2578-2585.

Ginn, T.R., B.D. Wood, K.E. Nelson, T.D. Scheibe, E.M. Murphy, and T.P. Clement. 2002. Processes in microbial transport in the natural subsurface. Advances in Water Resources 25:1017-1042.

Gregory, J. 1975. Interaction of unequal double-layers at constant charge. J. Colloid

Interface Sci. 51:44-51.

Gregory, J. 1981. Approximate expressions for retarded van der waals interaction. J. Colloid Interface Sci. 83:138-145.

Guldi, D.M., R.E. Huie, P. Neta, H. Hungerbuhler, and K.D. Asmus. 1994. Excitation of C-60, solubilized in water by Triton X-100 and gamma-cyclodextrin, and subsequent charge separation via reductive quenching. Chem. Phys. Lett. 223:511-516.

Guzman, K.A.D., M.P. Finnegan, and J.F. Banfield. 2006. Influence of surface potential on aggregation and transport of titania nanoparticles. Environ. Sci. Technol. 40:7688-7693.

Haasch, M.L., P. McClellan-Green, and E. Oberdorster. 2005. Consideration of the toxicity of manufactured nanoparticles. AIP Conference Proceedings:586.

Haddon, R.C., A.F. Hebard, M.J. Rosseinsky, D.W. Murphy, S.J. Duclos, K.B. Lyons, B. Miller, J.M. Rosamilia, R.M. Fleming, A.R. Kortan, S.H. Glarum, A.V. Makhija, A.J. Muller, R.H. Eick, S.M. Zahurak, R. Tycko, G. Dabbagh, and F.A. Thiel. 1991. Conducting films of C_{60} and C_{70} by alkali-metal doping. Nature 350:320-322.

Hahn, M.W., D. Abadzic, and C.R. O'Melia. 2004. Aquasols: On the role of secondary minima. Environ. Sci. Technol. 38:5915-5924.

Halford, B. 2006. Fullerene for the face. Chemical & Engineering News 84:47-47.

Hansen, C.M., and A.L. Smith. 2004. Using Hansen solubility parameters to correlate solubility of C-60 fullerene in organic solvents and in polymers. Carbon 42:1591-1597.

Happel, J. 1958. Viscous flow in multiparticle systems - slow motion of fluids relative to beds of spherical particles. AlChE J. 4:197-201.

Harvey, R.W., and S.P. Garabedian. 1991. Use of colloid filtration theory in modeling movement of bacteria through a contaminated sandy aquifer. Environ. Sci. Technol. 25:178-185.

Hayase, K., and H. Tsubota. 1983. Sedimentary humic-acid and fulvic-acid as surface-active substances. Geochim. Cosmochim. Acta 47:947-952.

Hazani, M., R. Naaman, F. Hennrich, and M.M. Kappes. 2003. Confocal fluorescence imaging of DNA-functionalized carbon nanotubes. Nano Lett. 3:153-155.

Hedberg, K., L. Hedberg, D.S. Bethune, C.A. Brown, H.C. Dorn, R.D. Johnson, and M. Devries. 1991. Bond lengths in free molecules of buckminsterfullerene, C_{60}, from gas-phase electron-diffraction. Science 254:410-412.

Heiney, P.A., J.E. Fischer, A.R. McGhie, W.J. Romanow, A.M. Denenstein, J.P. McCauley, A.B. Smith, and D.E. Cox. 1991. Orientational ordering transition in solid C_{60}. Phys. Rev. Lett. 66:2911-2914.

Henry, T.B., F.M. Menn, J.T. Fleming, J. Wilgus, R.N. Compton, and G.S. Sayler. 2007. Attributing effects of aqueous C-60 nano-aggregates to tetrahydrofuran decomposition products in larval zebrafish by assessment of gene expression. Environ. Health Perspect. 115:1059-1065.

Her, N., G. Amy, D. Foss, J. Cho, Y. Yoon, and P. Kosenka. 2002. Optimization of method for detecting and characterizing NOM by HPLC-size exclusion chromatography with UV and on-line DOC detection. Environ. Sci. Technol. 36:1069-1076.

Herzig, J.P., D.M. Leclerc, and P. Legoff. 1970. Flow of suspensions through porous media - application to deep filtration. Ind. Eng. Chem. 62:8-&.

Heymann, D. 1996a. Solubility of C-60 in alcohols and alkanes. Carbon 34:627-631.

Heymann, D. 1996b. Solubility of fullerenes C-60 and C-70 in seven normal alcohols and their deduced solubility in water. Fullerene Sci. Technol. 4:509-515.

Heymann, D., A. Korochantsev, M.A. Nazarov, and J. Smit. 1996. Search for fullerenes C-60 and C-70 in Cretaceous-Tertiary boundary sediments from Turkmenistan, Kazakhstan, Georgia, Austria, and Denmark. Cretaceous Research 17:367-380.

Hilding, J., E.A. Grulke, Z.G. Zhang, and F. Lockwood. 2003. Dispersion of carbon nanotubes in liquids. J. Dispersion Sci. Technol. 24:1-41.

Hinds, B.J., N. Chopra, T. Rantell, R. Andrews, V. Gavalas, and L.G. Bachas. 2004. Aligned multiwalled carbon nanotube membranes. Science 303:62-65.

Hirsch, A., and M. Brettreich. 2005. Fullerenes : chemistry and reactions Wiley-VCH, Weinheim.

Hong, S., and S. Myung. 2007. Nanotube electronics - A flexible approach to mobility. Nature Nanotechnology 2:207-208.

Hong, S.K., and M. Elimelech. 1997. Chemical and physical aspects of natural organic matter (NOM) fouling of nanofiltration membranes. Journal of Membrane Science 132:159-181.

Howard, J.B., A.L. Lafleur, Y. Makarovsky, S. Mitra, C.J. Pope, and T.K. Yadav. 1992. Fullerenes synthesis in combustion. Carbon 30:1183-1201.

Huang, W.J., S. Taylor, K.F. Fu, Y. Lin, D.H. Zhang, T.W. Hanks, A.M. Rao, and Y.P. Sun. 2002. Attaching proteins to carbon nanotubes via diimide-activated amidation. Nano Lett. 2:311-314.

Hubaux, A., and G. Vos. 1970. Decision and detection limits for linear calibration curves. Anal. Chem. 42:849-855.

Huffman, D.R. 1991. Solid C_{60}. Physics Today 44:22-29.

Hungerbuhler, H., D.M. Guldi, and K.D. Asmus. 1993. Influence of electrolyte species and concentration on the aggregation and transport of fullerene nanoparticles in quartz sands. JACS 115:3386-3387.

Hussain, M.A., M.A. Kabir, and A.K. Sood. 2009. On the cytotoxicity of carbon nanotubes. Current Science 96:664-673.

Hyung, H., J.D. Fortner, J.B. Hughes, and J.H. Kim. 2007. Natural organic matter stabilizes carbon nanotubes in the aqueous phase. Environ. Sci. Technol. 41:179-184.

Iijima, S. 1991. Helical microtubules of graphitic carbon. Nature 354:56-58.

Iqbal, Z., R.H. Baughman, B.L. Ramakrishna, S. Khare, N.S. Murthy, H.J. Bornemann, and D.E. Morris. 1991. Superconductivity at 45-k in rb/tl codoped C_{60} and C_{60}/C_{70} mixtures. Science 254:826-829.

Isaacson, C.W., C.Y. Usenko, R.L. Tanguay, and J.A. Field. 2007. Quantification of fullerenes by LC/ESI-MS and its application to in vivo toxicity assays. Anal. Chem. 79:9091-9097.

Isakovic, A., Z. Markovic, B. Todorovic-Markovic, N. Nikolic, S. Vranjes-Djuric, M. Mirkovic, M. Dramicanin, L. Harhaji, N. Raicevic, Z. Nikolic, and V. Trajkovic. 2006. Distinct Cytotoxic Mechanisms of Pristine versus Hydroxylated Fullerene. Toxicol. Sci. 91:173-183.

Islam, M.F., E. Rojas, D.M. Bergey, A.T. Johnson, and A.G. Yodh. 2003. High weight fraction surfactant solubilization of single-wall carbon nanotubes in water. Nano Lett. 3:269-273.

Ismail, I.M.K., and S.L. Rodgers. 1992. Comparisons between fullerene and forms of well-known carbons. Carbon 30:229-239.

Israelachvili, J. 1992. Intermolecular and surface forces. 2nd ed. Academic Press Inc., San Diego, CA.

Jaisi, D.P., N.B. Saleh, R.E. Blake, and M. Elimelech. 2008. Transport of Single-Walled Carbon Nanotubes in Porous Media: Filtration Mechanisms and Reversibility. Environ. Sci. Technol. 42:8317-8323.

Jensen, A.W., S.R. Wilson, and D.I. Schuster. 1996. Biological applications of fullerenes. Biorg. Med. Chem. 4:767-779.

Jia, G., H.F. Wang, L. Yan, X. Wang, R.J. Pei, T. Yan, Y.L. Zhao, and X.B. Guo. 2005. Cytotoxicity of carbon nanomaterials: Single-wall nanotube, multi-wall nanotube, and fullerene. Environ. Sci. Technol. 39:1378-1383.

Jiang, L.Q., L. Gao, and J. Sun. 2003. Production of aqueous colloidal dispersions of carbon nanotubes. J. Colloid Interface Sci. 260:89-94.

Johnson, R.D., G. Meijer, and D.S. Bethune. 1990. C-60 has icosahedral symmetry. JACS 112:8983-8984.

Johnson, W.P., and B.E. Logan. 1996. Enhanced transport of bacteria in porous media by sediment-phase and aqueous-phase natural organic matter. Water Res. 30:923.

Kahn, M.G.C., S. Banerjee, and S.S. Wong. 2002. Solubilization of oxidized single-walled carbon nanotubes in organic and aqueous solvents through organic derivatization. Nano Lett. 2:1215-1218.

Kalinichev, A.G., and R.J. Kirkpatrick. 2007. Molecular dynamics simulation of cationic complexation with natural organic matter. European Journal of Soil Science

58:909-917.

Kamat, P.V., M. Haria, and S. Hotchandani. 2004. C-60 cluster as an electron shuttle in a Ru(II)-polypyridyl sensitizer-based photochemical solar cell. J. Phys. Chem. B 108:5166-5170.

Kang, S., M. Pinault, L.D. Pfefferle, and M. Elimelech. 2007. Single-walled carbon nanotubes exhibit strong antimicrobial activity. Langmuir 23:8670-8673.

Kang, S., M. Herzberg, D.F. Rodrigues, and M. Elimelech. 2008. Antibacterial effects of carbon nanotubes: Size does matter. Langmuir 24:6409-6413.

Karagunduz, A., K.D. Pennell, and M.H. Young. 2001. Influence of a nonionic surfactant on the water retention properties of unsaturated soils. Soil Science Society of America Journal 65:1392-1399.

Kaya, A., and Y. Yukselen. 2005. Zeta potential of clay minerals and quartz contaminated by heavy metals. Canadian Geotechnical Journal 42:1280-1289.

Kelty, S.P., C.C. Chen, and C.M. Lieber. 1991. Superconductivity at 30-k in cesium-doped C_{60}. Nature 352:223-225.

Kim, P., L. Shi, A. Majumdar, and P.L. McEuen. 2001. Thermal transport measurements of individual multiwalled nanotubes. Phys. Rev. Lett. 87.

Kong, J., N.R. Franklin, C.W. Zhou, M.G. Chapline, S. Peng, K.J. Cho, and H.J. Dai. 2000. Nanotube molecular wires as chemical sensors. Science 287:622-625.

Korobov, M.V., A.L. Mirakian, N.V. Avramenko, E.F. Valeev, I.S. Neretin, Y.L. Slovokhotov, A.L. Smith, G. Olofsson, and R.S. Ruoff. 1998. C-60 center dot bromobenzene solvate: Crystallographic and thermochemical studies and their relationship to C-60 solubility in bromobenzene. J. Phys. Chem. B 102:3712-3717.

Koruga, D., L. Matija, N. Misic, and P. Rakin. 1996. Fullerene C-60: Properties and possible applications, p. 49-56 Advanced Materials for High Technology Applications, Vol. 214.

Koruga, D., S. Hameroff, W. James, R. Loutfy, and M. Sundareshan. 1993. Fullerene C_{60} : history, physics, nanobiology, nanotechnology North-Holland, Amsterdam.

Kowalczyk, P., and R. Holyst. 2008. Efficient adsorption of super greenhouse gas

(Tetrafluoromethane) in carbon nanotubes. Environ. Sci. Technol. 42:2931-2936.

Kratschmer, W., K. Fostiropoulos, and D.R. Huffman. 1990a. The infrared and ultraviolet-absorption spectra of laboratory-produced carbon dust - evidence for the presence of the C-60 molecule. Chem. Phys. Lett. 170:167-170.

Kratschmer, W., L.D. Lamb, K. Fostiropoulos, and D.R. Huffman. 1990b. Solid C-60 - a new form of carbon. Nature 347:354-358.

Kretzschmar, R., and H. Sticher. 1997. Transport of humic-coated iron oxide colloids in a sandy soil: Influence of Ca^{2+} and trace metals. Environ. Sci. Technol. 31:3497-3504.

Kroto, H.W., J.R. Heath, S.C. Obrien, R.F. Curl, and R.E. Smalley. 1985. C-60 - Buckminsterfullerene. Nature 318:162-163.

Krusic, P.J., E. Wasserman, P.N. Keizer, J.R. Morton, and K.F. Preston. 1991a. Radical reactions of C_{60}. Science 254:1183-1185.

Krusic, P.J., E. Wasserman, B.A. Parkinson, B. Malone, E.R. Holler, P.N. Keizer, J.R. Morton, and K.F. Preston. 1991b. Electron-spin-resonance study of the radical reactivity of C_{60}. JACS 113:6274-6275.

Kulkarni, P.P., and C.T. Jafvert. 2008. Solubility of C-60 in solvent mixtures. Environ. Sci. Technol. 42:845-851.

Kuznetsova, A., I. Popova, J.T. Yates, M.J. Bronikowski, C.B. Huffman, J. Liu, R.E. Smalley, H.H. Hwu, and J.G.G. Chen. 2001. Oxygen-containing functional groups on single-wall carbon nanotubes: NEXAFS and vibrational spectroscopic studies. JACS 123:10699-10704.

Lamparth, I., and A. Hirsch. 1994. Water-soluble malonic-acid derivatives of C-60 with a defined 3-dimensional structure. Journal Of The Chemical Society-Chemical Communications:1727-1728.

Langa, F., and J.-F. Nierengarten. 2007. Fullerenes : principles and applications Royal Society of Chemistry, Cambridge, UK.

Larsson, S., A. Volosov, and A. Rosen. 1987. Optical-spectrum of the icosahedral C_{60} - follene-60. Chem. Phys. Lett. 137:501-504.

Lecoanet, H.F., and M.R. Wiesner. 2004. Velocity effects on fullerene and oxide nanoparticle deposition in porous media. Environ. Sci. Technol. 38:4377-4382.

Lecoanet, H.F., J.-Y. Bottero, and M.R. Wiesner. 2004. Laboratory assessment of the mobility of nanomaterials in porous media. Environ. Sci. Technol. 38:5164-5169.

Lee, H.J., S.W. Han, Y.D. Kwon, L.S. Tan, and J.B. Baek. 2008. Functionalization of multi-walled carbon nanotubes with various 4-substituted benzoic acids in mild polyphosphoric acid/phosphorous pentoxide. Carbon 46:1850-1859.

Li, C., Y.H. Chen, Y.B. Wang, Z. Iqbal, M. Chhowalla, and S. Mitra. 2007. A fullerene-single wall carbon nanotube complex for polymer bulk heterojunction photovoltaic cells. J. Mater. Chem. 17:2406-2411.

Li, J., A. Takeuchi, M. Ozawa, X.H. Li, K. Saigo, and K. Kitazawa. 1993. C-60 fullerol formation catalyzed by quaternary ammonium hydroxides. Journal Of The Chemical Society-Chemical Communications:1784-1785.

Li, X., P. Zhang, C.L. Lin, and W.P. Johnson. 2005. Role of hydrodynamic drag on microsphere deposition and re-entrainment in porous media under unfavorable conditions. Environ. Sci. Technol. 39:4012.

Li, X.Q., T.D. Scheibe, and W.P. Johnson. 2004. Apparent decreases in colloid deposition rate coefficients with distance of transport under unfavorable deposition conditions: A general phenomenon. Environ. Sci. Technol. 38:5616-5625.

Li, Y.S., Y.G. Wang, L.M. Abriola, and K.D. Pennell. 2008. Investigation of the Transport and Deposition of Fullerene (C60) Nanoparticles in Quartz Sands under Varying Flow Conditions. Environmental Science & Technology In press.

Litton, G.M., and T.M. Olson. 1996. Particle size effects on colloid deposition kinetics: Evidence of secondary minimum deposition. Colloids and Surfaces a-Physicochemical and Engineering Aspects 107:273-283.

Litvinova, L.S., V.G. Ivanov, M.V. Mokeev, and V.N. Zgonnik. 2001. Water-soluble [60]fullerene compositions with carbohydrates. Mendeleev Commun.:193-194.

Liu, S.Z., Y.J. Lu, M.M. Kappes, and J.A. Ibers. 1991. The structure of the C_{60} molecule - x-ray crystal-structure determination of a twin at 110-k. Science 254:408-410.

Logan, B.E., D.G. Jewett, R.G. Arnold, E.J. Bouwer, and C.R. Omelia. 1995.

Clarification of clean-bed filtration models. Journal of Environmental Engineering-Asce 121:869-873.

Lyon, D.Y., L.K. Adams, J.C. Falkner, and P.J.J. Alvarez. 2006. Antibacterial activity of fullerene water suspensions: Effects of preparation method and particle size. Environ. Sci. Technol. 40:4360-4366.

Lyon, D.Y., J.D. Fortner, C.M. Sayes, V.L. Colvin, and J.B. Hughes. 2005. Bacterial cell association and antimicrobial activity of a C_{60} water suspension. Environ. Toxicol. Chem. 24:2757-2762.

Marcus, Y., A.L. Smith, M.V. Korobov, A.L. Mirakyan, N.V. Avramenko, and E.B. Stukalin. 2001. Solubility of C-60 fullerene. J. Phys. Chem. B 105:2499-2506.

Matarredona, O., H. Rhoads, Z.R. Li, J.H. Harwell, L. Balzano, and D.E. Resasco. 2003. Dispersion of single-walled carbon nanotubes in aqueous solutions of the anionic surfactant NaDDBS. J. Phys. Chem. B 107:13357-13367.

Maynard, A.D., R.J. Aitken, T. Butz, V. Colvin, K. Donaldson, G. Oberdorster, M.A. Philbert, J. Ryan, A. Seaton, V. Stone, S.S. Tinkle, L. Tran, N.J. Walker, and D.B. Warheit. 2006. Safe handling of nanotechnology. Nature 444:267-269.

McEwen, C.N., R.G. McKay, and B.S. Larsen. 1992. C-60 as a radical sponge. JACS 114:4412-4414.

Monthioux, M., and V.L. Kuznetsov. 2006. Who should be given the credit for the discovery of carbon nanotubes? Carbon 44:1621-1623.

Monthioux, M., B.W. Smith, B. Burteaux, A. Claye, J.E. Fischer, and D.E. Luzzi. 2001. Sensitivity of single-wall carbon nanotubes to chemical processing: an electron microscopy investigation. Carbon 39:1251-1272.

Muller, J., F. Huaux, N. Moreau, P. Misson, J.F. Heilier, M. Delos, M. Arras, A. Fonseca, J.B. Nagy, and D. Lison. 2005. Respiratory toxicity of multi-wall carbon nanotubes. Toxicol. Appl. Pharmacol. 207:221-231.

Murr, L.E., J.J. Bang, E.V. Esquivel, P.A. Guerrero, and A. Lopez. 2004. Carbon nanotubes, nanocrystal forms, and complex nanoparticle aggregates in common fuel-gas combustion sources and the ambient air. J. Nanopart. Res. 6:241-251.

Murray, J.S., S.G. Gagarin, and P. Politzer. 1995. Representation of C-60 solubilities in terms of computed molecular-surface electrostatic potentials and areas. J. Phys. Chem. 99:12081-12083.

Mylon, S.E., K.L. Chen, and M. Elimelech. 2004. Influence of natural organic matter and ionic composition on the kinetics and structure of hematite colloid aggregation: Implications to iron depletion in estuaries. Langmuir 20:9000-9006.

Nagano, Y., and T. Nakamura. 1997. C-60-CCl4 solvate: An AB(13) type binary crystal. Chem. Phys. Lett. 265:358-360.

Nel, A., T. Xia, L. Madler, and N. Li. 2006. Toxic potential of materials at the nanolevel. Science 311:622-627.

Nguyen, T.H., and K.L. Chen. 2007. Role of divalent cations in plasmid DNA adsorption to natural organic matter-coated silica surface. Environ. Sci. Technol. 41:5370-5375.

Niyogi, S., S. Boukhalfa, S.B. Chikkannanavar, T.J. McDonald, M.J. Heben, and S.K. Doorn. 2007. Selective aggregation of single-walled carbon nanotubes via salt addition. JACS 129:1898-1899.

O'Connell, M.J., P. Boul, L.M. Ericson, C. Huffman, Y.H. Wang, E. Haroz, C. Kuper, J. Tour, K.D. Ausman, and R.E. Smalley. 2001. Reversible water-solubilization of single-walled carbon nanotubes by polymer wrapping. Chem. Phys. Lett. 342:265-271.

O'Connell, M.J., S.M. Bachilo, C.B. Huffman, V.C. Moore, M.S. Strano, E.H. Haroz, K.L. Rialon, P.J. Boul, W.H. Noon, C. Kittrell, J.P. Ma, R.H. Hauge, R.B. Weisman, and R.E. Smalley. 2002. Band gap fluorescence from individual single-walled carbon nanotubes. Science 297:593-596.

Oberdorster, E. 2004a. Manufactured nanomaterials (Fullerenes, C-60) induce oxidative stress in the brain of juvenile largemouth bass. Environ. Health Perspect. 112:1058-1062.

Oberdorster, E. 2004b. Toxicity of nC_{60} fullerenes to two aquatic species: Daphnia and largemouth bass. Abstracts of Papers of the American Chemical Society 227:U1233-U1233.

Oberdorster, G., E. Oberdorster, and J. Oberdorster. 2005. Nanotoxicology: An emerging discipline evolving from studies of ultrafine particles. Environ. Health Perspect.

113:823-839.

Pan, Z.W., S.S. Xie, B.H. Chang, C.Y. Wang, L. Lu, W. Liu, M.Y. Zhou, and W.Z. Li. 1998. Very long carbon nanotubes. Nature 394:631-632.

Pelley, A.J., and N. Tufenkji. 2008. Effect of particle size and natural organic matter on the migration of nano- and microscale latex particles in saturated porous media. J. Colloid Interface Sci. 321:74-83.

Peng, X.J., Z.K. Luan, J. Ding, Z.H. Di, Y.H. Li, and B.H. Tian. 2005. Ceria nanoparticles supported on carbon nanotubes for the removal of arsenate from water. Mater. Lett. 59:399-403.

Pennell, K.D., L.M. Abriola, and W.J. Weber, Jr. 1993. Surfactant-enhanced solubilization of residual dodecane in soil columns. 1. Experimental investigation. Environ. Sci. Technol. 27:2332-2340.

Pennell, K.D., S.A. Boyd, and L.M. Abriola. 1995. Surface area of soil organic matter reexamined. Soil Science Society of America Journal 59:1012-1018.

Pennell, K.D., A.M. Adinolfi, L.M. Abriola, and M.S. Diallo. 1997. Solubilization of dodecane, tetrachloroethylene, and 1,2-dichlorobenzene in micellar solutions of ethoxylated nonionic surfactants. Environ. Sci. Technol. 31:1382-1389.

Pierson, H.O. 1993. Handbook of Carbon, Graphite, Diamond and Fullerenes - Properties, Processing and Applications Noyes Publications, Park Ridge, N.J., U.S.A.

Poland, C.A., R. Duffin, I. Kinloch, A. Maynard, W.A.H. Wallace, A. Seaton, V. Stone, S. Brown, W. MacNee, and K. Donaldson. 2008. Carbon nanotubes introduced into the abdominal cavity of mice show asbestos-like pathogenicity in a pilot study. Nature Nanotechnology 3:423-428.

Pompeo, F., and D.E. Resasco. 2002. Water solubilization of single-walled carbon nanotubes by functionalization with glucosarnine. Nano Lett. 2:369-373.

Prassides, K., H.W. Kroto, R. Taylor, D.R.M. Walton, W.I.F. David, J. Tomkinson, R.C. Haddon, M.J. Rosseinsky, and D.W. Murphy. 1992. Fullerenes and fullerides in the solid-state - neutron-scattering studies. Carbon 30:1277-1286.

Raja, P.M.V., J. Connolley, G.P. Ganesan, L.J. Ci, P.M. Ajayan, O. Nalamasu, and D.M. Thompson. 2007. Impact of carbon nanotube exposure, dosage and aggregation on smooth muscle cells. Toxicol. Lett. 169:51-63.

Rajagopalan, R., and C. Tien. 1976. Trajectory Analysis Of Deep-Bed Filtration With Sphere-In-Cell Porous-Media Model. AlChE J. 22:523-533.

Ramsburg, C.A., and K.D. Pennell. 2001. Experimental and economic assessment of two surfactant formulations for source zone remediation at a former dry cleaning facility. Ground Water Monit. Rem. 21:68-82.

Ramsburg, C.A., K.D. Pennell, L.M. Abriola, G. Daniels, C.D. Drummond, M. Gamache, H.-L. Hsu, E.A. Petrovskis, K.M. Rathfelder, J.L. Ryder, and T.P. Yavaraski. 2005. Pilot-scale demonstration of surfactant-enhanced PCE solubilization at the Bachman Road site. 2. System operation and evaluation. Environ. Sci. Technol. 39:1791-1801.

Rausch, H., and T. Braun. 2001. Sublimation behaviour of C-60 and of the endohedral radiofullerenes formed by nuclear recoil implosion via neutron irradiation. Chem. Phys. Lett. 350:15-18.

Regueiro, M.N., P. Monceau, and J.L. Hodeau. 1992. Crushing C_{60} to diamond at room-temperature. Nature 355:237-239.

Rinzler, A.G., J.H. Hafner, P. Nikolaev, L. Lou, S.G. Kim, D. Tomanek, P. Nordlander, D.T. Colbert, and R.E. Smalley. 1995. Unraveling nanotubes - field-emission from an atomic wire. Science 269:1550-1553.

Ruoff, R.S., D.S. Tse, R. Malhotra, and D.C. Lorents. 1993a. Solubility of C-60 in a variety of solvents. J. Phys. Chem. 97:3379-3383.

Ruoff, R.S., R. Malhotra, D.L. Huestis, D.S. Tse, and D.C. Lorents. 1993b. Anomalous solubility behavior of C_{60}. Nature 362:140-141.

Saiers, J.E., and J.J. Lenhart. 2003. Ionic-strength effects on colloid transport and interfacial reactions in partially saturated porous media. Water Resour. Res. 39.

Saito, R., M. Fujita, G. Dresselhaus, and M.S. Dresselhaus. 1992. Electronic-structure of chiral graphene tubules. Appl. Phys. Lett. 60:2204-2206.

Saleh, N.B., L.D. Pfefferle, and M. Elimelech. 2008. Aggregation kinetics of multiwalled carbon nanotubes in aquatic systems: measurements and environmental implications. Environ. Sci. Technol. 42:7963-7969.

Salerno, M.B., M. Flamm, B.E. Logan, and D. Velegol. 2006. Transport of rodlike colloids through packed beds. Environ. Sci. Technol. 40:6336-6340.

Salzmann, C.G., S.A. Llewellyn, G. Tobias, M.A.H. Ward, Y. Huh, and M.L.H. Green. 2007. The role of carboxylated carbonaceous fragments in the functionalization and spectroscopy of a single-walled carbon-nanotube material. Adv. Mater. 19:883-887.

Sano, M., J. Okamura, and S. Shinkai. 2001a. Colloidal nature of single-walled carbon nanotubes in electrolyte solution: The Schulze-Hardy rule. Langmuir 17:7172-7173.

Sano, M., A. Kamino, J. Okamura, and S. Shinkai. 2001b. Self-organization of PEO-graft-single-walled carbon nanotubes in solutions and Langmuir-Blodgett films. Langmuir 17:5125-5128.

Sawada, H., J. Iidzuka, T. Maekawa, R. Takahashi, T. Kawase, K. Oharu, H. Nakagawa, and K. Ohira. 2003. Solubilization of fullerene into water with fluoroalkyl end-capped amphiphilic oligomers-novel fluorescence properties. J. Colloid Interface Sci. 263:1-3.

Sayes, C.M., A.M. Gobin, K.D. Ausman, J. Mendez, J.L. West, and V.L. Colvin. 2005. Nano-C-60 cytotoxicity is due to lipid peroxidation. Biomaterials 26:7587-7595.

Sayes, C.M., J.D. Fortner, W. Guo, D. Lyon, A.M. Boyd, K.D. Ausman, Y.J. Tao, B. Sitharaman, L.J. Wilson, J.B. Hughes, J.L. West, and V.L. Colvin. 2004. The differential cytotoxicity of water-soluble fullerenes. Nano Lett. 4:1881-1887.

Schenkel, J.H., and J.A. Kitchener. 1960. A Test of the Derjaguin-Verwey-Overbeek Theory with a Colloidal Suspension. Transactions of the Faraday Society 56:161-173.

Scrivens, W.A., J.M. Tour, K.E. Creek, and L. Pirisi. 1994. Synthesis of C-14-labeled C-60, its suspension in water, and its uptake by human keratinocytes. JACS 116:4517-4518.

Service, R.F. 2004. Nanotoxicology: Nanotechnology grows up. Science 304:1732-1734.

Shani, C., N. Weisbrod, and A. Yakirevich. 2008. Colloid transport through saturated sand columns: Influence of physical and chemical surface properties on deposition. Colloids and Surfaces a-Physicochemical and Engineering Aspects 316:142-150.

Shen, C.Y., Y.F. Huang, B.G. Li, and Y. Jin. 2008. Effects of solution chemistry on straining of colloids in porous media under unfavorable conditions. Water Resour. Res. 44:W05419.

Sijbesma, R., G. Srdanov, F. Wudl, J.A. Castoro, C. Wilkins, S.H. Friedman, D.L. Decamp, and G.L. Kenyon. 1993. Synthesis of a fullerene derivative for the inhibition of HIV enzymes. JACS 115:6510-6512.

Sivaraman, N., R. Dhamodaran, I. Kaliappan, T.G. Srinivasan, P.R.V. Rao, and C.K. Mathews. 1992. Solubility of C-60 in organic-solvents. J. Org. Chem. 57:6077-6079.

Smalley, R.E. 1997. Discovering the fullerenes (Nobel lecture). Angewandte Chemie-International Edition in English 36:1595-1601.

Stanton, R.E., and M.D. Newton. 1988. Normal vibrational-modes of buckminsterfullerene. J. Phys. Chem. 92:2141-2145.

Talukdar, S., P. Pradhan, and A. Banerji. 1997. Electron donor-acceptor interactions of C-60 with n- and pi-donors: A rational approach towards its solubility. Fullerene Sci. Technol. 5:547-557.

Taylor, R., J.P. Hare, A.K. Abdulsada, and H.W. Kroto. 1990. Isolation, separation and characterization of the fullerenes C-60 and C-70 - the 3rd form of carbon. Journal Of The Chemical Society-Chemical Communications:1423-1424.

Terashima, M., and S. Nagao. 2007. Solubilization of [60]fullerene in water by aquatic humic substances. Chem. Lett. 36:302-303.

Tong, Z.H., M. Bischoff, L. Nies, B. Applegate, and R.F. Turco. 2007. Impact of fullerene (C-60) on a soil microbial community. Environ. Sci. Technol. 41:2985-2991.

Toride, N., F.J. Leij, and M.T. vanGenuchten. 1999. The CXTFIT code for estimating transport parameters from laboratory or field tracer experiments, Version 2.1 Research report No. 137.

Torrens, F. 2006. Calculations of organic-solvent dispersions of single-wall carbon nanotubes. Int. J. Quantum Chem 106:712-718.

Trembley, J.F. 2002. Mitsubishi Chemical Aims at Breakthrough. Chemical & Engineering News 80:16-17.

Tufenkji, N., and M. Elimelech. 2004. Deviation from the classical colloid filtration theory in the presence of repulsive DLVO interactions. Langmuir 20:10818-10828.

Tufenkji, N., J.A. Redman, and M. Elimelech. 2003. Interpreting deposition patterns of microbial particles in laboratory-scale column experiments. Environ. Sci. Technol. 37:616-623.

Ungurenasu, C., and A. Airinei. 2000. Highly stable C-60/poly(vinylpyrrolidone) charge-transfer complexes afford new predictions for biological applications of underivatized fullerenes. J. Med. Chem. 43:3186-3188.

Utsunomiya, S., K.A. Jensen, G.J. Keeler, and R.C. Ewing. 2002. Uraninite and fullerene in atmospheric particulates. Environ. Sci. Technol. 36:4943-4947.

Wang, P., Q.H. Shi, H.J. Liang, D.W. Steuerman, G.D. Stucky, and A.A. Keller. 2008. Enhanced Environmental Mobility of Carbon Nanotubes in the Presence of Humic Acid and Their Removal from Aqueous Solution. Small 4:2166-2170.

Warheit, D.B., P.J.A. Borm, C. Hennes, and J. Lademann. 2007. Testing strategies to establish the safety of nanomaterials: Conclusions of an ECETOC workshop. Inhalation Toxicology 19:631-643.

Weeks, D.E., and W.G. Harter. 1988. Vibrational frequencies and normal-modes of buckminsterfullerene. Chem. Phys. Lett. 144:366-372.

Wei, X.W., M.F. Wu, L. Qi, and Z. Xu. 1997. Selective solution-phase generation and oxidation reaction of C-60(n-) (n=1,2) and formation of an aqueous colloidal solution of C-60. Journal Of The Chemical Society-Perkin Transactions 2:1389-1393.

Weiss, T.H., A.L. Mills, G.M. Hornberger, and J.S. Herman. 1995. Effect of bacterial-cell shape on transport of bacteria in porous-media. Environ. Sci. Technol. 29:1737-1740.

Wiesner, M.R., G.V. Lowry, P. Alvarez, D. Dionysiou, and P. Biswas. 2006. Assessing the risks of manufactured nanomaterials. Environ. Sci. Technol. 40:4336-4345.

Wilson, R.J., G. Meijer, D.S. Bethune, R.D. Johnson, D.D. Chambliss, M.S. Devries, H.E.

Hunziker, and H.R. Wendt. 1990. Imaging C-60 clusters on a surface using a scanning tunneling microscope. Nature 348:621-622.

Xia, X.R., N.A. Monteiro-Riviere, and J.E. Riviere. 2006. Trace analysis of fullerenes in biological samples by simplified liquid-liquid extraction and high-performance liquid chromatography. J. Chromatogr. A 1129:216-222.

Xie, B., Z.H. Xu, W.H. Guo, and Q.L. Li. 2008. Impact of natural organic matter on the physicochemical properties of aqueous C-60 nanoparticles. Environ. Sci. Technol. 42:2853-2859.

Xu, S.P., B. Gao, and J.E. Saiers. 2006. Straining of colloidal particles in saturated porous media. Water Resour. Res. 42.

Xu, S.P., Q. Liao, and J.E. Saiers. 2008. Straining of nonspherical colloids in saturated porous media. Environ. Sci. Technol. 42:771-778.

Yamago, S., H. Tokuyama, E. Nakamura, K. Kikuchi, S. Kananishi, K. Sueki, H. Nakahara, S. Enomoto, and F. Ambe. 1995. In-vivo biological behavior of a water-miscible fullerene - C-14 labeling, absorption, distribution, excretion and acute toxicity. Chemistry & Biology 2:385-389.

Yamakoshi, Y., S. Sueyoshi, K. Fukuhara, and N. Miyata. 1998. center dot OH and O-2(center dot-) generation in aqueous C-60 and C-70 solutions by photoirradiation: An EPR study. JACS 120:12363-12364.

Yamakoshi, Y., N. Umezawa, A. Ryu, K. Arakane, N. Miyata, Y. Goda, T. Masumizu, and T. Nagano. 2003. Active oxygen species generated from photoexcited fullerene (C-60) as potential medicines: O-2(-center dot) versus O-1(2). JACS 125:12803-12809.

Yamakoshi, Y.N., T. Yagami, K. Fukuhara, S. Sueyoshi, and N. Miyata. 1994. Solubilization Of Fullerenes Into Water With Polyvinylpyrrolidone Applicable To Biological Tests. Journal Of The Chemical Society-Chemical Communications:517-518.

Yang, J.Z., L.B. Alemany, J. Driver, J.D. Hartgerink, and A.R. Barron. 2007. Fullerene-derivatized amino acids: Synthesis, characterization, antioxidant properties, and solid-phase peptide synthesis. Chemistry-a European Journal 13:2530-2545.

Yannoni, C.S., P.P. Bernier, D.S. Bethune, G. Meijer, and J.R. Salem. 1991. NMR determination of the bond lengths in C_{60}. JACS 113:3190-3192.

Yao, K.M., M.M. Habibian, and C.R. Omelia. 1971. Water and waste water filtration - concepts and applications. Environ. Sci. Technol. 5:1105-1112.

Yu, M.F., B.S. Files, S. Arepalli, and R.S. Ruoff. 2000. Tensile loading of ropes of single wall carbon nanotubes and their mechanical properties. Phys. Rev. Lett. 84:5552-5555.

Zhang, Y., Z. Shi, Z. Gu, and S. Iijima. 2000. Structure modification of single-wall carbon nanotubes. Carbon 38:2055-2059.

Zhao, B., H. Hu, A.P. Yu, D. Perea, and R.C. Haddon. 2005. Synthesis and characterization of water soluble single-walled carbon nanotube graft copolymers. JACS 127:8197-8203.

Zhao, W., C.H. Song, and P.E. Pehrsson. 2002. Water-soluble and optically pH-sensitive single-walled carbon nanotubes from surface modification. JACS 124:12418-12419.

Zheng, L.X., M.J. O'Connell, S.K. Doorn, X.Z. Liao, Y.H. Zhao, E.A. Akhadov, M.A. Hoffbauer, B.J. Roop, Q.X. Jia, R.C. Dye, D.E. Peterson, S.M. Huang, J. Liu, and Y.T. Zhu. 2004. Ultralong single-wall carbon nanotubes. Nature Materials 3:673-676.

Zhu, S.Q., E. Oberdorster, and M.L. Haasch. 2006. Toxicity of an engineered nanoparticle (fullerene, C-60) in two aquatic species, Daphnia and fathead minnow. Marine Environmental Research 62:S5-S9.